PROPERTIES OF LIME BINDERS AND AGGREGATES OF ROMAN MORTARS IN WESTERN ANATOLIA

A Thesis Submitted to
the Graduate School of Engineering and Sciences of
İzmir Institute of Technology
In Partial Fulfillment of the Requirements for the Degree of

DOCTOR OF PHILOSOPHY

in Architectural Restoration

by
Burcu TAŞCI

March 2021
İZMİR

ACKNOWLEDGMENT

ABSTRACT

PROPERTIES OF LIME BINDERS AND AGGREGATES OF ROMAN MORTARS IN WESTERN ANATOLIA

In this study, the characteristics of Roman lime mortars taken from a wide area in Western Anatolia were determined in order to understand whether there was a common production technology of lime mortar in the Roman Empire by making a comparison between Europe and Western Anatolia.

For this purpose, *opus caementicium* and *opus signinum* mortars were collected from twenty-six archaeological sites in Western Anatolia. Basic physical properties, raw material compositions, mineralogical and chemical compositions, mechanical, microstructural, and hydraulic properties of mortars, pozzolanicity and geochemical characteristics of aggregates were identified by SEM-EDS, MIP, XRD, TGA, FTIR analyses, and point load tests. Results showed Roman lime mortars were compact, low dense, and high porous materials. *Opus caementicium* mortars were grayish with the use of crushed stones, however *opus signinum* mortars were light brownish due to the use of crushed bricks/tiles. *Opus caementicium* mortars were used in various types of structures, while *opus signinum* mortars were generally used in water-related structures. Lime/aggregate ratios of mortars varied between 1:4-3:2 parallel to ideal lime/aggregate written in Roman sources. Despite using high calcium lime in the production of mortars, the compressive strengths of mortars were found compatible with NHL3.5 type of lime due to the use of pozzolanic aggregates which were produced from rhyolite and dacite (silicic rocks).

These results indicated that the properties of Roman lime mortars were similar in Western Anatolia and other regions of the Roman Empire. This finding can be evidence of common lime mortar technology produced using similar local sources throughout the Roman Empire.

ÖZET

BATI ANADOLU ROMA HARÇLARININ KİREÇ BAĞLAYICI VE AGREGALARININ ÖZELLİKLERİ

Bu çalışmada, Batı Anadolu'da geniş bir alandan alınan Roma kireç harçlarının özellikleri, Avrupa ile Batı Anadolu arasında karşılaştırma yapılarak Roma İmparatorluğu'nda ortak bir kireç harç üretim teknolojisi olup olmadığını anlamak için belirlenmiştir.

Bu amaçla, Batı Anadolu'da bulunan yirmi altı arkeolojik alandan *opus caementicium* ve *opus signinum* harçları toplanmıştır. Harçların temel fiziksel özellikleri, ham madde kompozisyonları, mineralojik ve kimyasal yapıları, mekanik, mikro yapısal ve hidrolik özellikleri ile agregaların puzolanik ve jeokimyasal özellikleri SEM-EDS, MIP, XRD, TGA, FTIR analizleri ve nokta yükleme deneyleri ile belirlenmiştir. Sonuçlar, Roma kireç harçlarının kompakt, düşük yoğunluklu ve yüksek gözenekli malzemeler olduğunu göstermiştir. *Opus caementicium* harçları kırma taş kullanımı ile grimsi renk alırken, *opus signinum* harçları kırma tuğla/kiremit kullanımı nedeniyle açık kahverengimsi renktedir. *Opus caementicium* harçları çeşitli yapı türlerinde kullanılırken, *opus signinum* harçları genellikle su yapılarında kullanılmıştır. Harçların kireç/agrega oranları, Roma kaynaklarında yazılan ideal kireç/agrega oranlarına paralel olarak 1:4-3:2 arasında değişmektedir. Harç üretiminde saf kireç kullanılmasına rağmen, harçların basınç dayanımları riyolit ve dasitten (silisli kayaçlar) üretilen puzolanik agregalar kullanılması nedeniyle NHL3.5 tür kireç ile uyumlu bulunmuştur.

Bu sonuçlar, Roma kireç harçlarının özelliklerinin Batı Anadolu'da ve Roma İmparatorluğu'nun farklı bölgelerinde benzer olduğunu göstermiştir. Bu bulgu, Roma İmparatorluğu genelinde benzer yerel kaynaklar kullanılarak üretilen ortak bir kireç harç teknolojisinin kanıtı olabilir.

TABLE OF CONTENTS

LIST OF TABLES

LIST OF FIGURES

CHAPTER 1

INTRODUCTION

Mortar is a composite material obtained by mixing binder, aggregate, water, and additives with suitable proportions in historic and modern structures. In historic structures, mortars are one of the primary materials and fulfilled different functions such as bedding, jointing, bonding, and surface finishing (UNI EN 16572 2015).

There have been several types of mortars used from the beginning of construction history until today. Clay, gypsum, and lime are the most prevalent binding materials found in the mortars just before the invention of the modern cement in the 19th century. Among historic binders, lime is the most widely used binding material in archaeological sites and historic structures.

Many different civilizations such as Incas, Mayas, Chinese, Egyptians, Greeks, and Romans used lime mortars for the construction of brick or stone masonry and rendering the surfaces (Boynton 1980; Cowper 1998). The invention of lime plaster could be traced back to at least the Epi-Paleolithic Geometric Kebaran (ca.12.000 B.C.) and its use in architecture to the Natufian (10.300-8500 B.C.) in the Levant (Kingery, Vandiver, and Prickett 1988). In Anatolia, lime was used as a plaster in Çatal Höyük (ca. 6500 B.C.), Hacılar, Aşıklı Höyük (ca. 7000 B.C.), and Çayönü during the Neolithic Period (Gourdin and Kingery 2016). Lime, as a mortar, was used in Egypt in 4000 B.C. (Cowan 1977; Cowper 1998). Apparently, the practice of limestone calcination has been known since 2450 B.C. in ancient Mesopotamia where the ruins of a lime kiln were found (Davey 1961).

It is considered that lime mortar technology was diffused from the Middle East to the Greeks and then to the Romans (Davey 1961). However, the Greeks used lime only for stuccos, painted renderings, and the lining of cisterns instead of using it as a binding agent in the mortars for structural purposes (MacDonald 1982; Adam 2005; Cowper 1998). Studies on the lime plaster of the cistern of Kameiros (Rhodes) (500 B.C.) confirmed this statement (Moropoulou, Bakolas, and Anagnostopoulou 2005). Written documents on the use of lime in mortar production are available in Roman sources. Accordingly, the first known use of lime mortars in Roman times could be accepted in the first half of the 3rd century B.C. (Ward-Perkins 2003).

The Romans can be distinguished from other civilizations with their widespread use of lime mortars for building purposes in architecture (Lugli 1957; Moropoulou, Bakolas, and Anagnostopoulou 2005). The skilled and clever use of the lime mortar in architecture was one of the main parameters of the expansion of the Roman Empire (Artioli, Secco, and Addis 2019).

Lime mortars are produced mixing lime as binder and aggregates as filling material. The raw material of lime is calcareous stones which are primarily consisted of calcium carbonate ($CaCO_3$) minerals (Cowper 1998; Davey 1961). Vitruvius described the properties of suitable limestone for lime mortar production. Limestones should be white and less porous (Vitruvius 1960).

The calcination process is the first step of lime production and it starts with heating limestones ($CaCO_3$). In ancient times, the calcination of limestones used to be done in kilns made of stone or bricks. Such kilns used to be burned after piles of wood and limestone were put in them. Those kilns used to be left to cool after burning for a day or two, and then quicklime would be taken out from the lower part of the kiln. Even though burning those kilns required ability and experience, criminals were generally used in running the lime kilns during the Roman Period (Krumnacher 2001).

After the calcination, calcium carbonate is converted into calcium oxide (CaO) called quicklime. The last step is to slake the quicklime with water. During slaking, quicklime is hydrated, a strong heat is evolved and calcium hydroxide ($Ca(OH)_2$) known as lime is obtained (Boynton 1980; Wingate 1985).

The aging of lime putty is carried out after the slaking under excess water for extended periods. Upon aging, portlandite (calcium hydroxide) crystal size reduces and platelike portlandite crystals occur due to dissolution of prism faces and secondary crystallization of sub-micrometer large portlandite crystals. This leads to an increase in surface area. As a result, more water can penetrate newly formed large portlandite crystals. Aging improves plasticity, workability, and water retention capacity of mortar (Cazalla et al. 2000; Mascolo et al. 2010; Margalha et al. 2013). The use of the aged lime has been known since the Roman and succeeding periods. In the Roman Period, it was advised to keep lime at least for three years before using it (Peter 1850).

Aggregates used as filling material can be classified as inert aggregates and pozzolanic aggregates (Lea 1940). Inert aggregates do not react with lime. However, the pozzolanic aggregates composed of reactive silicates and aluminates, react with lime in the presence of water and produce hydraulic products such as calcium silicate hydrate

(CSH) and calcium aluminate hydrate (CAH) (Davey 1961). Inert aggregates are available in some stone mines, streams, and seas, but pozzolans are materials made up of active silicates and aluminates which enable the mortars and plasters to harden under water through a reaction with lime. Pozzolans can be grouped as natural and artificial (Lea 1940).

Natural pozzolans are generally of volcanic origin. Santorin earth, glassy rhyolite, zeolitic tuff, clay, and diatomaceous earth as natural pozzolans are some of the oldest construction materials. Pozzolans of volcanic origin are composed of reactive silicates and contain glassy and crystalline particles (Lea 1940). However, all volcanic ashes do not have a pozzolanic property and some of them can be used as inert aggregates (Lea 1940). Diatomaceous earth is mainly comprised of opal which is an amorphous form of hydrous silica (Lea 1940). Reactivity of opal with lime is derived from its amorphous character and its structure which allows pores to absorb alkali solutions into all parts of the aggregate. Therefore, amorphous silica contributes to the hydraulic properties of lime mortars (Diamond 1976).

Artificial pozzolans are mainly obtained by heat treatment of natural materials such as clays, certain siliceous rocks, and fly-ash (Lea 1940). Crushed bricks, tiles and ceramic fragments are some of the artificial pozzolans. Lime mortars produced using artificial pozzolans were widely used in water-related structures such as bath, cistern, and aqueduct. Vitruvius stated that fired bricks should be used instead of sand in the first plaster layers of the walls which would be subjected to high humidity (Vitruvius 1960).

The most important contribution of the Romans to lime mortar technology was the use of pozzolans (Ward-Perkins 1994; Ward-Perkins 2003). The word pozzolan was derived from the Latin "*pulvis puteolanus*" meaning "Puteoli powder" and indicating volcanic deposits around Puteoli (modern Pozzuoli, a city near Naples, Italy) (Ward-Perkins 2003). The ancient treatises, among which Vitruvius's *De Architectura* was the most important, have described the use of pozzolans that bring hydraulic properties to lime mortars. Vitruvius defined pozzolan as a kind of powder formed as a result of natural causes and found in the neighborhood of Baiae near Mount Vesuvius and recommended its use in lime mortars to obtain hydraulic properties. In fact, the use of lime mortars and plasters in Greek buildings, as mentioned and in detail described by Vitruvius, indicates that the concrete probably was known in the pre-Roman Periods (Vitruvius 1960). However, in pre-Roman Periods, there was no hard evidence for the structural use of lime mortar (Artioli, Secco, and Addis 2019). In the Roman Period, adding pozzolanic

materials to the lime mortars was spread throughout the empire, including Europe, northern Africa, and Anatolia (Turkey) (Moropoulou, Bakolas, and Anagnostopoulou 2005).

The use of lime mortars containing natural pozzolans developed dramatically during the Roman Period and resulted in astonishing changes in construction techniques (Cowan 1977). This technology produced a strong and durable material called "Roman concrete" or "*opus caementicium*" (Cowan 1977). The new material Roman concrete (*opus caementicium*), which was made of lime and pozzolans, allowed to form a compact and monolithic building material (Ward-Perkins 1994; Adam 2005). In Anatolia (Asia Minor), the mortared rubble could be regarded as a simple substitute for Roman concrete (Waelkens 1989). The mortared rubble was typical to Asia Minor. Even though the mortared rubble was not completely a replacement for Roman concrete, it included considerable Western influence. In Italian Peninsula, this material often covered by dressed stones or bricks, and gave rise to different wall facing techniques such as *opus incertum, opus reticulatum* etc. (Adam 2005; MacDonald 1982; Waelkens 1989). In Anatolia, local wall construction techniques that can be grouped as walls comprised of mortared rubble core and facing, and walls comprised of mortared materials preferred (Uğurlu Sağın 2012). Thus, it can be said that Anatolia was not the only recipient in this process, but also it adapted Roman influences to local traditions and locally available building material (Waelkens 1989; Yegül and Favro 2019).

The previous research on Roman lime mortars figured out that the type of mortar can be varied according to the function of structures (Ontiveros-Ortega, Rodríguez-Gutiérrez, and Navarro 2016; Leone et al. 2016; Velosa et al. 2007; Ergenç and Fort 2019). Besides *opus caementicium* mortars, *opus signinum* or *cocciopesto* mortars produced by lime and crushed bricks/tiles/ceramic fragments, were mainly used for water-bearing and hydraulic structures. These reddish color mortars can increase impermeability and hydraulicity.

Roman concrete technology was more efficient than the traditional ones in terms of durability, long-term performance, setting underwater, the construction of the vaults and domes, and shortening the construction time. When the construction time for the domes of the most famous monuments compared, domes of Pantheon, Rome, and Ste-Sophia, Istanbul made of concrete were built within 5-7 years, but others lasted several decades (Rasch 1985) (Table 1).

Using lime mortars in constructions had been continued until the invention of modern cement, though in careless preparation made the mortars low quality and degradable in many cases (Artioli, Secco, and Addis 2019). After the invention of modern cement, the manuals still suggested the use of traditional materials, but after explaining the details about their right use and composition to the professionals (Baronio and Binda 1997; Moropoulou, Bakolas, and Anagnostopoulou 2005).

Table 1. Construction time for the domes.
(Source: Rasch 1985)

Monument (location)	Dome Diameter (m)	Date (AD)	Time (years)	Material
Pantheon (Rome)	43.3	118-125	7	concrete
Ste-Sophia (Istanbul)	32.6	532-537	5	concrete
St-Peter (Rome)	42	1400-1564	>50	stone
Cathedral (Florence)	42.2	1420-1434	14	tiles+concrete
St-Paul (London)	30.8	1675-1710	35	stone
Pantheon (Paris)	21	1755-1792	37	stone

Today, ancient structures with lime-based mortars from the Roman Period can be found in archaeological sites. In order to decide on appropriate interventions for these structures, the characterization of a lime mortar is an essential step in the conservation plan. Documentation of mortars related to the Roman Period and required research must be done before all sorts of intervention.

1.1. Literature Review

Roman lime mortars have been a broad range of research area mainly composed of characterization, local raw material sources, and repair mortars studies. Starting with the second half of the 20th century, characterization of Roman lime mortars has gained importance for cultural heritage. However, in the last decade, new methodologies on the characterization, test methods, dating of archeological sites, durability, consolidation,

design repair mortars with different additives and nanotechnology could be regarded as the major research topics.

Existing studies regarding characterization can be classified into three groups according to the location of case areas: Anatolia (Turkey) as a province of the Roman Empire, Italy as a center of the Roman Empire and the other regions of the Roman Empire particularly located in Europe (Spain, Greece, Portugal, Serbia, etc.) (Figure 1). Previous research has focused mainly on archeological sites in Italy which was the center of the Roman Empire. However, despite its cultural importance, a limited number of studies have been conducted on Roman lime mortars used in Anatolia (Figure 2).
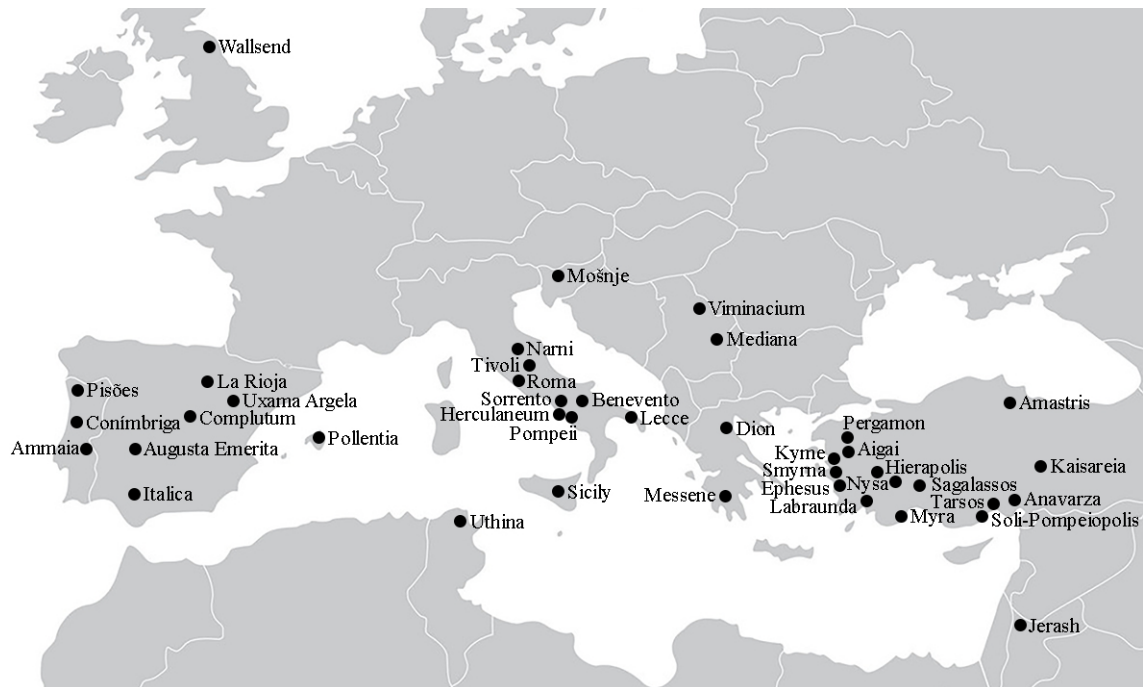
Figure 1. Roman cities studied in literature review.

1.1.1. Anatolia (Turkey)

In Anatolia, the determination of Roman lime mortar characteristics became an important research subject at the end of the 1990s, parallel to the studies conducted in Europe. The properties of lime mortars belonging to archaeological sites in Anatolia were investigated in the following studies: Roman buildings in Sagalassos (Degryse, Elsen, and Waelkens 2002), terrace houses in Ephesus (Kuleli 2005), Serapis Temple in

6

Pergamon (Aslan Özkaya and Böke 2009), bridge and castle in Kaisareia (Kozlu 2010), theatre, house and seashore buildings in Kyme (Miriello et al. 2011, 2015), ancient harbor in Soli-Pompeiopolis (Stanislao et al. 2011), many types of buildings in Aigai and Nysa (Uğurlu Sağın 2012), in Tarsos and Anavarza (Polat Pekmezci 2012) and Hierapolis (De Luca 2014), ancient harbor in Myra (Oğuz et al. 2015), a basilica in Amastris (Kurugöl and Güleç 2015), many types of buildings in Nysa (Ergenç, Fort, and Öztaner 2016), bouleuterion in Smyrna (Felekoğlu et al. 2016) and many types of buildings in Labraunda (Ergenç et al. 2019) (Figure 2). The brief information on these studies was given in this section.
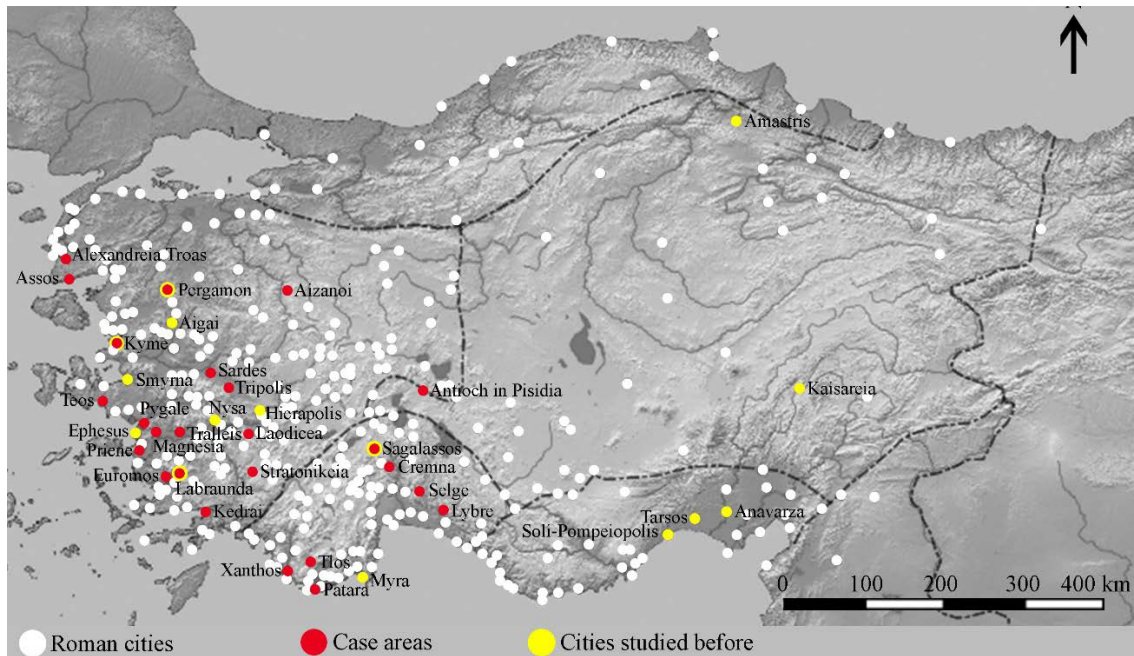
Figure 2. Roman cities studied before and case areas in Anatolia.
(Source: Willet 2020)

Sagalassos: Characteristics of Roman lime mortars used in structures such as water-related structures and tomb in Sagalassos were investigated to produce repair mortars compatible with the existing ones (Degryse, Elsen, and Waelkens 2002). The Roman mortars were composed of lime and pozzolanic aggregates. Lime/aggregate ratios were between 1/3-2/3 by weight (Table 2). Aggregates greater than 1 mm constituted the largest fraction of aggregates in the mortars (Table 2). They had submicroscopic crystal structures and a glass phase, and consisted of plagioclase, alkali-feldspar, augite,

7

diopside, biotite, and amphibole minerals (Table 17). The mortar matrices were composed of sanidine, anorthite, and amorphous glass (Table 24). The study concluded that the proposed repair mortar, a mix of lime and volcanic aggregates, had similar composition to the original Roman lime mortars and showed high durability (Degryse, Elsen, and Waelkens 2002).

Ephesus: Roman lime mortars found in terrace houses of Ephesus were studied to investigate physical, mechanical, and raw material characteristics of mortars and to evaluate the construction periods (Kuleli 2005). The density and porosity values of mortars were between 1.3-1.9 g/cm^3 and 24-45%, by volume, respectively (Table 2). The lime/aggregate ratios were between 1/1-4/1 by weight (Table 2). Aggregates coarser than 1 mm were determined as the largest fraction (Table 2). The aggregates consisted of quartz, muscovite, mica, feldspar, epidote, opal-CT, amphibole, serpantine, schist, mica schist , and albite schist (Table 17). The lime lumps were mainly composed of calcium oxide (Table 8). The mortars were hydraulic due to the use of pozzolanic amorphous silica (Table 2). Their modulus of elasticity values were between 524-2401 MPa (Table 9). The lime lumps were comprised of micritic calcite crystals. The study revealed that mortars had similar characteristics that may be the result of traditional construction technology for the Roman Period in Ephesus (Kuleli 2005).

Pergamon: Properties of mortars used in the Serapis Temple were defined to describe the characteristics of the intervention materials (Aslan Özkaya and Böke 2009). The mortars were composed of lime and pozzolanic aggregates. The lime/aggregate ratios of mortars were 1/4 by weight (Table 2). The aggregates greater than 1 mm constituted the largest fraction of the total aggregates (Table 2). The density and porosity values of mortars were 1.50 g/cm^3 and between 34-38%, by volume, respectively (Table 2). The fine aggregates were composed of quartz, albite, K-feldspar, and amorphous minerals (Table 17). The fine matrices were comprised of quartz and carbonated lime (Table 24). Carbonated lime was mainly composed of calcium oxide. Fine aggregates consisted of high amounts of SiO_2, Al_2O_3, and Fe_2O_3, and low amounts of Na_2O_3, MgO, K_2O, and TiO_2 (Table 6). The mortars were hydraulic due to the use of pozzolanic amorphous silica (Table 2). Gel-like formations composed of calcium, silicon, and aluminum were determined in the mortar matrices. Compressive strengths and modulus of elasticity of mortars were 6.6 MPa and 630.6 MPa, respectively (Table 9). As a result, mortars were stiff, compact, and hydraulic due to using pozzolanic aggregates (Aslan Özkaya and Böke 2009).

Kaisareia: Mortars of Roman bridge and castle in Kaisareia were investigated to design the recipes of the repair mortars for the conservation works (Kozlu 2010). The density and porosity values were determined between 1.2-1.7 g/cm^3 and 29-54%, by volume, respectively (Table 2). The lime/aggregate ratios were between 1/2-1/6 by weight (Table 2). The aggregates greater than 8 mm constituted half of the total aggregates in the mortars (Table 2). The fine aggregates were comprised of quartz, plagioclase, pyroxene, and opaque minerals (Table 17). The mortars were hydraulic but not pozzolanic (Table 2). Compressive strengths of mortars were between 5.3-9.70 MPa (Table 9). The study concluded that Roman mortars were durable and hydraulic due to the use of pozzolanic aggregates and produced repair mortars were compatible with the original ones (Kozlu 2010).

Kyme: Characteristics of Roman mortars used in theatre and house in Kyme were studied to understand the compositional differences within mortars of the same historical period (Miriello et al. 2011). Lime/aggregate ratios of mortars were between 1/7-1/2 by weight (Table 2). The aggregates were composed of calcite, quartz, anorthite, goethite, muscovite, chlorite, albite, biotite, vaterite, heulandite, and opaque minerals (Table 17). The mortars were comprised of calcite, quartz, anorthite, goethite, muscovite, chlorite, albite, and vaterite (Table 23). The fine matrices consisted of high amounts of SiO_2, CaO, Al_2O_3, MgO, and Fe_2O_3 and, low amounts of Na_2O_3, K_2O, and P_2O_5 (Table 5). The fine aggregates included high amounts of SiO_2, CaO, Al_2O_3, Fe_2O_3, MgO, Na_2O_3, and K_2O, and low amounts of TiO_2, P_2O_5, and MnO (Table 6). The mortars were composed of high amounts of SiO_2, CaO, Al_2O_3, MgO, and Fe_2O_3, and low amounts of Na_2O_3, K_2O, TiO_2, P_2O_5, and MnO (Table 7). Lime lumps mainly consisted of calcium oxide (Table 8). Volcanic aggregates presented the andesite, dacite, rhyolite, trachyandesite, and trachydacite fragments on the TAS diagram (Figure 66). The mortars were found as hydraulic, but lime lumps were non-hydraulic. The study revealed the use of *cocciopesto* as a pozzolanic additive made the mortars hydraulic and more durable (Miriello et al. 2011).

Soli-Pompeiopolis: Properties of ancient seawater concrete from the Roman harbor of Soli-Pompeiopolis were investigated to find out the extraordinary durability of ancient concretes in the marine environment (Stanislao et al. 2011). The aggregates were comprised of quartz, mica, sanidine, phillipsite, halite, chabazite, and smectite (Table 17). The mortar matrices were composed of calcite, tobermorite, and ettringite (Table 24). The long curing time in the marine environment was probably found as the key-factor of the

formation of tobermorite from gel-like CSAH at ordinary temperatures. The study concluded that the Romans produced mortars by using coarse tuff aggregate, lime hydrated in seawater, and pozzolanic volcanic fine sand (Stanislao et al. 2011).

Aigai and Nysa: Characteristics of mortars used in theatre, agora, bath, stadium, macellum, bouleuterion, temple, library, water basin, bridge, and cistern in Aigai and Nysa were determined to investigate the technology of Roman lime mortars (Uğurlu Sağın 2012). The density and porosity values were between 1.1-1.9 g/cm^3 and 24-55%, by volume, respectively (Table 2). The lime/aggregate ratios were between 1/5-4/5 by weight (Table 2). The aggregates greater than 1 mm constituted the major fraction in the mortars (Table 2). The fine aggregates were composed of quartz, albite, anorthite, muscovite, and phillipsite (Table 17). The mortar matrices were comprised of calcite, quartz, albite, anorthite, and muscovite (Table 24). The mortar matrices consisted of high amounts of SiO_2, CaO, and Al_2O_3, and low amounts of Fe_2O_3, MgO, Na_2O_3 and TiO_2 (Table 5). The fine aggregates included high amounts of SiO_2, Al_2O_3 and Fe_2O_3, and low amounts of MgO, CaO, Na_2O_3, K_2O, and TiO_2 (Table 6). Lime lumps were composed of mainly calcium oxide (Table 8). Lime lumps of mortars can be regarded as non-hydraulic, but mortars were hydraulic due to the use of pozzolanic aggregates (Table 2). Needle-like formations were found in binders, and irregular morphology was observed within aggregates. Results indicated that the properties of Roman lime mortars in Anatolia and Central Roman Empire were similar and mortars were hydraulic due to the use of pozzolans (Uğurlu Sağın 2012).

Anavarza and Tarsos: Characterization of mortars found in a bath, road, gate, temple, and arch structures in Anavarza and Tarsos was carried out to design compatible repair mortars (Polat Pekmezci 2012). The density and porosity values of mortars were found between 1.1-2.0 g/cm^3 and 6-52%, by volume, respectively (Table 2). The lime/aggregate ratios of mortars were between 1/3-1/1 by weight (Table 2). The aggregates greater than 1 mm were the major fragments in the mortars (Table 2). The aggregates were composed of quartz, feldspar, and opaque minerals (Table 17). The mortar matrices included calcite, quartz, gypsum, muscovite, and mica (Table 24). The mortar matrices and aggregates of the mortars consisted of high amounts of SiO_2, CaO, Al_2O_3, MgO, and Fe_2O_3, and low amounts of Na_2O_3, K_2O, and TiO_2 (Table 5-6). The mortars were weakly hydraulic (Table 2). Their compressive strength values were between 3-5 MPa (Table 9). The study concluded that most of the samples were non-hydraulic lime mortars with sand aggregates. The physical and mechanical properties of

the repair mortars were compatible values with the original samples (Polat Pekmezci 2012).

Hierapolis: Roman mortars and plasters used in a door, temple, stoa, nymphaeum, and sanctuary buildings in Hierapolis were characterized to provide more information about the production technology of the Romans (De Luca 2014). The aggregates were mainly composed of travertine, marble, phyllite, quartzite, and bioclasts. The mortars were hydraulic due to the use of pozzolanic additives. Results indicated a great difference between the groups of mortar and plaster of the same period (De Luca 2014).

Myra: Roman mortars found in Granariumin, Myra were investigated to understand the characteristics of mortars (Oğuz, Türker, and Koçkal 2015). The density and porosity values were between 1.5-1.8 g/cm^3 and 29-40%, by volume, respectively (Table 2). The lime/aggregate ratios were between 1/9-1/3 by weight (Table 2). The aggregates coarser than 1 mm constituted the major fraction of aggregates in the mortars (Table 2). The fine matrices were composed of calcite, quartz, and dolomite (Table 24). The mortars were hydraulic, and almost half of the mortars were pozzolanic (Table 2). The compressive strength values of mortars were between 3.1-8.1 MPa (Table 9). The study concluded that most of the analyzed Roman mortars were hydraulic due to the using pozzolanic aggregates, and properties of mortars were almost similar to the other sites (Oğuz, Türker, and Koçkal 2015).

Amastris: Roman lime mortars from the basilica in Amastris were characterized to obtain information about their composition (Kurugöl and Güleç 2015). The density and porosity values of mortars were between 1.6-1.8 g/cm^3 and 26-33 %, by volume, respectively (Table 2). The lime/aggregate ratios were between 1/2-1/1 by weight (Table 2). The aggregates were composed of quartz and feldspar (Table 17). The mortars included calcite, quartz, sanidine, muscovite, biotite, plagioclase, feldspar, and chlorite minerals (Table 23). All mortars can be classified as moderately or highly hydraulic due to the use of pozzolanic aggregates (Table 2). Their compressive strength, flexural strength, and modulus of elasticity values were between 4.5-8.9 MPa, 2.5-4.7 MPa, and 8300-13500 MPa, respectively (Table 9). Results revealed that Roman mortars were mainly composed of slaked non-hydraulic lime and crushed andesite fragments. They were hydraulic due to the addition of volcanic rock (Kurugöl and Güleç 2015).

Kyme: Roman mortars used many buildings in Kyme were investigated to have information of properties of mortars (Miriello et al. 2015). The lime/aggregate ratios were between 1/2-2/1 by weight (Table 2). The aggregates were composed of calcite, quartz,

plagioclase, orthoclase, muscovite, amphibole, biotite, pyroxene, chlorite, and opaque minerals (Table 17). The fine matrices consisted of calcite, quartz, chlorite, dolomite, mica, plagioclase, halite, and heulandite (Table 24). The fine matrices included high amounts of SiO_2, CaO, Al_2O_3, MgO and Fe_2O_3, and low amounts of Na_2O_3 and K_2O (Table 5). The study indicated that the mortars were comprised of aerial lime which became hydraulic lime by the addition of ceramic fragments and the non-intentional presence of volcanic rock fragments (Miriello et al. 2015).

Nysa: Characteristics of Roman mortars collected from theatre, gymnasium, library, gerontikon, basilica, stadium, water structures, and agora road in Nysa were defined in order to investigate the technology of mortars (Ergenç, Fort, and Öztaner 2016). The mortars were composed of highly porous un/carbonated lime binder and pozzolanic aggregates (Table 2). The mortars were comprised of calcite, quartz, albite, anorthite, plagioclase, muscovite, biotite, pyroxene, and garnet (Table 23). The mortars were hydraulic due to the use of pozzolanic aggregates (Table 2). The study concluded that the Roman used mica and argillaceous aggregates for improving hydraulicity and pozzolanicity, and ceramics for improving mechanical quality (Ergenç, Fort, and Öztaner 2016).

Smyrna: Roman lime plaster and mortar used in bridge, tunnel, and agora road in Smyrna were investigated to understand the characteristics of mortars (Felekoğlu et al. 2016). The density values were between 1.29-1.82 g/cm^3 (Table 2). The aggregates greater than 1 mm constituted the half of total aggregates (Table 2). The aggregates were comprised of quartz, biotite, and feldspar (Table 17). The fine matrices were composed of calcite and quartz (Table 24). Mortars showed homogeneous texture with rock fragments such as sandstone, metasandstone, quartz schist, quartzite, and brick fragments. Their compressive strength values were between 3.2-4.5 MPa (Table 9). Results showed that Roman mortars had a compact and homogeneous matrix structure that gave a high compressive strength due to the presence of crushed brick particles (Felekoğlu et al. 2016).

Labraunda: Characteristics of Roman mortars found in Androns, hypostile, baths, and pool structures in Labraunda were studied to understand the advantage of the analytical methods (Ergenç et al. 2019). The fine matrices were composed of calcite, silicates, and magnesite (Table 5). The mortars were comprised of illite, quartz, or montmorillonite. The mortars revealed highly angular augen gneiss, mica schist, and marble rock fragments. The mortars consisted of high amounts of SiO_2, low amounts of Al_2O_3, CaO, MgO, and Fe_2O_3 (Table 7). The study indicated the efficiency of analytical

characterization methods. Analyzed mortars were rich in ceramic fragments and they had CSH gels and fibrous crystals due to the pozzolanic reactions (Ergenç et al. 2019).

1.1.2. Italy

In Italy, the characterization and conservation of Roman lime mortars have been widely studied up to now (Figure 1). Studies were carried out on characteristics of lime mortars taken from a villa in Sorrento (Benedetti et al. 2004), Colosseum and cistern in Rome (Silva et al. 2005), catacombs in Rome (Sánchez-Moral et al. 2005), water-related buildings in Sicily (Rizzo et al. 2008), Markets of Trajan in Rome (Jackson et al. 2009), a house in Pompeii (Miriello et al. 2010), Theatre of Marcellus in Rome (Jackson et al. 2011), bridge in Narni (Cantisani et al. 2002; Drdácký et al. 2013), a house in Herculaneum (Leone et al. 2016), palace and amphitheater in Lecce (Gulotta et al. 2016), baths in Tivoli (Columbu et al. 2017), theatre and arch in Benevento (Izzo et al. 2018), and theatre in Tivoli (Columbu et al. 2018).

Sorrento: The mortars found in a Roman villa in Sorrento were studied to define the characteristics of mortars (Benedetti et al. 2004). The lime/aggregate ratios were between 1/2-2/1 by weight (Table 3). The fraction between 0.1 mm and 0.5 mm was the major fraction among the total of the aggregates (Table 3). The fine aggregates were comprised of calcite, quartz, diopside, sanidine, dolomite, biotite, hematite, and serandite (Table 18). The mortars were composed of calcite, quartz, sanidine, muscovite, hematite, diopside, analcime, periclase, labradorite, pyrope, aragonite, and graphite (Table 23). They concluded that volcanic materials were abundant in the mortars and showing the lava material was used not only to pave the roads but also for structures (Benedetti et al. 2004).

Rome (Colosseum): Characterization of mortars from the Colosseum and a cistern in Rome was carried out to compare the mortars from different structures (Silva et al. 2005). The mortars were composed of lime and pozzolanic aggregates. The fine matrices were comprised of calcite, aluminum, and siliceous materials such as diatoms as pozzolanic material. The mortars were hydraulic due to the use of pozzolanic aggregates (Table 3). Calcite crystals were found within the mortars. The spaces between aggregates were filled by calcite crystals. The crystals were covered by small prismatic particles composed of silicon. The study indicated that cistern mortar was high-quality pozzolanic

material, but Colosseum mortar was a lower quality mortar with a different lime/aggregate ratio. The mortar of the Colosseum was mainly calcareous lime, while the mortar of the cistern was pozzolanic siliceous material (Silva et al. 2005).

   Rome (Catacombs): Lime mortars taken from catacombs in Rome were studied to have information on their characteristics (Sánchez-Moral et al. 2005). The porosity values were between 39-42% by volume (Table 3). The pore sizes were <100 μm for the mortars produced by natural pozzolanic aggregates. The lime/aggregate ratios of mortars were between 1/2-1/1 by weight (Table 3). The largest fraction of the aggregates was between 0.5-2 mm and 100-300 μm (Table 3). The mortars were composed of calcite, analcime, augite, phyllosilicate, feldspar, and quartz (Table 23). Mortars consisted of high amounts of SiO_2, CaO, Al_2O_3, Fe_2O_3, and MgO, and low amounts of Na_2O_3, K_2O, TiO_2, P_2O_5, and MnO (Table 7). They concluded that Roman builders used local aggregates with a high proportion of clay. In the aggregates, the high content in volcanic glass helped the chemical reactions around the aggregates. The aggregate/lime mixture showed a higher content of the binder in comparison to other studies (Sánchez-Moral et al. 2005).

   Sicily: Mortars used in water-related structures in Sicily were investigated to compare both the hydraulic properties and the textural characteristics of mortars (Rizzo et al. 2008). The porosity values of mortars were between 25-35% by volume (Table 3). The lime/ aggregate ratios were between 2/3-3/2 by weight (Table 3). The aggregates were comprised of calcite, magnesite, anorthite, anorthoclase, augite, quartz, halite, hematite, diopside, feldspar, pyroxene, orthoclase, plagioclase, clinopyroxene, olivine, enigmatite, arenite, and mica rocks (Table 18). The fine matrices included calcite, quartz, magnesite, anorthite, anorthoclase, dolomite, diopside, feldspar, and halite (Table 24). Results revealed that all mortars were highly hydraulic due to the pozzolanic characteristics of aggregates (Rizzo et al. 2008).

   Rome (Markets of Trajan): The mortars from Markets of Trajan in Rome were studied to assess the material characteristics of the concrete wall (Jackson et al. 2009). The density values were between 1.4-1.7 g/cm^3 (Table 3). The aggregates were comprised of quartz, sanidine, analcime, biotite, feldspar, and ignimbrite (Table 18). The fine matrices were composed of calcite, diopside, sanidine, leucite, analcime, and strätlingite (Table 24). The fine matrices included high amounts of SiO_2, CaO, Al_2O_3, MgO, and Fe_2O_3, and low amounts of Na_2O_3, K_2O, P_2O_5, TiO_2, and MnO (Table 5). The aggregates included high amounts of SiO_2, Al_2O_3, and Fe_2O_3, and low amounts of MgO, CaO, Na_2O_3, K_2O, MnO, P_2O_5, and TiO_2 (Table 6). Blade-like strätlingite crystals composed of calcium

aluminate hydrate were determined. Their compressive and tensile strength and modulus of elasticity values were between 2.00-6.97 MPa, 0.8-0.9 MPa, and 1750–9170 MPa, respectively (Table 9). They concluded that Roman builders used complex aggregate mixes to optimize the performance of the concretes. The strätlingite and CSH pozzolanic cementitious phases of the mortars were a key factor for the long-term durability of the concretes (Jackson et al. 2009).

Pompeii: The characterization of mortars from a villa in Pompeii was carried out to describe the compositions of *coccciopesto* and natural pozzolanic mortars (Miriello et al. 2010). The lime/aggregate ratios were between 1/2-1/1 by weight (Table 3). The mortars were comprised of calcite, quartz, anorthite, analcime, leucite, sanidine, augite, plagioclase, albite, tobermorite, goethite, cowlesite, wollastonite, phlogopite, sillimanite, zircon, ludwigite, CSH phases, montmorillonite, andradite, nepheline, and dypingite (Table 23). The mortars consisted of high amounts of SiO_2, CaO, and Al_2O_3, and low amounts of MgO, Fe_2O_3, Na_2O_3, K_2O, TiO_2, P_2O_5, and MnO (Table 7). The fine matrices included high amounts of SiO_2, CaO, Al_2O_3, MgO, and Fe_2O_3, and low amounts of Na_2O_3, K_2O and TiO_2 (Table 5). Basalt, basaltic andesite, tephrite, phonotephrite, tephriphonolite, phonolite, trachyte, trachyte-andesite, and basaltic trachyte-andesite fragments were identified on the TAS diagram (Figure 66). The study indicated that properties of the aggregate were compatible with pyroclastic deposits from the volcano Vesuvius. CSH phases in the binder were due to the pozzolanic hydration phenomena of hydrated lime with *cocciopesto* and natural pozzolans (Miriello et al. 2010).

Rome (Theatre of Marcellus): The mortars collected from the Theatre of Marcellus in Rome were investigated to understand the construction methods and materials of the theatre (Jackson et al. 2011). The density value of the mortar was 1.8 g/cm^3 (Table 3). The aggregates consisted of calcite, analcime, leucite, diopside and hematite (Table 18). The fine matrices were composed of calcite, analcime, leucite, diopside, vaterite, and strätlingite (Table 24). The fine matrices included high amounts of SiO_2, CaO, Al_2O_3, MgO, and Fe_2O_3, and low amounts of Na_2O_3, K_2O, TiO_2, P_2O_5, and MnO (Table 5). Blade-like strätlingite crystals were composed of calcium aluminate hydrate in the fine matrices. They concluded that the exploratory concrete masonry and the integration of these materials showed the highly skilled workmanship, work-site management, and technical supervision of Roman builders trained in the Republican era (Jackson et al. 2011).

Narni: Characteristics of mortars from a bridge in Narni were studied, particularly focusing on the mechanical behaviors of mortars (Cantisani et al. 2002; Drdácký et al. 2013). The density and porosity values were between 1.1-1.7 g/cm^3 and 31%, by volume, respectively (Table 3). The lime/aggregate ratios were between 1/3-1/2 by weight (Table 3). The distribution of aggregates was inhomogeneous due to larger amounts of the middle grain classes. The aggregates were comprised of quartz, pyroxene, sanidine, leucite, chert, travertine, tuff, and carbonatic rocks (Table 18). The fine matrices were composed of calcite and tobermorite (Table 24). The fine matrices consisted of high amount of SiO_2, CaO, Al_2O_3, and MgO, and low amount of Fe_2O_3, K_2O, Na_2O_3, TiO_2, P_2O_5, and MnO (Table 5). The lime lumps were comprised of a high amount of SiO_2 and CaO, and a low amount of Al_2O_3, MgO, Fe_2O_3, K_2O, Na_2O_3, P_2O_5, and MnO (Table 8). The mortars were hydraulic due to the presence of pozzolanic materials (Table 3). Their compressive strength and the bending strength values were between 1.8-4.7 MPa and 0.3-1.5 MPa, respectively (Table 9). The volcanic deposit can be classified as foidite on the TAS diagram. Results showed that Romans did not produce different compositions of mortars for the different load carrying capacity, but the strongest mortar was used and produced logically (Cantisani et al. 2002; Drdácký et al. 2013).

Herculaneum: Roman mortars collected from several houses in Herculaneum were investigated to increase the knowledge of the use of ancient mortars (Leone et al. 2016). The porosity values of most mortars were lower than 15% by volume (Table 3). The lime/aggregate ratios were between 2/1-5/1 by weight (Table 3). The minimum and maximum sizes of aggregates were 0.05-0.25 mm and 0.3-12.5 mm, respectively (Table 3). The aggregates were composed of calcite, quartz, sanidine, pyroxene, plagioclase, leucite, muscovite, biotite, tephrite, pumice, trachyte, glassy slags, calcareous grains, iron oxides, zeolites, chamotte, shell, flint, microcline, bricks, and ceramics (Table 18). As a result, mortars were found as hydraulic due to using a high amount of pozzolanic material (Leone et al. 2016).

Lecce: Characterization of mortars found in the palace and amphitheater in Lecce was carried out to interpret the Roman mortars (Gulotta et al. 2016). The mortars were composed of calcium, iron, sulfur, mercury, and copper. The mortars consisted of calcite, quartz and feldspar (Table 23). The fine matrices were comprised of an aerial lime and the aggregates, including quartz-siliceous sand, feldspar, and crushed bricks. Lime was mainly composed of calcium oxide. They concluded that there were common properties

in the preparation of mortars in terms of the presence of an aerial lime with selected or heterogeneous aggregates (Gulotta et al. 2016).

Tivoli: Roman mortars from baths in Tivoli were studied to characterize the mortars (Columbu et al. 2017). The density and porosity values were between 1.2-1.5 g/cm^3 and 34-52%, by volume, respectively (Table 3). Most of the analyzed mortars presented a poorly sorted particle size distribution. The lime/aggregate ratios were between 1/5-1/3 by volume (Table 3). The aggregates were composed of scoria, leucite, *cocciopesto,* and marble. The aggregates included quartz, leucite, mica, muscovite, leucite, feldspar, clinopyroxenes, and opaque minerals (Table 18). The fine matrices were composed of calcite, quartz, gypsum, leucite, muscovite, ettringite, ridymite, cristobalite, and vuagnatite (Table 24). All mortars were found as hydraulic (Table 3). The compressive strength and the tensile strength of mortars were between 1.2-13.3 MPa and 0.10-1.19 MPa, respectively (Table 9). The point load test strength index was determined between 0.08-0.95 MPa (Table 9). The study proved a close relation between pozzolanic characteristics and the physical-mechanical properties of the mortars (Columbu et al. 2017).

Benevento: Properties of Roman mortars found in theatre and arch in Benevento were investigated to have information on the technology of mortar-based materials (Izzo et al. 2018). The lime/aggregate ratios were between 1/1-3/1 by volume (Table 3). The aggregates were composed of calcite, quartz, alkali feldspar, diopside, plagioclase, leucite, *cocciopesto,* olivine, anisotropic, isotropic, microcrystalline, cryptocrystalline, sedimentary lithics, igneous lithics, and charcoal fragments (Table 18). The fine matrices included pure carbonate phases, silicon, aluminum, and iron. The mortars were comprised of calcite, quartz, gypsum and/or nitrates. Mortars were hydraulic due to the use of pozzolanic aggregates generally formed by pumices and scoriae (Table 3). Volcanic lithics have chemical compositions ranging from phonotephrite to phonolite/trachyphonolite (Figure 66). Results indicated three types of mortars: lime-based pozzolanic mortar, hydraulic mortar, and highly hydraulic mortar. A hydraulic mortar was due to the occurrence of natural pozzolanic admixture in air-hardening lime and highly hydraulic was a consequence of the concomitant effect of a pozzolana-based aggregate and a binder deriving from a marly-limestone–like stone (Izzo et al. 2018).

Tivoli (Maritime Theatre): Roman mortars in Tivoli were studied to improve the knowledge of the constructive technologies of the Maritime Theatre (Columbu et al. 2018). The density and porosity values were between 1.2-1.81 g/cm^3 and 30-48 %, by volume, respectively (Table 3). The lime/aggregate ratios were between 1/5-1/1 by

weight (Table 3). The aggregates greater than 1 mm constituted the largest fraction of aggregates in the mortars (Table 3). The aggregates were composed of volcanic rocks, crystal clasts, *cocciopesto,* and rare marble fragments. The volcanic aggregate consisted of leucitic basalt scoria and leucites. The aggregates were composed of quartz, leucite, biotite, hematite, plagioclase, green hornblende, clinopyroxene, and opaque minerals (Table 18). They concluded that the ancient theatre was built using various kinds of brick, pyroclastic rocks, and other ornamental stones with hydraulic and lime mortars (Columbu et al. 2018).

1.1.3. Other Countries

A number of studies that were particularly in Spain have been determined on Roman lime mortars outside of Italy and Turkey (Figure 1). These studies can be given as follows: cistern in Uthina, Tunisia (Farci et al. 2005), forum and house in Pollentia, Spain (Genestar, Pons, and Más 2006), heroon in Messene, Greece (Zamba et al. 2007), bath in Conímbriga, Portugal (Velosa et al. 2007), villa in Augusta Emerita, Spain (Franquelo et al. 2008; Robador, Perez-Rodriguez, and Duran 2010), many different buildings in La Rioja, Spain (Pavía and Caro 2008), villa in Mošnje, Slovenia (Kramar et al. 2011), many buildings in Jerash, Jordan (Yaseen et al. 2013), odeion in Dion, Greece (Papayianni, Pachta, and Stefanidou 2013), many buildings in Ammaia, Portugal (Cardoso et al. 2014), villa in Mediana, Serbia (Topličić-Ćurčić et al. 2014), amphitheater in Viminacium, Serbia (Nikolić et al. 2016), many buildings in Italica, Spain (Ontiveros-Ortega, Rodríguez-Gutiérrez, and Navarro 2016), bath complex in Uxama Argela, Spain (Olazabal et al. 2019), many buildings in Pisões, Portugal (Borsoi et al. 2019) and Complutum, Spain (Ergenç and Fort 2019), and a bath in Wallsend, United Kingdom (Laycock et al. 2019).

Uthina, Tunisia: The mortars used in cisterns in Uthina were investigated to obtain information about their characteristics (Farci, Floris, and Meloni 2005). The density and porosity values were between 1.5-1.7 g/cm^3 and 24-44%, by volume, respectively (Table 4). The pore sizes of mortars were found as <0.01-30 μm (Table 4). The aggregates were composed of calcite, quartz, feldspar, sanidine, plagioclase, biotite, and gehlenite (Table 19). The study concluded that mortars were composed of lime-based binder medium, and pottery sherds and pozzolana as aggregates (Farci, Floris, and Meloni 2005).

Pollentia, Spain: Properties of Roman mortars from forum and house buildings in Pollentia were studied to identify the construction mode of the mortars (Genestar, Pons, and Más 2006). A considerable number of fragments with a diameter greater than 4 mm could be found in some mortars, and the finest particle size containing the binder represented less than 10% of the whole sample in all the samples analyzed (Table 4). The fine matrices consisted of calcite and quartz (Table 24). Mortars were hydraulic due to the use of pozzolanic aggregates (Table 4). As a result, they grouped the studied mortars into four: artificial pozzolanic mortars, hydraulic lime mortars with aggregates of siliceous and calcareous nature, and non-hydraulic ones (Genestar, Pons, and Más 2006).

Messene, Greece: Characteristics of Roman mortars collected from the Heroon Podium in Messene were defined to understand the nature of filling material used for the construction (Zamba et al. 2007). The aggregates were composed of mostly massive and porous sandy limestone angular fragments. The aggregates consisted of calcite and quartz (Table 19). Lime lumps were observed, and one group of lumps was composed of solely calcite and traces of quartz grains, and the other one included additionally CaO–SiO_2-rich compounds, typical of hydraulic lime. Results showed that the mortar used for the filling material was semi-hydraulic lime derived from the pure limestone and siliceous limestone fragments, possibly the waste material from the ancient walls (Zamba et al. 2007).

Conímbriga, Portugal: Mortars used in Roman baths in Conímbriga were investigated to produce a repair mortar (Velosa et al. 2007). The lime/aggregate ratios were about 1/4 by weight (Table 4). The aggregates greater than 1 mm constituted the largest fraction of aggregates in the mortars (Table 4). The mortars were composed of calcite, quartz, feldspar, dolomite, magnesite, pyrite, and phyllosilicates (Table 23). The mortars included high amounts of SiO_2 and CaO, and low amounts of Al_2O_3, MgO, Fe_2O_3, K_2O Na_2O_3, TiO_2, and MnO (Table 7). Calcite crystals were detected inside the pores of brick aggregates. The study concluded that mortars were produced using lime, quartzitic sand, and crushed ceramic particles (Velosa et al. 2007).

Augusta Emerita, Spain (Mithraeum House): Characterization of Roman mortars from Mithraeum house in Augusta Emerita was carried out to understand the behavior of ceramics as aggregates (Franquelo et al. 2008). The lime/aggregate ratios were between 1/2-1/1 by weight (Table 4). The brick aggregates were composed of calcite, quartz, anorthite, hematite, mica, and muscovite (Table 19). The mortars consisted of calcite, quartz, mica, and anorthite (Table 23). They concluded that the

carbonates and the new phases formed inside the pores were responsible for the formation of new phases during the heating of the ceramics (Franquelo et al. 2008).

La Rioja, Spain: The mortars used in the city wall, bridge, road, bath, thermal complex, and living space in La Rioja were investigated to provide fundamental information on mortar technology (Pavía and Caro 2008). The mortars were hydraulic due to the addition of ceramics. Lime lumps were detected as fine-grained and did not show a low shrinkage that can be attributed to the soft burn of raw limestone. Reaction and strong adhesion between binder and aggregates were detected. Results showed that the presence of ceramics can be partially responsible for better quality and performance of the Roman mortars (Pavía and Caro 2008).

Augusta Emerita, Spain: Roman mortars collected from the water-related structures in Augusta Emerita were studied to describe and characterize the hydraulic mortars (Robador, Perez-Rodriguez, and Duran 2010). The lime/aggregate ratios were about 1/3 by weight (Table 4). The major fraction of the aggregates was between 0.4-0.5 mm (Table 4). The aggregates were composed of quartz, anorthite, mica, feldspar, and hematite (Table 19). The fine matrices included calcite, quartz, anorthite, and mica (Table 24). The mortars consisted of high amounts of SiO_2 and CaO; and low amounts of Al_2O_3, Fe_2O_3, K_2O, MgO, Na_2O_3, and TiO_2 (Table 7). The carbonate particles were found in the pores of brick aggregates. Different formations composed of silicon, aluminum, and calcium representing the reaction between lime and silicate compounds were also observed inside the pores of aggregates. They concluded that the mortars, which were heterogeneous due to the presence of different calcite, composed of hydrated lime as a binder and siliceous sand and ceramic fragments as aggregates (Robador, Perez-Rodriguez, and Duran 2010).

Mošnje, Slovenia: Characterization of mortars from the bath complex of the Roman villa in Mošnje was carried out to identify the effect of the brick aggregates in the mortars (Kramar et al. 2011). The density and porosity values were between 1.2-2.0 g/cm^3 and 23-49%, by volume, respectively (Table 4). The lime/aggregate ratios were between 1/2-1/1 by weight (Table 4). The particle sizes of the aggregates varied between 0.02-14.9 mm (Table 4). The fine matrices were composed of high amounts of CaO, SiO_2, low amounts of Al_2O_3, MgO Na_2O_3, K_2O TiO_2, and P_2O_5 (Table 5). The aggregates consisted of a high amount of CaO and a low amount of SiO_2, Al_2O_3, MgO, Na_2O_3, K_2O, MnO, P_2O_5, and TiO_2 (Table 6). The aggregates included calcite, quartz, dolomite, and muscovite minerals (Table 19). The fine matrices were comprised of calcite, quartz,

dolomite, and muscovite (Table 24). The study revealed that the calcium carbonate rims around individual brick grains and the rim between brick aggregates and lime were observed. The mortars produced with a greater amount of brick aggregates showed a higher porosity but a lower average pore diameter (Kramar et al. 2011).

Jerash, Jordan: Roman mortars found in the arch, temple, piazza, and nymphaeum in Jerash were investigated to obtain information on their compositions (Yaseen et al. 2013). The mortars were composed of calcite, quartz, dolomite, gypsum, magnesite, biotite, amphibole, sulfide, and clay minerals (Table 23). The mortars included a high amount of CaO and SiO_2, and a low amount of Al_2O_3, MgO, Fe_2O_3 Na_2O_3, K_2O TiO_2, MnO, and P_2O_5 (Table 7). The aggregates were well embedded in the matrix. The areas of the surface and pores were filled with calcite crystals. They concluded that analyzed mortars composed of calcic lime and aggregates including crushed carbonate rocks (limestone), gypsum, and siliceous sand (Yaseen et al. 2013).

Dion, Greece: Characteristics of mortars from Roman Odeion in Dion were studied to determine the criteria for the selection of suitable repair mortars (Papayianni, Pachta, and Stefanidou 2013). The porosity values were between 8-12% by volume (Table 4). The lime/aggregate ratios were between 2/5-2/3 by weight (Table 4). The aggregates were of calcitic origin and their gradation varied from 0–16 mm (Table 4). The mortars were composed of a high amount of SiO_2, CaO, MgO, Al_2O_3, Fe_2O_3, and a low amount of Na_2O_3 and K_2O (Table 7). Their compressive strength values were between 2.1-4.8 MPa (Table 9). Results showed that lime and pozzolan kept as the main binders, and aggregates followed the one found in ancient mortars. Particle size distribution and binder/aggregate ratio were preserved according to the mortars' type (Papayianni, Pachta, and Stefanidou 2013).

Ammaia, Portugal: Roman mortars used in tower, residential area, macellum, peristylium, public bath building, temple, forum structures in Ammaia were studied in a multidisciplinary approach (Cardoso et al. 2014). The lime/aggregate ratios of mortars were between 1/6-1/2 by weight (Table 4). Major grain sizes of aggregates were between 0.5 mm and 1 mm (Table 4). The aggregates were composed of quartz, feldspar, muscovite, biotite, and amphibole (Table 19). The mortars consisted of calcite, quartz, feldspar, illite, chlorite, aragonite, kaolinite, amphibole, sepiolite, and cordierite (Table 23). As a result, the mortars were hydraulic. They were heterogeneous, composed of light-colored calcitic binders and various types of aggregates. The compositions of mortars varied depending on their function in the structure (Cardoso et al. 2014).

Mediana, Serbia: The mortars collected from the Roman residential building in Mediana were characterized to determine their properties (Topličić-Ćurčić et al. 2014). The density and porosity values of mortars were between 1.6-1.7 g/cm^3 and 31-34 %, by volume, respectively (Table 4). The mortars were composed of aggregates with grain size between 0.05 to 2 mm (Table 4). The mortars included calcite, quartz, dolomite, feldspar, mica, gypsum, vaterite, and clay materials (Table 23). The mortars consisted of a high amount of SiO_2 and CaO, and a low amount of MgO, Al_2O_3, Na_2O_3, P_2O_5, and SO_3 (Table 7). They concluded that the analyzed mortars were made of carbonate binder and the aggregate, including limestone, quartz, metarmorphite, and vulcanite (Topličić-Ćurčić et al. 2014).

Viminacium, Serbia: The mortars of the Roman amphitheater in Viminacium were investigated to provide information on their compositions (Nikolić et al. 2016). The density and porosity values were between 1.1-1.8 g/cm^3 and 24-47%, by volume, respectively (Table 4). The lime/aggregate ratios were between 2-4 by volume (Table 4). The largest fraction of aggregates was between 0-4 mm (Table 4). The aggregates were comprised of quartz, feldspar, mica, and pyroxene (Table 19). The mortars consisted of high amounts of SiO_2 and CaO, and low amounts of MgO, Al_2O_3, Fe_2O_3, Na_2O_3, and K_2O (Table 7). Their compressive strength values were between 2-5.3 MPa (Table 9). The study concluded that analyzed mortars were mixtures of a carbonate binder and fine natural aggregate which was assumed to be of a river origin. They were prepared in different ways according to their role in the structure, particularly for compressive strength (Nikolić et al. 2016).

Italica, Spain: Roman mortars used in tetrapylon, bath, and sewer in Italica were studied to understand their compositions (Ontiveros-Ortega, Rodríguez-Gutiérrez, and Navarro 2016). The density and porosity values were around 1.6 g/cm^3 and 32%, by volume, respectively (Table 4). The lime/aggregate ratios were between 1/4-1/2 (Table 4). The aggregates were generally sand-sized and well-sorted. The mortars were comprised of calcite, quartz, albite, feldspar K, mica, amphibole, dolomite, tobermorite, gypsum, and phyllosilicate (Table 19). The mortars included a high amount of SiO_2 and CaO, and a low amount of Al_2O_3, MgO, Fe_2O_3, K_2O Na_2O_3, TiO_2, P_2O_5, MnO, SO_3, and Cl (Table 7). They concluded that, in this area, Romans produced four types of lime-based mortar with different proportions of metamorphic, igneous, and sedimentary rock depending on the structural needs of the construction (Ontiveros-Ortega, Rodríguez-Gutiérrez, and Navarro 2016).

Uxama Argela, Spain: Roman mortars from the bath complex in Uxama Argela were investigated to obtain information on their characteristics (Olazabal et al. 2019). The lime/aggregate ratios were between 1/2-2/1 by weight (Table 4). The grain size of the aggregates was lower than 4 mm (Table 4). The fine matrices were composed of calcite, quartz, illite, kaolinite, and phyllosilicates (Table 24). The aggregates consisted of calcite, quartz, and K-feldspar (Table 19). The study concluded that analyzed mortars were composed of lime binder and sandy siliceous aggregates (Olazabal et al. 2019).

Pisões, Portugal: Characteristics of Roman mortars collected from the residential area, baths, dam, and mill in Pisões were defined to have information on the construction materials and techniques used in the Roman Period (Borsoi et al. 2019). The lime/aggregate ratios were 1/3 and 2/3 by weight (Table 4). The aggregates were greater than 1 mm (Table 4). The mortars were comprised of calcite, quartz, alkali feldspar, mica, kaolinite, chlorite, amphiboles, pyroxenes, and hematite (Table 23). The aggregates were composed of quartz, pyroxene, amphibole, feldspar, mica, schist, and basalt (Table 19). The mortars were hydraulic due to the use of pozzolanic aggregates (Table 4). The mortars had a compact microstructure with a high amount of ceramic materials. These materials provided alumina and silica to an alkaline environment, inducing reactions with the formation of CSH and/or CASH. The binder matrix was found as fully carbonated. They concluded that the mortars can be categorized as aerial lime mortars with siliceous aggregates, crushed ceramic-lime mortars, and lime mortars with natural pozzolanic aggregates (Borsoi et al. 2019).

Complutum, Spain: Properties of Roman mortars found in sewer and bath structures in Complutum were investigated by a multi-technical characterization (Ergenç and Fort 2019). The lime/aggregate ratios of mortars were between 1/2-1/1 by weight (Table 4). The aggregates greater than 1 mm constituted the largest fraction (Table 4). The mortars were composed of calcite, quartz, feldspar, biotite, muscovite, augite, pyroxene, plagioclase, mica, gypsum, portlandite, gehlenite, opaque minerals, and CSH phases (Table 23). The mortars consisted of a high amount of SiO_2, CaO and a low amount of Al_2O_3, MgO, Fe_2O_3, K_2O, Na_2O_3, TiO_2, P_2O_5 and MnO (Table 7). The mortars were hydraulic due to the use of pozzolanic aggregates (Table 4). Siliceous aggregates embedded into hexagonal rhombohedral calcite crystals were observed. There were amorphous gel forms, fibrous and needle-like CSH crystals. The study concluded that sub-rounded sand aggregates and limestones obtained from local sources were used in mortar production. Ceramic dust, fly ash, chamotte, and charcoal were the materials that

made the mortars hydraulic. Mortar samples without ceramics can also be accepted naturally hydraulic, and ceramics were probably produced in local workshops (Ergenç and Fort 2019).

Wallsend, United Kingdom: Characterization of mortars used in the baths and walls in Wallsend were studied to explore potential sources (Laycock et al. 2019). The lime/aggregate ratios were between 1/5-1/3 by weight (Table 4). The particle size of the aggregates ranged between 2-10 mm (Table 4). The mortars were composed of calcite, quartz, dolomite, anorthite, and kaolinite (Table 23). The aggregates consisted of quartz, plagioclase, K-feldspar, amphibole, pyroxene, biotite, muscovite, mica, chlorite, dolerite/basalt, and opaque minerals (Table 19). The mortars included high amounts of SiO_2 and CaO, and low amounts of Al_2O_3, MgO, Fe_2O_3, K_2O, Na_2O_3, TiO_2, P_2O_5, and SO_3 (Table 7). As a result, various sources were suggested for the quarried limestone and the aggregates, but Carboniferous limestone that was poorly sieved and contained charcoal was the most likely source for some mortars (Laycock et al. 2019).

1.2. Evaluation of Literature Review

Previous studies on lime mortars used in several Roman Period buildings in Turkey, Italy, Spain, Portugal, Serbia, Greece, Slovenia, United Kingdom, Jordan, and Tunisia, which were the provinces of the Roman Empire, were investigated to understand the technology of Roman lime mortars.

Based on these studies, the most common investigated properties were density and porosity values as a basic physical characteristic, lime/aggregate ratio and particle size distribution as raw material composition, mineralogical and chemical compositions of aggregate, lime, and fine mortar matrices (binder), hydraulic properties of binder and petrographic analysis of mortars. Reporting the presence of hydraulic formations (CSH and CAH) was also one of the primary objectives of the studies in order to understand the reaction between lime and fine aggregates (pozzolans). Besides all these, the least emphasized properties were identified as; pore size distribution of mortars, mineralogical and chemical compositions of lime lumps, hydraulic indexes, and microstructural properties of lime lumps, and pozzolanic activity and geochemical characteristics of fine aggregates. Moreover, existing research on Roman lime mortars used in Anatolia has

failed to explore geochemical characteristics of fine aggregates which deserves more research attention.

Based on the results given in the previous studies, Roman lime mortars can be described according to their following characteristics:

- Roman mortar compositions have generally varied according to the type of structure (water-related buildings, theatre, stadium, etc.) and type of their uses in the masonry structures (arches, vaults, domes, etc.)

- The mortars, produced with calcitic lime and natural pozzolans, called *opus caementicium* were mainly used as a coating, lining, or flooring.

- The mortars, produced with artificial pozzolans such as crushed pottery or ceramic fragments, called *opus signinum* or *cocciopesto* were generally used in water-related and hydraulic structures, as a plaster, paving, and supporting for mosaics and marble coverings.

- The majority of the mortars presented low density (1.2-1.9 g/cm^3) and high porosity (25-50%) (Table 2-4).

- The particle size distributions of aggregates were almost similar to each other, and the aggregates coarser than 1 mm constituted the largest fraction of the total aggregate in most cases (Table 2-4).

- The mortars were produced using lime and flat aggregates.

- Most of the mortars respected the ideal 1:2, 1:3, and 1:4 lime/aggregate ratios given in the historic sources written in the Roman Period by Vitruvius, Cato, and Plinius, whereas few of them presented broader lime/aggregate ratios (Table 2-4).

- Lime lumps, regarded as the main indicator of the lime used in mortar preparation, were classified as high calcium lime regarding the high content of CaO%.

- Raw material compositions of mortars were similar to each other in Kyme, Turkey; in Pompeii, Italy; in Dion, Greece; in Augusta Emerita, Italica and Complutum, Spain; in Conímbriga, Portugal; in Jerash, Jordan; In Viminacium and Mediana, Serbia; and in Wallsend, United Kingdom. Accordingly, it could be said that Roman lime mortars used in various regions were produced with similar raw materials. However, the small differences in raw material compositions could be regarded as the use of local raw material sources.

- The compressive strength values of the Roman lime mortars were found in the range of 2-13 MPa (Table 9).

- The composition of mortars played a significant role in mechanical properties. Therefore, the mortars were prepared in various types according to their role in the structure. Hydraulic lime mortars had higher mechanical strength than the non-hydraulic ones. Pozzolanic additives made the mortars more durable.

- Fine mortar matrices (binder) were composed of mainly calcite, quartz, feldspar, dolomite, muscovite, mica, diopside, anorthite, leucite minerals (Table 24). Having different types of minerals such as biotite, analcime, plagioclase, pyroxene, kaolinite, magnesite, tobermorite, goethite, leucite, and illite may be due to the use of volcanic origin aggregates (Table 24).

- The most common minerals identified in the composition of aggregates were quartz, feldspar, biotite, leucite, muscovite, mica, diopside, anorthite, and plagioclase minerals (Table 17-19).

- The binders consisted of mainly calcium and a minor amount of magnesium, silica, alumina, and iron.

- The aggregates were composed of mainly high amounts of SiO_2, moderate amounts of Al_2O_3 and Fe_2O_3, and low amounts of MgO, CaO, Na_2O_3, K_2O, MnO, P_2O_5, and TiO_2 (Table 6).

- Fine aggregates had mainly good pozzolanicity due to the use of volcanic ash as a pozzolan (Table 2-4).

- Binders of many mortars were hydraulic due to the use of pozzolans (Table 2-4).

- Carbonated lime was composed of mainly the small size of micritic crystals with needle-like or rod-like forms which could be attributed to the use of aged lime putty. Fine aggregates were well adhered to the lime.

In the literature on Roman lime mortars, there were a number of studies, but there was a lack of comprehensive comparative study according to locations. Roman Empire had a large influence both on Europe and Anatolia with construction techniques and building materials in architecture. Thus, it could be important to compare data from various archeological sites in terms of materials, production techniques, and so on if there would be a connection between Europe and Anatolia. In the present study, besides making an investigation in a wider area, the least examined characteristics of Roman mortars, particularly geochemical characteristics of fine aggregates, were also analyzed to understand the technology better.

Table 2. Properties of Roman lime mortars as a result of the previous studies in Turkey.

Case area (Reference)	BASIC PHYSICAL PROPERTIES		RAW MATERIAL COMPOSITIONS		HYDRAULIC PROPERTIES (TGA)			POZZOLANIC ACTIVITY
	Density (g/cm³)	Porosity (%)	Lim/Agg	Particle Size Distributions of Aggregates (%)	200-600 °C (H₂O %)	600-900 °C (CO₂ %)	CO₂/H₂O	Electrical Differences (mS/cm)
Sagalassos (Degryse, Elsen, and Waelkens 2002)	–	–	1/3-2/3	<4.75 mm 3.87, <4 mm 30.58, <2 mm 25.61, <1 mm 14.09, <500 μm 11.42, <250 μm 8.82, <125μm 5.64	–	–	–	–
Ephesus (Kuleli 2005)	1.3-1.9	24.9-45.2	1/1-4/1	the largest fraction: > 1 mm	–	–	–	0.45-3.93
Pergamon (Aslan Özkaya 2005; Özkaya and Böke 2009)	1.5	34-38	1/4	<1 mm 38, <500 μm 32, <250 μm 9, <125 μm 2, <53 μm 0.5	2.33	6.87	2.95	6.03-7.70
Kaisareia (Kozlu 2010)	1.2-1.7	29.4-54.9	1/2-1/6	<8 mm 50	3.79-6.99	6.84-12.61	1.21-2.50	0.06-0.29
Kyme (Miriello et al. 2011)	–	–	1/7-1/2	–		–	–	–
Aigai and Nysa (Uğurlu Sağın 2012)	1.1-1.9	24.9-55.5	1/5-4/5	>1 mm 11.2-65.1, 500 μm-1 mm 7.1-37.5, 250-500 μm 3.0-18.3, 125-250 μm 2.1-9.3, 53-125 μm 0.8-8.0, <53 μm 0.3-4.7	2.85-9.86	7.66-22.05	1.12-6.41	3.25-8.09
Tarsos and Anavarza (Polat Pekmezci 2012)	1.1-2.2	6-52	1/3-1/1	>8 mm 0.0-14.8, 4-8 mm 0.0-19.6, 2-4 mm 0.0-15.6, 1-2 mm 0.0-42.1, 500 μm-1 mm 0.0-14.6, 250-500 μm 0.0-55.5, 125-250 μm 0.7-37.7, <125 μm 9.6-64.3	–	–	–	–
Amastris (Kurugöl and Güleç 2015)	1.6-1.8	26.7-33.1	1/2-1/1	–	–	–	–	3.9-4.6 N/mm2
Myra (Oğuz et al. 2015)	1.5-1.8	29-40	1/3-1/9	4-8 mm 36, 2-4 mm 25, 1-2 mm 16, 500 μm-1 mm 10, 250-500 μm 8, 125-250 μm 4, <125 μm 1	2.17-3.63	30.71-34.99	10.0-16.0	0.04-0.49
Kyme (Miriello et al. 2015)	–	–	1/2-2/1	–	–	–	–	–
Smyrna (Felekoğlu et al. 2016)	1.3-1.8	–	–	4-8 mm 17, 2-4 mm 20, 1-2 mm 13, 500 μm-1 mm 12, 250-500 μm 6, 125-250 μm 5, 63-125 μm 3, <63 μm 3	–	–	–	–

TURKEY

Table 3. Properties of Roman lime mortars as a result of the previous studies in Italy.

Case area (Reference)	BASIC PHYSICAL PROPERTIES		RAW MATERIAL COMPOSITIONS		HYDRAULIC PROPERTIES (TGA)			POZZOLANIC ACTIVITY
	Density (g/cm³)	Porosity (%)	Lim/Agg	Particle Size Distributions of Aggregates (%)	200-600 °C (H₂O %)	600-900 °C (CO₂ %)	CO₂/H₂0	Electrical Differences (mS/cm)
Sorrento (*Benedetti et al. 2004*)	–	–	1/2-2/1	<0.1 mm 30, 0.1-0.5 mm 35, >0.5 mm Few	–	–	–	–
Rome (*Sánchez-Moral et al. 2005*)	–	39-42	1/2-1/1	the largest fraction: 0.5-2 mm, 100-300 μm	5.62-7.84	2.25 - 11.88	0.29-2.11	–
Sicily (*Rizzo et al. 2008*)	–	<15-35	2/3-3/2	–	1.6-8.4	11.0-40.2	1.8-6.6	–
Rome (*Jackson et al. 2009*)	1.4-1.7	–	–	–	–	–	–	–
Pompeii (*Miriello et al. 2010*)	–	–	1/2-1/1	–	–	–	–	–
Rome (*Jackson et al. 2011*)	1.80	–	–	–	–	–	–	–
Narni (*Cantisani et al. 2002; Drdácký et al. 2013*)	1.1-1.7	31	1/3-1/2	0.01-0.1 mm 30, 0.1-1 mm 12, 1-10 mm 33, 10-100 mm 3	4.2-6.6	11.4-22.2	1.9-5.3	–
Herculaneum (*Leone et al. 2015*)	–	<20-40>	2/1-5/1	min size: 0.05-0.25 mm max size: 0.3-12.5 mm	2.1-21.0	7.1-30.9	0.9-7.5	–
Tivoli (*Columbu et al. 2017*)	1.2-1.5	34.1-52.0	1/5-1/3	<6.3 mm 100, <4 mm 24-94, <2 mm 14-67, <1 mm 9-51, <500 μm 5-35, <250 μm 2-19, <125 μm 0.8-4.2	1.9-6.8	7.4-17.0	1.6-5.1	–
Benevento (*Izzo et al. 2018*)	–	–	1/1-3/1	–	–	–	–	–
Tivoli (*Columbu et al. 2018*)	1.2-1.8	30-48	1/5-1/1	4-8 mm 42-53, 2-4 mm 16-22, 1-2 mm 8-11, 00 μm-1 mm 6-12, 250-500 μm 5-9, 125-250 μm 4-5, 63-125 μm 2-4, <63 μm 1-2	–	–	–	–

ITALY

Table 4. Properties of Roman lime mortars as a result of the previous studies in other countries.

Case area (Reference)	BASIC PHYSICAL		RAW MATERIAL COMPOSITIONS		HYDRAULIC PROPERTIES (TGA)			POZZOLANIC ACTIVITY
	Density (g/cm³)	Porosity (%)	Bin/Agg	Particle Size Distributions of Aggregates (%)	200-600 °C (H$_2$O %)	600-900 °C (CO$_2$ %)	CO$_2$/H$_2$0	Electrical Differences (mS/cm)
OTHER COUNTRIES								
Uthina, Tunisia (*Farci et al. 2005*)	1.5-1.7	24.2-44.3	–	–	–	–	–	–
Conimbriga, Portugal (*Velosa et al. 2007*)	–	–	1/4	the largest fraction: >1 mm	–	–	–	–
Augusta Emerita, Spain (*Franquelo et al. 2008; Robador et al. 2010*)	–	–	1/2-1/1	1-2 mm 24.16, 0.595-1 mm 13.97, 0.420-0.595 mm 32.13, 0.32-0.42 mm 13.52	–	–	–	–
Mošnje, Slovenia (*Kramar et al. 2011*)	1.2-2.0	23.9-49.7	1/2-1/1	0.02-14.9 mm	–	–	–	–
Dion, Greece (*Papayianni et al. 2013*)	–	8.8-12.9	2/5-2/3	0-16 mm	–	–	–	–
Ammaia, Portugal (*Cardoso et al. 2014*)	–	–	1/6-1/2	the largest fraction: 0.5-1 mm	1.4-4.1	9.4-23.4	2.4-8.0	–
Mediana, Serbia (*Gordona et al. 2014*)	1.6-1.7	31.3-34.8	–	0.05-2 mm	–	–	–	–
Viminacium, Serbia (*Nikolić et al., 2016*)	1.1-1.8	24.7-47.1	2/1-4/1	the largest fraction: 0-4 mm	–	–	–	–
Italica, Spain (*Ontiveros-Ortega et al. 2016*)	1.6	32	1/4-1/2	–	–	–	–	–
Uxama Argela, Spain (*Alonso-Olazabal et al. 2019*)	–	–	1/2-2/1	<4 mm	–	–	–	–
Pisões, Portugal (*Borsoi et al. 2019*)	–	–	1/3-2/3	the largest fraction: >1 mm	0.3-4.4	0.2-20.1	2.5-5.5	–
Complutum, Spain (*Ergenç and Fort 2019*)	–	–	1/2-1/1	<2 mm 0-53, < 1-2 mm 4-36,< 0.5-1 mm 8-50,< 0.25-0.5 mm 9-44, < 0.063-0.25 mm 4-20, < 0.063 mm 0.4-5.5	1.5-6.7	2.8-37.6	1.7-11.13	–
Wallsend, United Kingdom (*Laycock et al. 2019*)	–	–	1/5-1/3	2-10 mm	–	–	–	–

Table 5. Chemical compositions of binders of Roman lime mortars as a result of the previous studies.

Case area (Reference)	Method	CHEMICAL COMPOSITIONS (%)									
		CaO	MgO	SiO₂	Al₂O₃	Fe₂O₃	P₂O₅	K₂O	Na₂O₃	TiO₂	MnO
TURKEY Kyme (*Miriello et al. 2011*)	SEM-EDS	75-91	1-2	4-15	1-4	0-1	0-1	0-1	0-1	–	–
Aigai and Nysa (*Uğurlu Sağın 2012*)	SEM-EDS	13-61	2-8	24-55	8-22	1-7	–	–	1-6	0-1	–
Tarsos and Anavarza (*Polat Pekmezci 2012*)	SEM-EDS	45-99	0-3	1-14	1-5	1-2	–	0-7	0-7	–	–
Kyme (*Miriello et al. 2015*)	XRF	48-86	1-2	7-39	2-8	0-1	–	0-1	0-2	–	–
ITALY Rome (*Sánchez-Moral et al. 2005*)	ICP	19-29	2	27-35	10-12	3-4	0-0.3	1	1-2	0-0.4	0-0.2
Rome (*Jackson et al. 2009*)	XRF	20-22	2-4	31-36	11-13	4-7	0-1	2-4	0-1	0-1	0-0.2
Pompeii (*Miriello et al. 2010*)	SEM-EDS	18-91	2-13	5-51	1-16	0-4	–	0-4	0-2	0-1	–
Rome (*Jackson et al. 2011*)	ICP	14-27	2-3	27-39	10-13	4-6	0-1	1-2	1-2	0-1	0-0.2
Narni (*Cantisani et al. 2002*)	XRF	32	1	36	2	1	0.03	0.5	0.1	0.1	0.04
OTHERS Mošnje, Slovenia (*Kramar et al. 2011*)	ICP-OES	35-54	2-13	0-2	0-2	0-0.4	0-1	0-0.2	0-0.04	0-0.01	0-0.03

Table 6. Chemical compositions of aggregates of Roman lime mortars as a result of the previous studies.

Case area (Reference)	Method	CHEMICAL COMPOSITIONS (%)									
		CaO	MgO	SiO$_2$	Al$_2$O$_3$	Fe$_2$O$_3$	P$_2$O$_5$	K$_2$O	Na$_2$O$_3$	TiO$_2$	MnO
Pergamon (*Aslan Özkaya 2005*)	SEM-EDS	–	1	80	6	9	–	1	2	1	–
Kyme (*Miriello et al. 2011*)	SEM-EDS	0-6	0-4	64-85	6-18	0-4	0-1	1-7	1-4	0-1	0-0.2
Aigai and Nysa (*Uğurlu Sağın 2012*)	XRF	0-3	0-3	40-79	5-16	2-7	–	0-3	0-2	0-1	–
Tarsos and Anavarza (*Polat Pekmezci 2012*)	SEM-EDS	3-98	0-25	1-97	1-22	6-32	–	1-95	0-7	0-3	–
Rome (*Jackson et al. 2009*)	XRF	2-11	1-5	43-52	12-21	9-11	0-1	3-7	0-1	0-1	0-0.2
Pompeii (*Miriello et al. 2010*)	XRF	0-13	0-26	46-64	12-24	1-17	0-1	1-18	0-13	0-2	0-1
Mošnje, Slovenia (*Kramar et al. 2011*)	ICP-OES	29-43	4-13	0-3	0.001-0.023	0-1	0.055-0.442	0.039-0.258	0.023-0.043	0.001-0.023	0.012-0.033

TURKEY (Pergamon, Kyme, Aigai and Nysa, Tarsos and Anavarza)
ITALY (Rome, Pompeii)
OTHERS (Mošnje, Slovenia)

Table 7. Chemical compositions of Roman lime mortars as a result of the previous studies.

Case area (Reference)	Method	CHEMICAL COMPOSITIONS (%)									
		CaO	MgO	SiO₂	Al₂O₃	Fe₂O₃	P₂O₅	K₂O	Na₂O₃	TiO₂	MnO
TURKEY Kyme (*Miriello et al. 2011*)	XRF	21-31	1-2	31-42	7-9	1-3	0-0.3	1-2	0-0.4	0-0.5	0-0.1
ITALY Pompeii (*Miriello et al. 2010*)	XRF	12-27	3-8	32-45	10-15	5-7	0-1	2-5	1-3	0-1	0-0.2
Conímbriga, Portugal (*Velosa et al. 2007*)	XRF	13-22	1-4	28-51	7-11	2-4	0-0.4	0-1	0-1	0-1	0-0.04
Augusta Emerita, Spain (*Robador et al. 2010*)	XRF	19-20	–	54-58	2-3	4-5	–	1	0.1	–	–
Dion, Greece (*Papayianni et al. 2013*)	AAS	31-46	4-9	13-41	0-3	0-2	–	0-1	0-0.4	–	–
Jerash, Jordan (*Yaseen et al. 2013*)	XRF	42-51	0-1	1-18	0-1	0-1	0-0.4	0-1	0-1	0-0.1	0-0.02
Mediana, Serbia (*Gordona et al. 2014*)	SEM-EDS	32-64	0-2	28-54	0-12	–	0-3	–	0-3	–	–
Viminacium, Serbia (*Nikolić et al. 2016*)	SRPS	13-43	0-1	16-67	3-5	1-2	–	0-0.5	0-0.3	–	–
Italica, Spain (*Ontiveros-Ortega et al., 2016*)	XRF	10-49	0-4	6-62	0-10	0-4	0-0.4	0-4	0-1	0-0.4	0-0.2
Complutum, Spain (*Ergenç and Fort 2019*)	XRF	1-48	0-7	8-73	2-20	0-8	0-0.4	0-5	0-1	0-1	0-0.1
Wallsend, United Kingdom (*Laycock et al. 2019*)	XRF	12-19	1-6	35-57	4-7	3-6	0-0.2	0-1	0-1	0-1	–

(Rows from Conímbriga, Portugal through Wallsend, United Kingdom fall under the **OTHER COUNTRIES** group.)

Table 8. Chemical compositions of lime lumps of Roman lime mortars as a result of the previous studies.

	Case area (Reference)	Method	CHEMICAL COMPOSITIONS (%)									
			CaO	MgO	SiO$_2$	Al$_2$O$_3$	Fe$_2$O$_3$	P$_2$O$_5$	K$_2$O	Na$_2$O$_3$	TiO$_2$	MnO
TURKEY	Ephesus (*Kuleli 2005*)	SEM-EDS	95-98	0-0.4	1-2	0-0.1	0-0.2	–	0-0.2	0-1	0-0.1	0-1
	Kyme (*Miriello et al. 2011*)	SEM-EDS	84-94	1-2	1-8	1-3	0-1	1-2	0-1	0-2	0-0.2	0-0.3
	Aigai and Nysa (*Uğurlu Sağın 2012*)	SEM-EDS	89-100	0-2	0-8	0-3	–	0-1	–	0-3	–	–
ITALY	Narni (*Cantisani et al. 2002*)	XRF	30	1	37	2	0.2	0.01	0.4	0.02	–	0.02

Table 9. Mechanical properties of Roman lime mortars as a result of the previous studies.

Case area (Reference)	Method	Compressive Strength (MPa)	Elasticity Moduls (MPa)	Flexural Strength (MPa)	Tensile Strength (MPa)	Point Load Test Strength Index (MPa)
TURKEY Ephesus (*Kuleli 2005*)	Ultrasonic Pulse Velocity	–	524-2401	–	–	–
Pergamon (*Aslan Özkaya and Böke 2009*)	Mechanical Test Instrument	6.6	630.6	–	–	–
Kaisareia (*Kozlu 2010*)	Point Load Test	5.3-9.70		–	–	–
Tarsos and Anavarza (*Polat Pekmezci 2012*)	Point Load Test	3-5	–	–	–	–
Amastris (*Kurugöl and Güleç 2015*)	Universal Hydraulic Press	4.5-8.9	8300-13500	2.5-4.7	–	–
Myra (*Oğuz et al. 2015*)	Point Load Test	3.1-8.1		–	–	–
Smyrna (*Felekoğlu et al. 2016*)	Loading Frame Scheme	3.2-4.5	–	–	–	–
ITALY Rome (*Jackson et al. 2009*)	Point Load Test Brazilian tests	0.98-6.7	1750–9170	–	0.8-0.9	–
Narni (*Drdácký et al. 2013*)	ITAM methodology Point Bending Test	2.0-4.7	–	0.3-1.5	–	–
Tivoli (*Columbu et al. 2017*)	Point Load Test	1.2-13.3	–	–	0.10-1.19	0.08-0.95
OTHERS Dion, Greece (*Papayianni et al. 2013*)	with shaped cubic sample	2.1-4.8	–	–	–	–
Viminacium, Serbia (*Nikolić et al. 2016*)	BS EN 1015-11:2019	2.0-5.3	–	–	–	–

1.3. Problem Statement, Aim, and Scope of the Study

The purpose of the present study was to determine the characteristics of Roman lime mortars in Western Anatolia. Western Anatolia referred to the coastal and inner parts of the Mediterranean and the Aegean Sea. This region was part of Asia Province which was one of the most important provinces of the Roman Empire throughout history. Despite the cultural importance of Anatolia, less attention has been paid to this region. Detailed studies were carried out for the characterization and conservation of Roman lime mortars that were in the Italian Peninsula, but the studies involving the lime mortar used in Anatolia have focused mainly on a few cases. Hence, this study aimed to investigate the characteristics of Roman lime mortars of Western Anatolia to understand whether there was a common production technology of lime mortar in the Roman Empire by making a comparison between Europe and Western Anatolia.

1.4. Significance of the Study

Preliminary literature review showed that studies were mainly about Roman lime mortars used in the imperial buildings in the Italian Peninsula. Although Western Anatolia (Asia Province) was one of the important regions of the Roman Empire, a limited number of studies have addressed on Roman lime mortars in this region. Ancient cities located in Anatolia, particularly Western Anatolia where had been settled densely in the Roman Period have not been examined in detail regarding lime mortar. Therefore, this study will contribute to compare the production technology of Roman lime mortar in Europe and Western Anatolia. Existing studies related to Anatolia have focused mainly on characterization of lime mortars used in a few case areas. However, this study provided an opportunity to examine a wider area, including numerous archaeological sites from different parts of the Mediterranean and Aegean Sea.

In this study, the least examined characteristics of Roman mortars, mentioned before, were also analyzed to figure out the materials and the production technology of mortars. Among the least examined properties, particularly the geochemical characteristics of fine aggregates, which were investigated in this study, were an important research area. Similarities and differences in the properties of mortars can play an important role in understanding Roman construction techniques.

The results of this study can make a significant contribution to whether there was a common mortar production technology regarding location, geography, and raw material resources. Results may be attributed to the production of a standard quality mortar with local raw materials in the Roman Empire.

1.5. Research Questions

This study aims to answer the following questions in the research process:

- What are the characteristics of Roman lime binders and aggregates used in Western Anatolia?

- What are the geochemical characteristics of fine aggregates (pozzolans) used in Roman lime mortars in Anatolia?

- Are there any differences or similarities of Roman lime mortars produced in geographical regions of Anatolia?

- Is there any common mortar production technology in different regions of the Roman Empire?

CHAPTER 2

METHOD

In this study, characteristics of Roman lime mortars taken from twenty-six archaeological sites in Western Anatolia were investigated based on a methodology specified by European Standard called "Conservation of Cultural Heritage-Characterization of Mortars Used in Cultural Heritage" (UNI EN 17187 2020). A series of laboratory tests were carried out by visual analysis, standard test methods, Munsell Soil Color Chart, point load tests, electrical conductivity measurements, Scanning electron microscope (SEM) equipped with X-Ray energy dispersive system (EDS), X-ray diffraction (XRD), Fourier transformed infrared spectroscopy (FTIR), Mercury intrusion porosimetry (MIP) and thermogravimetric analysis (TGA) to determine basic physical properties, mechanical properties, raw material compositions, mineralogical and chemical compositions, hydraulic properties, pozzolanic activities and microstructural characteristics of mortars.

2.1. Sampling

In the case areas mentioned below, sampling was performed mainly on archaeological sites, on monuments or buildings in a good state of conservation. Sampling was conducted following the European Standard (UNI EN 16085). The mortars were taken in sufficient sizes for the analysis not to cause damage to the original material characteristics of historic structures (UNI EN 16085 2012).

Ancient structures with original mortar were selected for sampling with the help of excavation reports, information signboards, and visual analysis. In 2016, fifty-seven original lime mortar samples were taken from various types of buildings in twenty-six case areas. Samples were collected from the walls by a chisel with careful and non-destructive work.

2.1.1. Case Areas

Roman Empire was one of the empires with the largest lands in history and the Romans divided their land into the provinces such as Achaia, Asia, Hispania, Macedonia, Sicilia, and Syria. Roman provinces were administrative and territorial units of the Roman Empire, established by various emperors throughout Italy and then the rest of Europe. The number and border of the provinces under Roman rule changed throughout history (Kretzchmer 2010).

Case areas in Asia province (Western Anatolia) of Roman Empire were selected based on the criteria of location, distribution, accessibility, state of excavation, and construction period.

Figure 3. Location of Asia province in the Roman Empire.
(Source: Kretzchmer 2010)

Figure 4. Ancient geographical regions of Anatolia.

Asia province, one of the most important provinces of the Roman Empire, was determined as the main site of this study since Western Anatolia with its coastal and inner sites had been settled densely in the Roman Period (Figure 3). There were nine geographical regions in Western Anatolia: Aiolis, Caria, Ionia, Lycia, Lydia, Mysia, Pamphylia, Phrygia, Pisidia, and Troas (Kaya 2005) (Figure 4). Nowadays, in these regions, there are many Roman archeological sites, whose primary building material was a lime mortar. In this study, at least one ancient city was selected in each region to provide a homogeneous distribution of case areas. All selected case areas have had systematic archeological excavations so far. Accessibility to the remains of the structures played a significant role in sampling. Thus, all case areas have ruins above ground.

The use of lime in construction works has been known since the earliest civilizations. However, the widespread use of lime and pozzolans in mortar production was the important contribution of the Romans to mortar technology. The major innovations and/or technological optimization of lime binders were introduced rapidly and systematically at the beginning of the 2nd century B.C. or shortly after (Adam 2005). For that reason, the construction period of the structures was determined as the Roman Imperial Period (1st century BC and 3rd century AD) when the greatest innovations in Roman architecture took place (Ward-Perkins 1994).

There are about three hundred archeological sites dated Roman period in Anatolia (Willet 2020) (Figure 5). In this study, twenty-six archeological sites were selected as a case area based on the criteria above: Aizanoi, Alexandria Troas, Anaia, Antiocheia in Pisidia, Assos, Cremna, Cyme, Euromos, Kedrai, Labraunda, Laodicea, Lyrbe, Magnesia

ad Meander, Patara, Pergamon, Priene, Pygela, Sagalassos, Sardes, Selge, Stratonikeia, Teos, Tlos, Tralleis, Tripolis, and Xanthos (Figure 5).

Cyme (Kyme), located in İzmir Province, was the major city of the Aiolis. Sea trade and agriculture were its main economic activities thanks to its harbor. It had a strategic political position in the region. Harbor, city walls, agora, theatre, and bath are some important monuments of Cyme (Miriello et al. 2011).

Euromos, located in Muğla Province, was a city in Caria. It has the Temple of Zeus, which is one of the best-preserved ancient temples in Anatolia. Besides the temple, there are remains of an agora, theatre, baths, and city walls (Kızıl and Doğan 2018).

Anaia is one of the Ionian cities, famous for the ruins of Kadıkalesi, located in Aydın Province. Besides the castle, there are water-related buildings such as baths and aqueducts (Akdeniz 2007).
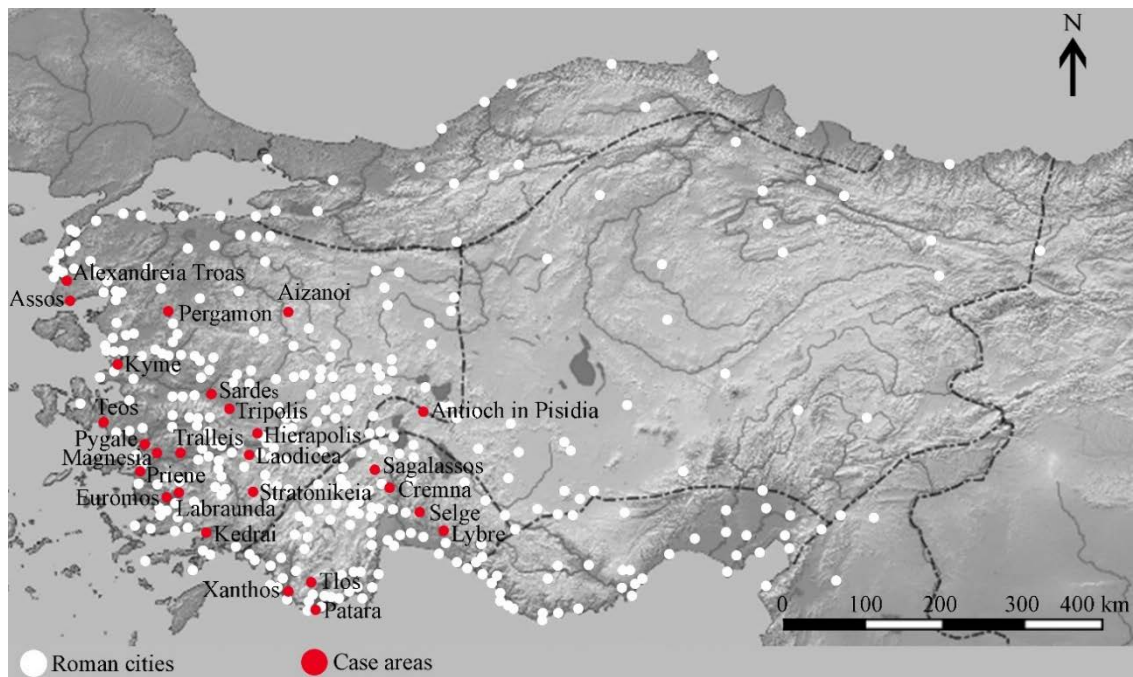

Figure 5. Case areas in Western Anatolia.
(Source: Ligt et al. 2017)

Magnesia on the Meander was a city in Ionia, today located in Aydın Province. It was called "on the Meander" to distinguish it from the nearby Lydian city Magnesia ad Sipylum. Its stadium is one of the best-preserved stadiums in Anatolia (Figure 6). Agora, bath, gymnasium, theatre, and city walls are the other ruins of the site (Yegül 2007).

Figure 6. Stadium of Magnesia on the Meander.
(Source: Author)

Priene was a coastal city of Ionia, located in Aydın Province. It was founded on the seacoast. Today, it is an inland site because of changes in the landscape thanks to Meander. In 2018, it was included in the UNESCO Tentative List of World Heritage. Temple of Athena, theatre, bouleuterion, and baths are some finds on the site (UNESCO 2018).

Pygela was a harbor city in Ionia near Ephesus, located in Aydın Province. Today, there is a holiday village in most parts of the city (Stock et al. 2013).

Teos was an ancient port city in Ionia, located in İzmir Province. The modern settlement is situated close to the ruins of Teos. Port, theatre, gymnasium, cistern, bouleuterion, and agora are some ruins in the city (Tuna 1995).

Kedrai (Cleopatra Island) is an island settlement on the eastern coast of the Bay of Keramos, in Caria. The ancient city is located on Sedir Island, Muğla Province. Kedrai was surrounded by walls and there are remains of a Temple of Apollo, agora, necropolis, and the theatre. It is believed that the Roman Emperor Marcus Antonius brought the golden sand by ship from Egypt for Cleopatra and that is why the beach was called "Beach of Cleopatra" (Diler 2008).

Labraunda (Labranda), located in Muğla Province, was an important sanctuary in the Caria region with the cult to Zeus. Today, there are remains of the Temple of Zeus, stoa buildings, baths, pools, and fountains (Karlsson et al. 2012).

Stratonikeia, a city in the interior part of Caria, was located in Muğla Province. The most important feature of the area is having remains from different periods, such as the ancient period as well as the Ottoman and Turkish Republican Period. In 2015, it was included in the UNESCO Tentative List of World Heritage. There are city walls, gymnasium, bouleuterion, theatre, bath, also a Turkish bath, mosque, streets, houses, and shops (UNESCO 2015).

Patara, located in Antalya Province, was the principal port of Lycia. It was one of the main ancient maritime and trade centers of the eastern Mediterranean. In 2009, Patara was added to the UNESCO Tentative List of World Heritage. Some significant finds at Patara are acropolis, baths, theatre, bouleuterion, a triumphal arch, and lighthouse (UNESCO 1988).

Tralleis was a famous city of sculpture in Caria, located in Aydın Province. The best-preserved building in the city is a ruin of gymnasium and called "Üçgözler" by local people (Figure 7). Besides, an agora, a theatre, and a stadium are the other structures of the city (Saraçoğlu 2011).

Figure 7. Gymnasium (Uçgözler) in Tralleis.
(Source: Author)

Tlos, located in Muğla Province, is another important city in the Lycia region. In 2009, Tlos was included in the UNESCO Tentative List of World Heritage. The rock-cut tombs, the stadium, the agora, the baths, the city basilica, and the theater are some outstanding examples of the city (UNESCO 2009a).

Xanthos, located in Antalya Province, was the capital of ancient Lycia. In 1998, Xanthos was designated a UNESCO World Heritage Site with the ancient city of Letoon. The tombs, the theatre, the bath, the agora, and the basilica are the most important architectural examples of the city (Figure 8) (UNESCO 2009a).

Figure 8. Theatre and tomb of Xanthos.
(Source: Author)

Sardes, situated in Manisa Province, was the capital of ancient Lydia. In 2013, it was added to the UNESCO Tentative List of World Heritage. It is famous for the Temple of Artemis, a synagogue which was a section of a large bath-gymnasium complex and its gold coins. Also, it was a terminus point of Royal Road (UNESCO 2013a).

Tripolis, also called Neapolis, Apollonia, and Antoniopolis was a Lydia city and located in Denizli Province. There are ruins of a theatre, baths, agora, city walls, and necropolis (Figure 9) (Duman 2013).

Figure 9. Excavations in Tripolis.
(Source: Author)

Pergamon, was one of the biggest metropolises of Anatolia, was a Mysia city and situated in İzmir Province. In 2014, Pergamon and its multi-layered cultural landscape were declared as a UNESCO World Heritage Site. The city has many outstanding monuments such as Serapis Temple, altar, theatre, library, gymnasium, baths, and Asklepion (UNESCO 2014).

Lybre, which is also known as Seleukeia, was a city in the ancient Pamphylia region. It is located in Antalya Province and has many remains of city walls, bath, cistern, temple, and agora (Figure 10) (İnan 1998).

Figure 10. Theatre and tomb of Lybre.
(Source: Author)

Aizonai is an archeological site of Phrygia, located in Kütahya Province. In 2012, it was added to the UNESCO Tentative List of World Heritage. Temple of Zeus, one of the well-preserved ancient temples in Anatolia, theatre-stadium complex, baths, and macellum are some important ruins in the city (Figure 11) (UNESCO 2012).

Figure 11. Temple of Zeus in Aizonai.
(Source: Author)

Laodiceia, is one of the important archaeological remains in Phrygia along with Hierapolis and Tripolis, located in Denizli Province. In 2013, the city was included in the UNESCO Tentative List of World Heritage. It has the largest ancient stadium in Anatolia, theatres, bath complexes, bouleuterion, and many other ruins (UNESCO 2013b).

Cremna, was an ancient city founded on the hill in Pisidia, is situated in Burdur Province. Today, the ruins of theatre, agora, bath, cistern, forum, and city walls stand in the city (Mitchell and Waelkens 1987).

Sagalassos, founded on the slopes of the Taurus mountain range, was the metropolis of Pisidia. Today it is situated in Burdur Province. In 2009, it was designated a UNESCO Tentative List of Word Heritage. The site is almost completely preserved, with monumental structures such as theatre, fountains, temples, agora, baths, and bouleuterion (UNESCO 2009b).

Selge was an important city in Pisidia, on the southern slope of Mount Taurus, in Antalya Province. The best-preserved monument of the site is theater, but it has also the remains of a bath, stadium, gymnasium, temple (Figure 12) (Nolle 2015).

Figure 12. The remains of Selge.
(Source: Author)

Antiocheia in Pisidia, also known as Antiochia Caesareia, is situated in Isparta Province. The remains of the city consist of theatre, bath, aqueduct, fountain, and churches (Özhanlı 2013).

Assos, one of the most important archaeological sites of the Troas region, is in Çanakkale Province. In 2017, it was added to the UNESCO Tentative List of World Heritage. It is famous for the Temple of Athena, but it also has the remains of a theatre, bath, cistern, and bouleuterion (Figure 13) (UNESCO 2017).
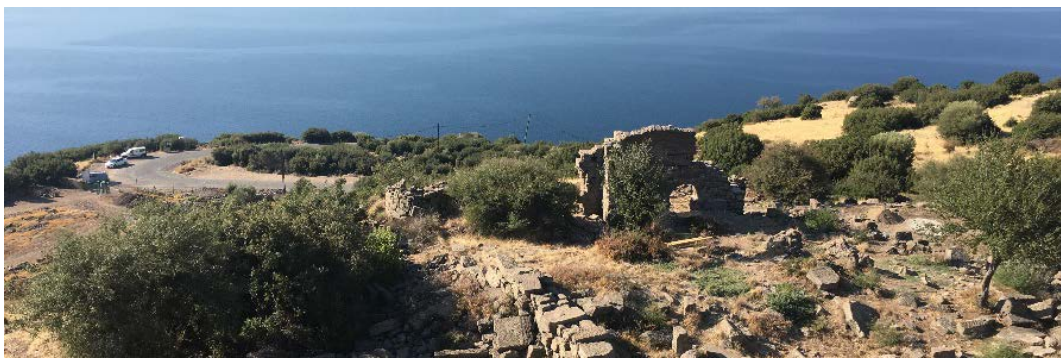
Figure 13. Bath ruins in Assos.
(Source: Author)

Alexandria Troas, which was an important coastal city in the Troas region, located in Çanakkale Province. Today, some remains of a gymnasium, bath, odeon, theatre, and stadium stand on the site (Feuser 2011).

2.1.2. Samples

Fifty-seven mortar samples were collected from the aforementioned twenty-six case areas (Table 10). Forty-eight of the samples were *opus caementicium* and nine of the samples were *opus signinum.* Ancient and current locations of the archeological sites, type, and date of construction of building that samples were collected were given (Table 10). The places where the samples were collected were marked on photographs of the structures (Table 11).

Samples were categorized according to the presence of ceramic as *opus caementicium* and *opus signinum*. Mortars, identified as *opus caementicium*, were prepared with lime, aggregates, and natural pozzolanic additions without ceramic fragments. O*pus signinum* mortars were produced by using artificial pozzolanic additions such as ceramic fragments or crushed pottery.

The mortars were identified in terms of function in the structure, such as wall, vault, and arch. Collected samples belonged to bath (twenty-one samples), theatre (twelve samples), agora (four samples), city wall (five samples), cistern (four), stadium (three samples), house (three samples), gymnasium (three samples), aqueduct (one sample), and undefined (one sample). Mortars were also defined as follows: mortar from the rubble core of the ashlar masonry, mortar from the ashlar masonry, and the rubble masonry (Table 11).

Samples were labeled as the first letter showing the name of the ancient geographical region (A: Aiolis, C: Caria, I: Ionia, L: Lycia, Ld: Lydia, M: Mysia, P: Pisidia, Pm: Pamphylia, Ph: Phrygia, T: Troas), the second letter showing the anem of the ancient city they were taken from (A: Assos, Az: Aizanoi, Ax: Alexandria Troas, An: Anaia, At: Antiocheia, C: Cremna, Cy: Cyme, E: Euromos, K: Kedrai, L: Labraunda, Ld: Laodicea, Ly: Lybre, M: Magnesia ad Meander, P: Pergamon, Pt: Patara, Pr: Priene, Py: Pygela, S: Sagalassos, Sr: Sardes, Sl: Selge, St: Stratonikeia, T: Teos, Tl: Tlos, Tr: Tralleis, Tp: Tripolis, X: Xanthos) and the third letter showing the name of the building type (B: Bath, T: Theatre, A: Agora, C: City Wall, Cs: Cistern, S: Stadium, H: House, G: Gymnasium, Aq: Aqueduct, U: Undefined) (Table 11). The codes of *opus signinum* mortars were written in italic and underlined in this study.

Table 10. Information of Roman lime mortar samples.
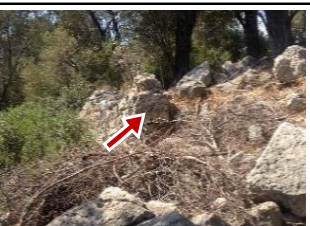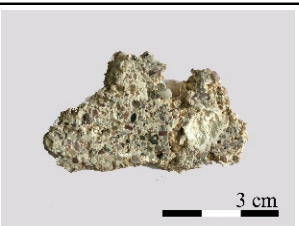
Code	Site	Region	Building Type	Date of Construction	Location
ACyH	Cyme	Aiolis	House	Roman Imperial Period - *I Century AD*	Aliağa/İzmir
ACyT	Cyme	Aiolis	Theatre	Roman Imperial Period - *III Century AD*	Aliağa/İzmir
CEB	Euromos	Caria	Bath	Roman Imperial Period - *I-II Century AD*	Milas/Muğla
CKC	Kedrai	Caria	City Wall	Roman Period - *n.d.*	Marmaris/Muğla
CKCs	Kedrai	Caria	Cistern	Roman Period - *n.d.*	Marmaris/Muğla
CLB1	Labraunda	Caria	Bath	Roman Imperial Period - *I-II Century AD*	Milas/Muğla
CLB2	Labraunda	Caria	Bath	Roman Imperial Period - *I-II Century AD*	Milas/Muğla
CStB	Stratonikeia	Caria	Bath	Roman Imperial Period - *II Century AD*	Yatağan/Muğla
CStT	Stratonikeia	Caria	Theatre	Roman Imperial Period - *I Century AD*	Yatağan/Muğla
CTrG	Tralleis	Caria	Gymnasium	Roman Imperial Period - *II Century AD*	Merkez/Aydın
CTrB	Tralleis	Caria	Bath	Roman Imperial Period - *II Century AD*	Merkez/Aydın
IAnAq	Anaia	Ionia	Aquadict	Roman Imperial Period - *I Century AD*	Kuşadası/Aydın
IAnB	Anaia	Ionia	Bath	Roman Period - *n.d.*	Kuşadası/Aydın
IMA	Magnesia	Ionia	Agora	Roman Imperial Period - *I-III Century AD*	Germencik/Aydın
IMG	Magnesia	Ionia	Gymnasium	Roman Imperial Period - *II-III Century AD*	Germencik/Aydın
IMS	Magnesia	Ionia	Stadium	Roman Imperial Period - *I-II Century AD*	Germencik/Aydın
IPyH	Pygela	Ionia	House	Roman Imperial Period - *III Century AD*	Kuşadası/Aydın
IPrB	Priene	Ionia	Bath	Roman Imperial Period - *I-II Century AD*	Söke/Aydın
IPrH	Priene	Ionia	House	Roman Imperial Period - *n.d.*	Söke/Aydın
IPrT	Priene	Ionia	Theatre	Roman Imperial Period - *II Century AD*	Söke/Aydın
ITCs	Teos	Ionia	Cistern	Roman Period - *n.d.*	Seferihisar/İzmir
ITT	Teos	Ionia	Theatre	Roman Imperial Period - *I Century AD*	Seferihisar/İzmir
LPtB	Patara	Lycia	Bath	Roman Period - *n.d.*	Kaş/Antalya
LPtC	Patara	Lycia	City Wall	Roman Imperial Period - *I Century AD*	Kaş/Antalya
LPtT	Patara	Lycia	Theatre	Roman Imperial Period - *I Century BC*	Kaş/Antalya
LTlB	Tlos	Lycia	Bath	Roman Imperial Period - *II-III Century AD*	Fethiye/Muğla
LTlS	Tlos	Lycia	Stadium	Roman Period - *n.d.*	Fethiye/Muğla
LTlT	Tlos	Lycia	Theatre	Roman Imperial Period - *I Century BC*	Fethiye/Muğla

(cont. on next page)

Table 10. (cont.)

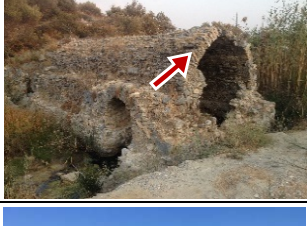| Code	Site	Region	Building Type	Date of Construction	Location
LXA	Xanthos	Lycia	Agora	Roman Imperial Period - *n.d.*	Kaş/Antalya
LXB	Xanthos	Lycia	Bath	Roman Imperial Period - *n.d.*	Kaş/Antalya
LXT	Xanthos	Lycia	Theatre	Roman Imperial Period - *n.d.*	Kaş/Antalya
LySrU	Sardes	Lydia	Undefined	Roman Period - *n.d.*	Salihli/Manisa
LyTpA	Tripolis	Lydia	Agora	Roman Imperial Period - *IV Century AD*	Buldan/Denizli
LyTpB	Tripolis	Lydia	Bath	Roman Imperial Period - *II Century AD*	Buldan/Denizli
LyTpT	Tripolis	Lydia	Theatre	Roman Imperial Period - *II Century AD*	Buldan/Denizli
MPB	Pergamon	Mysia	Bath	Roman Imperial Period - *n.d.*	Bergama/İzmir
MPB2	Pergamon	Mysia	Bath	Roman Imperial Period - *n.d.*	Bergama/İzmir
MPC	Pergamon	Mysia	City Wall	Roman Imperial Period - *n.d.*	Bergama/İzmir
PhAzB	Aizonai	Phrygia	Bath	Roman Imperial Period - *II Century AD*	Çavdarhisar/Kütahya
PhLdB	Laodiceia	Phrygia	Bath	Roman Imperial Period - *II Century AD*	Merkez/Denizli
PCT	Cremna	Pisidia	Theatre	Roman Imperial Period - *I Century BC*	Bucak/Burdur
PCB	Cremna	Pisidia	Bath	Roman Imperial Period - *I Century BC*	Bucak/Burdur
PCC	Cremna	Pisidia	City Wall	Roman Imperial Period - *I Century BC*	Bucak/Burdur
PmLyB	Lyrbe	Pamphylia	Bath	Roman Period - *n.d.*	Manavgat/Antalya
PmLyCs	Lyrbe	Pamphylia	Cistern	Roman Period - *n.d.*	Manavgat/Antalya
PmLyC	Lyrbe	Pamphylia	City Wall	Roman Period - *n.d.*	Manavgat/Antalya
PAtT	Pisidia Antiocheia	Pisidia	Theatre	Roman Imperial Period - *I-III Century AD*	Yalvaç/Isparta
PSlB	Selge	Pisidia	Bath	Roman Imperial Period - *II Century AD*	Manavgat/Antalya
PSlS	Selge	Pisidia	Stadium	Roman Imperial Period - *II Century AD*	Manavgat/Antalya
PSlT	Selge	Pisidia	Theatre	Roman Imperial Period - *III Century AD*	Manavgat/Antalya
PSB	Sagalassos	Pisidia	Bath	Roman Imperial Period - *n.d.*	Ağlasun/Burdur
PSA	Sagalassos	Pisidia	Agora	Roman Imperial Period - *I Century AD*	Ağlasun/Burdur
PST	Sagalassos	Pisidia	Theatre	Roman Imperial Period - *II Century AD*	Ağlasun/Burdur
TAB	Assos	Troas	Bath	Roman Imperial Period - *I Century AD*	Ayvacık/Çanakkale
TACs	Assos	Troas	Cistern	Roman Imperial Period - *n.d.*	Ayvacık/Çanakkale
TAxB	Alexandria Troas	Troas	Bath	Roman Imperial Period - *n.d.*	Ezine/Çanakkale
TAxG	Alexandria Troas	Troas	Gymnasium	Roman Imperial Period - *II Century AD*	Ezine/Çanakkale

Table 11. Definitions of Roman lime mortar samples.

Code	Location	Images	Definition
ACyH		3 cm	Wall _Opus signinum_ Mortar from the rubble core of the ashlar masonry
ACyT		3 cm	Wall _Opus caementicium_ Mortar from the rubble masonry
CEB		3 cm	Wall _Opus caementicium_ Mortar from the rubble masonry
CKC		3 cm	Wall _Opus caementicium_ Mortar from the rubble core of the ashlar masonry
CKCs		3 cm	Wall _Opus caementicium_ Mortar from the rubble masonry
CLB1		3 cm	Wall _Opus signinum_ Mortar from the rubble core of the ashlar masonry
CLB2		3 cm	Wall _Opus caementicium_ Mortar from the rubble masonry
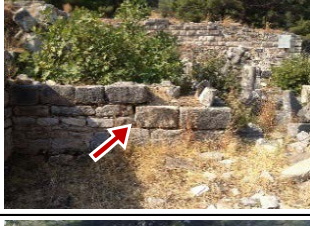
(cont. on next page)

Table 11. (cont.)

Code	Location	Images	Definition
CStB		3 cm	Wall *Opus signinum* Mortar from the rubble masonry
CStT		3 cm	Wall *Opus signinum* Mortar from the rubble core of the ashlar masonry
CTrG		3 cm	Vault *Opus caementicium* Mortar from the rubble masonry
CTrB		3 cm	Wall *Opus signinum* Mortar from the ashlar masonry
IAnAq		3 cm	Wall *Opus caementicium* Mortar from the rubble core of the ashlar masonry
IAnB		3 cm	Vault *Opus caementicium* Mortar from the rubble masonry
IMA		3 cm	Wall *Opus caementicium* Mortar from the rubble core of the ashlar masonry
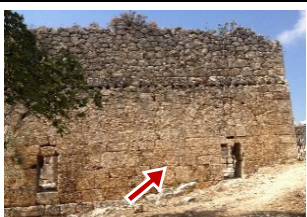
(cont. on next page)

Table 11. (cont.)

Code	Location	Images	Definition
IMG			Wall *Opus caementicium* Mortar from the rubble masonry
IMS			Wall *Opus caementicium* Mortar from the rubble masonry
IPyH			Wall *Opus caementicium* Mortar from the rubble masonry
IPrB			Wall *Opus caementicium* Mortar from the rubble core of the ashlar masonry
IPrH			Wall *Opus caementicium* Mortar from the rubble core of the ashlar masonry
IPrT			Wall *Opus caementicium* Mortar from the rubble masonry
ITT			Vault *Opus caementicium* Mortar from the rubble masonry
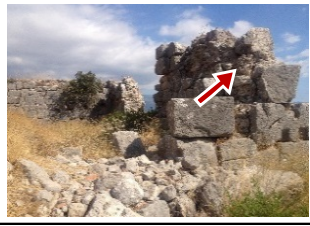
Table 11. (cont.)

Code	Location	Images	Definition
ITCs		3 cm	Arch *Opus caementicium* Mortar from the rubble masonry
LPtB		3 cm	Wall *Opus signinum* Mortar from the rubble core of the ashlar masonry
LPtC		3 cm	Wall *Opus caementicium* Mortar from the rubble core of the ashlar masonry
LPtT		3 cm	Wall *Opus signinum* Mortar from the ashlar masonry
LTlB		3 cm	Wall *Opus signinum* Mortar from the ashlar masonry
LTlS		3 cm	Wall *Opus caementicium* Mortar from the ashlar masonry
LTlT		3 cm	Wall *Opus caementicium* Mortar from the ashlar masonry
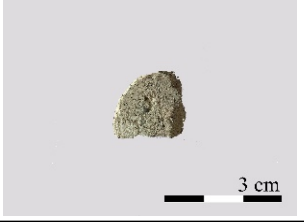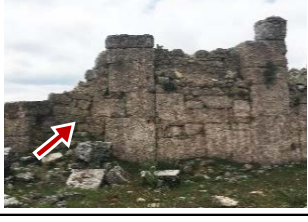
(cont. on next page)

Table 11. (cont.)

Code	Location	Images	Definition
LXA		3 cm	Wall *Opus caementicium* Mortar from the rubble masonry
LXB		3 cm	Wall *Opus signinum* Mortar from the rubble core of the ashlar masonry
LXT		3 cm	Wall *Opus caementicium* Mortar from the rubble masonry
LySrU		3 cm	Wall *Opus caementicium* Mortar from the rubble masonry
LyTpA		3 cm	Wall *Opus caementicium* Mortar from the rubble masonry
LyTpB		3 cm	Wall *Opus caementicium* Mortar from the rubble core of the ashlar masonry
LyTpT		3 cm	Vault *Opus caementicium* Mortar from the rubble masonry

(cont. on next page)

54
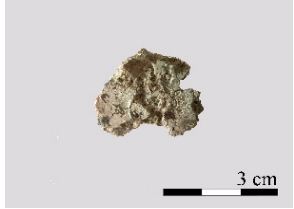
Table 11. (cont.)

Code	Location	Images	Definition
MPB			Wall *Opus caementicium* Mortar from the rubble core of the ashlar masonry
MPB2			Vault *Opus caementicium* Mortar from the rubble core of the ashlar masonry
MPC			Wall *Opus caementicium* Mortar from the rubble masonry
PhAzB			Wall *Opus caementicium* Mortar from the rubble core of the ashlar masonry
PhLdB			Wall *Opus caementicium* Mortar from the rubble core of the ashlar masonry
PCT			Wall *Opus caementicium* Mortar from the rubble masonry
PCB			Wall *Opus caementicium* Mortar from the rubble core of the ashlar masonry

(cont. on next page)

Table 11. (cont.)

Code	Location	Images	Definition
PCC			Wall *Opus caementicium* Mortar from the rubble core of the ashlar masonry
PmLyB			Wall *Opus caementicium* Mortar from the rubble masonry
PmLyCs			Wall *Opus caementicium* Mortar from the rubble masonry
PmLyC			Wall *Opus caementicium* Mortar from the rubble masonry
PAtT			Wall *Opus caementicium* Mortar from the rubble core of the ashlar masonry
PSlB			Vault *Opus caementicium* Mortar from the rubble masonry
PSlS			Wall *Opus caementicium* Mortar from the rubble core of the ashlar masonry

(cont. on next page)

Table 11. (cont.)

Code	Location	Images	Definition
PSIT		3 cm	Wall *Opus caementicium* Mortar from the rubble core of the ashlar masonry
PSB		3 cm	Wall *Opus caementicium* Mortar from the rubble masonry
PSA		3 cm	Wall *Opus caementicium* Mortar from the rubble masonry
PST		3 cm	Wall *Opus caementicium* Mortar from the rubble core of the ashlar masonry
TAB		3 cm	Wall *Opus signinum* Mortar from the rubble core of the ashlar masonry
TACs		3 cm	Vault *Opus caementicium* Mortar from the rubble core of the ashlar masonry
TAxB		3 cm	Vault *Opus caementicium* Mortar from the rubble masonry

(cont. on next page)

Table 11. (cont.)

Code	Location	Images	Definition
TAxG		3 cm	Arch *Opus caementicium* Mortar from the rubble masonry

2.2. Experimental Study

Experimental studies have been conducted to determine macroscopic properties (color-compactness-grain size distribution), basic physical properties of mortars (density-porosity-pore size distribution), mechanical properties (uniaxial compressive strength), raw material compositions (lime/aggregate ratios and particle size distribution of aggregates), mineralogical and chemical compositions of lime lump, aggregate and fine mortar matrices (binder), hydraulic properties of the binder, pozzolanic activities and geochemical characteristics of fine aggregates (pozzolans) and microstructural properties of lime lump, aggregate, and binder.

2.2.1. Determination of Macroscopic Properties

The color and compactness of mortars, and grain size distribution and shape of aggregates were determined by visual analysis. The determination of the color of aggregates (coarser than 1 mm) was carried out by visual examination. Munsell Soil Color Chart was used to determine the color of fine aggregates (less than 63 μm) (Munsell Color 2013).

2.2.2. Determination of Density and Porosity

Bulk density and porosity of the mortars were determined by standard RILEM test methods (RILEM 1980). Bulk density is the ratio of the mass to its bulk volume and is

expressed in grams per cubic centimeters (g/cm^3). Porosity is the ratio of the pore volume to the bulk volume of the sample and is usually expressed in percent (% volume).

Measurement of bulk density and porosity was carried out on two specimens of each sample. At first, samples were dried in an oven at low temperatures (40ºC) at least for 24 hours. Afterward, they were weighed by a precision balance (AND HF-3000G) to determine their dry weights (M_{dry}). Subsequently, samples were completely saturated with distilled water in a vacuum oven (Lab-Line 3608-6CE Vacuum Oven). Saturated weights (M_{sat}) were measured, and Archimedes weight (M_{arch}) was determined with hydrostatic weighing in distilled water by using the precision balance. Bulk densities (D) and porosities (P) of the mortars were calculated by using the following formulas:

D (g/cm^3) = M_{dry} / (M_{sat}- M_{arch})

P (%) = [(M_{sat}-M_{dry}) / (M_{sat}- M_{arch})] x 100

where;

M_{dry}: Dry weight (g)

M_{sat}: Saturated weight (g)

M_{arch}: Archimedes weight (g)

M_{sat}-M_{dry}= Pure volume (g)

M_{sat}-M_{arch}= Bulk volume (g)

2.2.3. Determination of Pore Size Distribution

The pore sizes of selected mortars were determined by Mercury intrusion porosimetry (MIP). Micromeritics Auto Pore IV 9500 apparatus (Micromeritics, Norcross, GA, USA) was applied to study the pore structure of the mortars with a pressure range between 0.0015 and 207 MPa, allowing the study of pore sizes in the range of 1.000 to 0.001 μm. The MIP results were obtained in the form of raw data representing logarithmic differential intruded volume versus pore diameter of mortars.

Twelve samples, approximately 1 cm^3 in size, were dried in an oven for 24 h at 105 °C, and then the binder parts of mortars were analyzed using penetrometers for solid samples. This technique allows for the determination of pore size (radius or diameter), using Laplace's equation and the structure of capillary tubes in porous media.

2.2.4. Determination of Mechanical Properties

Mechanical properties of historic mortars in the dry state were determined by point load tests due to the size and shape of the samples. Measurements were carried out on two specimens of each sample. Point load test allows working with irregular shape and relatively smaller samples than conventional test techniques. It has not been possible to take large enough samples from the archeological sites to carry out the other tests.

Mortars were prepared by using a cutting machine according to the standards with a minimum thickness of 20 mm (ASTM 1985). Subsequently, they were dried in an oven at 60°C for at least 24 hours. The specimens with thicknesses varying between 20-55 mm could be prepared since it is hard to obtain samples of such sizes in historic masonry. Point load tests were carried out by using ELE-Point Load Test Apparatus / 77-0110. Load configuration for irregular lumps was applied to the samples (Figure 14) (ASTM 1985).
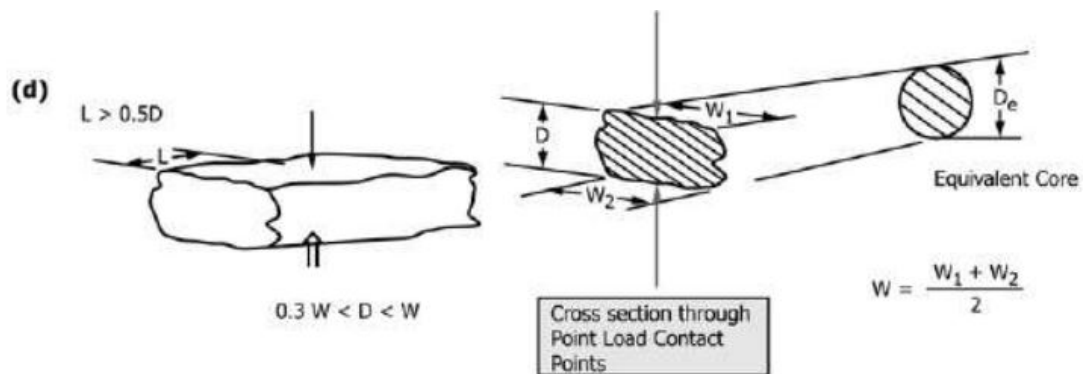
Figure 14. Load configurations for the irregular lump test.
(Source: ASTM 1985)

Uniaxial compressive strength (S_c, MPa) of the mortars were calculated by equations given in ASTM standard (ASTM 1985).

L = distance between contact points and nearest free face

D = equivalent core diameter

W = (W1 + W2) /2 (If the sides are not parallel)

The ratio, D/W, should be between 1∕3 and 1, preferably close to 1. The distance L should be at least 0.5 W.

Steadily increase the load such that failure occurs within 10 to 60 s, and record the failure load, P.

P = failure load, N

D_e = equivalent core diameter, mm

$De^2 = 4A/\pi$ for axial, block, and lump tests, mm^2

A = W x D = minimum cross-sectional area of a plane through the platen contact points

The index value is referred to a standard cylindrical specimen with diameter D = 50 mm, for which I_S has been corrected with a shape coefficient (F) and calculated as

$$I_{S\,(50)} = F \times I_s$$

$$F = (D_e\,/\,50)^{0.45}$$

F = Size Correction Factor

$I_{S\,(50)}$ = Uncorrected point load strength index from a specimen with a specific test diameter (D)

$$S_c = K \times I_{S\,(50)}$$

S_c = Uniaxial compressive strength, MPa

K = Index to strength conversion factor that depends on the site-specific correlation between S_c and I_s for a specific specimen with a test diameter (D), MPa

Table 12. Generalized index to strength conversion factor (K).
(Source: Bieniawski 1975)

Core Size, mm	Value of "K" (Generalized)
21.5 (Ex Core)	18
30	19
42 (Bx Core)	21
50	23
54 (Nx Core)	24
60	24.5

In this study, a test diameter (D) of samples varied between 20-30 mm (Appendix B). The strength conversion factor (K) was determined as 19 according to the generalized values for the site-specific correlation factor given in ASTM (1985) to calculate the uniaxial compressive strengths of the mortars (Table 12).

2.2.5. Determination of Raw Material Compositions

Raw material composition analyses provided information about binder/aggregate ratios and the particle size distributions of the aggregates. The ratio of lime and acid-insoluble aggregate used in the preparation of the mortars were determined by dissolving carbonated lime ($CaCO_3$) in dilute hydrochloric acid (Jedrzejevska 1981). Determination of particle size distributions of aggregates was carried out by sieving analysis.

In the analysis, one sample was prepared from each mortar and dried in an oven then weighed (M_{sam}) by a precision balance. Afterward, samples were left under the solution of dilute hydrochloric acid (5%) until all carbonated lime was entirely dissolved. After filtering the acid-insoluble aggregates with distilled water, aggregates were dried in an oven, and weighed (M_{agg}) by precision balance. Ratios of acid-soluble and insoluble parts were calculated by formulas given below:

Insoluble % = [($M_{sam} - M_{agg}$) / M_{sam}] × 100

Acid Soluble % = 100 – Insoluble %

where;

M_{sam}: Weight of the mortar sample

M_{agg}: Weight of the aggregates

The acid-soluble ratio does not show the accurate composition of mortars, since both carbonated lime and calcareous aggregates are dissolved in dilute hydrochloric acid. Hence, the rough lime ratio must be calculated by taking into consideration of the following formula:

Aggregate % = (100 × Insoluble %) / [((Acid Soluble % × M.W.$_{Ca(OH)2}$) / M.W.$_{Ca(CO3)}$) + Insoluble %]

Lime % = 100 – Aggregate %

where;

M.W.$_{Ca(CO3)}$: Molecular weight of $CaCO_3$ which is 100.

M.W.$_{Ca(OH)2}$: Molecular weight of $Ca(OH)_2$ which is 74.

The particle size distributions of aggregates in mortars were determined by an analytical sieve shaker (Retsch AS200) with a series of sieves 53 µm, 500 µm, 1180 µm. Then, particles remaining on each sieve surface were weighed by a precision balance and their percentages were calculated.

2.2.6. Mineralogical Compositions of Binders, Aggregates, and Lime Lumps

Mineralogical compositions of fine mortar matrices (binders) and aggregates were determined by X-ray diffraction (XRD). Fourier transformed infrared spectroscopy (FTIR) analysis was also used to determine the mineralogical compositions of binders and lime lumps.

XRD analyses were performed by using a Philips X-Pert Pro X-ray diffractometer and a Bruker D8 Advance ECO X-ray Diffractometer (Bruker, Karslruhe, Germany). For the Philips X-Pert Pro X-ray diffractometer, the XRD spectra were collected with CuKα radiation with Ni filter adjusted to 45 kV and 40mA from 2° to 60° with 2θ and a scan speed of 1.6o per minute. The analyses were performed on finely ground samples of less than 63 μm. The mineral phases in each X-ray diffraction spectrum were identified by using The Philips X'Pert Graphics and Identity software program.

For the Bruker D8 Advance ECO X-ray Diffractometer (Bruker, Karslruhe, Germany), the XRD spectra were collected with CuKα radiation with Ni filter adjusted to 40 kV and 40 mA from 5° to 60° with 2θ and using a step interval of 0.02°, with a step counting time of 3 s. The analyses were performed on mortar samples. Minerals have been identified by using Diffrac Eva software.

FTIR analyses were performed by Spectrum BX II FTIR spectrometer (Perkin Elmer). The powdered binders and lime lumps scraped from mortars were in about 80 milligrams of spectral grade potassium bromide (KBr) and pressed into pellets under 10 tons/cm^2 pressure. Spectra were normally acquired with the use of 4 cm^{-1} resolution yielding IR traces over the range of 400 to 4000 cm^{-1}. All data were corrected for pure KBr spectrum.

2.2.7. Chemical Compositions of Binders, Aggregates, and Lime Lumps

Chemical compositions of binders, aggregates, and lime lumps were determined by Scanning Electron Microscope (SEM) equipped with X-Ray Energy Dispersive System (EDS). SEM-EDS analyses were performed by a Quanta 250FEG. SEM-EDS analyses of lime lumps were performed on pieces scraped from broken surfaces of mortar samples. SEM-EDS analysis of binders and aggregates was performed with samples that

were ground to the fineness of less than 63μm, then pressed into pellets prepared by pressing powder samples under 10 tons/cm^2 pressures. Proper sizes of samples were prepared and dried in an oven (40 ℃) for at least 24 hours for the analysis. In the analysis, samples were not coated with gold. Results were taken from three areas and average values were calculated. The elemental compositions were given in the form of oxides and normalized to 100%.

2.2.8. Pozzolanic Activities of Aggregates

Pozzolanic activities of fine aggregates (less than 63 μm) were determined by measurement of electrical conductivity differences. The differences in electrical conductivities (mS/cm) before and after the addition of fine aggregates into saturated calcium hydroxide solution with a ratio of 1g./40 ml. were measured after 120 seconds (Luxán, Madruga, and Saavedra 1989). Electrical conductivity differences of more than 2 mS/cm can be accepted as a good pozzolanicity (Luxán, Madruga, and Saavedra 1989).

2.2.9. Geochemical Characterization of Aggregates

The total alkali-silica (TAS) diagrams as a geochemical study were the widely used diagrams to classify volcanic aggregates used in mortars. The TAS diagram contributed to find the provenance of aggregates used in Roman lime mortars, and it helped us to determine the type of volcanic rocks (Le Maitre et al. 2002). In the present study, this method was used in the geochemical characterization of fine aggregates of *opus caementicium* mortars. The results of chemical compositions of aggregates determined by EDS analysis were used to create the total alkali-silica (TAS) diagram (Le Maitre et al. 2002). This diagram included the percentages of SiO_2 and $Na_2O_3 + K_2O$ and the type of rocks such as trachyte, foidite, basalt, andesite, dacite, rhyolite.

2.2.10. Hydraulic Properties of Binders

The hydraulic properties of fine mortar matrices (binders) were defined with thermogravimetric analysis (TGA) by using Shimadzu TGA-21. The analysis was carried out in a static nitrogen atmosphere at a temperature range of 30-1000 ℃ with a heating

rate of 10ºC/min. The weight losses at 200º-600ºC and 600-900 ºC were measured. Weight loss at 200ºC is due to the loss of hygroscopic (absorbed) water and at 200º-600ºC weight loss is due to the loss of chemically bound (H_2O) water of hydraulic products. Weight loss over 600ºC is mainly due to the loss of carbon dioxide (CO_2) released during the decomposition of carbonated lime. If the CO_2/H_2O ratio is between 1 and 10, the mortars can be accepted as hydraulic (Bakolas et al. 1995; Moropoulou, Bakolas, and Bisbikou 2000).

In addition, hydraulic index (H.I.) calculated by SEM-EDS analysis of the binder was used to determine the hydraulic properties of mortars. Hydraulic index of binders and lime lumps were defined by Boynton formula (Boynton 1980) and expressed as follows:

$$H.I. = (Al_2O_3\% + Fe_2O_3\% + SiO_2\%) / (CaO\% + MgO\%)$$

Boynton formula referred to the ratio of total percentages of Al_2O_3, Fe_2O_3, and SiO_2 to the total percentages of CaO and MgO that can be used to calculate hydraulic indexes (Boynton 1980).

2.2.11. Microstructural Properties

The microstructure of mortars was determined by using a Quanta 250FEG Scanning Electron Microscope (SEM) equipped with X-Ray Energy Dispersive System (EDS). SEM-EDS analyses were performed to understand the characteristics of fine aggregates-binder interfaces and the general microstructure of mortars. Proper sizes of samples were prepared and dried in an oven (40 ºC) for at least 24 hours for the analysis. In the analysis, samples were not coated with gold. These analyses were carried out on powder samples of fine aggregates and broken and polished surfaces of mortar samples by using backscattered electron (BSE) modes at several magnifications.

CHAPTER 3

RESULTS AND DISCUSSIONS

Basic physical properties, raw material compositions, mechanical properties, mineralogical and chemical compositions, microstructural and hydraulic properties of Roman lime mortars, characteristics of lime, and mineralogical and chemical compositions, microstructural properties, pozzolanic activities, and geochemical characteristics of aggregates in these mortars were determined. Besides, visual analyses of the mortars were carried out to understand their macroscopic features. The results of the analyses and the discussions are given in this chapter.

3.1. Visual Analyses

Roman mortars can be described according to the presence (*opus signinum)* and absence (*opus caementicium)* of crushed brick/tile/ceramic fragments by visual analyses. In this study, forty-eight of mortars were *opus caementicium* and nine of mortars were *opus signinum. Opus caementicium* mortars were found in various types of structures such as bath, stadium, agora, while *opus signinum* mortars were generally used in water-related structures such as bath and cistern.

Opus caementicium mortars were mainly whitish, greyish, and light brownish color and had crushed stones aggregates. They were relatively compact and heterogeneous mortars. Lime lumps were visible to the naked eye in most of the samples. The grain size was diverse and poorly sorted. The aggregates coarser than 1 mm were greyish/light greyish and rarely brownish and pinkish (Table 13, Appendix E). According to the Munsell Soil Color Chart, the colors of fine aggregates varied between "white", "pinkish white", "gray", "pinkish gray", "grayish brown", "light brown" and "brown" (Munsell Color 2013).

Table 13. Colors of aggregates defined by visual analyses and Munsell Soil Color Chart

Sample Name	Color of Aggregates	
	>1180 µm	< 53 µm
	Visual Analysis	Munsell Soil Color Chart
ACyH	Reddish	2.5YR 5/3 Reddish Brown
ACyT	Greyish	7.5YR 8/1 White
CEB	Brownish	7.5YR 6/2 Pinkish Gray
CKC	Brownish	7.5YR 6/4 Light Brown
CKCs	Pinkish	5YR 7/3 Pinkish Gray
CLB1	Reddish	5YR 7/3 Pinkish Gray
CLB2	Greyish	10YR 8.5/1 White
CStB	Reddish	10YR 8/1 White
CStT	Reddish	10YR 8/1 White
CTrG	Pinkish	10YR 8/2 Very Pale Brown
CTrB	Reddish	2.5YR 8/3 Pink
IAnAq	Greyish	10YR 6/2 Light Grayish Brown
IAnB	Greyish	10YR 6/2 Light Grayish Brown
IMA	Greyish	10YR 6/1 Gray
IMG	Brownish	7.5YR 5/3 Brown
IMS	Brownish	10YR 6/1 Gray
IPyH	Greyish	10YR 6/2 Light Grayish Brown
IPrB	Brownish	7.5YR 5/3 Brown
IPrH	Brownish	7.5YR 5/3 Brown
IPrT	Brownish	7.5YR 5/3 Brown
ITCs	Greyish	5YR 7/2 Pinkish Gray
ITT	Greyish	N 9.5 White
LPtB	Reddish	5YR 7/4 Pink
LPtC	Pinkish	7.5YR 8/2 Pinkish White
LPtT	Reddish	2.5YR 6/3 Light Reddish Brown
LTlB	Reddish	5YR 7/3 Pink
LTlS	Whitish	10YR 5/2 Grayish Brown
LTlT	Whitish	7.5YR 8/2 Pinkish White

(cont. on next page)

Table 13. (cont.)

Sample Name	Color of Aggregates	
	>1180 µm	< 53 µm
	Visual Analysis	Munsell Soil Color Chart
LXT	Brownish	10YR 5/2 Grayish Brown
LySrU	Pinkish	5YR 7/2 Pinkish Gray
LyTpA	Greyish	10YR 6/2 Light Grayish Brown
LyTpB	Greyish	7.5YR 8.5/1 White
LyTpT	Greyish	10YR 8.5/1 White
MPB	Greyish	5YR 7/1 Light Gray
MPB2	Greyish	5YR 7/1 Light Gray
MPC	Greyish	5YR 7/1 Light Gray
PhAzB	Pinkish	7.5YR 5/2 Brown
PhLdB	Greyish	7.5YR 6/1 Gray
PCT	Brownish	10YR 6/3 Pale Brown
PCB	Brownish	10YR 6/2 Light Brownish Gray
PCC	Brownish	10YR 4/2 Dark Grayish Brown
PmLyB	Brownish	7.5YR 6/4 Light Brown
PmLyCs	Brownish	10YR 5/2 Grayish Brown
PmLyC	Greyish	10YR 8.5/1 White
PAtT	Greyish	10YR 8/1 White
PSlB	Greyish	7.5YR 8/2 Pinkish White
PSlS	Greyish	7.5YR 8/1 White
PSlT	Greyish	7.5YR 9/1 White
PSB	Greyish	7.5YR 8/1 White
PSA	Greyish	7.5YR 9/1 White
PST	Greyish	7.5YR 9/1 White
TAB	Reddish	2.5YR 7/2 Pale Red
TACs	Greyish	10YR 8.5/1 White
TAxB	Greyish	10YR 8.5/1 White
TAxG	Greyish	10YR 8.5/1 White

Opus signinum mortars had light brownish and greyish color with crushed brick and/or ceramic additions. They are relatively compact and heterogeneous mortars. Unmixed lime lumps appeared in different sizes and shapes, and in some samples, they had large cracks in them. The grain size was diverse and poorly sorted. The apparent type of the aggregate was generally crushed brick/tile/ceramic fragments, and they were reddish (Table 13, Appendix E). The colors of fine aggregates determined as "white", "pink" and "reddish brown" by the Munsell Soil Color Chart (Munsell Color 2013). Regarding the shapes of aggregates, the angular shape was predominant in the aggregates due to the use of crushed stones and crushed ceramic additions.

Similar colors of mortars and fine aggregates have been observed in many studies conducted on Roman lime mortars (Cardoso et al. 2014; Belfiore et al. 2015; Benedetto et al. 2018; Izzo et al. 2018; Moreno-Alcaide and Compaña-Prieto 2018; Borsoi et al. 2019).

3.2. Basic Physical Properties

The basic physical properties of mortars could be described by density and porosity values, and pore size distribution of the mortars.

3.1.2. Density and Porosity

Density values of mortars were in the range of 1.2-1.9 g/cm^3 and the average value of 1.7 g/cm^3 (Figure 15, Appendix A). Density values of *opus caementicium* and *opus signinum* samples were between 1.3-1.9 g/cm^3 and 1.2-1.9 g/cm^3, respectively.

Related to the density values, the porosity values of samples were between 26-53% and the average of 37% by volume (Figure 16, Appendix A). Porosity values were between 27-46% for *opus caementicium* and 26-53% for *opus signinum* samples.

Opus signinum samples were relatively less dense and more porous than o*pus caementicium* ones. This can be explained by the use of porous and light ceramic materials as aggregates.

All samples showed lower density and higher porosity according to cement mortar. Cement mortars need more water for workable consistency which makes the

mortar denser due to less air content in the mortar (Chen, Wu, and Zhou 2013; Odler and Rößler 1985).

Density and porosity values for all regions were almost similar to each other except the Lycia region. Lycia presented a broader range of values due to the two exceptions (*LPtB* and LXT). These exceptions may be explained by the use of calcareous aggregates in these mortars (Figure 15 and Figure 16).

	Aiolis	Caria	Ionia	Lycia	Lydia	Mysia	Pamphylia	Phrygia	Pisidia	Troas
Max.	1.68	1.79	1.86	1.93	1.82	1.72	1.65	1.81	1.86	1.64
Min.	1.35	1.43	1.52	1.20	1.73	1.57	1.40	1.72	1.33	1.52
Ave.	1.52	1.64	1.71	1.66	1.78	1.64	1.56	1.77	1.60	1.58
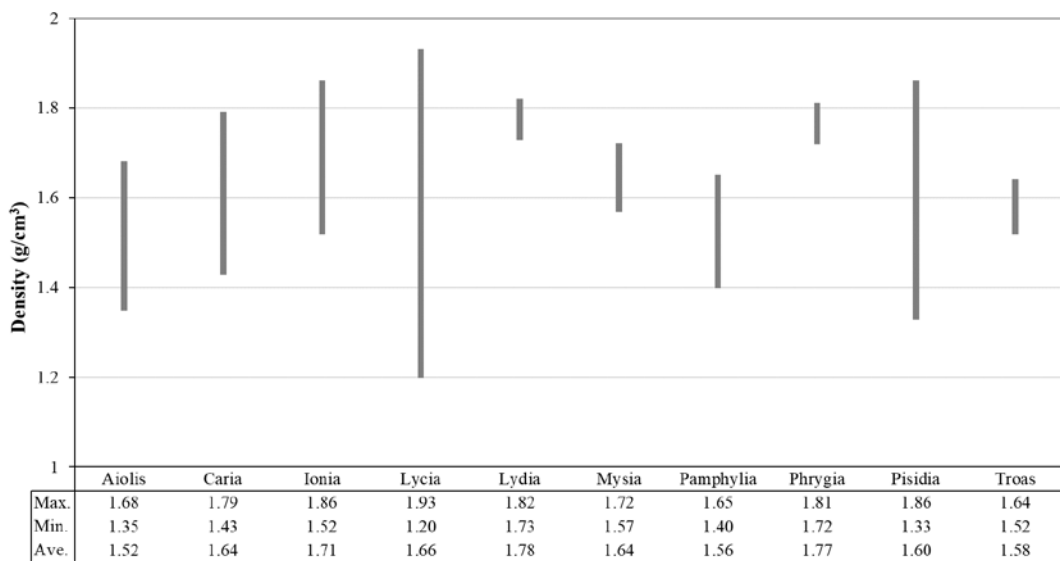
Figure 15. Density values of Roman lime mortars.

	Aiolis	Caria	Ionia	Lycia	Lydia	Mysia	Pamphylia	Phrygia	Pisidia	Troas
Max.	48.21	42.21	44.27	53.21	34.43	38.74	45.67	34.77	48.03	43.94
Min.	35.41	30.99	29.02	25.99	30.52	34.00	37.73	31.65	28.50	35.75
Ave.	41.81	36.15	34.84	36.83	32.69	36.50	40.48	33.21	38.27	38.90
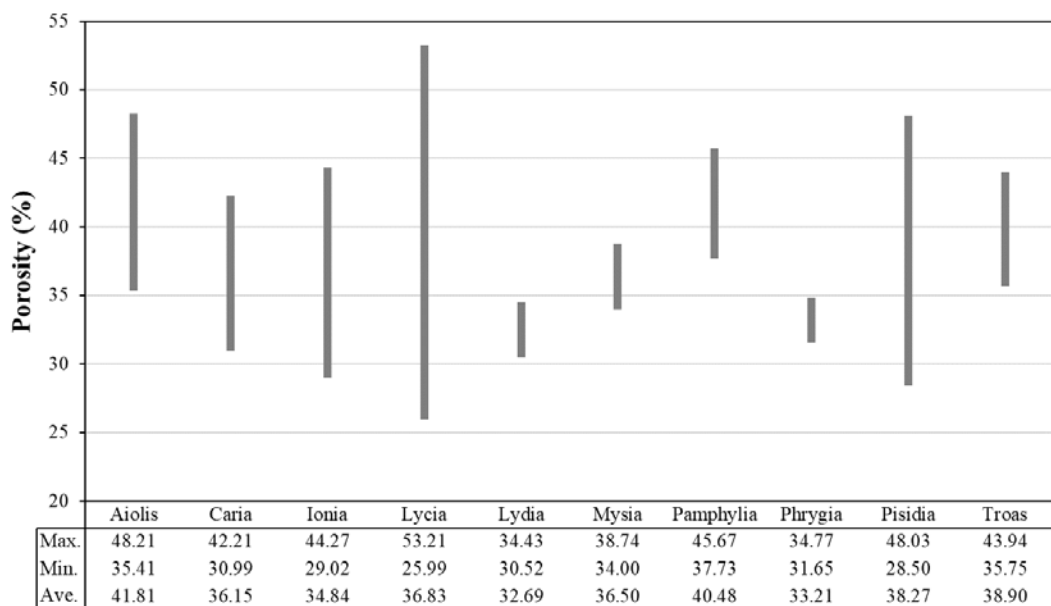
Figure 16. Porosity values of Roman lime mortars.
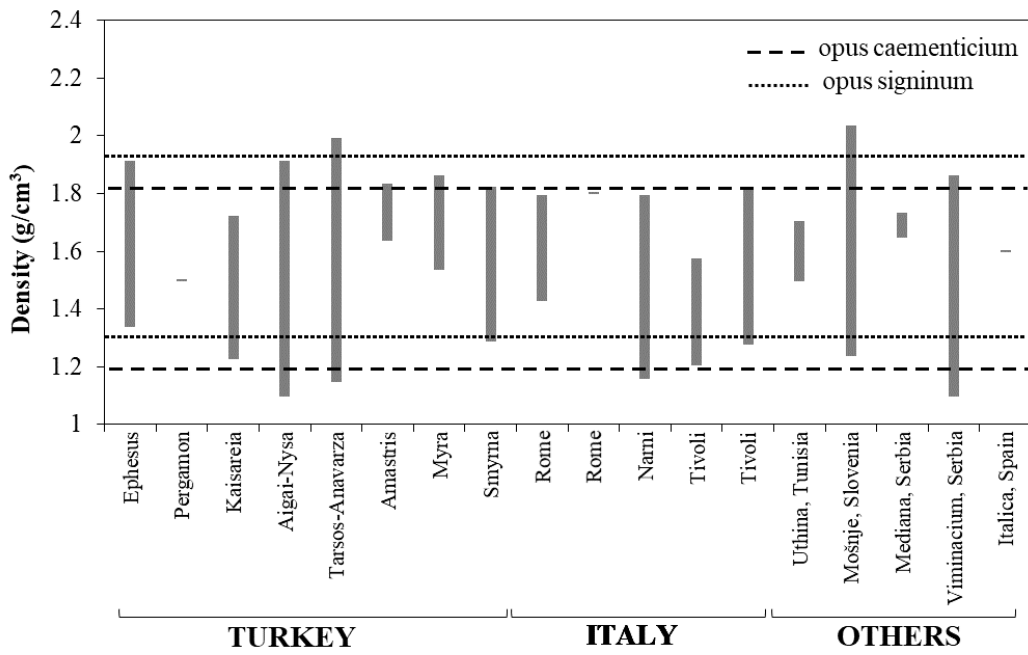
Figure 17. Comparison of density values with the literature review.
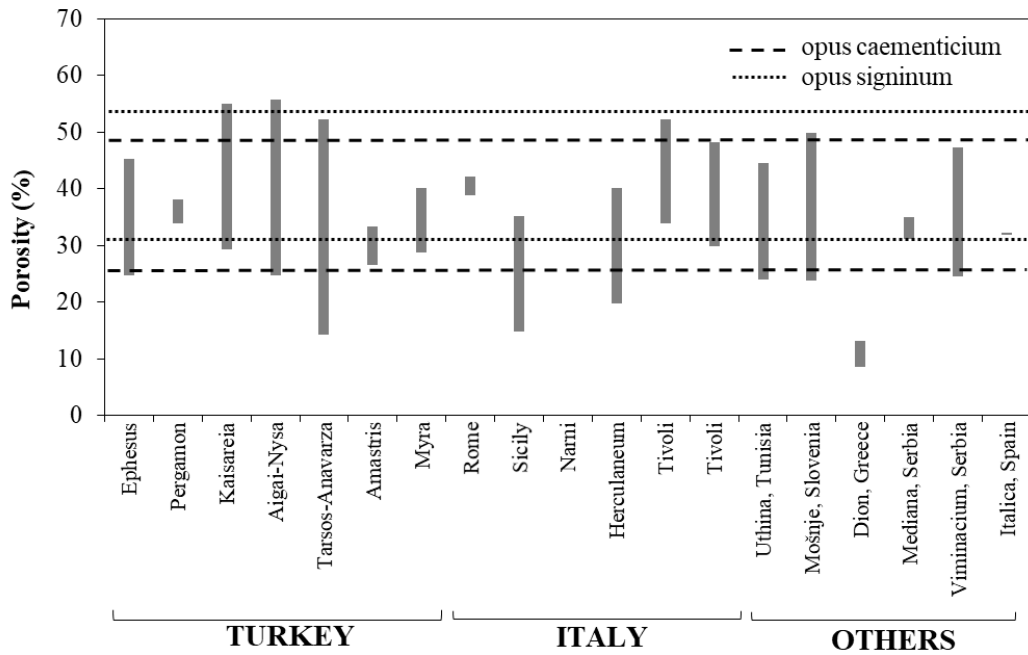
Figure 18. Comparison of porosity values with the literature review.

In general, all density values were almost in the same ranges with lime mortars used in several Roman Period buildings located in Turkey (1.1-2.0 g/cm^3), Italy (1.2-1.8 g/cm^3), and other countries (1.1-2.0 g/cm^3) (Table 2-4, Figure 17). Also, the porosity values of the Roman lime mortars showed nearly similar values to other structures from

Turkey (14.5-55.5%), Italy (15-52%), and other countries (8.8-49.7%) (Table 2-4, Figure 18). References were given in Table 2-4. These behaviors can be ascribed to the similarities of the raw material source, ratios of materials, and production technology.

3.1.3. Pore Size Distribution

Porosity and pore size distribution were one of the important physical properties of lime mortars. They affect the carbonatation process and hardening, and therefore, the strength and durability of the lime mortars. Previous studies have explained the relationship between strength and porosity (Odler and Rößler 1985; Kumar and Bhattacharjee 2003; Jackson et al. 2009; Arandigoyen et al. 2006; Izaguirre, Lanas, and Álvarez 2010; Santos et al. 2018). Although porosity was not the only factor on strength, finer pores mortar had higher strength than the coarser one at the same total porosity (Chen, Wu, and Zhou 2013; Odler and Rößler 1985). Previous studies also indicated that the reduction in the mean pore size prevented the absorption of liquid water, blocking its later freezing and expansion damage, and thus providing better resistance against freezing-thawing cycles (Nikolić et al. 2016).

The pore size distributions and mean pore size diameter of the twelve selected mortars were determined by MIP (Figure 19). Three of these samples were *opus signinum* mortars.
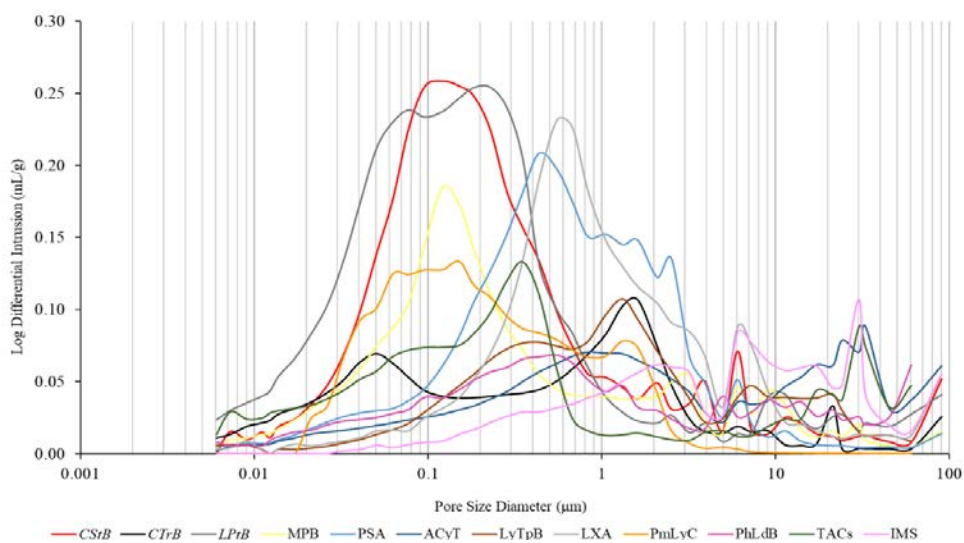
Figure 19. Log differential intrusion versus pore size of the analyzed samples.

According to the results, _CStB_ was unimodally distributed, with a well-defined peak being around 0.1 μm. _CTrB_ indicated the bimodal distribution of pores with peaks around 0.5 μm and 3 μm. _LPtB_ was unimodally distributed with a broad pore size distribution within the range of 1 to 0.01 μm, without a well-defined peak.

MPB showed unimodal distribution with a clear peak of around 0.1 μm. PSA differed from the others by exhibiting a broad pore size distribution within the range of 3 to 0.06 μm. ACyT was unimodally distributed, with a peak of around 0.2 μm. LyTpB indicated the bimodal distribution of pores with peaks around 0.5 μm and 2 μm. LXA indicated the bimodal distribution of pores with peaks around 0.5 μm. PmLyC was bimodally distributed with a broad pore size distribution without a well-defined peak around 0.1 μm. PhLdB was unimodally distributed, with a well-defined peak being around 0.6 μm. TACs was bimodally distributed with a minor intrusion peak at around 32 μm and a larger intrusion peak at around 0.4 μm. IMS showed three different peaks around 2 μm, 6 μm, and 30 μm.

The main peaks were around 0.5 to 0.1 μm, except in the case of _CTrB_, where the distribution curve was slightly shifted to the right (Figure 19). _Opus signinum_ mortars, _CStB_ and _LPtB_ presented the highest porosity with the unimodal distribution and well-defined peaks. In addition, regarding the mean pore size diameter of analyzed samples, _opus signinum_ mortars had lower mean pore size diameter than _opus caementicium_ mortars (Table 14).

Table 14. Mean pore size diameter of analyzed mortars.

Opus caementicium samples	Mean Pore Size Diameter (μm)	_Opus signinum_ samples	Mean Pore Size Diameter (μm)
ACyT	0.29	_CStB_	0.13
IMS	1.37	_CTrB_	0.09
LyTpB	0.32	_LPtB_	0.08
LXA	0.39		
MPB	0.11		
PmLyC	0.79		
PhLdB	0.23		
PSA	0.22		
TACs	0.11		

An in-depth analysis of pore size distribution is not within the scope of this study regarding the impact of the mechanical chracteristics of mortars. However, in a limited number of analyzed samples, the lower mean pore size diameter of *opus signinum* mortars can provide the better durability to them than *opus caementicium* mortars parallel to the results of the point load test (Table 14). Different distribution of pore sizes could be attributed to the nonhomogeneous characteristics of Roman mortars, even though some predominant results were obtained.

3.3. Mechanical Properties

Uniaxial compressive strength measurements in the dry state obtained by the point load test were used to evaluate the mechanical properties of the mortars. The strength values of the three samples (*LTIB*, LTIS, PhAzB) could not be calculated due to the insufficient size of the samples. The compressive strength values of the mortars were found between 2.01-12.22 MPa and this range corresponded to NHL3.5 type of lime based on the compressive strength of laboratory mortars after 28 days (Appendix B) (UNI EN 459-1 2001). However, CKC (17.15 MPa), a non-hydraulic lime mortar, had the highest value as an exception. The compressive strength values of *opus caementicium* and *opus signinum* mortars were 2.01-12.22 MPa and 2.63-10.49 MPa, respectively. The compressive strength of mortars used in structural elements such as arch and vault was more than 5 MPa for hydraulic mortars with pozzolanic aggregates.

In the literature on mortars, there seems to be general agreement that pozzolanic activity, hydraulicity, porosity, binder content, the presence of ceramic and limestone aggregates in the mortars could affect the strength and durability of the mortar (Schiller 1971; Odler and Rößler 1985; Kumar and Bhattacharjee 2003; Velosa et al. 2010; Degryse, Elsen, and Waelkens 2002; Lanas and Alvarez 2003; Santos et al. 2018). The mortars having high pozzolanic activity and hydraulicity showed higher compressive strength values. A lower porosity in mortars with adequate binder content led to higher strength (Schiller 1971; Odler and Rößler 1985; Kumar and Bhattacharjee 2003). A higher binder content can increase durability due to the self-healing properties of lime (Velosa et al. 2010). The type and shape of aggregates can also make an impact on durability in addition to their mineralogy (Degryse, Elsen, and Waelkens 2002; Velosa et al. 2010; Santos et al. 2018). However, in the present study, it was not possible to define

the relationship between these parameters in detail. This was due to the similar results varying in a rather narrow range of values and also point load test may not provide precise measurements regarding the durability of mortars (Appendix H).

Nevertheless, it can be said that most of lime mortars with compressive strength values more than 9 MPa presented binder content greater than 90%, fine aggregates of these mortars showed SiO_2 content more than 85% and lime lumps in these mortars had SiO_2 content more than 5%.
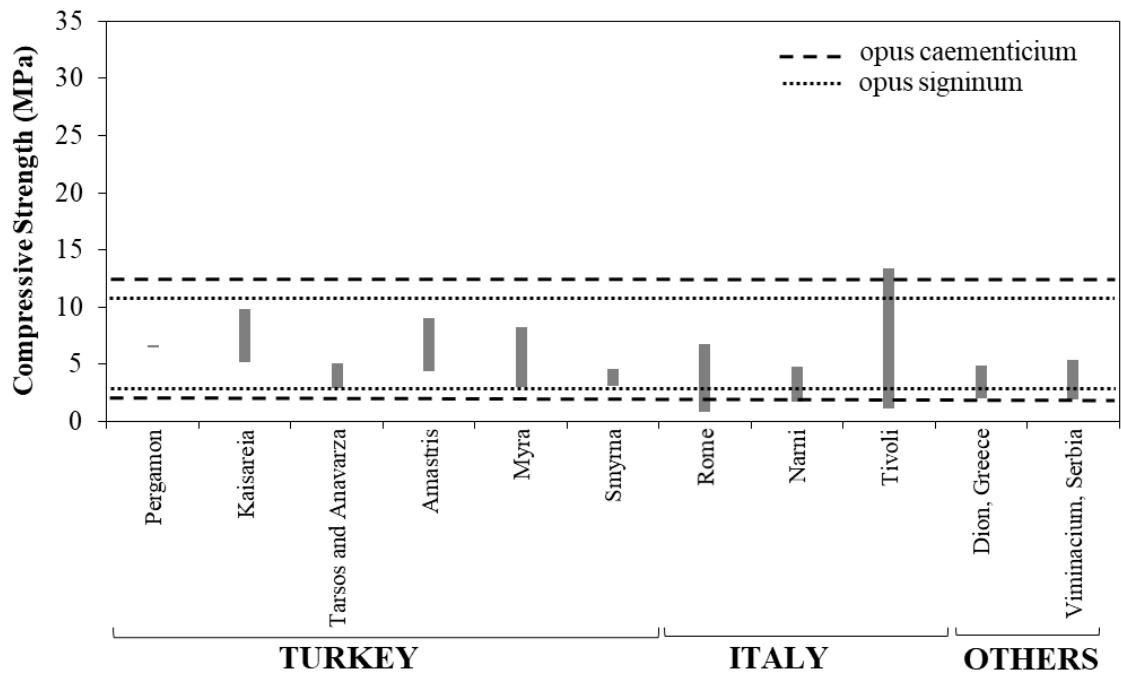
Figure 20. Comparison of the compressive strength values with the literature review.

In this study, Roman lime mortars with pozzolanic aggregates were also found as hydraulic with the compressive strength values varying 2 MPa and 12 MPa. The compressive strength values were in almost similar ranges with the values of lime mortars used in other structures from the Roman Period located in Turkey (3-9.7 MPa), Italy (2-13 MPa), and other countries (2-5.3 MPa) (Table 9, Figure 20). References can be found in Table 9.

3.4. Raw Material Compositions

The raw material compositions of mortars define their physical, mechanical, and durability characteristics. In this study, lime/aggregate ratios and particle size distribution of aggregates by weight were investigated to understand the raw material compositions of Roman lime mortars.

3.4.1. Lime/Aggregate Ratios

Lime/aggregate ratios of mortars varied between 1:4-3:2 by weight without the exceptions (Figure 21, Appendix B). Exceptions from Lycia, Pisidia, and Pamphylia regions showed lime/aggregate ratios in the range of 5:2-28:1 by weight (Appendix B). This broad range can be due to the high content of acid-soluble calcareous aggregates in the mortars which was proved by XRD and SEM-EDS analysis. In this respect, lime/aggregate ratios of some mortars (LTIT, LTIS, *LTIB*, PCB, PCT, PCC, LPtC, PSIT, PmLyC) taken from Lycia, Pisidia, and Pamphylia regions cannot be determined due to the dissolution of calcareous aggregates by the current method. Aggregates of mortars sampled from Lycia, Pamphylia, and Pisidia regions showed a high content of CaO that can be regarded as the abundance of calcareous aggregates in these regions. These regions were also lack of volcanic zones, as seen in maps (Figure 67 and Figure 68). On the contrary, limestones were abundant in these regions (Erkanol and Aydındağ 2013).

Lime/aggregate ratios of *opus caementicium* and o*pus signinum* samples were between 1:6-5:2 and 1:2-2:1 by weight, respectively. The average lime/aggregate ratio was found almost 1:1 by weight.
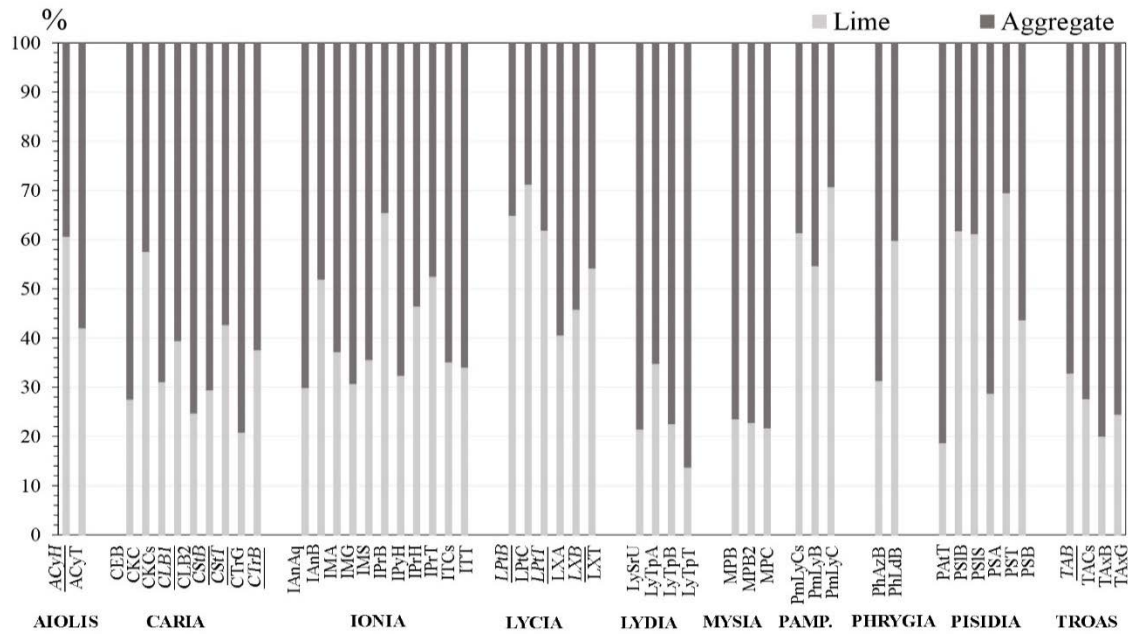
Figure 21. Lime/aggregate ratios of Roman lime mortars.

According to the results, the lime/aggregate ratios of mortars were almost in similar ranges. Furthermore, there was a tendency in similar lime/aggregate ratios in each region. The amount of binder used was mainly high in all mortars (Appendix B). However, the exceptionally high content of acid-soluble (70.7-96.5%) found in some mortars was due to the calcareous aggregates which were observed in the analyses. Moreover, mortars with higher lime content (over 60%) were more porous (over 40%) than the others due to the need for a less amount of water.
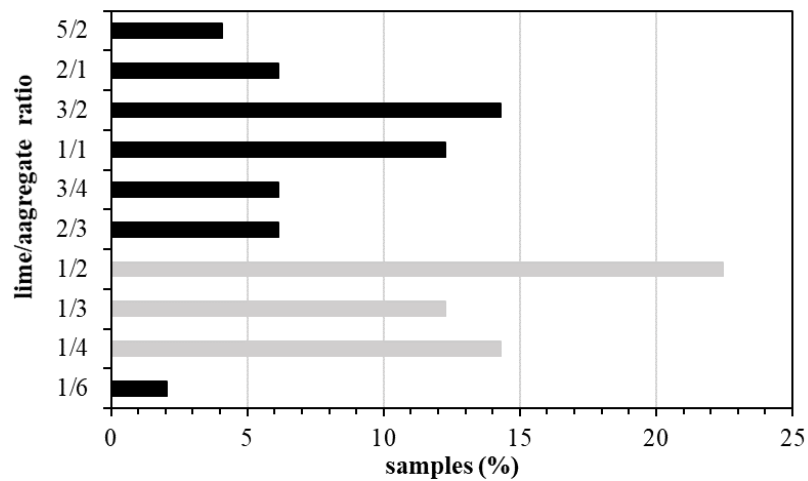
Figure 22. Percentages of lime/aggregate ratios of Roman lime mortars.
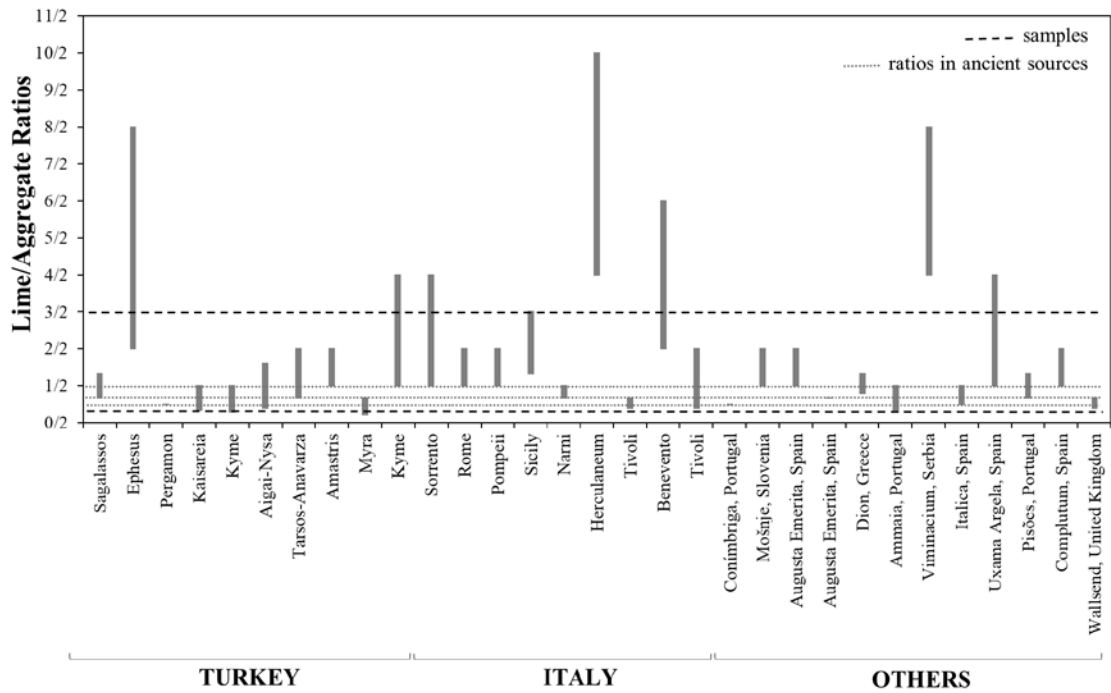
Figure 23. Comparison of lime/aggregate ratios with the literature review.

Half of the mortars presented the 1:2, 1:3, and 1:4 lime/aggregate ratios given in the historic sources written in the Roman Period (Figure 22). These values were considerably similar to many sites in Turkey (Sagalassos, Pergamon, Kyme, Aigai, Nysa, Tarsos, Anavarza, Amastris), Italy (Rome, Narni, Tivoli), Spain (Augusta Emerita, Italica, Comptulum), Portugal (Conímbriga, Ammaia, Pisões), Slovenia (Mošnje), Greece (Dion) and United Kingdom (Wallsend) (Table 2-4, Figure 23). References were given in Table 2-4. However, the rest of the analyzed mortars presented various lime/aggregate ratios like mortars in Turkey (1:9-4:1), Italy (1:5-5:1), and other countries (1:6-4:1) which had a higher lime/aggregate ratio as an exception (Figure 23).

3.4.2. Particle Size Distribution

The distribution of particle sizes of the aggregates is an important feature in the quality of Roman mortars. The well-graded aggregates with a broad range of particle sizes and evenly distributed should be used for higher quality in mortar production (Davey 1961; Holmes and Wingate 1997). In this study, smaller size aggregates were analyzed in a limited range regarding particle size distribution (Figure 24, Appendix C). The

average aggregate content in the mortars was found 53%. Aggregates greater than 1 mm constituted the major fraction of total aggregates in 62% of analyzed samples (Figure 25).
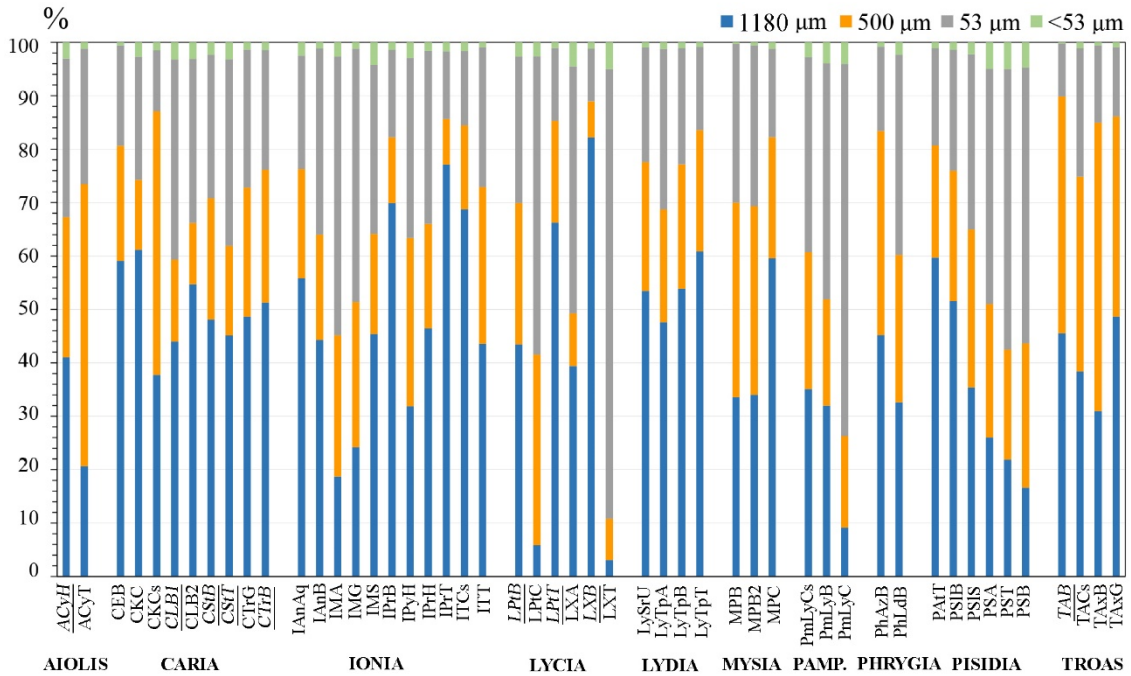
Figure 24. The particle size distribution of aggregates of Roman lime mortars.
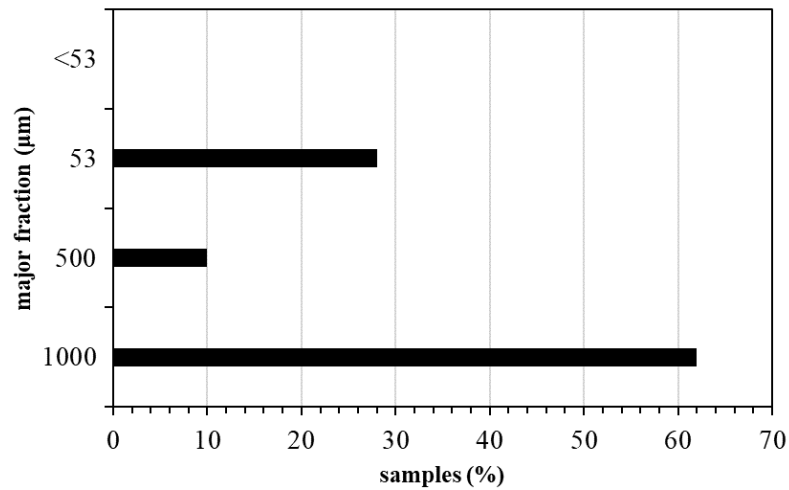
Figure 25. Percentage of the major aggregate fractions in the mortars

The particle size distribution of all samples, given in Table 2-4, presented great similarities with Roman lime mortars from different sites in Turkey (Sagalassos, Ephesus,

Pergamon, Aigai, Nysa, Tarsos, Anavarza, Myra, Smyrna), Italy (Sorrento, Rome, Pompeii, Narni, Tivoli), Spain (Augusta Emerita, Complutum), Portugal (Conímbriga and Pisões) and Serbia (Viminacium) (Table 2-4). Moreover, aggregates with particle sizes coarser than 1180 μm constituted the largest fraction of total aggregates by the recent studies (Columbu, Sitzia, and Ennas 2017; Degryse, Elsen, and Waelkens 2002; Aslan Özkaya 2005; Uğurlu Sağın 2012; Oğuz, Türker, and Koçkal 2015; Felekoğlu et al. 2016; Kuleli 2005; Columbu et al. 2018; Velosa et al. 2007; Nikolić et al. 2016; Borsoi et al. 2019; Ergenç and Fort 2019). These results demonstrated that Romans produced lime mortars by using aggregates of different sizes, particularly coarser than 1 mm.

The particle size distribution of the aggregates determined the volume of space between particles and the quantity of binder needed. For the particle size distribution in inert aggregates, it was suggested that the voids between large grains must be filled with smaller ones (Davey 1961; Santos et al. 2018)). Thus, the total surface area to be covered with lime will be small. This meant less amount of carbon dioxide and less amount of lime which required a less amount of water. After drying, less porous mortar with high strength was obtained (Davey 1961). In addition to this, excessive use of fine aggregates provided a higher surface area to be covered with lime which resulted in a porous mortar with a lower strength (Ashurts and Dimes 1990). Having regard to this information, analyzed mortars composed of more quantity of fine aggregates (63 μm) were more porous than the others.

Overall results provide information on the role of raw materials in Roman lime mortar production. Accordingly, raw material compositions were almost the same in different locations of the Roman Empire, including Turkey, Spain, Portugal, United Kingdom, etc. (Table 2-4). This idea can be a proof of the availability of the local sources of raw materials in these regions.

3.5. Characteristics of Lime

Lime lumps found as round and soft fragments in the mortars were accepted as being the carbonated lime particles used in the production of mortars. Hence, their mineralogical, microstructural, and chemical properties can give information about the lime used in the preparation of the mortars. Some authors demonstrated that these lumps

may have a variety of textures that reflect the nature of the original limestone source rock (Hughes and Leslie 2001; Kurugöl and Güleç 2015).

Limestones provide lime as a raw material of Roman mortars. However, it is hard to find a pure form of calcite in nature. Limestones have mostly impurities and the quantity of these impurities determines the type of limestone (Davey 1961; Boynton 1980). If the quantity of magnesia exceeds 5%, it is not pure lime. If the quantity of silicate exceeds 5%, the lime gains hydraulic properties (Holmes and Wingate 1997).

In the present study, lime lumps in various dimensions were detected in all mortars as a result of the poor labor and mixing used in their production. Detected lime lumps were mainly white color, homogeneous, and hard lumps. They can be considered as calcitic aggregates in the mortars due to incomplete carbonization in lime pits, thus they cannot be mixed with the other aggregates. These lime lumps were analyzed to understand the mineralogical and chemical compositions and hydraulicity.

3.5.1. Mineralogical Compositions

Mineralogical compositions of lime lumps were determined by FTIR analysis instead of XRD analysis due to the small quantity of samples. These analyses showed mortars collected from all regions were composed of calcite crystals and showed the characteristics of $CaCO_3$ bands at ~1430 cm^{-1} (C–O stretching), ~874, and ~712 cm^{-1} (C–O bending) (Figure 26-35). The small bands at ~1000-1200 cm^{-1} (Si-O stretching) and 470 cm^{-1} (Si-O bending) could be attributed to siliceous materials (Figure 26-35). Also, the broadband from ~3250 to 3580 cm^{-1} (O-H stretching) was due to bound water (Figure 26-35).

All regions showed almost similar characteristics concerning minerals of lime lumps. However, these results could not be compared due to the lack of studies. Lime lumps from Aigai and Nysa have been analyzed and XRD patterns of the lime lumps indicated only calcite peaks which were similar to the results of this study (Uğurlu Sağın 2012).
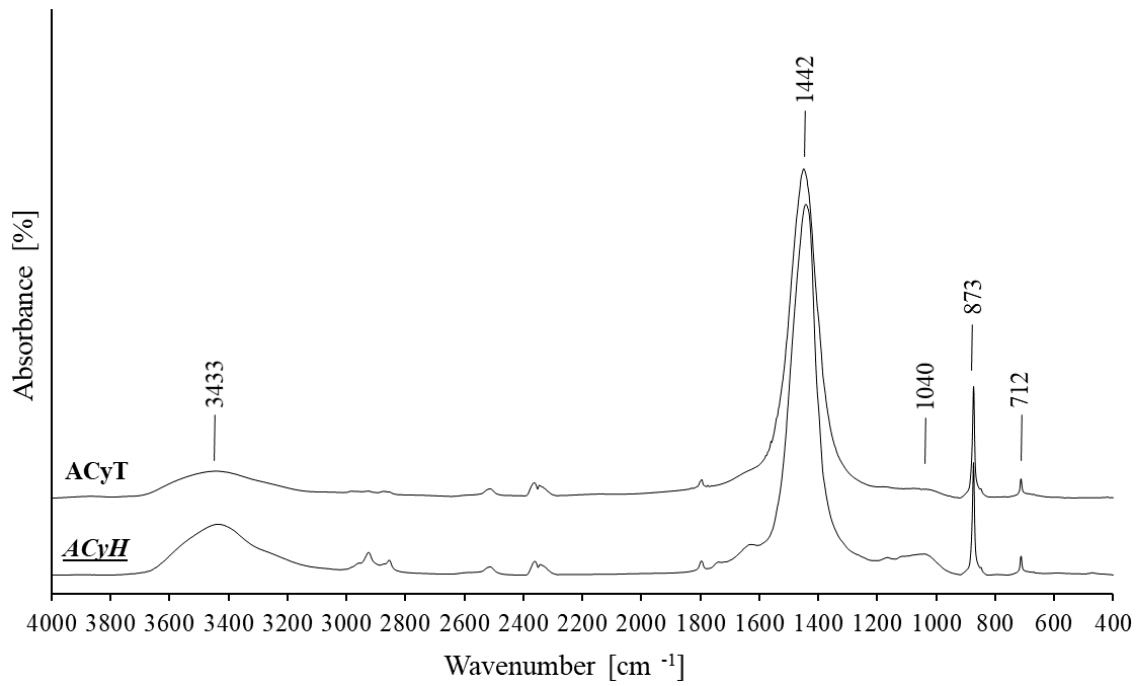
Figure 26. FTIR spectra of lime lumps of Roman lime mortars in Aiolis.
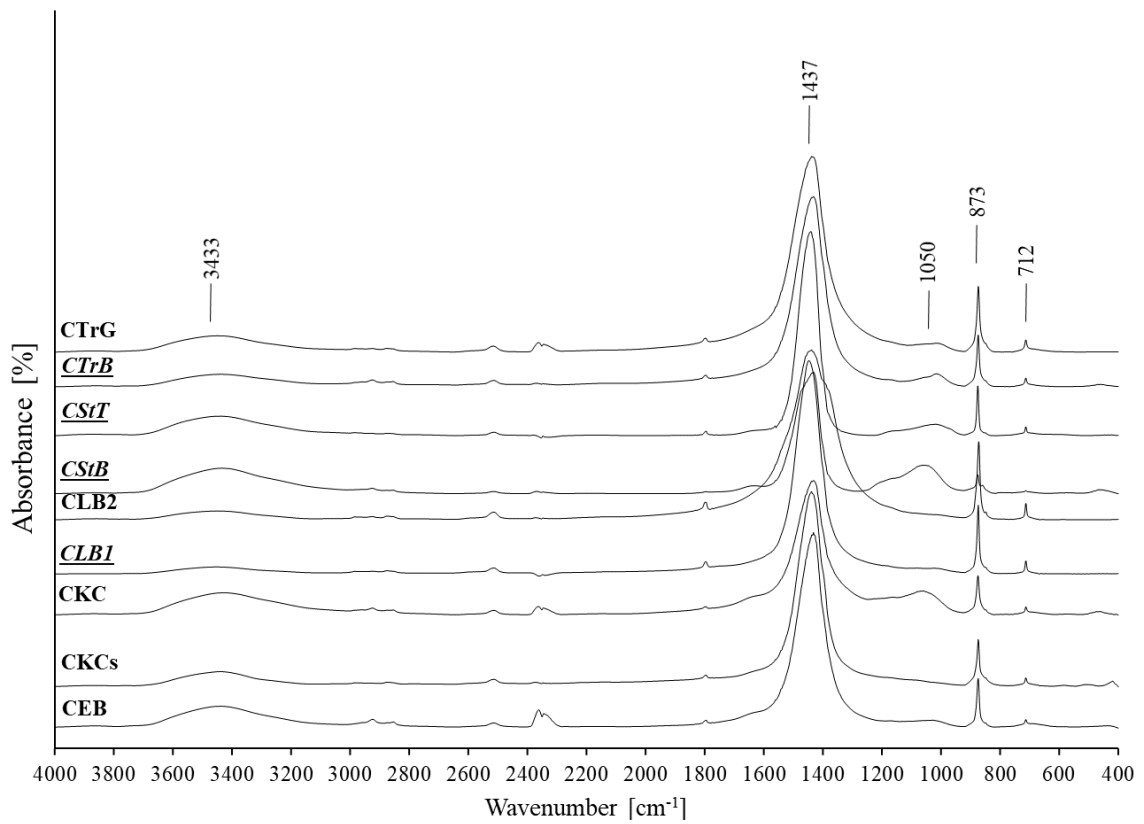
Figure 27. FTIR spectra of lime lumps of Roman lime mortars in Caria.
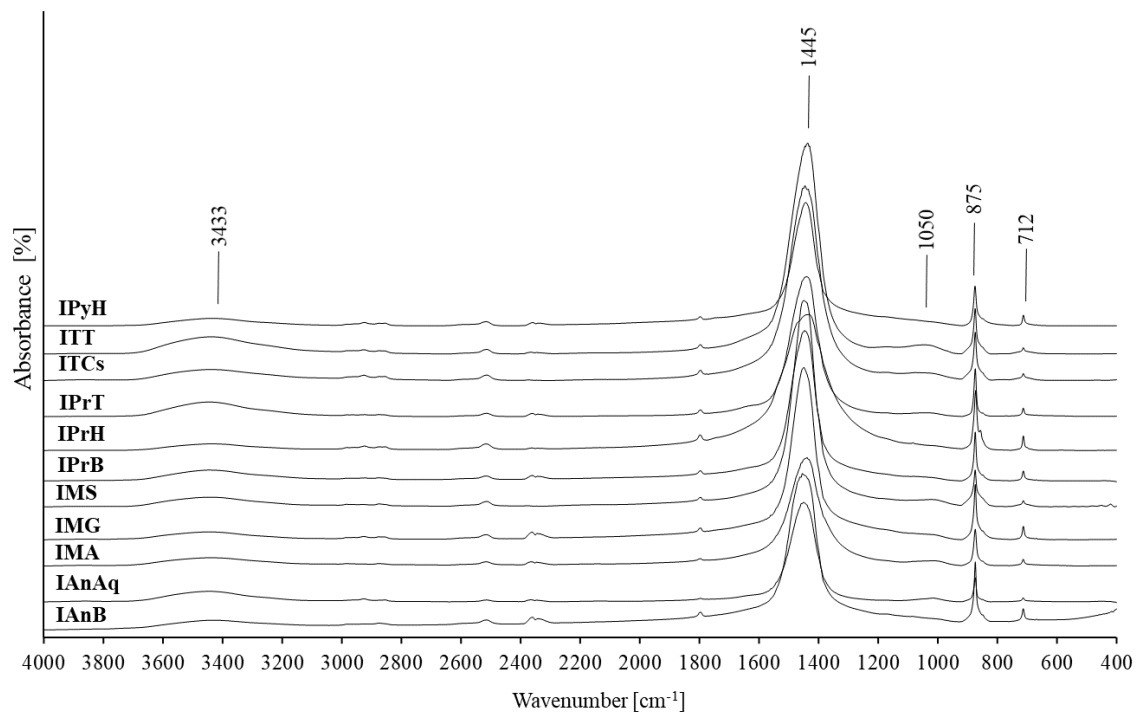
Figure 28. FTIR spectra of lime lumps of Roman lime mortars in Ionia.
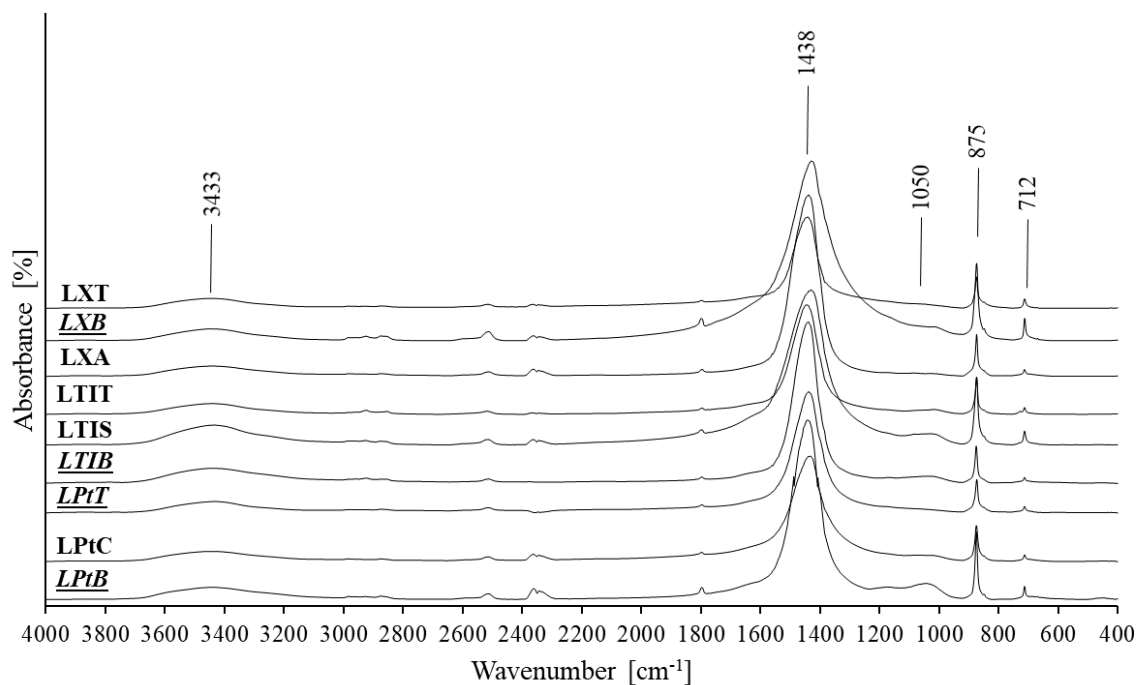
Figure 29. FTIR spectra of lime lumps of Roman lime mortars in Lycia.
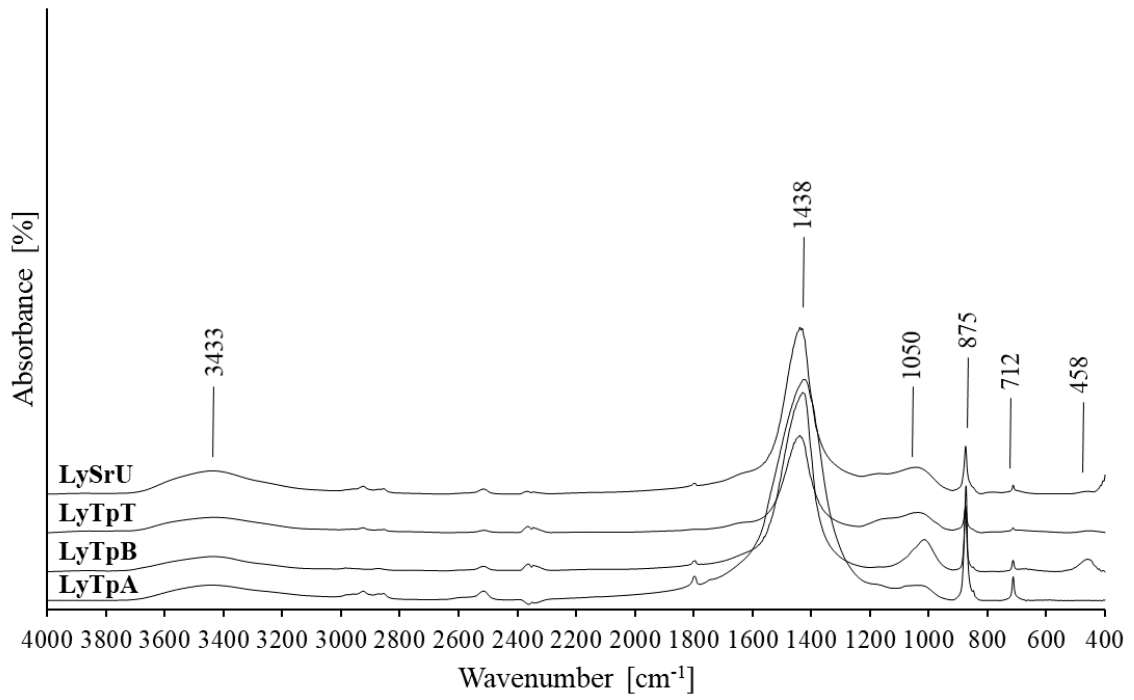
Figure 30. FTIR spectra of lime lumps of Roman lime mortars in Lydia.
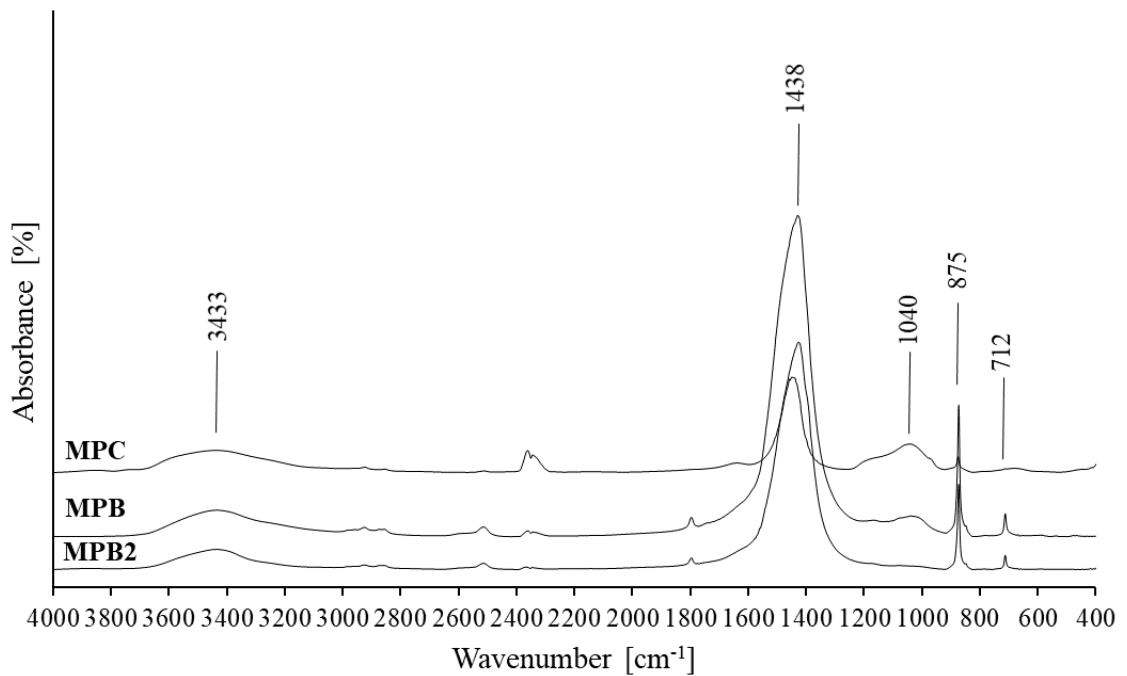
Figure 31. FTIR spectra of lime lumps of Roman lime mortars in Mysia.
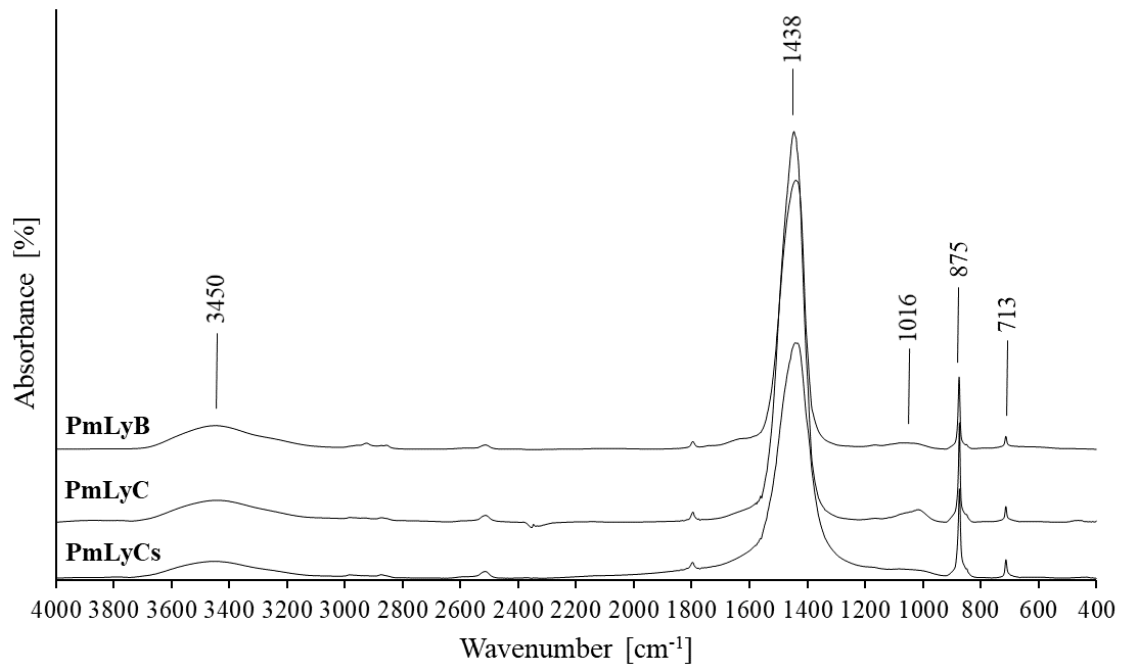
Figure 32. FTIR spectra of lime lumps of Roman lime mortars in Pamphylia.
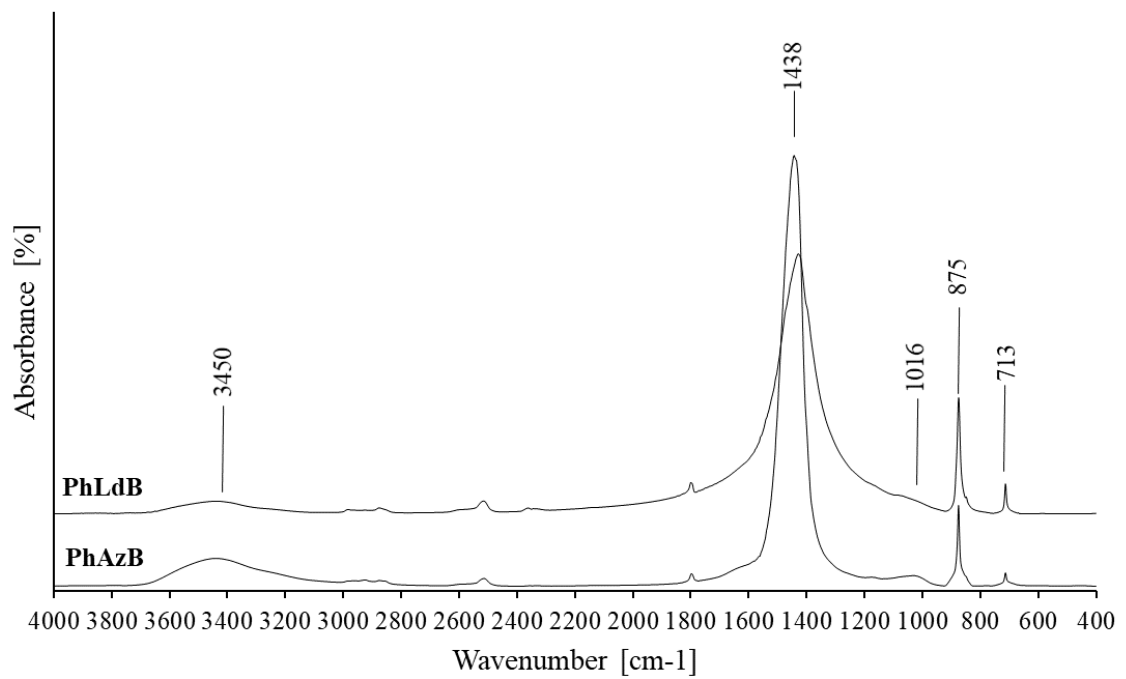
Figure 33. FTIR spectra of lime lumps of Roman lime mortars in Phrygia.
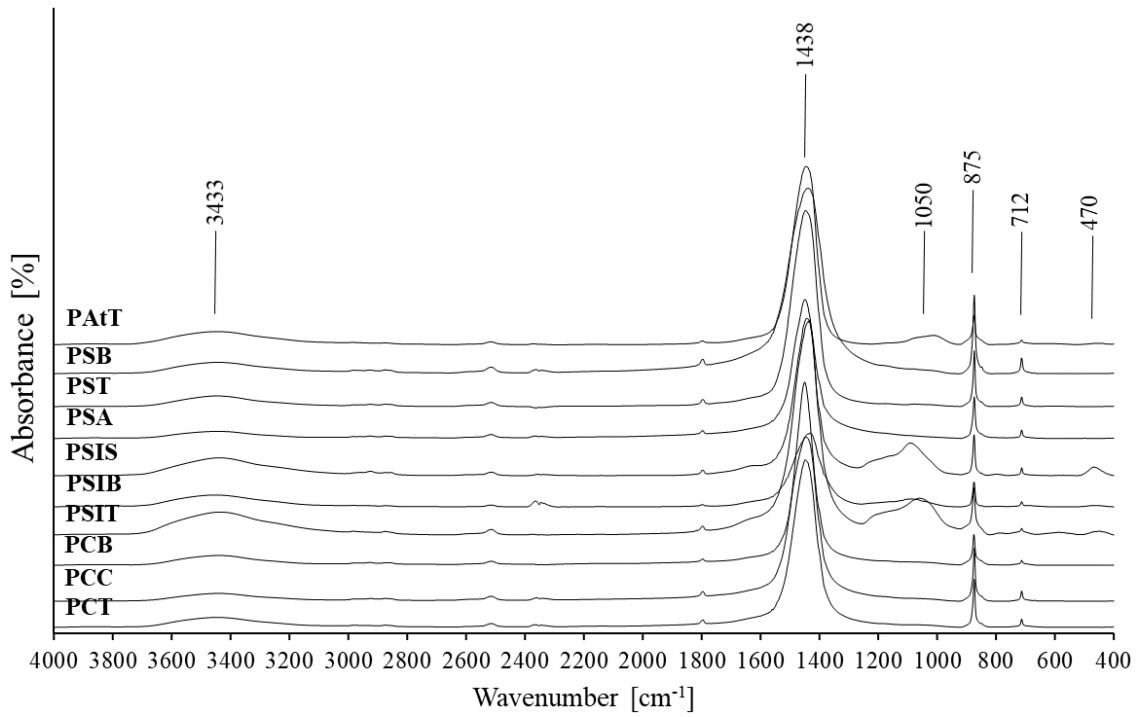
Figure 34. FTIR spectra of lime lumps of Roman lime mortars in Pisidia.
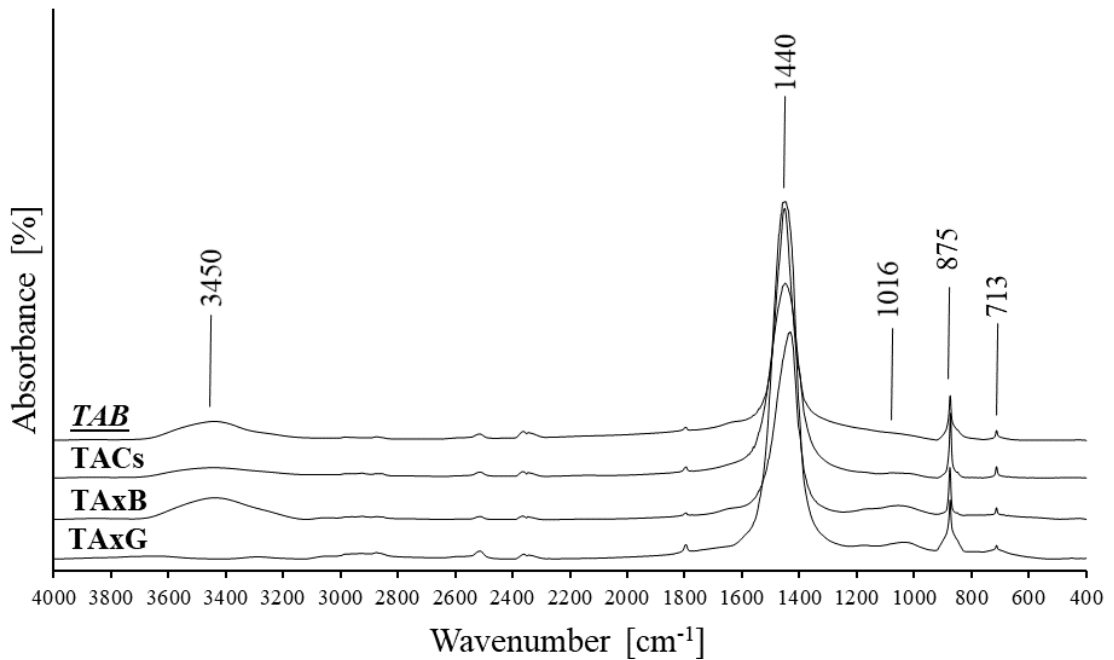
Figure 35. FTIR spectra of lime lumps of Roman lime mortars in Troas.

3.5.2. Chemical Compositions

Chemical compositions of lime lumps were determined by SEM-EDS analysis. The type of building lime can be classified according to their chemical content particularly their (CaO + MgO) content (UNI EN 459-1 2001; UNI EN 16572 2015) (Table 15). Accordingly, fat limes (rich or high calcium lime) presented a high content of calcium oxide (CaO + MgO >95%), and lean lime exhibited less calcium oxide than a fat lime (85% < CaO + MgO < 95%) (UNI EN 16572 2015). In addition to this classification, lime can be classified as CL which refers to "calcium limes" and it can be defined as "limes mainly consisting of calcium oxide or calcium hydroxide without any additions of hydraulic or pozzolanic materials" (UNI EN 459-1 2001).

SEM-EDS analysis showed that lime lumps were composed of mainly CaO (78.7-99.6%); and traces of SiO_2 (0-11.6%), Al_2O_3 (0-12.1%), MgO (0-6.6%), FeO (0-0.8%), and P_2O_5 (0-0.6%) (Appendix D). Having regard to these results, 62% of lime lumps were found as high calcium lime or fat lime, and 38% of lime lumps were lean lime.

Figure 36. The percentage of CaO in lime lumps.

77% of lime lumps presented CaO ranging between 90-100% (Figure 36). The lime lump of the mortar of *LPtT* was composed of CaO with an approximate proportion of 100% (Figure 36). Hence, the lime used in this mortar could be pure lime. Lime lump

of the mortar of LyTpB presented 79% CaO and 11% SiO_2 (Figure 36). High proportions of silicon dioxide in this lime lump could be derived from siliceous limestone from which the lime was produced.

Table 15. Chemical requirements of lime.
(Source: UNI EN 459-1 2001)

Type of building lime	CaO+MgO	MgO	CO$_2$	SO$_3$	Available lime
CL 90	≥90	≤5	≤4	≤2	—
CL 80	≥80	≤5	≤7	≤2	—
CL 70	≥70	≤5	≤12	≤2	—
DL 85	≥85	≥30	≤7	≤2	—
DL 80	≥80	≥5	≤7	≤2	—

In this study, 81% of limes can be regarded as CL 90 which has more than 90% CaO + MgO and less than 5% MgO content (Table 16). 18% of limes had more than 80% CaO + MgO and less than %5 MgO content and were called CL 80 (Table 16). 1% of limes can be regarded as DL 80 which has more than 85% CaO + MgO and 5% MgO content (Table 16).

Table 16. Classification of lime of Roman mortars.

Type of Lime	Sample Name
CL 90	*ACyH* , ACyT, CEB, CKC, CKCs, *CLB1* , CLB2, *CStB* , CTrG, *CTrB* , IAnAq, IAnB, IMA, IMG, IPrB, IPyH, IPrH, IPrT, ITCs, ITT, LPtC, *LPtT* , *LTIB* , LyTpA, LyTpB, LTIS, LTIT, LXA, *LXB* , LXT, MPB, MPB2, PhAzB, PCT, PCB, PCC, PmLyB, PmLyCs, PmLyC, PhLdB, PSB, PSIB, PSIS, PSIT, PSA, *TAB* , TACs, TAxG
CL 80	*CStT* , IMS, ITT, *LPtB* , LySrU, LyTpT, MPC, PAtT, PST, TAxB
DL 80	LyTpB

These results showed that lime used in these mortars could be regarded as high-calcium lime. According to the results, the lime used in the production of mortars had a

high amount of calcium and a low amount of magnesium and silicon due to the use of almost pure calcareous stones.

Only a few studies mentioned the chemical composition of lime lumps representing the lime part used in the mortar (Table 8). According to these studies, the chemical composition of the lime lump was composed of mainly CaO, small amounts of SiO_2, and minor amounts of other minerals (Al_2O_3, MgO, Fe_2O_3, Na_2O_3, K_2O, MnO, P_2O_5, TiO_2). Chemical compositions of lime lumps were considerably the same as lime lumps from Ephesus, Kyme, Aigai, and Nysa in Turkey (Table 8). References were given in Table 8. Having regard to chemical and mineralogical compositions of lime lumps, it could be considered that the lime used in the production of Roman mortars was almost pure.

3.5.3. Hydraulic Properties

Limes can also be classified as non-hydraulic, weakly hydraulic, moderately hydraulic, and highly hydraulic according to their hydraulic indexes (H.I.) (Vicat 2003). However, the aluminum and silicon content of lime lumps may not derive from hydraulic reaction products. Therefore, the results of weakly hydraulic mortars can be contradictory. The hydraulic index can be calculated by using chemical compositions of lime lumps according to the Boynton formula (Boynton 1980).
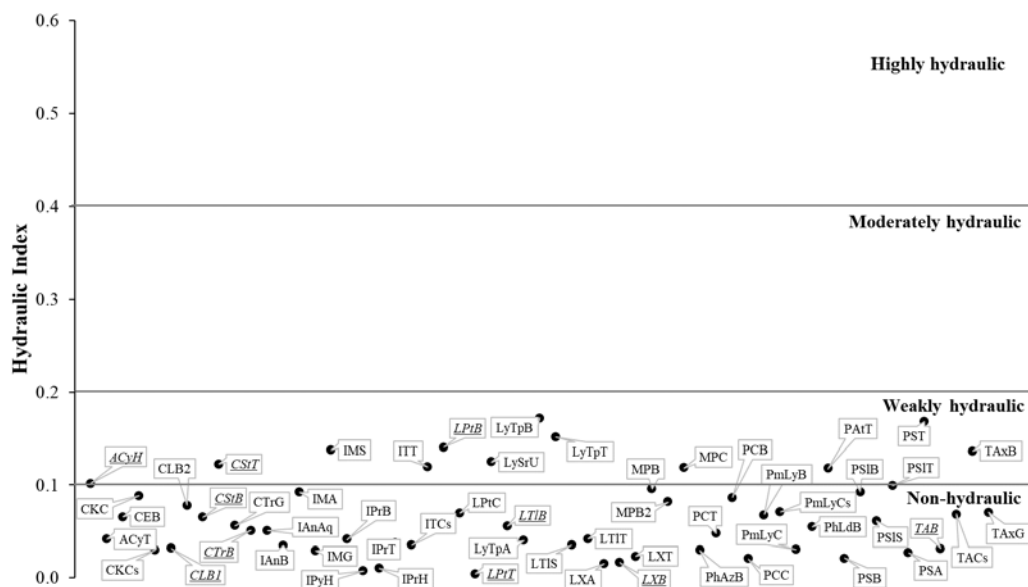
Figure 37. Hydraulic indexes of lime lumps of Roman mortars.

Non-hydraulic limes contained calcium carbonate over 90% (Eckel 1905). In this study, 77% of lime lumps presented CaO more than 90%. 25% of lime lumps showed silicate content of more than 5% which could give hydraulic properties to lime.

Fat limes (high-calcium limes) exhibited a hydraulic index less than 0.1 (Cowper 1998). Hydraulic indexes of lime lumps from all regions were in the range of 0.0-0.2 (Figure 37). Hydraulic indexes of 75% of lime lumps were between 0.0-0.1 and can be regarded as non-hydraulic (Figure 37). Hydraulic indexes of the 25% of lime lumps were between 0.1-0.2 and these lime lumps can be regarded as weakly hydraulic (Figure 37). Lime lumps with a high amount of silicate presented weak hydraulic properties.

Determination of hydraulic indexes of lime lumps has not been widespread in previous studies except for studies of Aigai, Nysa, and Kyme. Hydraulic indexes of lime lumps for Aigai and Nysa (0.0-0.1) and Kyme (0.03-0.12) mortars showed that they were non-hydraulic (Uğurlu Sağın 2012; Miriello et al. 2011). Considering these results, chemical compositions of lime lumps of analyzed mortars were almost the same as mortars from Aigai, Nysa, and Kyme regarding non-hydraulic behavior.

3.5.4. Microstructural Properties

Microstructural analysis carried out by SEM indicated that lime lumps were comprised of small-sized micritic calcite crystals with sizes smaller than 1 μm (Figure 38, Appendix D). More than half of lime lumps (65%) presented spongy texture of calcite crystals which can be the indicators of the hot lime mix method proved by recent studies (Figure 38) (Şerifaki, Sağın, and Böke 2020; Midtgaard, Brajer, and Taube 2020). However, lime lumps composed of lime containing silica at high ratios (more than 5%) consisted of calcite crystals having different crystal structures like cloudlike structures (Figure 39, Appendix D).
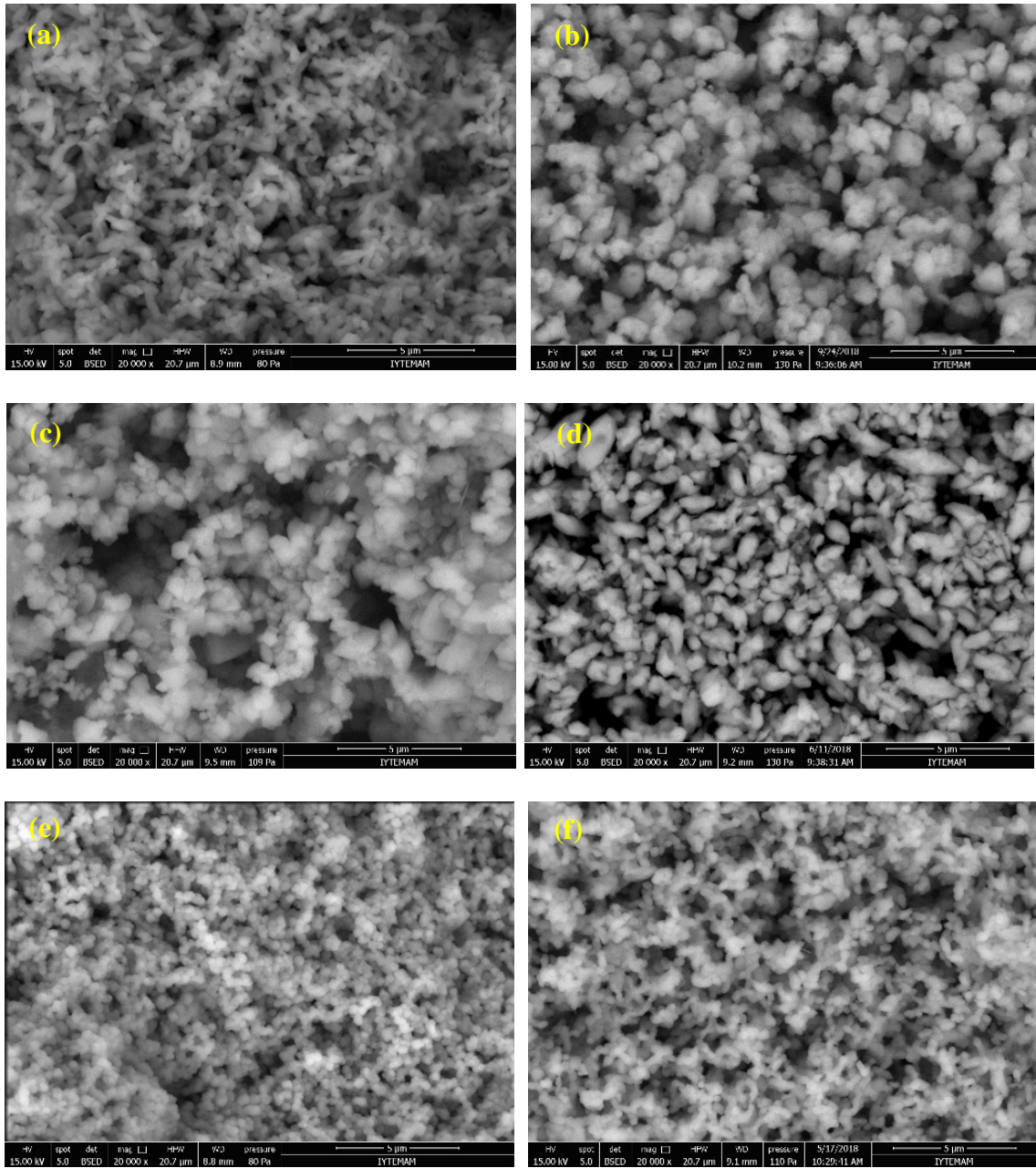
Figure 38. SEM-EDS images of calcite crystals of IAnAq (a), PmLyCs (b), PhLdB (c), PSIS (d), LXA (e), and _TAB_ (f) samples.
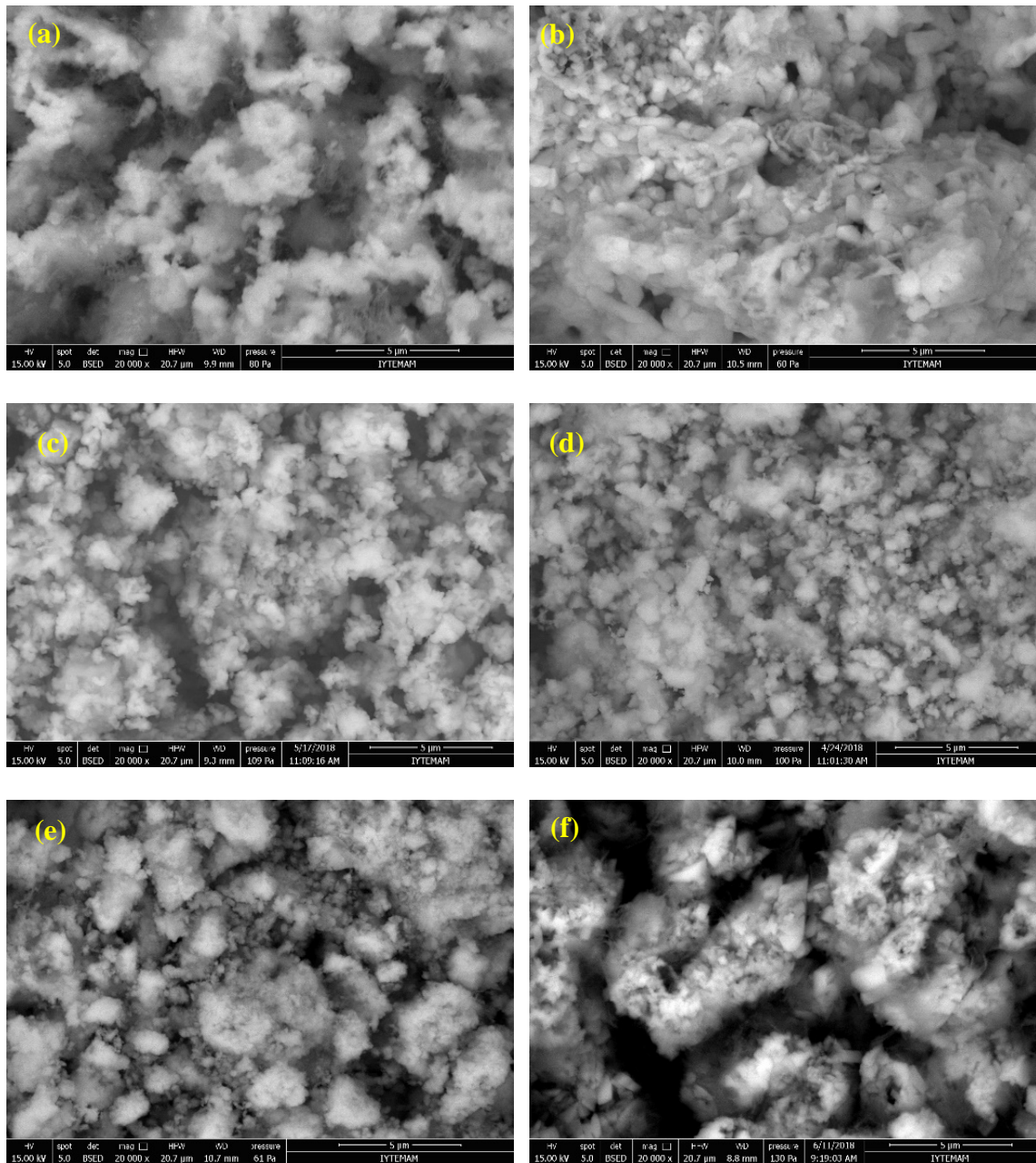
Figure 39. SEM-EDS images of calcite crystals of CKC (a), IMS (b), LyTpB (c), ITT (d), MPC (e), and PSIT (f) samples

Analyses showed that the lime used as a binder in the mortars was non-hydraulic and high calcium lime composed of small-sized micritic calcite crystals during the Roman Period. No significant differences were observed in the characteristics of lime used in *opus caementicium* and o*pus signinum* mortars.

3.6. Mineralogical Compositions of Aggregates

Mineralogical compositions of fine aggregates used in the mortars were determined by XRD analyses. XRD results of aggregates according to the regions were as follows:

The aggregates of mortars from Aiolis were composed of quartz (SiO_2), albite (Na ($AlSi_3O_8$), anorthite ($CaAl_2Si_2O_8$), sanidine (K ($AlSi_3O_8$), diopside ($MgCaSi_2O_6$), and hematite (Fe_2O_3) (Figure 40).
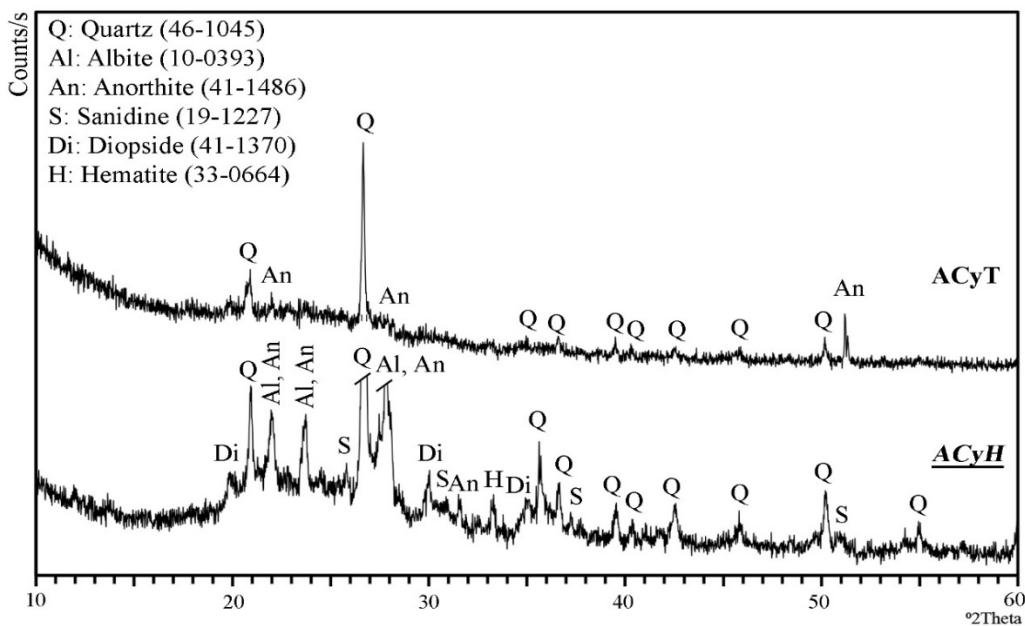
Figure 40. XRD pattern of fine aggregates from Roman lime mortars of Aiolis.

In Caria mortars, the aggregates were comprised of quartz, albite, anorthite, muscovite ($KAl_2(Si_3Al) O_{10}(OH, F)_2$), sanidine, and phillipsite (Ca, Na_2, $K_2)_3Al_6Si_{10}O_{32} \cdot 12H_2O$) (Figure 41). In XRD patterns of aggregates used in the mortars from Ionia, quartz, albite, anorthite, muscovite, sanidine, hematite, dolomite (CaMg $(CO_3)_2$), and phillipsite were observed (Figure 42). In the aggregates of Lycia mortars, quartz, albite, anorthite, muscovite, hematite, dolomite, and phillipsite were determined. (Figure 43). In Lydia, the aggregates were composed of quartz, albite, anorthite, muscovite, dolomite, sanidine, and phillipsite (Figure 44). The aggregates used in mortars from Mysia were composed of quartz, albite, anorthite, muscovite, sanidine, and

phillipsite (Figure 45). XRD results showed that fine aggregates used in the mortars from Pamphylia were composed of quartz, albite, and muscovite (Figure 46). In the mortars from Phrygia, quartz, albite, muscovite, and phillipsite peaks were identified (Figure 47). The aggregates used in the mortars from Pisidia were composed of quartz, albite, anorthite, muscovite, sanidine, dolomite, and phillipsite (Figure 48). In Troas, the aggregates were comprised of quartz, albite, anorthite, and sanidine (Figure 49).
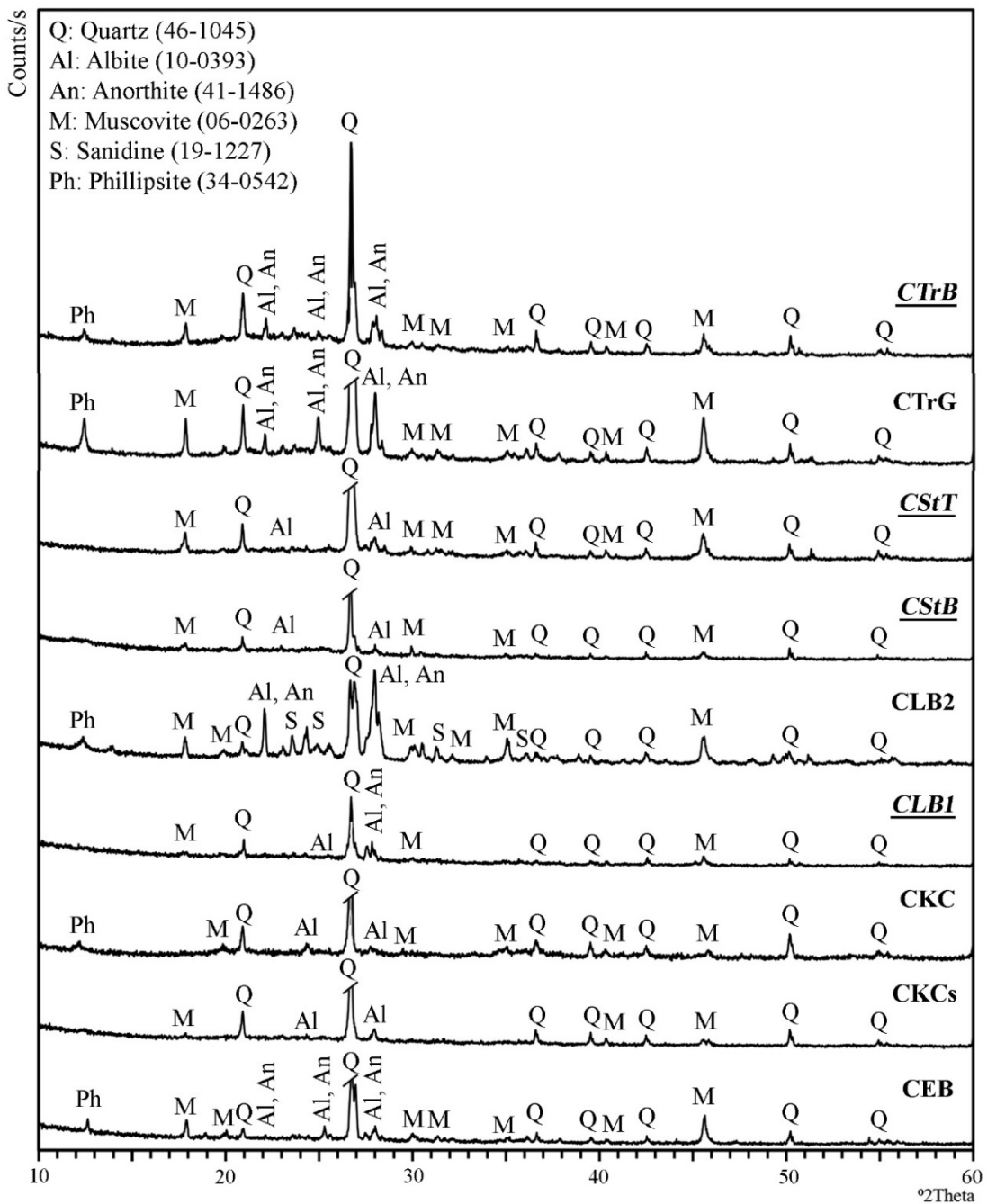
Figure 41. XRD pattern of fine aggregates from Roman lime mortars of Caria.
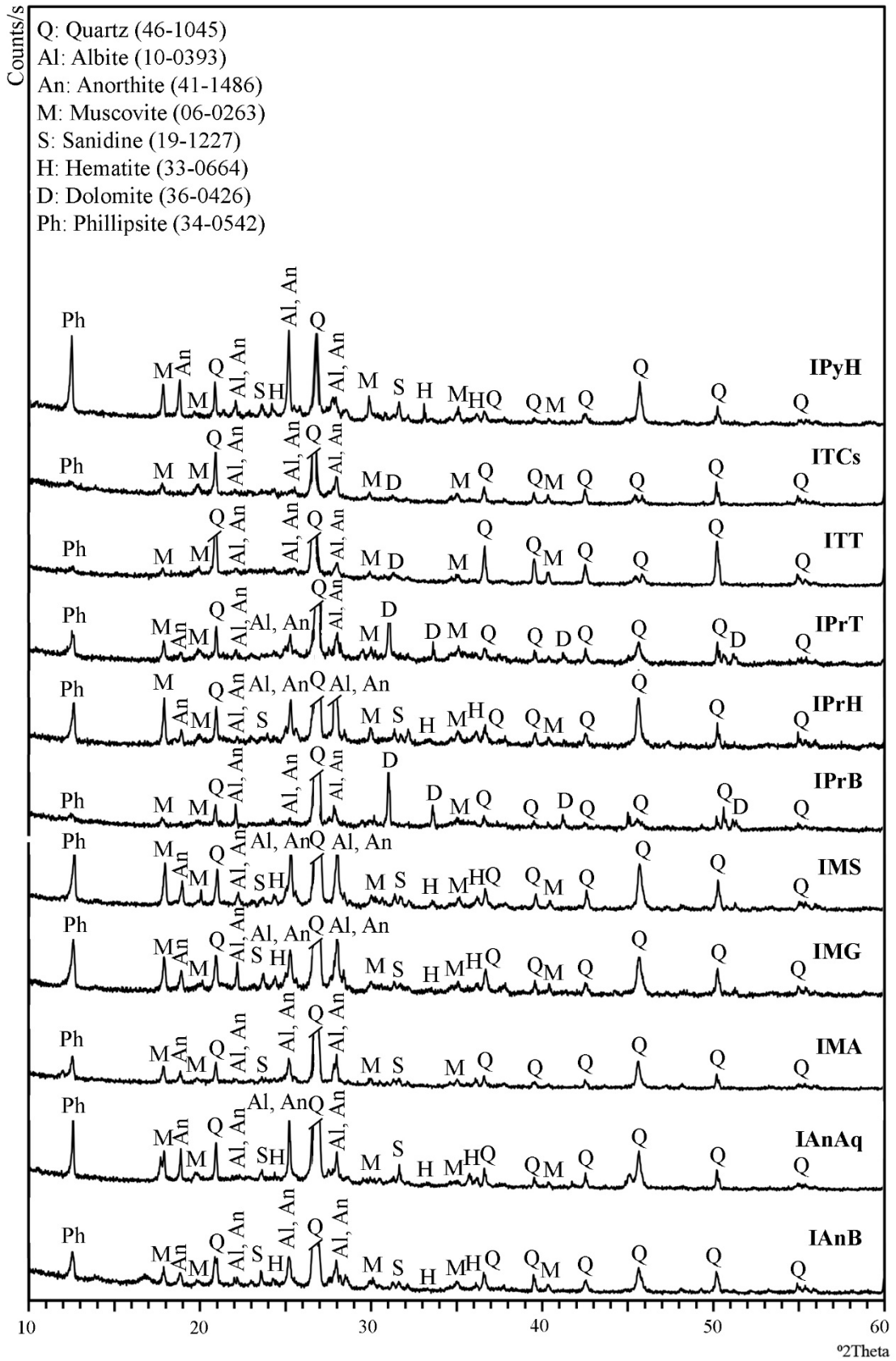
Figure 42. XRD pattern of fine aggregates from Roman lime mortars of Ionia.

Counts/s

Q: Quartz (46-1045)
Al: Albite (10-0393)
An: Anorthite (41-1486)
M: Muscovite (06-0263)
H: Hematite (33-0664)
D: Dolomite (36-0426)
Ph: Phillipsite (34-0542)

LXT

LXB

LXA

LTIT

LTIS

LTIB

LPtT

LPtC

LPtB

°2Theta
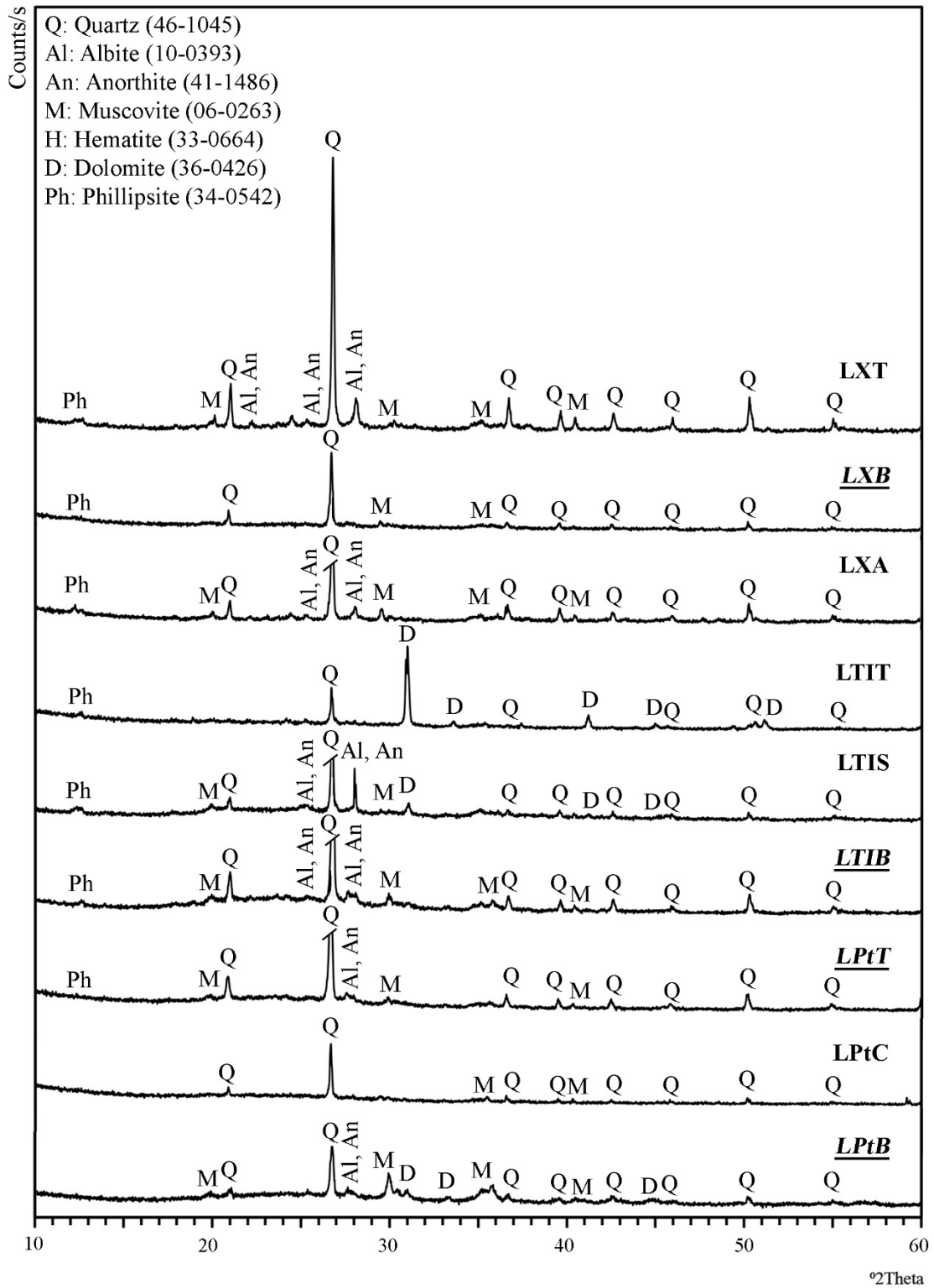
Figure 43. XRD pattern of fine aggregates from Roman lime mortars of Lycia.
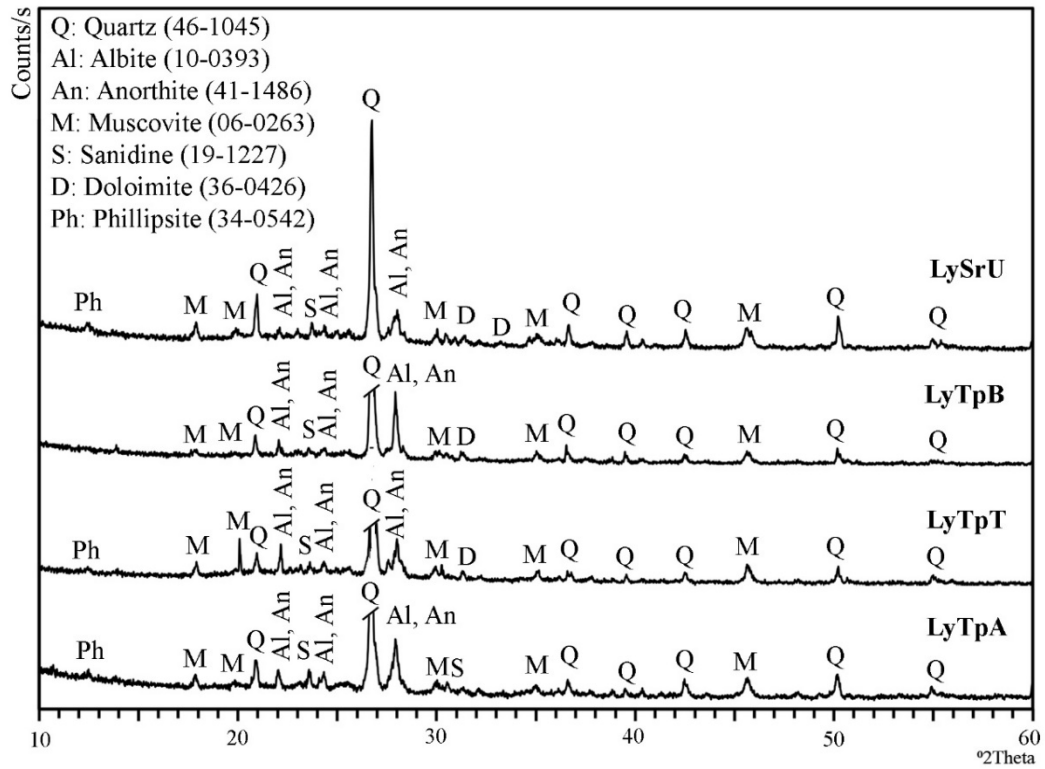
Figure 44. XRD pattern of fine aggregates from Roman lime mortars of Lydia.
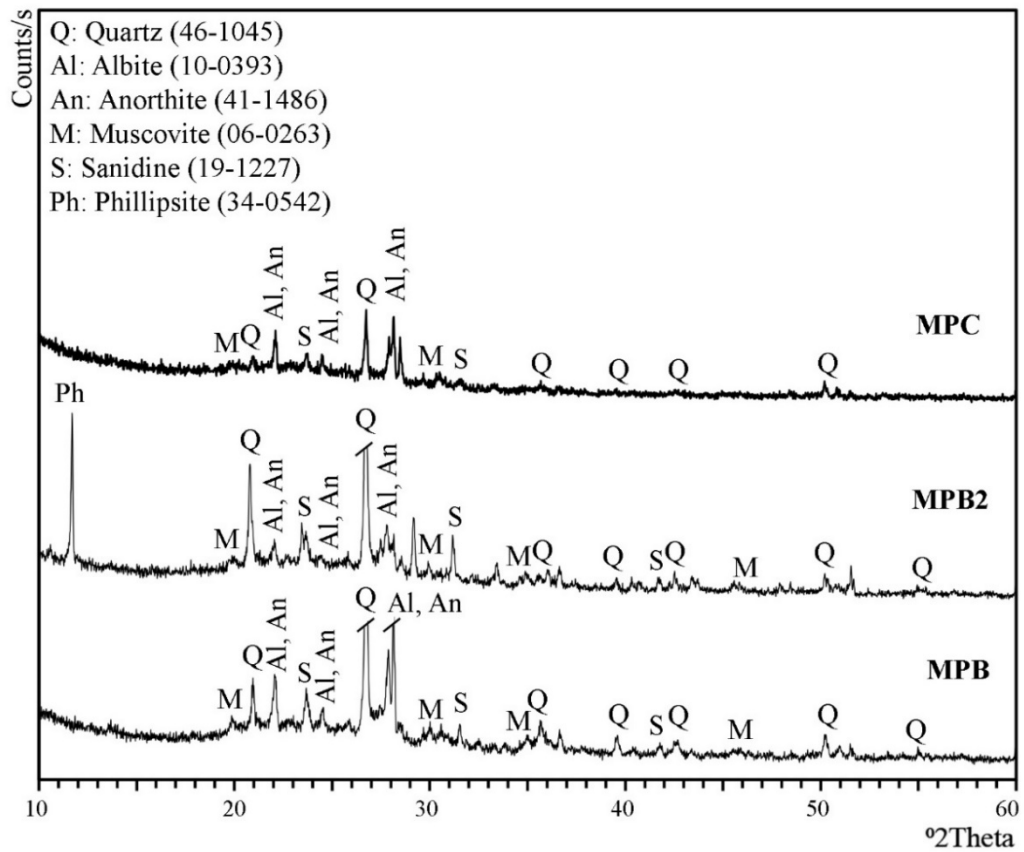
Figure 45. XRD pattern of fine aggregates from Roman lime mortars of Mysia.
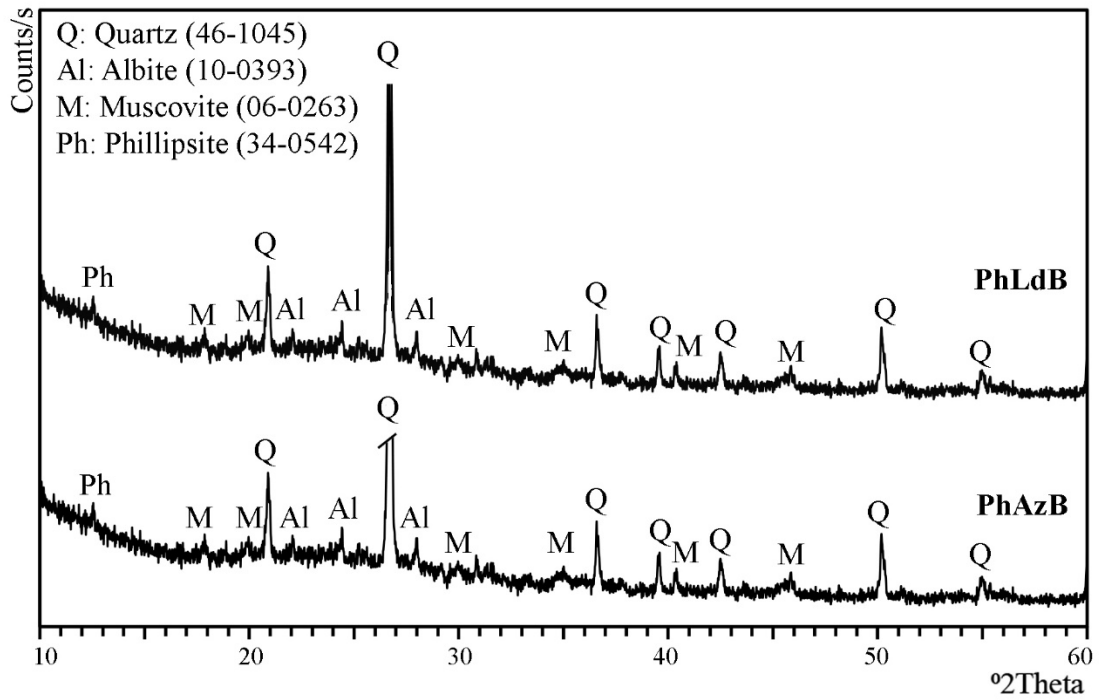
Figure 46. XRD pattern of fine aggregates from Roman lime mortars of Phrygia.
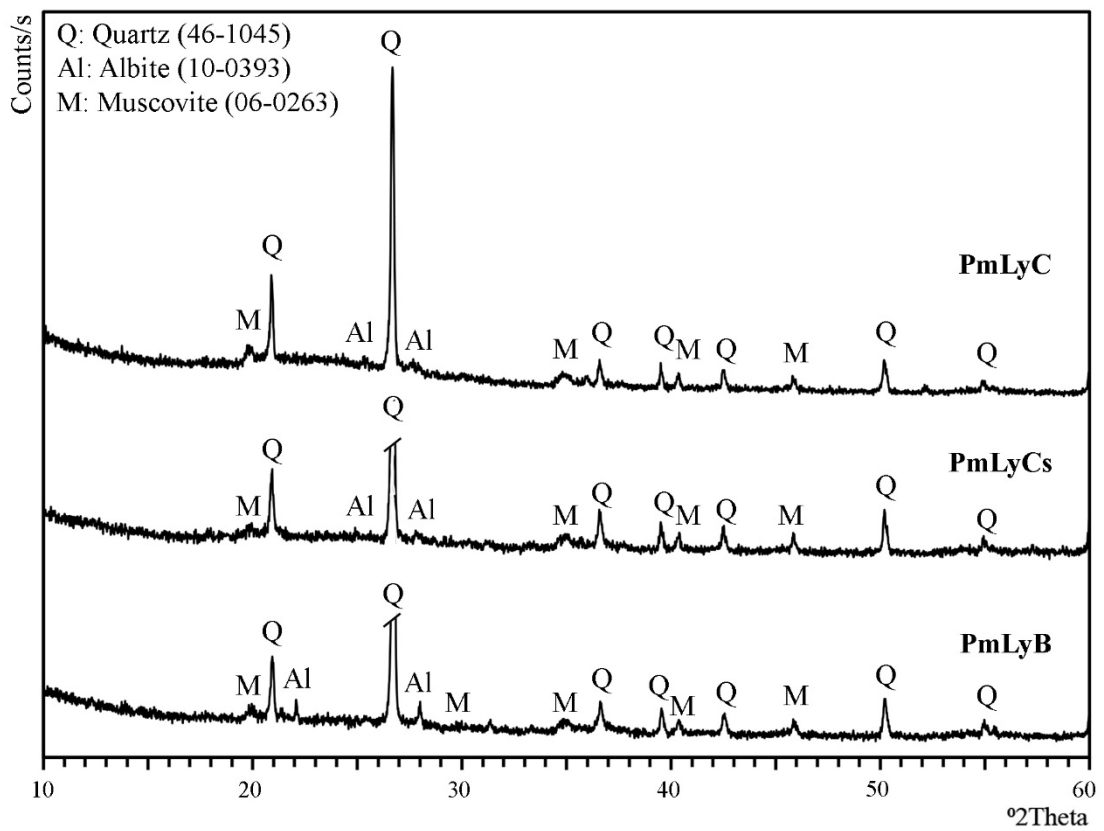
Figure 47. XRD pattern of fine aggregates from Roman lime mortars of Pamphylia.
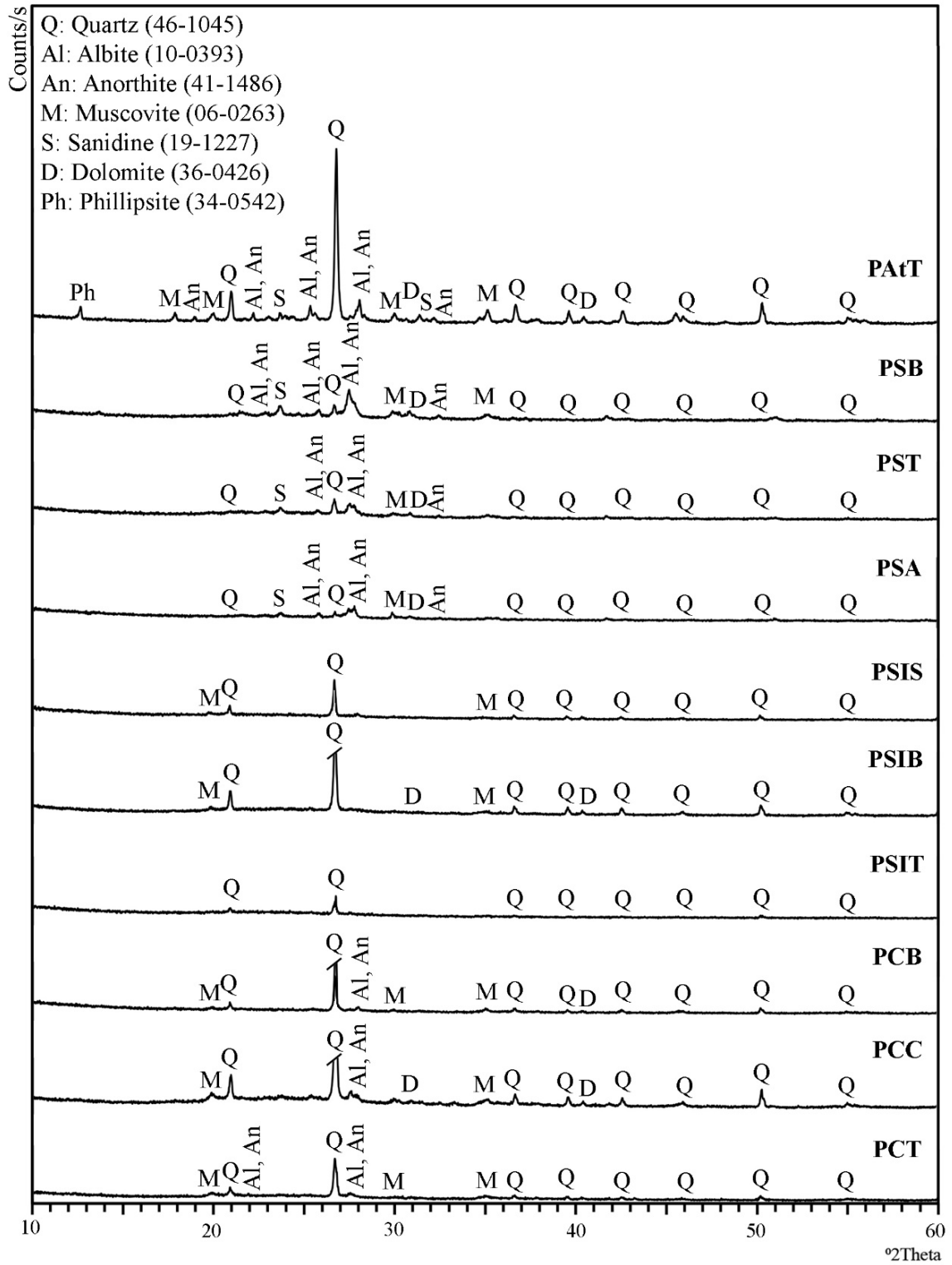
Figure 48. XRD pattern of fine aggregates from Roman lime mortars of Pisidia.
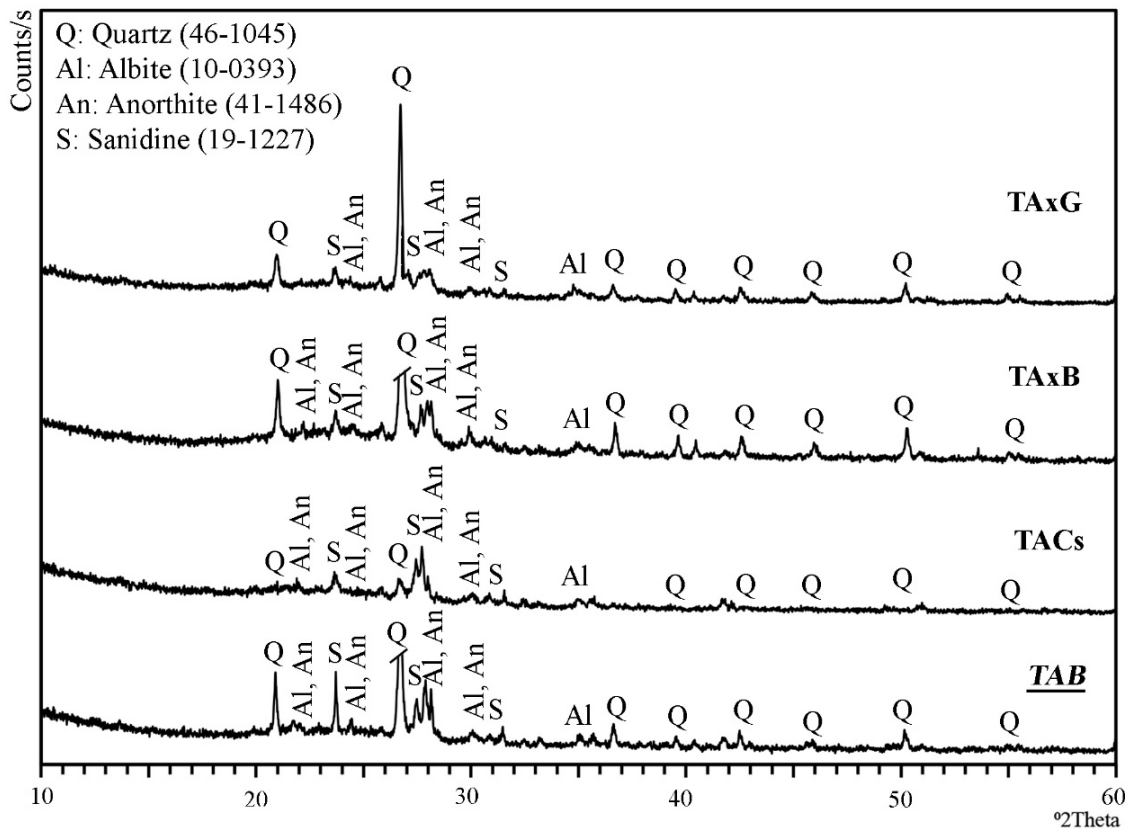
Figure 49. XRD pattern of fine aggregates from Roman lime mortars of Troas.

The presence of hydrated mineral phases was not identified in the XRD patterns. This situation was probably due to the overlapping of the peaks and/or the low crystallinity. However, their presence as amorphous phases could be observed via humps (between 20 and 30 2θ) in the XRD patterns of samples.

In this study, diffuse bands between 20-30 °2θ were slightly observed on the XRD patterns of more than half of mortars due to the amorphous aggregates (Figure 50 and Figure 51). The peaks of pozzolanic aggregates such as amorphous silicates were the ones that provide hydraulic features to Roman lime mortars. In this case, amorphous silicates can derive from the use of volcanic ash as a pozzolan. Despite a favorable pozzolanic activity, some samples did not show broadband between 20-30° 2θ on their XRD patterns. This situation may be a result of having a little quantity of amorphous silicates in their compositions. Almost all aggregates that presented SiO_2 content more than 80%, had a diffuse band between 20-30° 2θ on their XRD patterns (Figure 50 and Figure 51). This finding can be regarded as the result of using pozzolans in these mortars.
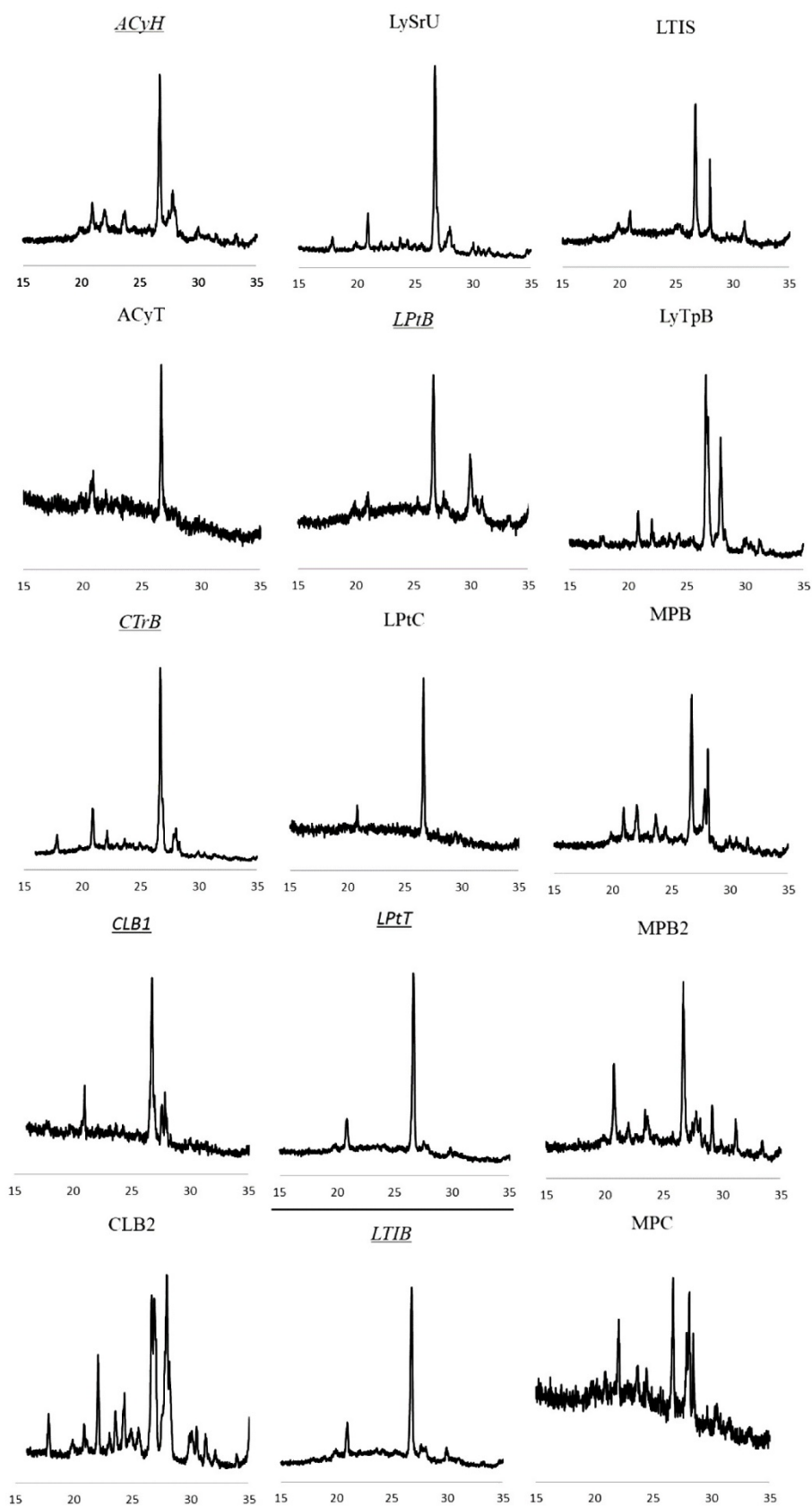
Figure 50. A broadband between 20-30º 2θ on the XRD pattern of samples-1.
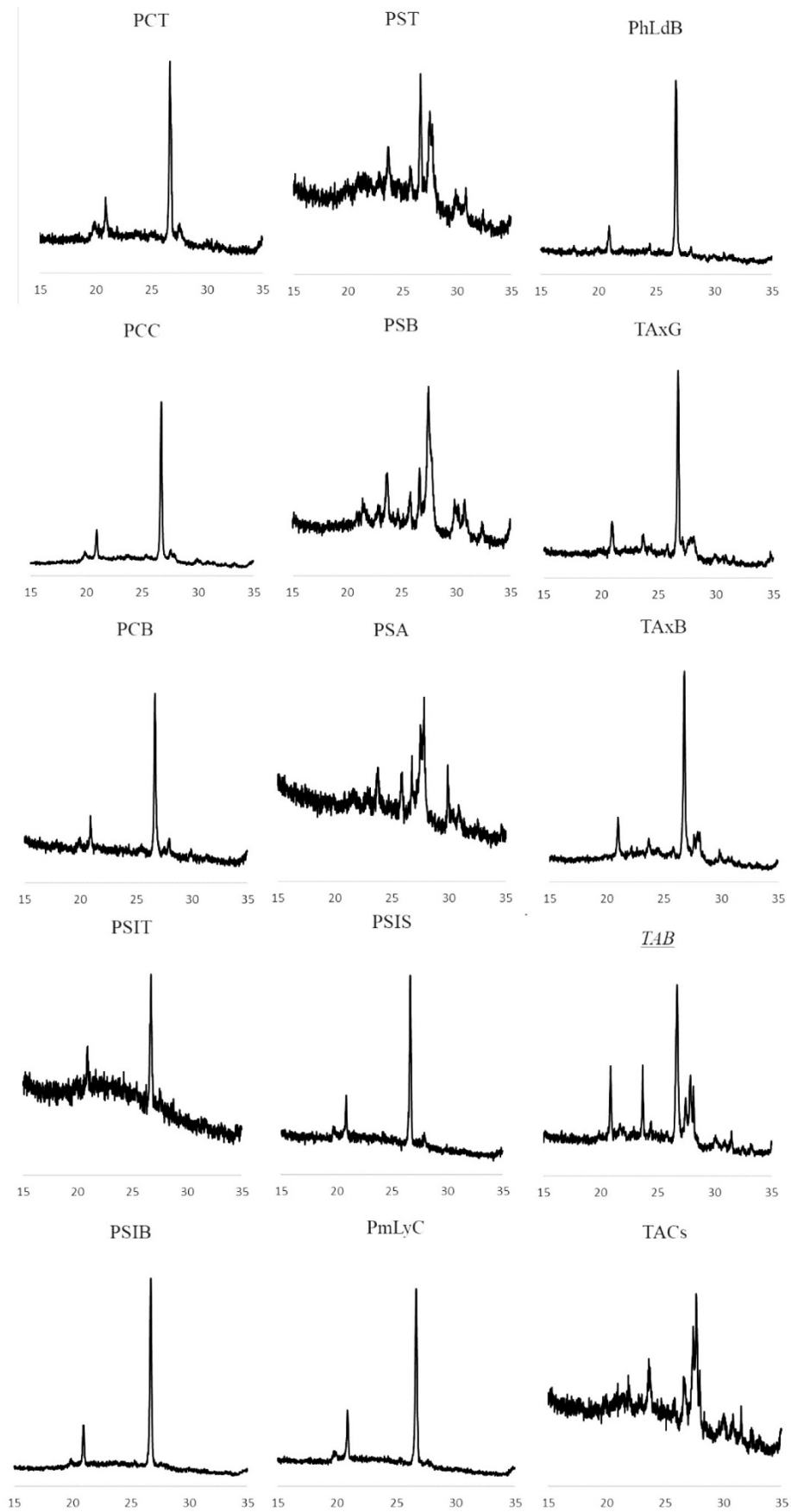
Figure 51. A broadband between 20-30º 2θ on the XRD pattern of samples-2.

Fine aggregates of *opus caementicium* and o*pus signinum* mortars from all regions showed almost similar characteristics concerning mineralogical compositions. Pamphylia, Phrygia, and Troas the ones that had the least number of minerals. However, Ionia, Lycia, Lydia, Pisidia, and Caria regions had much more different minerals as trace minerals such as dolomite, phillipsite, and hematite (Figure 52).
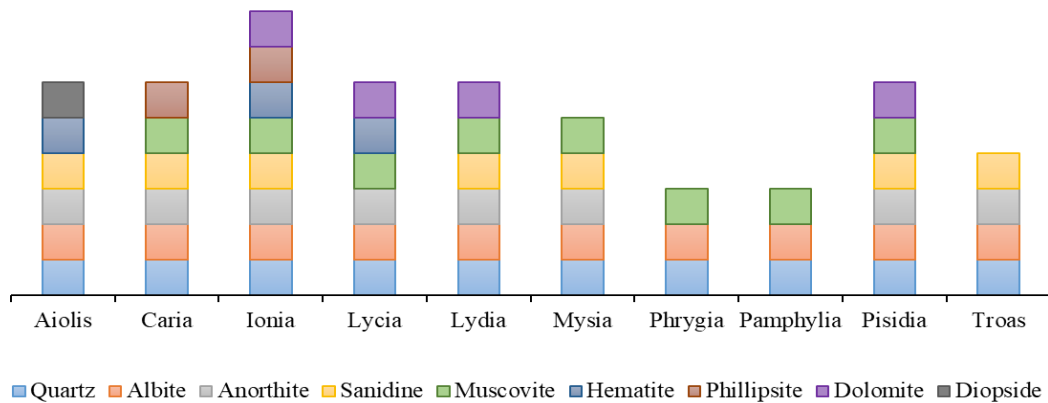
Figure 52. Mineralogical composition of fine aggregates from Roman lime mortars

Having regard to XRD analyses, fine aggregates of lime mortars were composed of mainly quartz, feldspar (albite, anorthite), mica (biotite, muscovite), and a trace of phillipsite minerals.

Mineralogical compositions of aggregates have been investigated by most of the studies due to their critical role in the performance of Roman mortars (Table 17-19). These studies indicated that fine aggregates of Roman Period mortars were composed of mainly quartz, muscovite, diopside, anorthite, sanidine, hematite, albite, and dolomite similar to fine aggregates of lime mortars studied. Moreover, calcite, feldspar, biotite, leucite, mica, plagioclase, pyroxene, amphibole, chlorite, augite, analcime, orthoclase, phillipsite, halite, magnesite, goethite were the other minerals determined by previous studies (Table 17-19). References were given in Table 17-19. Moreover, mineralogical compositions of aggregates of samples studied were found to be much more similar to aggregates of Ephesus, Kyme, Aigai, Nysa in Turkey, Sorrento, Sicily, Herculaneum in Italy, Augusta Emerita in Spain and Mošnje, Slovenia (Table 17-19). Small differences regarding mineralogical compositions of aggregates could be explained by the use of local material sources.

Table 17. Mineralogical compositions of fine aggregates of Roman lime mortars as a result of previous studies in Turkey.

Case area (Reference)	Method	MINERALS																											
		Cal	Qtz	Fsp	Bt	Lct	Ms	Mi	Di	An	Pl	Px	Sa	Am	Hem	Al	Chl	Aug	Anl	Or	Dol	Phl	Hl	Mgs	Gt	Gp	Ph	Kln	Oth
Samples of this study	XRD	+				+	+		+	+	+		+	+	+	+	+				+						+		
Sagalassos (*Degryse et al. 2002*)	OM		+	+			+	+	+	+	+		+	+	+	+													
Ephesus (*Kuleli 2005*)	XRD	+	+	+		+	+	+							+														+
Pergamon (*Özkaya and Böke 2009*)	XRD	+	+												+	+													+
Kaisareia (*Kozlu 2010*)	XRD	+									+	+																	+
Kyme (*Miriello et al. 2011*)	PM	+	+	+					+	+					+		+							+					+
Soli-Pompeiopolis (*Stanislao et al. 2011*)	XRD SEM-EDS	+						+					+					+	+	+									+
Aigai and Nysa (*Uğurlu Sağın 2012*)	XRD	+				+	+		+	+					+		+			+									
Tarsos and Anavarza (*Polat Pekmezci 2012*)	XRD	+	+												+														+
Amastris (*Kurugöl and Güleç 2015*)	XRD, OM	+	+			+																							
Kyme (*Miriello et al. 2015*)	XRD	+	+	+		+	+				+	+		+	+	+	+			+									+
Smyrna (*Felekoğlu et al. 2016*)	XRD	+	+	+	+																								

TURKEY

104

Table 18. Mineralogical compositions of fine aggregates of Roman lime mortars as a result of previous studies in Italy.

Case area (Reference)	Method	MINERALS																											
		Cal	Qtz	Fsp	Bt	Lct	Ms	Mi	Di	An	Pl	Px	Sa	Am	Hem	Al	Chl	Aug	Anl	Or	Dol	Phl	Hl	Mgs	Gt	Gp	Ph	Kln	Oth
Sorrento (*Benedetti et al. 2004*)	XRD	+	+					+	+				+		+	+				+									+
Sicily (*Rizzo et al. 2008*)	OM	+	+	+			+			+	+	+	+		+	+	+			+				+	+				+
Rome (*Jackson et al. 2009*)	XRD	+	+	+	+								+					+											+
Rome (*Jackson et al. 2011*)	XRD	+				+			+						+				+										
Narni (*Cantisani et al. 2002; Drdácký et al. 2013*)	OM	+	+						+			+	+																+
Herculaneum (*Leone et al. 2015*)	PM	+	+	+	+					+	+		+		+														+
Tivoli (*Columbu et al. 2017*)	OM, XRD	+	+	+		+	+	+																					+
Benevento (*Izzo et al. 2018*)	PM, FTIR	+	+	+					+		+												+						
Tivoli (*Columbu et al. 2018*)	OM, XRD	+	+	+	+	+					+				+														+

ITALY

Table 19. Mineralogical compositions of fine aggregates of Roman lime mortars as a result of previous studies in other countries.

Case area (Reference)	Method	Cal	Qtz	Fsp	Bt	Lct	Ms	Mi	Di	An	Pl	Px	Sa	Am	Hem	Al	Chl	Aug	Anl	Or	Dol	Phl	Hl	Mgs	Gt	Gp	Ph	Kln	Oth
Uthina, Tunisia (*Farci et al. 2005*)	XRD	+	+	+							+		+																+
Messene, Greece (*Zamba et al. 2007*)	XRD	+	+																										
Augusta Emerita, Spain (*Franquelo et al. 2008*)	XRD	+	+				+		+	+					+														
Augusta Emerita, Spain (*Robador et al. 2010*)	XRD	+	+				+			+					+														
Mošnje, Slovenia (*Kramar et al. 2011*)	XRD	+	+			+															+								
Ammaia, Portugal (*Cardoso et al. 2014*)	OM	+	+		+	+				+				+															
Viminacium, Serbia (*Nikolić et al. 2016*)	OM	+	+					+				+																	
Uxama Argela, Spain (*Alonso-Olazabal et al. 2019*)	OM	+	+	+																									
Pisões, Portugal (*Borsoi et al. 2019*)	PM	+	+					+				+		+															
Wallsend, United Kingdom (*Laycock et al. 2019*)	PM	+	+	+				+		+	+	+		+		+													+

OTHER COUNTRIES

3.7. Chemical Compositions of Aggregates

Chemical compositions of fine aggregates in the Roman lime mortars were determined by SEM-EDS analyses. The results of the analyses revealed that aggregates of *opus caementicium* were mainly composed of high amount of SiO_2 (52-93%), moderate amounts of Al_2O_3 (4-23%), Fe_2O_3 (0-18%), and low amounts of MgO (0-7%), CaO (0-10%), P_2O_5 (0-5%), K_2O (0-4%), TiO_2 (0-1%) (Table 20). The aggregates of *opus signinum* were comprised of mainly high amount of SiO_2 (66-91%), moderate amounts of Al_2O_3 (6-14%), Fe_2O_3 (0-7%), and low amounts of MgO (0-5%), CaO (0-5%), K_2O (0-3%), TiO_2 (0-1%) (Table 21). No significant difference was observed between the chemical compositions of aggregates of *opus caementicium* and *opus signinum* mortars.

The silica content of fine aggregates was high, ACyT, _CStB, CStT,_ PSIT, PST, PSIB _TAB_, TACs, TAxB, TAxG ones being the highest (90-93%). In addition to this, aluminum oxide and iron oxide contents of the mortars were also important for pozzolanic activity.

The low amounts of CaO content in the aggregates were probably from the acid-insoluble silicates or the remains of undissolved calcite. CaO contents of mortars from Lycia, Ionia, and Pisidia regions were considerably higher than others (Figure 53). This can be due to the presence of calcareous aggregates in these regions. K_2O contents were low enough to be considered as the production of damaging formations.

According to the results from chemical compositions and pozzolanic activity, the low pozzolanic activity of fine aggregates could be explained by the presence of high amounts of iron oxide and less amount of silicon dioxide. Samples (IMG, IMS, IPrH, IPrT, LXA, LXT, PmLyCs) had lower pozzolanicity less than 4 mS/cm, high amount of iron dioxide more than 5%, and low amount of silicon dioxide between 52.11-73.71%. However, CKCW as an exception presented good pozzolanicity with the highest amount of iron oxide 17.04%, and almost the lowest amount of silicon dioxide 57.69%.
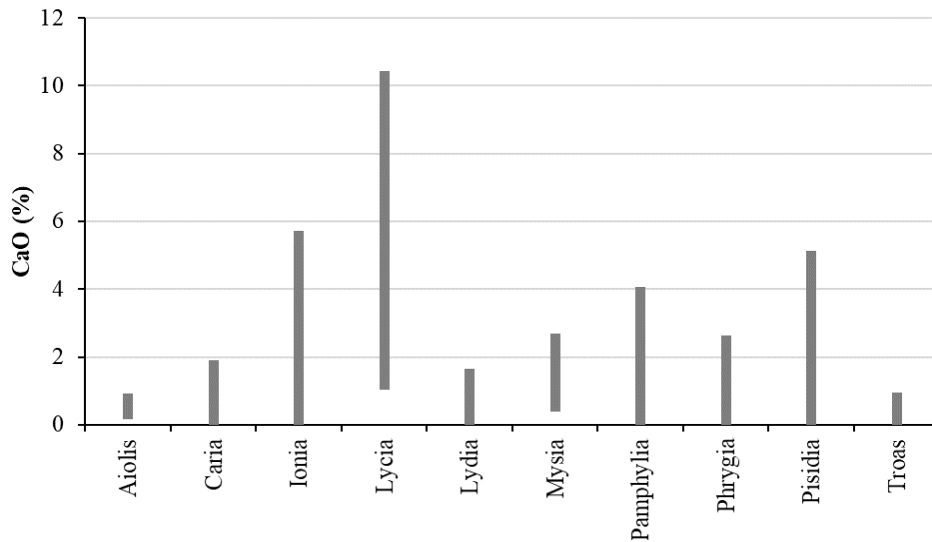
Figure 53. CaO content of fine aggregates.

SEM-EDS analysis was carried out to form the three different types of triangular diagrams (Figure 54-56). The majority of samples were far from pure carbonate phases and enriched in silicon and aluminum with higher than 90% $SiO_2+Al_2O_3$ content (Figure 54). Most of the aggregates were close to pure siliceous phases and presented SiO_2 content of more than 75% and Al_2O_3 content of less than 25% (Figure 55). The number of aggregates had less than 10% of Fe_2O_3 and they presented a variable composition enriched in silicon and aluminum (Figure 56).
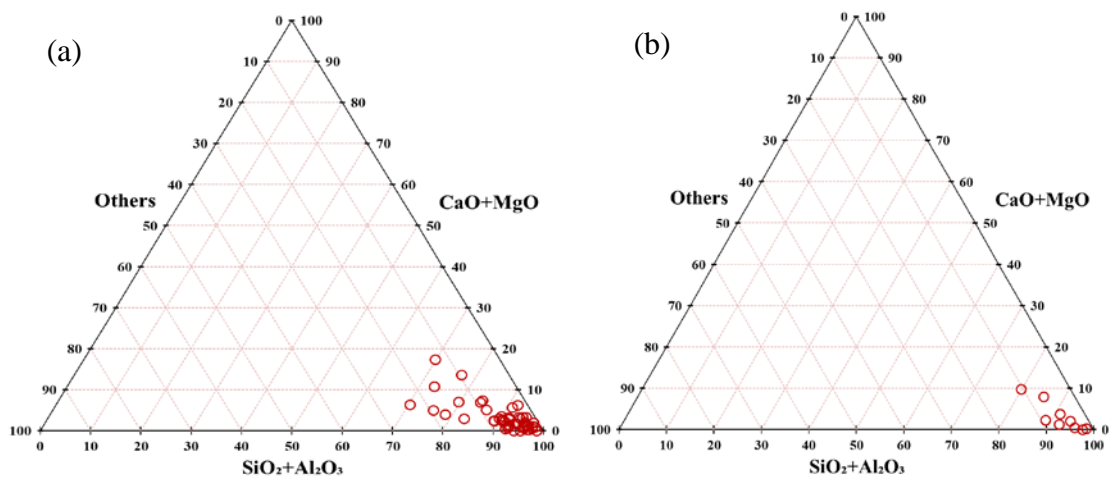
Figure 54. Triangular diagram (CaO+MgO-SiO$_2$+Al$_2$O$_3$-Others) of chemical compositions of fine aggregates of *opus caementicium* (a) and *opus signinum* (b)
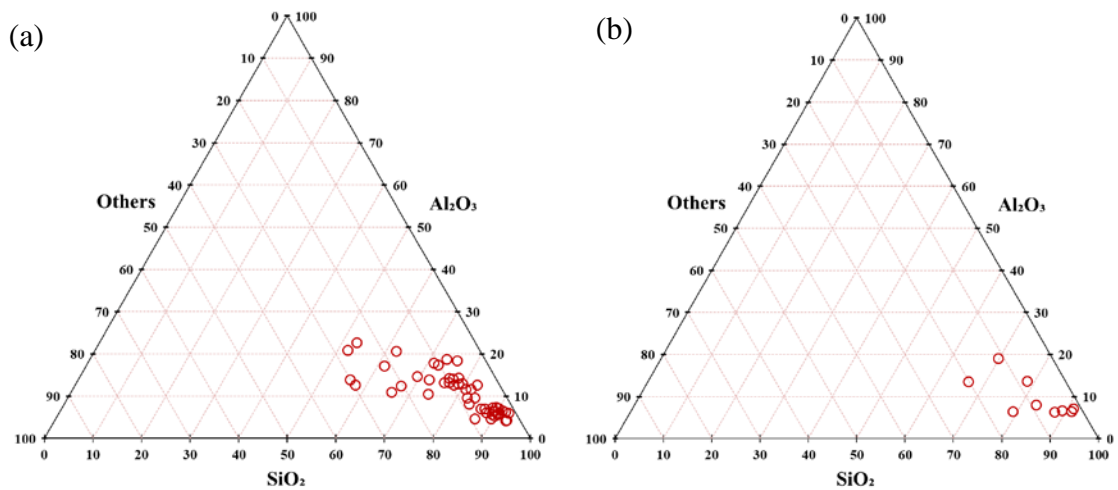
Figure 55. Triangular diagram (Al_2O_3-SiO_2-Others) of chemical compositions of fine aggregates of *opus caementicium* (a) and *opus signinum* (b)
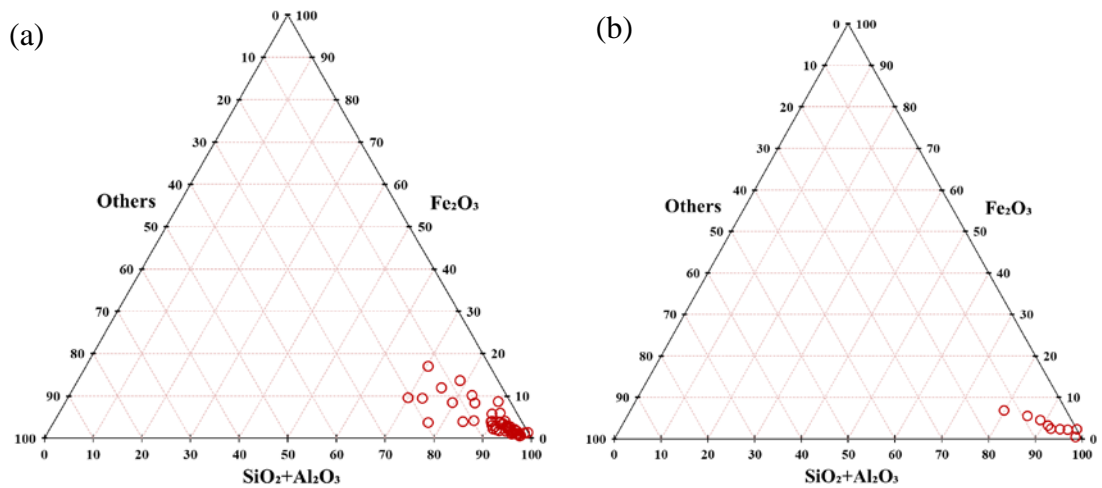
Figure 56. Triangular diagram (Fe_2O_3-SiO_2+ Al_2O_3-Others) of chemical compositions of fine aggregates of *opus caementicium* (a) and *opus signinum* (b)

Having regard to these results, chemical compositions of fine aggregates showed almost similar characteristics with aggregates used in Roman lime mortars from Pergamon, Kyme, Aigai, Nysa, Tarsos, and Anavarza in Turkey, Rome and Pompeii in Italy, and Mošnje in Slovenia (Table 6). References were given in Table 6.

Table 20. Chemical compositions of fine aggregates of *opus caementicium* mortars determined by SEM-EDS (%).

Region Name	SiO$_2$	Al$_2$O$_3$	FeO	MgO	CaO	P$_2$O$_5$	K$_2$O	TiO$_2$
Aiolis *(1 Sample)*	91	6	2	1	0.2	–	1	–
Caria *(5 Samples)*	58-86 75±10.7 (ave.)	7-19 13±4.6 (ave.)	2-18 7±6.1 (ave.)	0-5 2±1.9 (ave.)	0-1 0.5±0.7 (ave.)	0-4 1±1.9 (ave.)	0-4 2±1.4 (ave.)	–
Ionia *(11 Samples)*	52-89 69±11.3 (ave.)	6-23 16±4.6 (ave.)	1-14 6±4.3 (ave.)	0-5 3±1.2 (ave.)	0-6 1±1.7 (ave.)	3-5 1±2.0 (ave.)	1-4 3±0.7 (ave.)	0-1 1±0.5 (ave.)
Lycia *(5 Samples)*	56-90 70±12.3 (ave)	5-15 11±4.0 (ave.)	2-10 6±3.2 (ave.)	1-7 5±2.3 (ave.)	2-10 5±3.8 (ave.)	0-4 3±1.6 (ave.)	0-2 1±1.0 (ave.)	0-1 0.1±0.2 (ave.)
Lydia *(4 Samples)*	77-90 85±6.2 (ave.)	7-13 10±3.3 (ave.)	1-4 2±1.4 (ave.)	0-2 0.5±0.9 (ave.)	0-2 0.4±0.8 (ave.)	–	2-3 2±0.5 (ave.)	0-0.3 0.1±0.1 (ave.)
Mysia *(3 Samples)*	87-89 88±1.2 (ave.)	6-7 6±0.5 (ave.)	2-3 2±0.6 (ave.)	0-1 0.3±0.3 (ave.)	0-3 1±1.2 (ave.)	–	1-2 1±0.1 (ave.)	–
Pamphylia *(3 Samples)*	74-89 79±8.1 (ave.)	7-13 10±3.0 (ave.)	1-9 6±4.2 (ave.)	1-3 2±1.2 (ave.)	0-4 2±2.2 (ave.)	–	0-2 1±0.9 (ave.)	–
Phrygia *(2 Samples)*	78-86 82±5.8 (ave.)	5-14 10±6.8 (ave.)	2-4 3±0.9 (ave.)	1-3 2±1.4 (ave.)	0-3 1±1.9 (ave.)	–	1-3 2±1.3 (ave.)	–
Pisidia *(10 Samples)*	73-93 84±6.6 (ave.)	4-19 10±4.6 (ave.)	1-6 2±1.5 (ave.)	0-2 1±0.5 (ave.)	0-5 1±1.5 (ave.)	–	0-4 1±1.7 (ave.)	0-1 0.1±0.3 (ave.)
Troas *(3 Samples)*	91-93 92±1.4 (ave.)	4-6 5±1.0 (ave.)	0-1 1±0.4 (ave.)	0-0.3 0.1±0.1 (ave.)	0-1 0.4±0.5 (ave.)	–	0-2 1±0.9 (ave.)	–

Table 21. Chemical compositions of fine aggregates of *opus signinum* mortars determined by SEM-EDS (%).

Region Name	SiO$_2$	Al$_2$O$_3$	FeO	MgO	CaO	K$_2$O	TiO$_2$
Aiolis (1 Sample)	84	10	3	1	1	2	–
Caria (4 Samples)	78-91 85±5.9 (ave.)	7-14 9±3.4 (ave.)	0-3 2±1.0 (ave.)	0-1 0.9±0.4 (ave.)	0-2 0.5±1.0 (ave.)	1-3 2±1.0 (ave.)	0-1 0.2±0.5 (ave.)
Lycia (4 Samples)	66-88 79±8.6 (ave.)	6-14 9±5.7 (ave.)	2-7 5±2.1 (ave.)	1-5 3±1.7 (ave.)	1-5 3±2.2 (ave.)	0-1 0.9±1.3 (ave.)	0-1 0.2±0.4 (ave.)
Troas (*1 Sample*)	91	6	2	–	–	–	–

3.8. Pozzolanic Activity of Aggregates

Pozzolanic activity of aggregates plays a fundamental role in the mechanical strength and hydraulicity of lime mortars due to pozzolanic reactions that take place between pozzolans and lime in the presence of water (Lea 1940). This reaction can produce hydraulic reaction products such as CSH and CAH that give hydraulic properties to the lime mortars and provide high strength to them (Lea 1940).

In this study, electrical conductivity measurements were carried out to determine the pozzolanic activities of fine aggregates (pozzolans) less than 63 μm. In this method, the electrical conductivity differences higher than 2 mS/cm presented good pozzolanicity for aggregates (Luxán, Madruga, and Saavedra 1989).

The content of $SiO_2 + Al_2O_3 + Fe_2O_3$, the amorphous degree of their structure, and the material particle sizes are factors for the pozzolanic activity of the aggregates. The pozzolanic activity of aggregates depends mainly on the content of active SiO_2 and active Al_2O_3 below certain particle sizes (Yu, Zhou, and Deng 2015).

	Aiolis	Caria	Ionia	Lycia	Lydia	Mysia	Phrygia	Pamphylia	Pisidia	Troas
Max.	6.68	7.40	6.82	6.66	6.66	5.80	5.38	5.44	7.17	7.48
Min.	3.52	4.40	2.16	2.54	3.80	1.19	4.31	3.83	2.93	6.74
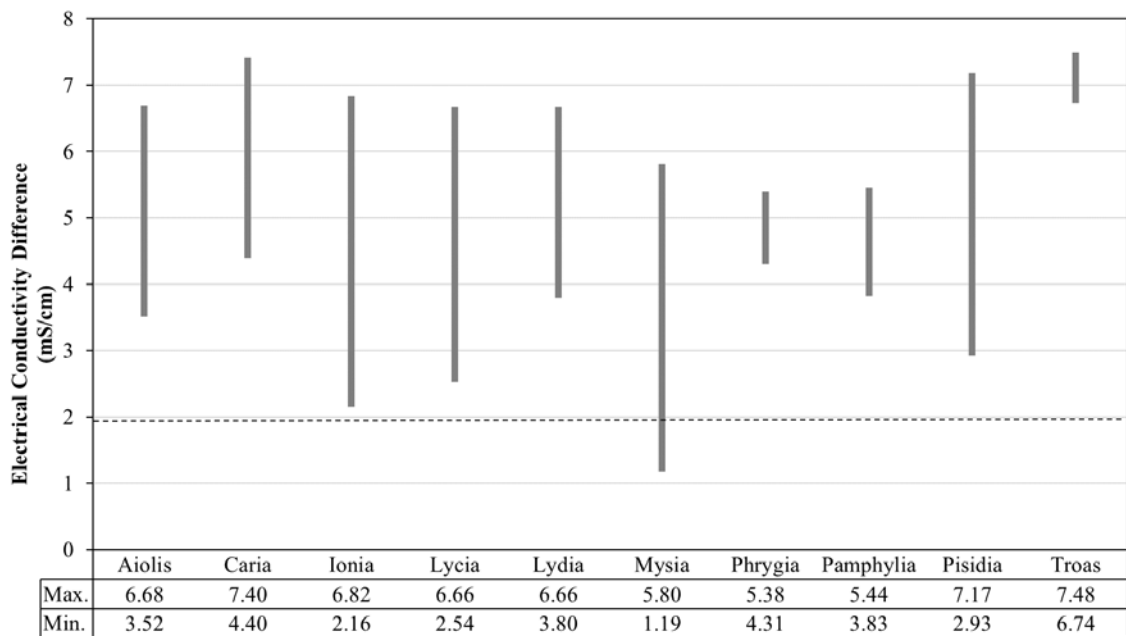
Figure 57. Electrical conductivity differences of aggregates of Roman lime mortars.

Electrical conductivity differences of aggregates were determined between 2.16-7.53 mS/cm (Figure 57). However, MPC (1.19 mS/cm) had the lowest value as an exception. Values were defined between 1.19-7.48 mS/cm for *opus caementicium* mortars and 4.15-7.53 mS/cm for *opus signinum* mortars. Electrical conductivity differences of aggregates were between 3.52-6.68 mS/cm for Aiolis mortars, between 4.40-7.40 mS/cm for Caria mortars, between 2.16-6.82 mS/cm for Ionia mortars, between 2.54-6.66 mS/cm for Lycia mortars, between 3.80-6.66 mS/cm for Lydia mortars, between 1.19-5.80 mS/cm for Mysia mortars, between 4.31-5.38 mS/cm for Phrygia mortars, between 3.83-5.44 mS/cm for Pamphylia mortars, between 2.93-7.17 mS/cm for Pisidia mortars and between 6.74-7.48 for Troas (Figure 57, Appendix E). No significant differences were observed among regions, and between aggregates of o*pus ceamentium* and *opus signinum* mortars regarding pozzolanicity.

These pozzolanic activity values indicated that fine aggregates of all mortars except one mortar had good pozzolanicity. MPC showed the lowest pozzolanicity values of 1.19 mS/cm and aggregates of this sample could not be accepted as a good pozzolan. Apart from this mortar, some samples (IMS, LXA, PAtT, IMG, LXT, IAnB, ACyT, IPrH, IPrB, LyTpA, PmLyCs) presented lower pozzolanicity than the rest of the samples with the value of 2.16-3.83 mS/cm. The silica content of fine aggregates was high in some mortars. In addition to silica content, aluminum oxide and iron oxide in the mortars were also effective compounds in pozzolanicity.
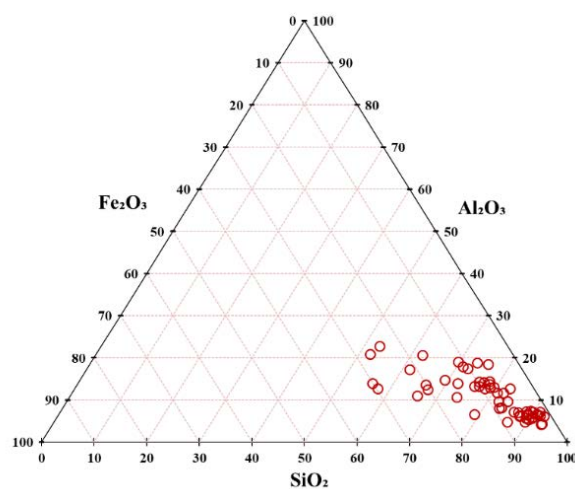
Figure 58. Triangular diagram (SiO_2+ Al_2O_3+ Fe_2O_3) of chemical compositions of fine aggregates.

This lower pozzolanicity can be due to the presence of a low amount of silica and a high amount of iron in the aggregates of these mortars with the range of 53-76% and 4-14%, respectively (Figure 58). However, the total of SiO_2, Al_2O_3, and Fe_2O_3 contents in analyzed mortars was higher than 70% which was the value of pozzolanicity required from pozzolanic aggregates by the current standards (ASTM 1978). In this study, siliceous aggregates with high pozzolanic activity constituted mainly the major fraction of fine aggregates. The use of highly pozzolanic aggregates played an important role in the formation of a silica network for CSH formation providing high mechanical strength and durability to the mortars.

Pozzolanic activity of fine aggregates was investigated in only a few sites from Turkey (Table 2). Among these studies, aggregates of Kaisareria, Myra, and Ephesus mortars showed poor pozzolanicity since their electrical differences values were below 2 mS/cm (Figure 59) (Table 2). However, pozzolanic activity values of mortar samples from Pergamon, Ephesus, Aigai, and Nysa were almost identical to the results of this study and these aggregates could be regarded as highly energetic (Figure 59) (Kuleli 2005; Aslan Özkaya and Böke 2009; Uğurlu Sağın 2012).
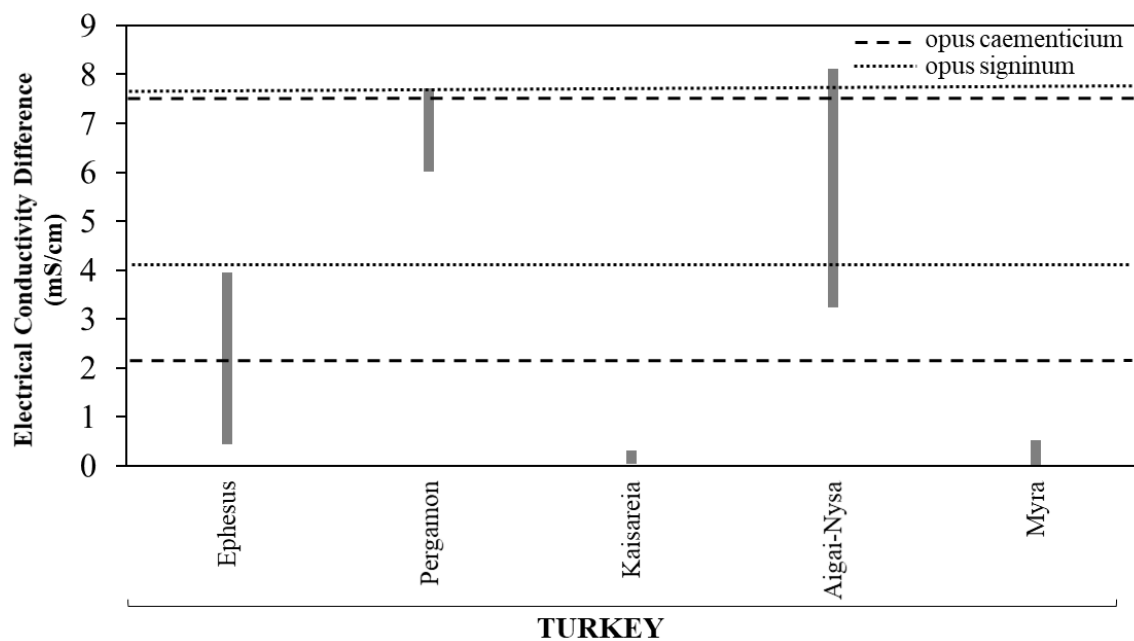
Figure 59. Comparison of electrical conductivity differences of aggregates with literature review.

3.9. Microstructural Properties of Aggregates

Microstructural properties of fine aggregates were determined by SEM-EDS analyses. These analyses were carried out with the small-sized particles less than 63 μm of aggregates used in Roman lime mortars. Increasing the magnification, we could observe the morphology of fine aggregates.

Fine aggregates presented irregular morphology in the SEM images; and consisted of small-sized amorphous particles with small crystal structures (Figure 60-64). SEM images also showed the glassy phases of silica. Amorphous particles enlarged the surface area of pozzolan that could increase the reactivity of pozzolan with lime. In analyzed samples, the frequency, shape, and size of the pozzolans were found highly similar.
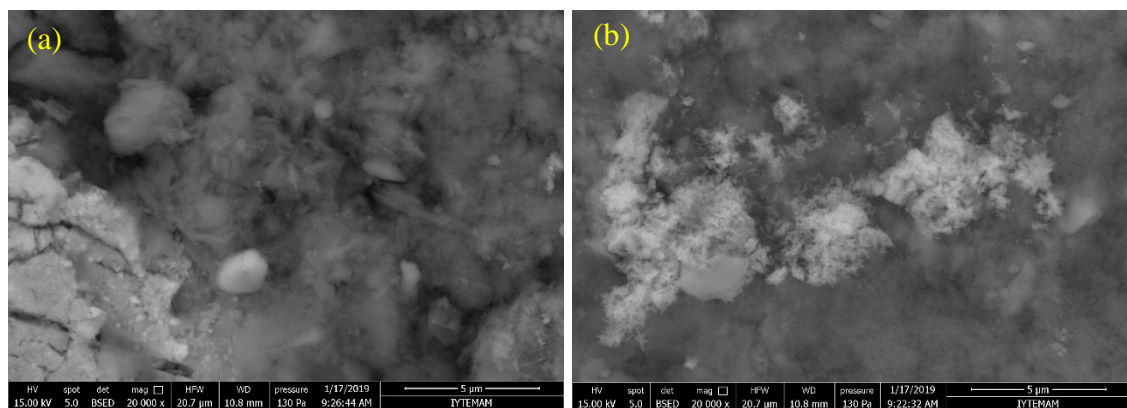
Figure 60. SEM images of fine aggregates (less than 63μm) used in *ACyH* and ACyT from Aiolis at magnifications of 20000 (a), 20000 (b).
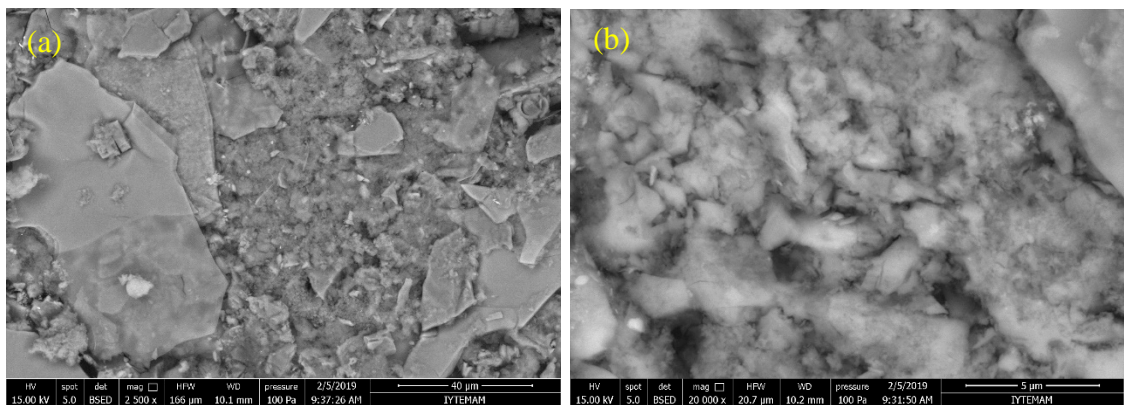
Figure 61. SEM images of fine aggregates (less than 63μm) used in CLB2 and CEB from Caria at magnifications of 2500 (a), 20000 (b).
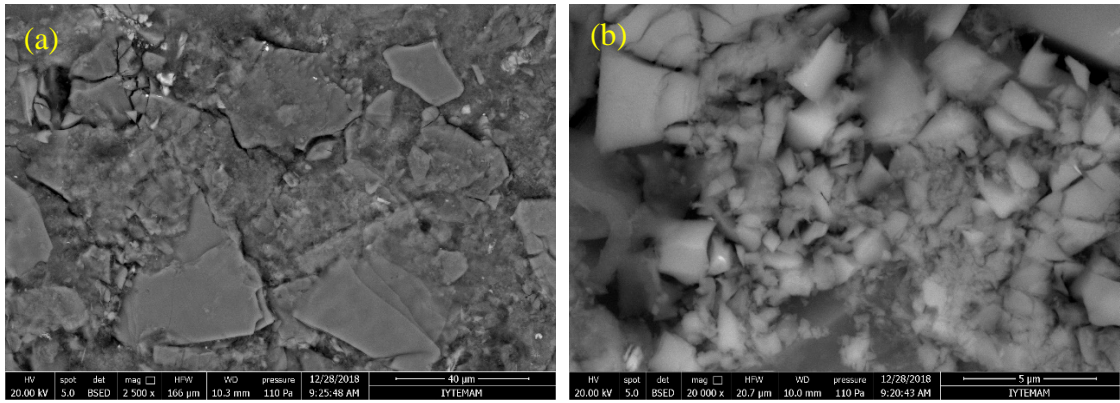
Figure 62 SEM images of fine aggregates (less than 63μm) used in IMA and IMG from Ionia at magnifications of 2500 (a), 20000 (b).
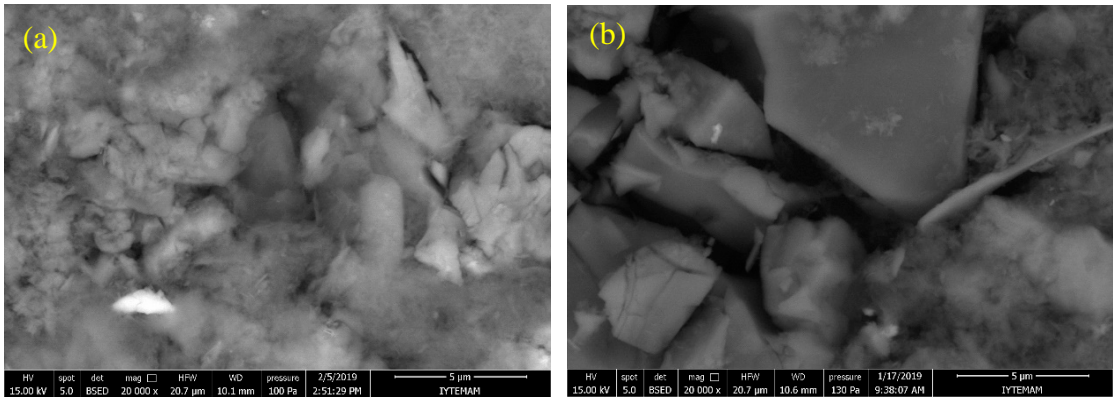
Figure 63.SEM images of fine aggregates (less than 63μm) used in LySrU and LyTpA from Lydia at magnifications of 20000 (a), 20000 (b).
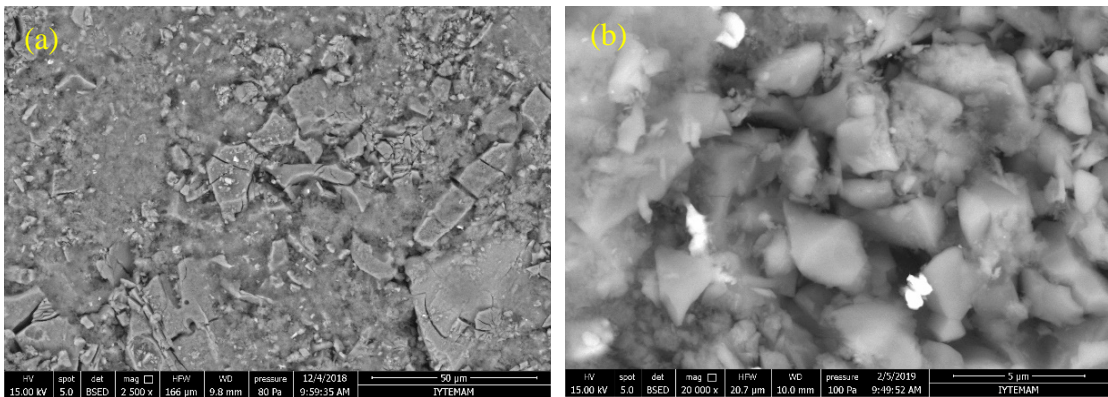
Figure 64.SEM images of fine aggregates (less than 63μm) used in PSA and PAtT from Pisidia at magnifications of 2500 (a), 20000 (b).

3.10. Geochemical Characterization of Aggregates

The geochemical characteristics of fine aggregates (pozzolans) of *opus caementicium* mortars were investigated based on their chemical compositions on the TAS diagram (Le Maitre et al. 2002). The geochemical composition of the fine aggregates could also provide information to determine the provenance of aggregates. The fine natural aggregates of *opus signinum* mortars could not be studied in terms of geochemical characteristics, due to the difficulty of separating small brick aggregates from natural ones that showed pozzolanic activity.

Results showed that fine aggregates had chemical composition ranging from basalt to rhyolite showing a highly variable silica content (SiO_2 ranges from 52-93%) and limited variability of alkali content (Na_2O_3 ranges from 0.2 to 0.7% and K_2O from 0 to 4%) (Figure 55). However, the predominant rock types were rhyolite and dacite in all the regions and archeological sites with a few exceptions (Figure 65).

The results of the TAS diagram were compatible with the mineralogical compositions of aggregates and pozzolanic activity measurements of aggregates. The minerals related to rhyolite and dacite were observed on the XRD patterns of aggregates of Roman lime mortars. Regarding the pozzolanicity, aggregates were found highly energetic parallel to the pozzolanic activity of rhyolite and dacite.

All the indicated five rocks, rhyolite, dacite, andesite, basaltic andesite, and basalt were extrusive igneous rocks formed by volcanic eruptions. However, rhyolite and dacite were distinct due to the high silica content (more than 63%). Rhyolite showed the pozzolanic activity that can be attributed to the chemical composition, fineness, and small amorphous phases (Richard et al. 1950; Massazza 1998; Baki et al. 2020). Literature showed that rhyolite tuffs, pumicites and dacite had the pozzolanic value while andesites, basalts and basaltic tuffs were found insufficient as a pozzolan (Hamidi et al. 2013; Yu, Zhou, and Deng 2015; Baki et al. 2020; Richard et al. 1950).

Rhyolite is a felsic (silica-rich) igneous extrusive volcanic rock, and it is generally glassy or fine-grained and dominated by quartz, alkali feldspar, oligoclase feldspar, sanidine, biotite, amphibole, or pyroxene. Rhyolite is available in grey, white, light black colors (Le Maitre et al. 2002).
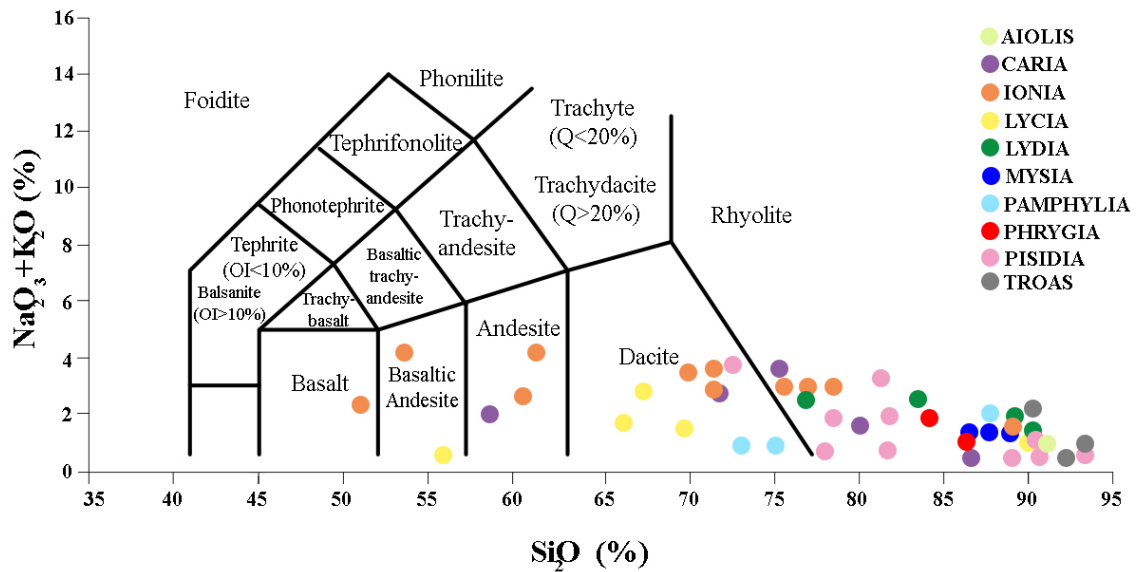
Figure 65. Classification of pozzolans by TAS diagram.
(Source: Le Maitre et al. 2002)

Dacite is a felsic igneous extrusive volcanic rock, and it is fine-grained. Dacite is composed of quartz and plagioclase with minor amounts of biotite, hornblende, or pyroxene. It is normally light in color. Dacite has less silica content than rhyolite (Le Maitre et al. 2002).

Andesite is an extrusive igneous volcanic rock and most commonly denotes fine-grained. The mineral assemblage is typically dominated by plagioclase, feldspar, pyroxene, or biotite. They are usually pale pink, yellow, or gray (Le Maitre et al. 2002).

Basaltic andesite is a volcanic rock, and it is different from basalt and andesite with a different percentage of silica content. In a general sense, it is the intermediate type between basalt and andesite, and containing about 55% silicon dioxide. Basaltic andesite is composed of olivine, augite, and plagioclase minerals. They are typically black (Le Maitre et al. 2002).

Basalt is an extrusive igneous volcanic rock that is comparatively rich in iron and magnesium. It is very fine-grained and compact. Basalt comprised of feldspar, plagioclase, augite, and pyroxene. Basalt is available in black, brown, light to dark grey colors (Le Maitre et al. 2002).

118
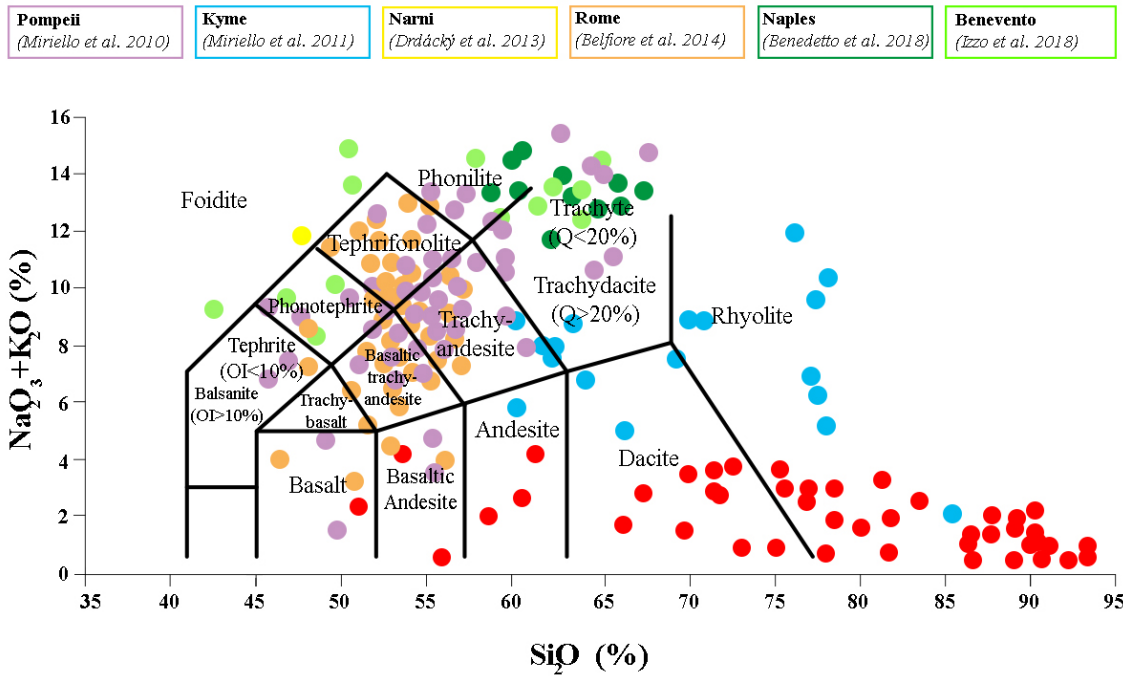
Figure 66. Geochemical comparison between literature review and samples of this study

Classification of fine aggregates identified on previous studies (colorful circles) and in this study (red dots) was made on TAS diagram (Figure 66) (Miriello et al. 2010, 2011; Drdácký et al. 2013; Benedetto et al. 2018; Izzo et al. 2018; Belfiore et al. 2015). Their compositions were variable, and pozzolans from Anatolia were not compatible with the pozzolans from Italy reported in the literature (Miriello et al. 2010; Benedetto et al. 2018; Izzo et al. 2018; Drdácký et al. 2013; Belfiore et al. 2015). The few samples in basalt and basaltic andesite fragments only matched with pozzolans from Pompeii and Rome. However, the majority of pozzolans identified in this study were in the same fragments as pozzolans from Kyme (Figure 66).

It seemed that there was a significant distinction on the TAS diagram between pozzolans from Italy and Anatolia. The locations of mortar containing volcanic ash and the volcanic zones in the Roman Empire were shown on the map (Figure 67). This map matched with the map showing the volcanic rock zones of Turkey (Figure 68). The predominance of volcanic rocks in the mortars suggested straight rhyolite deposits which were likely to have derived from the volcanic zones shown on map (Figure 68). These regions can be the sources of rhyolite in Anatolia, but future studies must be done to find the possible quarry regions.
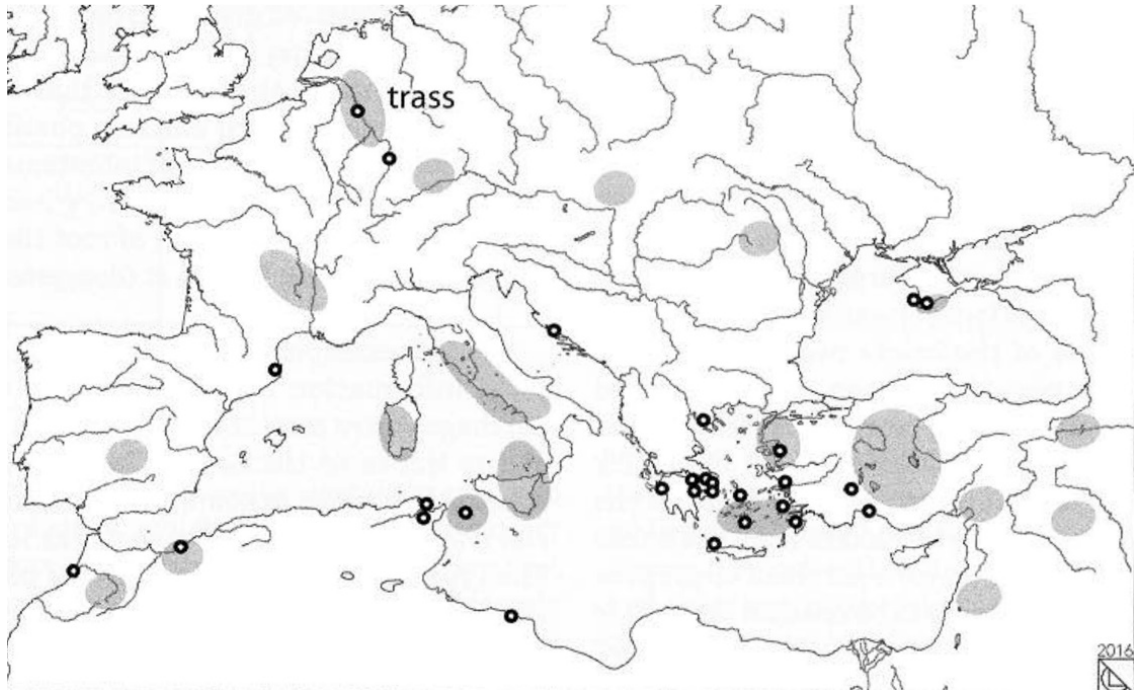
Figure 67. Locations of the volcanic zones (gray areas) and mortars containing volcanic ash (black dots) (Source: Lancaster 2019)
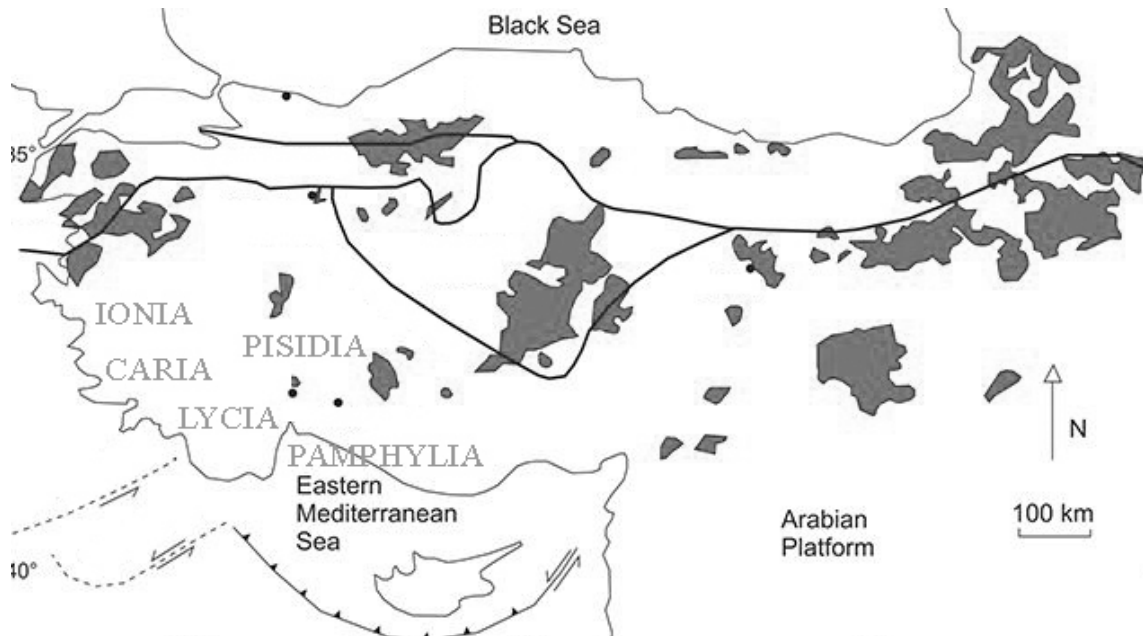
Figure 68. Volcanic rock zones of Turkey.
(Source: Robertson, Parlak, and Ünlügenç 2013)

The results of the comparison of studies could provide information regarding the role of geography on the use of pozzolans in mortar production in the Roman Empire. These results may be explained by the use of local aggregates as a raw material was common in Roman lime mortar production in Western Anatolia.

3.11. Mineralogical Compositions of Binders

Mineralogical compositions of fine mortar matrices (<63 µm) composed of the small size of aggregates and carbonated lime called "binder" were determined by XRD and FTIR analysis. XRD can be used to identify minerals in crystalline structure but it is not suitable for the detection of amorphous substances and organic additives. However, FTIR enables both the identification of amorphous minerals and organic additives (Uğurlu Sağın et al. 2012).

XRD analyses based on the surface and a powder were carried out to compare the results. Analyses based on the surface were conducted on twelve samples selected according to the results of the other analyses. Representative samples of each type and location were selected for the analysis.

Table 22. Mineralogical compositions of mortars based on surface and powder by XRD.

Sample	Minerals	
	Surface	**Powder**
ACyT	calcite, quartz, albite, anorthite, hematite, diopside	calcite, quartz, albite, phillipsite
CStB	calcite, quartz, albite, muscovite, diopside	calcite
CTrB	calcite, quartz, albite, muscovite	calcite, quartz, albite, hematite
IMS	calcite, quartz, albite, muscovite, hematite	calcite, quartz, albite, anorthite, muscovite
LPtB	calcite, quartz, sanidine, diopside	calcite, quartz, albite, dolomite, hematite
LyTpB	calcite, quartz, albite, anorthite, muscovite	calcite, quartz, albite
LXA	calcite, quartz, albite, anorthite, muscovite, diopside	calcite, quartz, albite, hematite
MPB	calcite, quartz, sanidine, muscovite	calcite, quartz, albite
PmLyC	calcite, quartz, diopside	calcite, quartz
PhLdB	calcite, quartz, albite, muscovite, diopside	calcite, quartz
PSA	calcite, quartz, sanidine, diopside	calcite, quartz
TACs	calcite, quartz, albite, anorthite, sanidine, muscovite, hematite	calcite, quartz, albite

Mineralogical compositions of mortars identified on the surface indicated that Roman mortars were composed of calcite, quartz, sanidine, albite, anorthite, hematite, muscovite, and diopside (Figure 69 and Figure 70) (Table 22). The differences between mineralogical compositions of mortars based on surface and powder by XRD were given (Table 22). An in-depth analysis of comparison of the two methods was not within the scope of this study. However, it can be said that XRD analyses conducted on surface of mortars detected more types of minerals than the other method.

Having regard to this, analyzed Roman mortars had almost the same mineralogical compositions as mortars in different areas such as Turkey, Italy, Spain, Portugal, and Serbia (Table 23). However, mortars from Kyme, Amastris, Nysa in Turkey containing calcite, quartz, muscovite, hematite, and albite were much more similar than other regions with analyzed mortars (Table 23). References were given in Table 23.

XRD patterns of binders according to the regions were as follows:

Binders of lime mortars from Aiolis were mainly composed of calcite, quartz, albite, and phillipsite (Figure 71). In the XRD patterns of binders from Caria, calcite and quartz showed strong peaks, and albite and hematite showed weaker peaks (Figure 72). In the Ionia region, calcite and quartz were observed as the primary minerals, and albite, anorthite, muscovite, dolomite, and phillipsite were observed as the secondary minerals (Figure 73). In Lycia, binders were comprised of calcite and quartz as the primary minerals and albite, hematite, and dolomite as the secondary minerals (Figure 74). XRD patterns revealed that binders of lime mortars from Lydia, Mysia, Pamphylia were mainly composed of calcite, quartz, and albite (Figure 75-76 and Figure 78). In Phrygia and Pisidia, calcite and quartz as the primary minerals were identified in XRD patterns of binders (Figure 77 and Figure 79). XRD patterns indicated that binders of lime mortars from Troas were mainly composed of calcite, quartz, and albite and hematite (Figure 80).
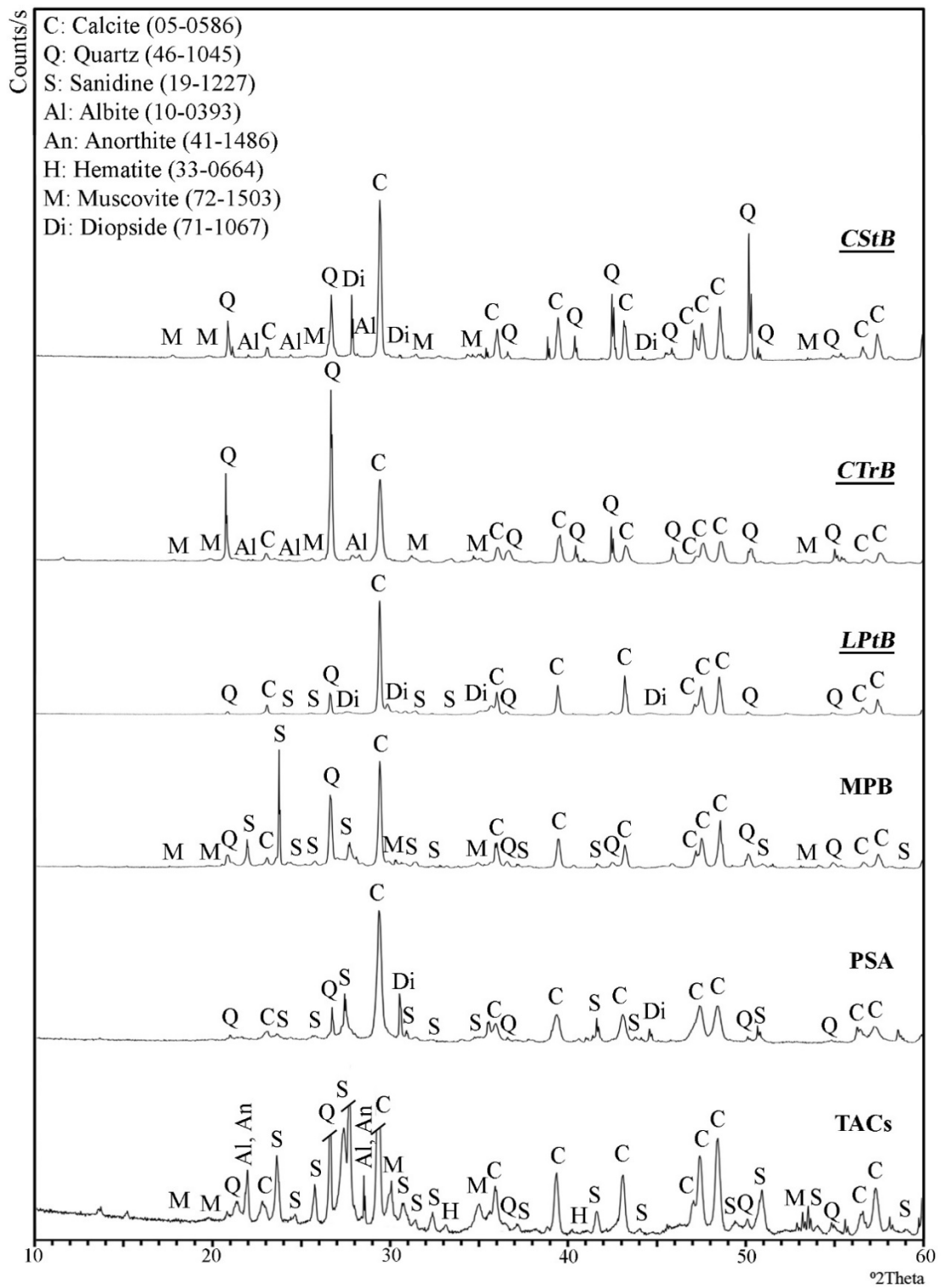
Figure 69. XRD patterns of binders of Roman lime mortars – 1.
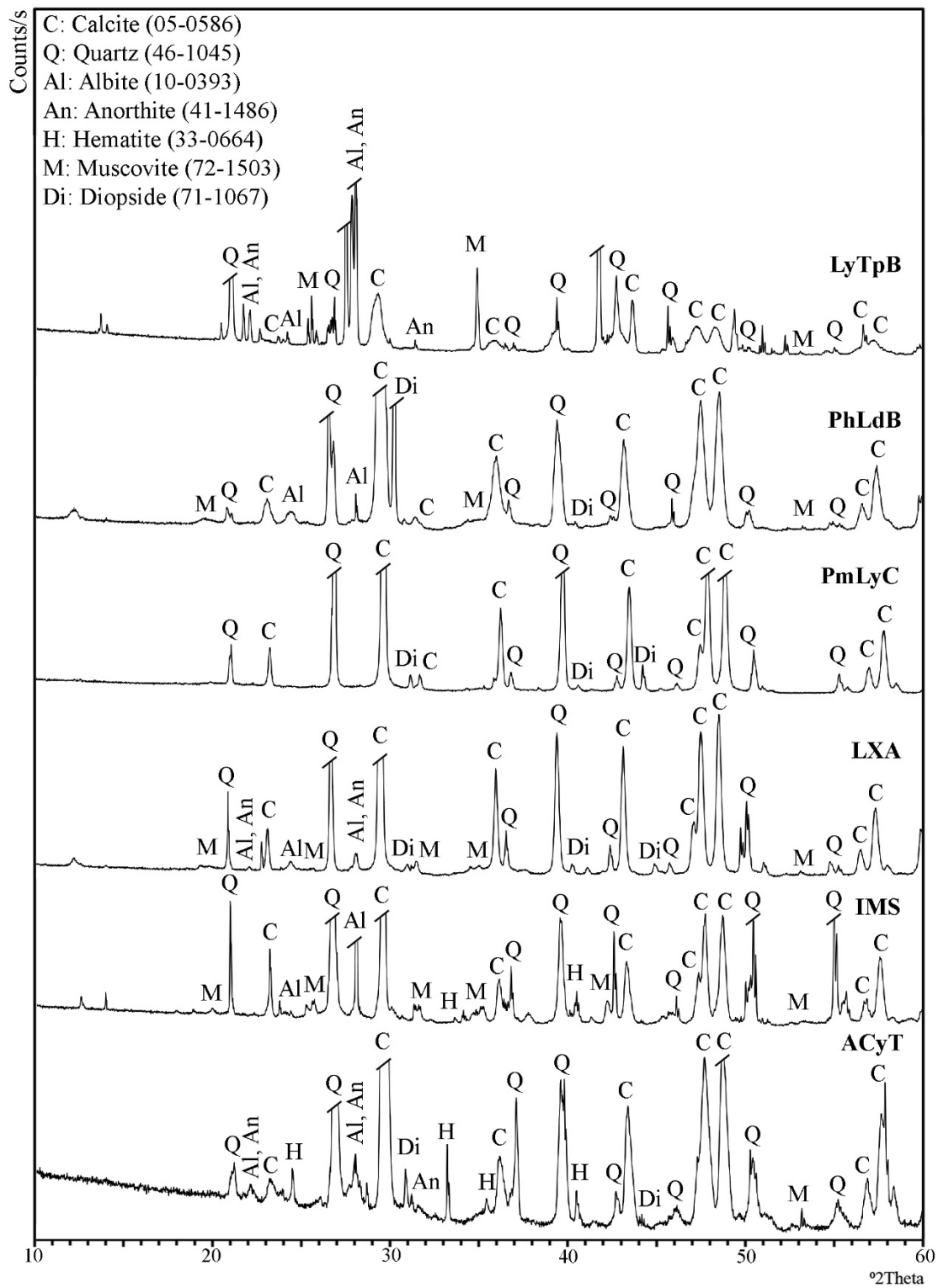
Figure 70. XRD patterns of binders of Roman lime mortars – 2.

Table 23. Mineralogical compositions of Roman lime mortars as a result of previous studies.

Region	Case area (Reference)	Method	MINERALS																								
			Cal	Qtz	Fsp	Dol	Ms	Mi	Am	Hem	Aug	Gp	Chl	Bt	Anl	Pl	An	Sa	Px	Kln	Mgs	Tbr	Al	Gt	Di	Lct	Ill	Oth
	Analyzed samples of this study	XRD	+	+			+			+						+	+	+					+	+				+
TURKEY	Kyme (*Miriello et al. 2011*)	XRD, SEM-EDS	+	+			+			+			+			+							+	+				+
TURKEY	Amastris (*Kurugöl and Gülec 2015*)	XRD, OM	+	+	+		+						+	+			+	+										
TURKEY	Nysa (*Ergenç et al. 2016*)	POM, XRD, Raman	+	+	+		+			+	+		+	+		+		+	+									+
ITALY	Sorrento (*Benedetti et al. 2004*)	XRD	+	+			+			+					+		+	+						+				+
ITALY	Rome (*Sánchez-Moral et al. 2005*)	XRD	+	+	+						+		+	+	+													+
ITALY	Pompeii (*Miriello et al. 2010*)	XRD, OM	+	+							+					+		+	+		+	+	+		+			
ITALY	Lecce (*Gulotta et al. 2016*)	XRD	+	+	+					+																		
OTHER COUNTRIES	Conímbriga, Portugal (*Velosa et al. 2007*)	XRD	+	+	+	+															+							+
OTHER COUNTRIES	Augusta Emerita, Spain (*Franquelo et al. 2008*)	XRD	+	+				+								+												
OTHER COUNTRIES	Jerash, Jordan (*Yaseen et al. 2013*)	XRD, OM	+	+	+	+		+			+			+						+								+
OTHER COUNTRIES	Mediana, Serbia (*Gordona et al. 2014*)	XRD	+	+	+	+		+			+																	+
OTHER COUNTRIES	Ammaia, Portugal (*Cardoso et al. 2014*)	XRD	+	+	+			+			+	+														+	+	+
OTHER COUNTRIES	Italica, Spain (*Ontiveros-Ortega et al. 2016*)	XRD, SEM, PM	+	+	+	+	+				+	+		+							+	+						+
OTHER COUNTRIES	Pisões, Portugal (*Borsoi et al. 2019*)	XRD	+	+			+				+								+	+								
OTHER COUNTRIES	Complutum, Spain (*Ergenç and Fort 2019*)	XRD, PM	+	+	+		+				+	+				+		+	+									+
OTHER COUNTRIES	Wallsend, United Kingdom (*Laycock et al. 2019*)	XRD	+	+	+	+										+			+									

125
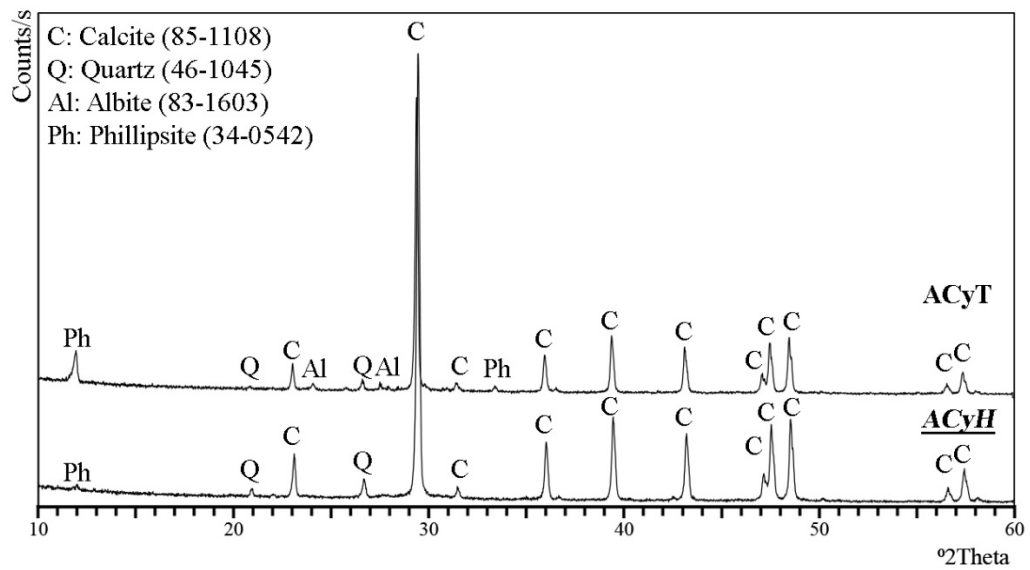
Figure 71. XRD patterns of binders of Roman lime mortars in Aiolis.
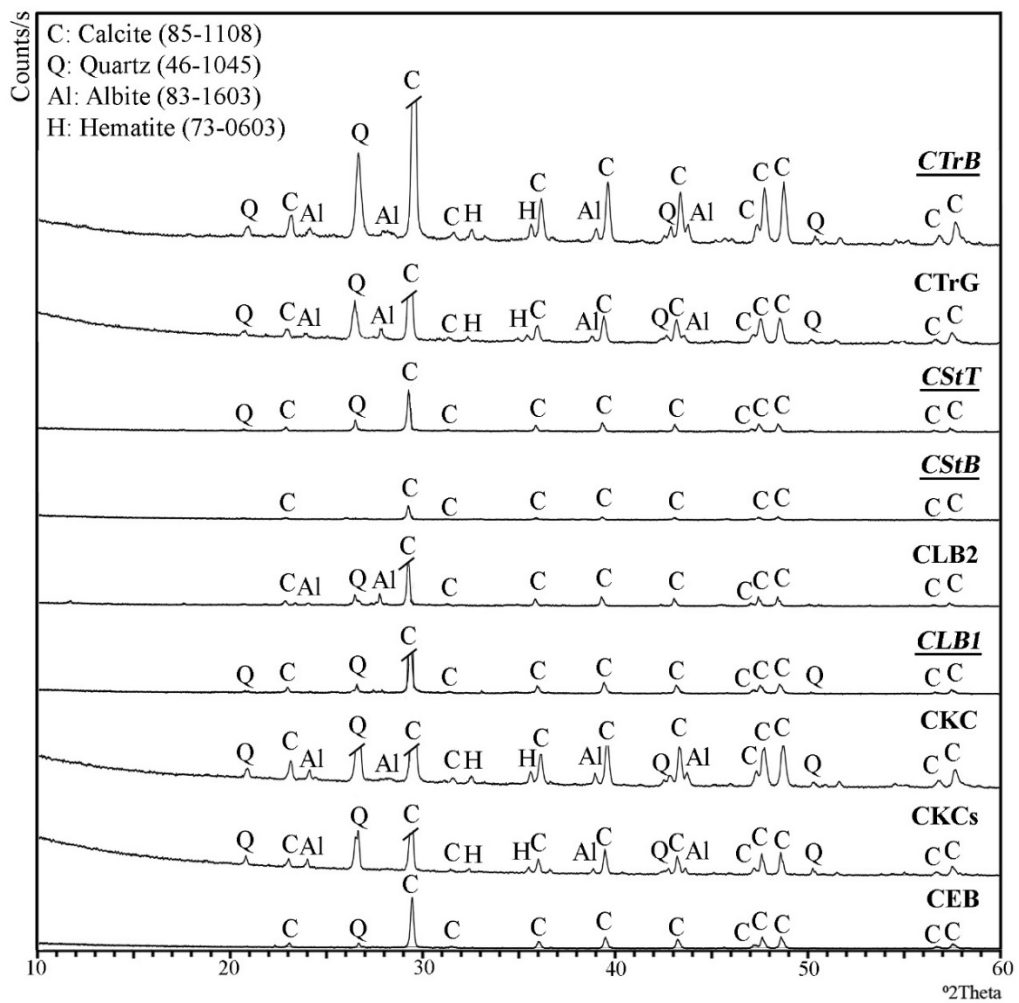
Figure 72. XRD patterns of binders of Roman lime mortars in Caria.

126
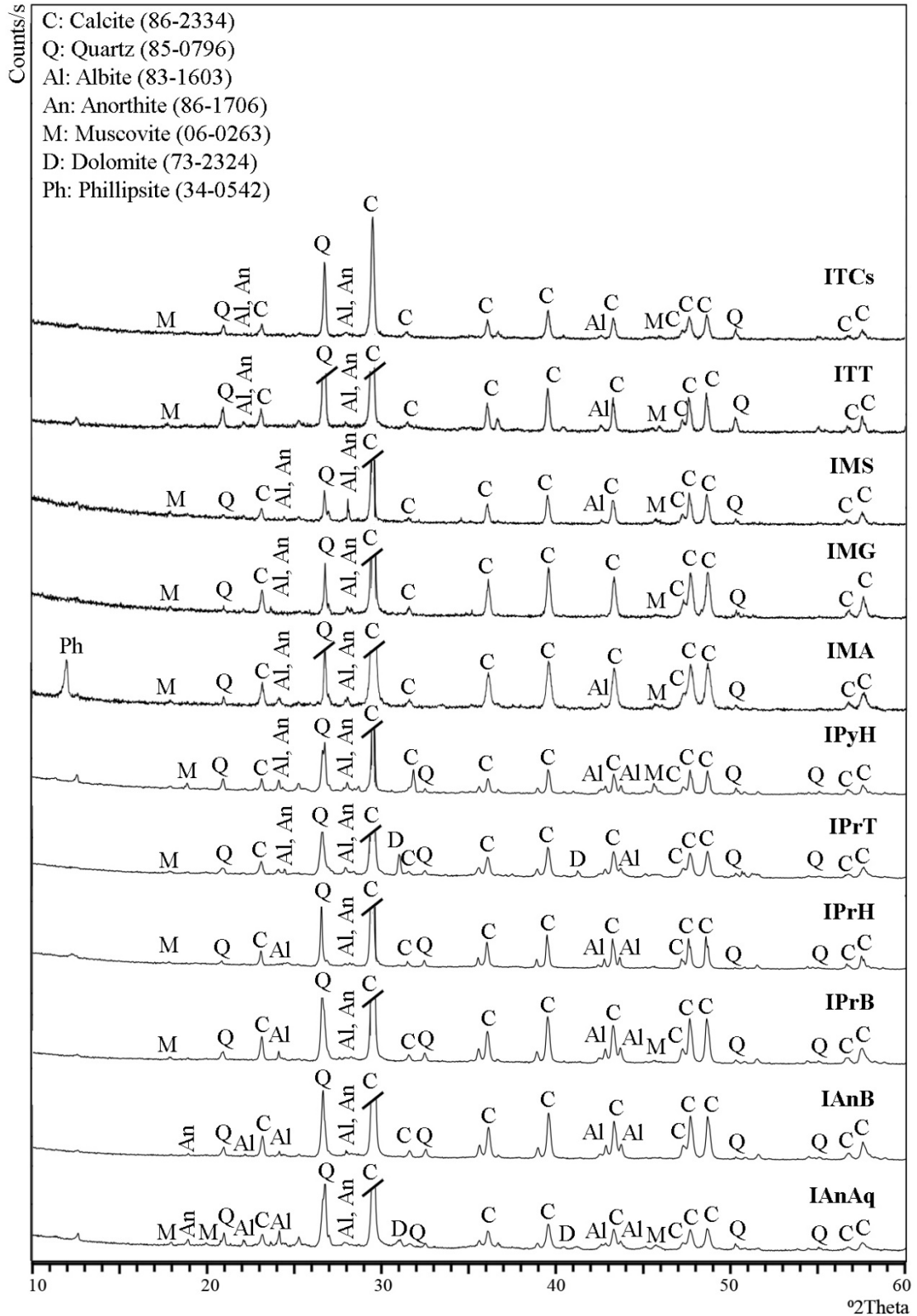
Figure 73. XRD patterns of binders of Roman lime mortars in Ionia.
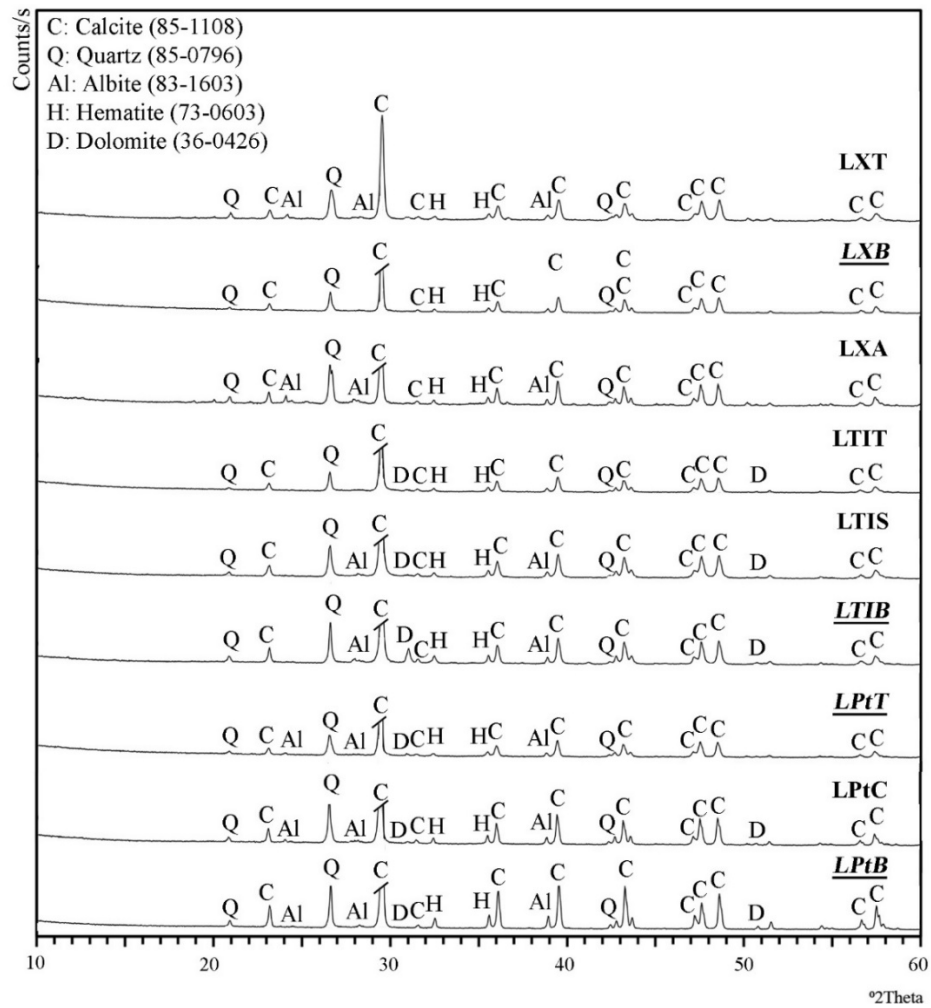
Figure 74. XRD patterns of binders of Roman lime mortars in Lycia.
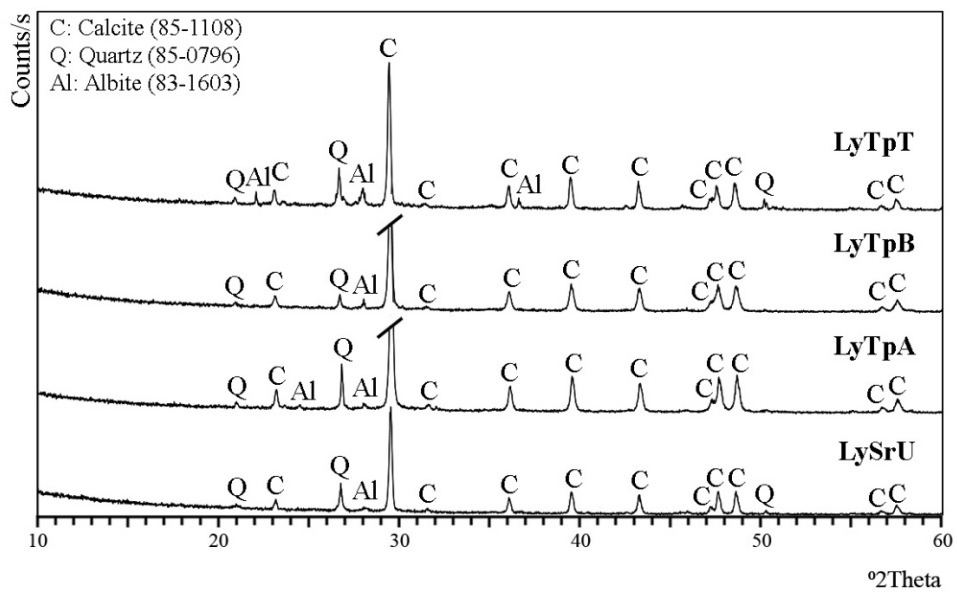
Figure 75. XRD patterns of binders of Roman lime mortars in Lydia.
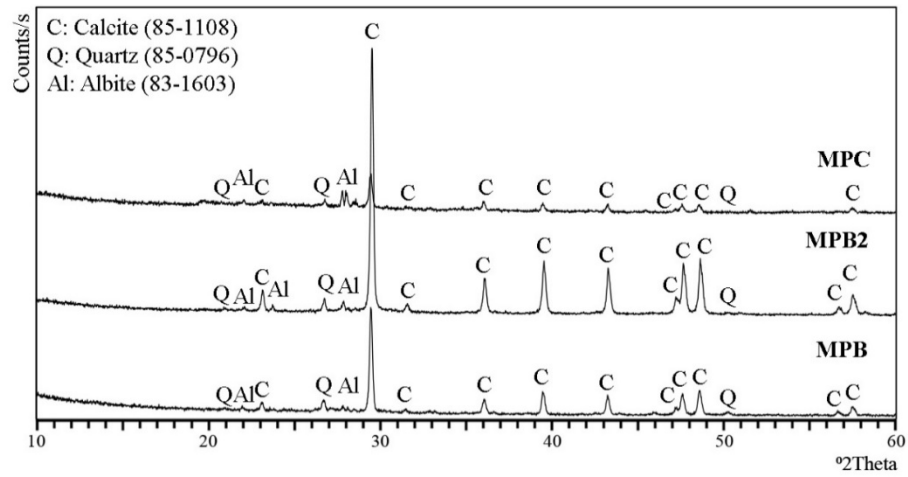
Figure 76. XRD patterns of binders of Roman lime mortars in Mysia
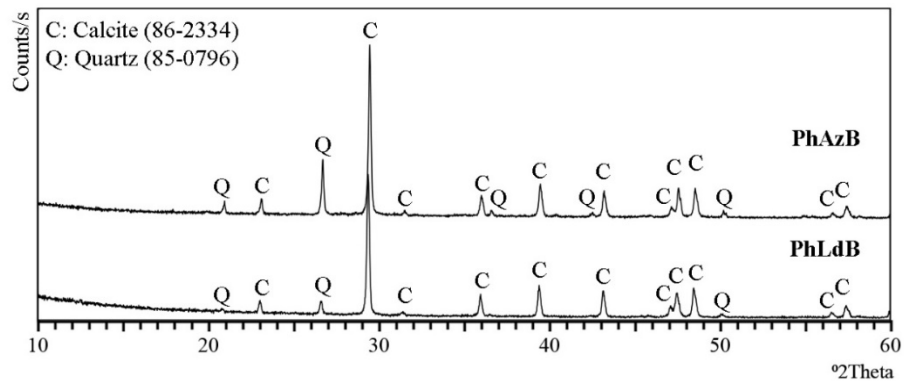
Figure 77. XRD patterns of binders of Roman lime mortars in Phrygia
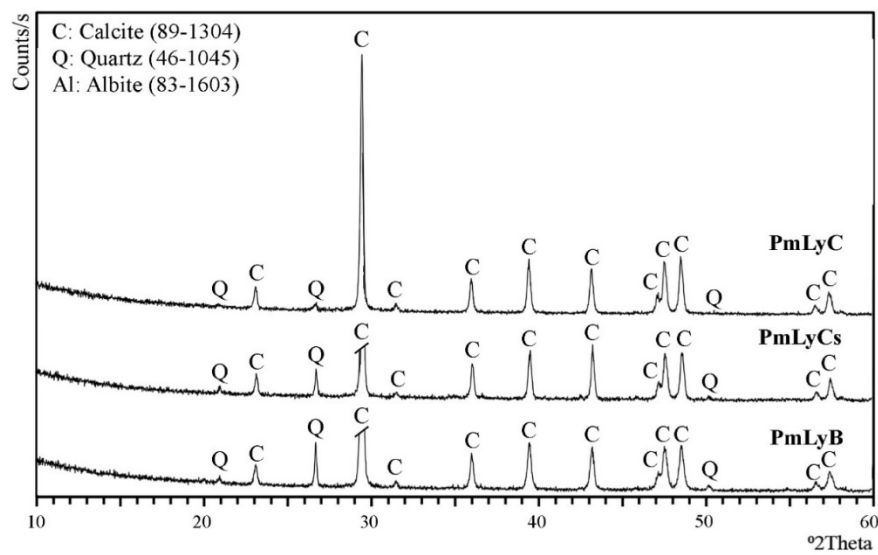
Figure 78. XRD patterns of binders of Roman lime mortars in Pamphylia
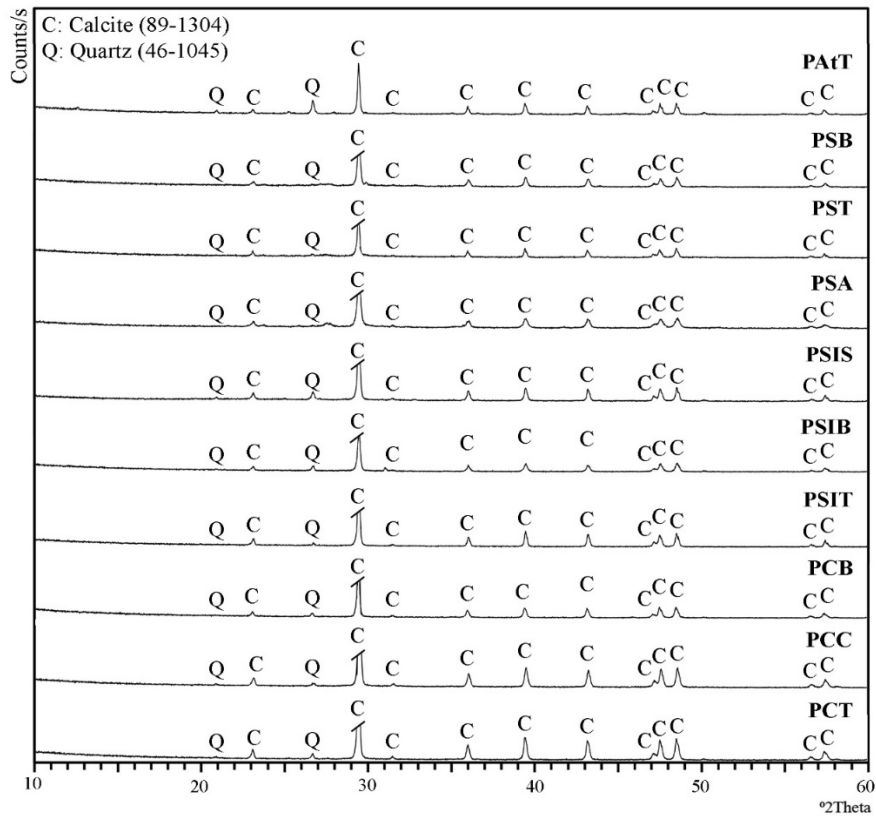
Figure 79. XRD patterns of binders of Roman lime mortars in Pisidia.
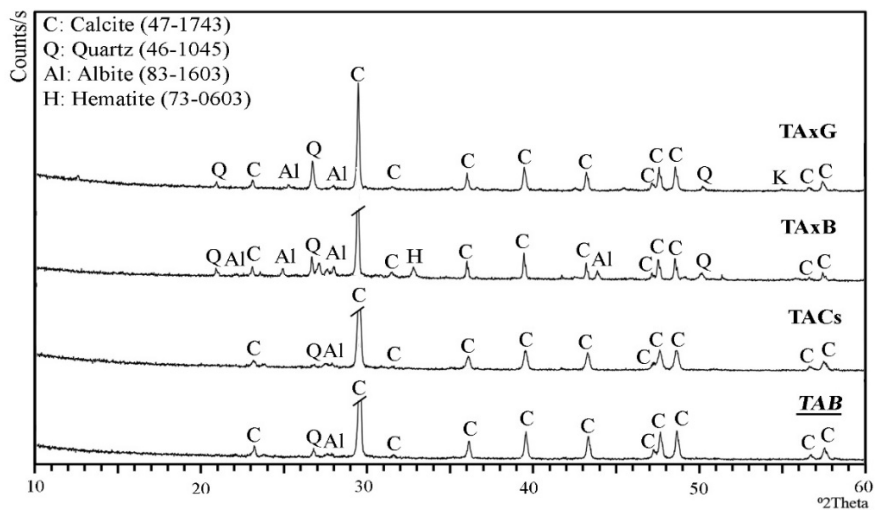
Figure 80. XRD patterns of binders of Roman lime mortars in Troas.

These results revealed that mineralogical compositions of binders of mortars from different regions were almost the same as each other by having calcite, quartz, and albite. In addition to these minerals, binders of mortars from Aiolis, Caria, Ionia, Lycia, and

Troas had also phillipsite, muscovite, anorthite, hematite, dolomite, minerals as trace minerals (Figure 81).
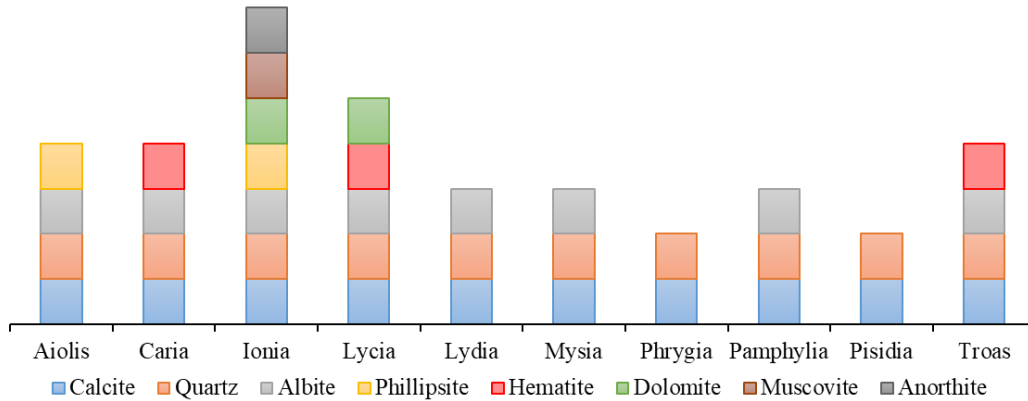
Figure 81. Mineralogical compositions of binders from Roman lime mortars.

According to results, it can be said that binders were comprised of mainly calcite, quartz, feldspar, and mica minerals. Calcite was originated from carbonated lime, while quartz and other minerals were from fine aggregates. Feldspars and biotite can be originated from volcanic aggregates.

It was expected that peaks of amorphous silicas as a pozzolanic mineral, and calcium silicate hydrate and calcium aluminate hydrate as hydraulic products formed as a result of the reaction between lime and pozzolanic aggregates could be observed. However, the peaks of the pozzolanic minerals and the hydraulic reaction products were not observed on the XRD patterns. This unexpected situation may be due to the overlapping of principal peaks of calcite and the hydraulic reaction products or due to their amorphous character.

Mineralogical compositions of binders were also determined by FTIR. The FTIR spectrum of the binders indicated the bands of stretching and bending vibrations of $CaCO_3$ ($\sim$1430, 874, and 712 cm^{-1}) and SiO_2 ($\sim$1031 and 470 cm^{-1}) (Figure 82-91). FTIR spectra of some samples showed small bands at $\sim$1630 and $\sim$536 cm^{-1} showing the presence of iron oxide (Figure 82-91). Also, the band at $\sim$3400 cm^{-1} was due to bound water. The minor peaks at $\sim$2502-2535 and 1788 cm^{-1} (C-O stretching) were due to the adsorption of the atmospheric CO_2 (Figure 82-91).
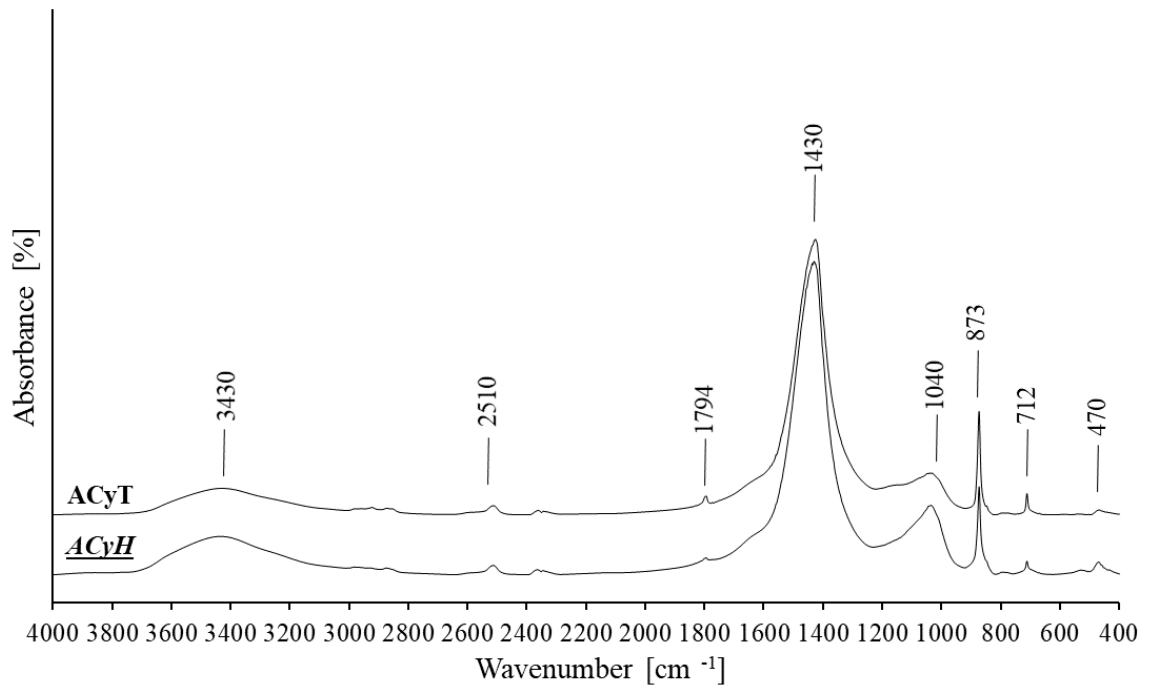
Figure 82. FTIR spectra of binders of Roman lime mortars in Aiolis.
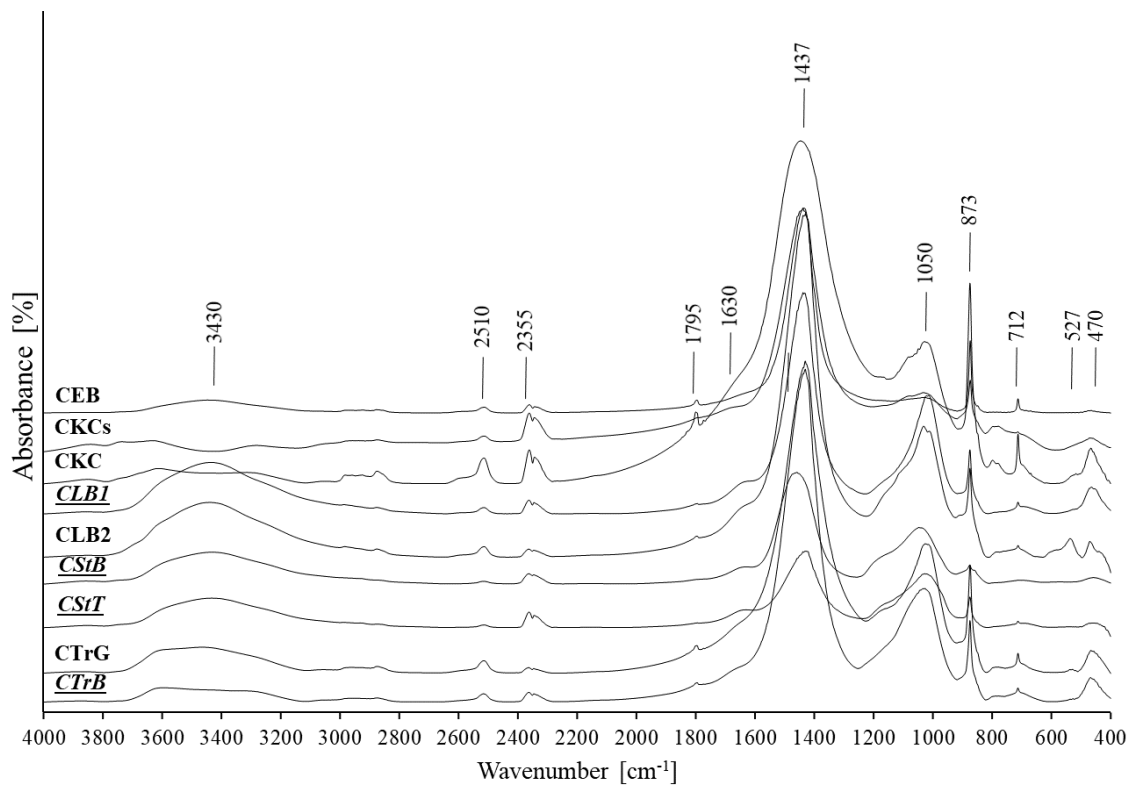
Figure 83. FTIR spectra of binders of Roman lime mortars in Caria.
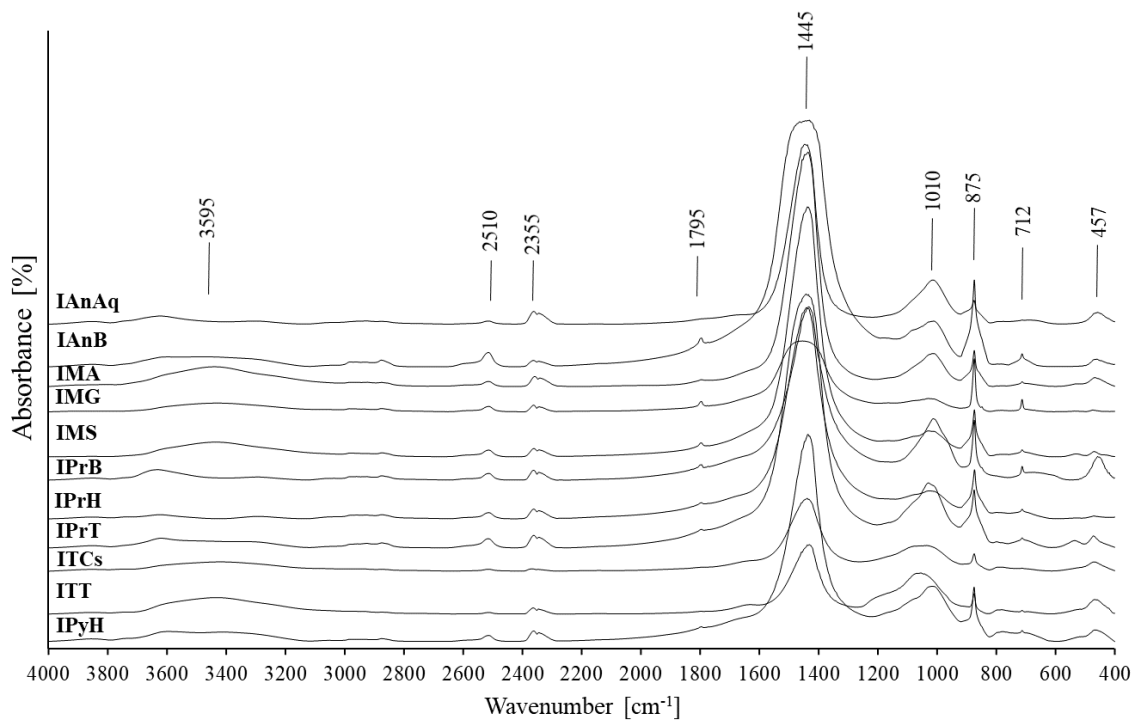
Figure 84. FTIR spectra of binders of Roman lime mortars in Ionia.
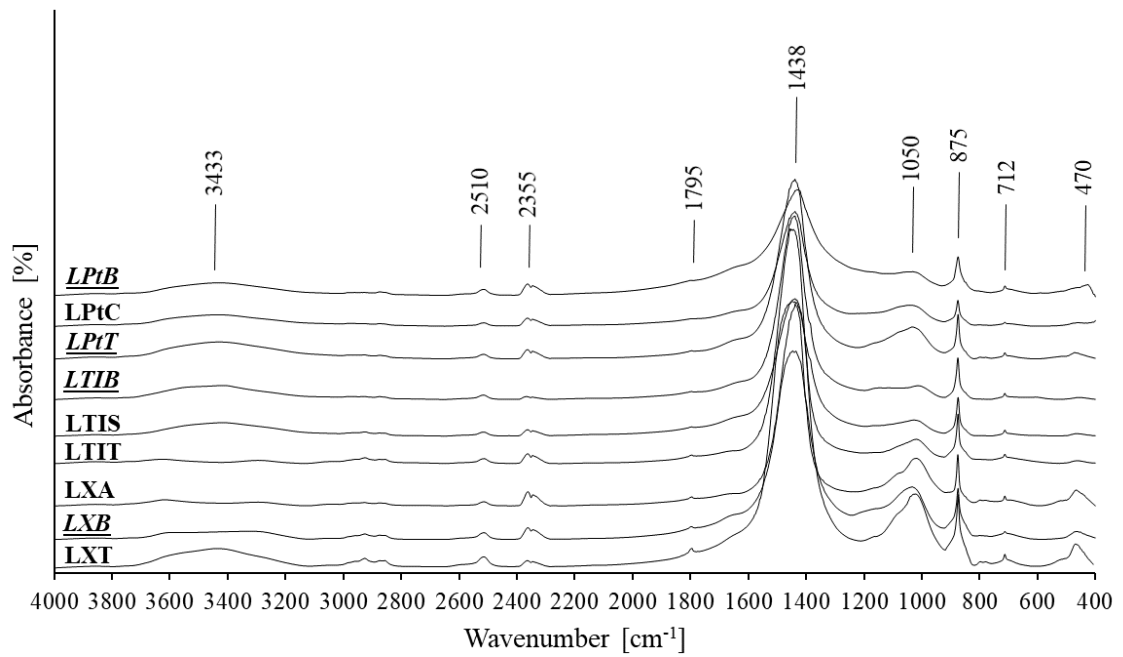
Figure 85. FTIR spectra of binders of Roman lime mortars in Lycia.

133
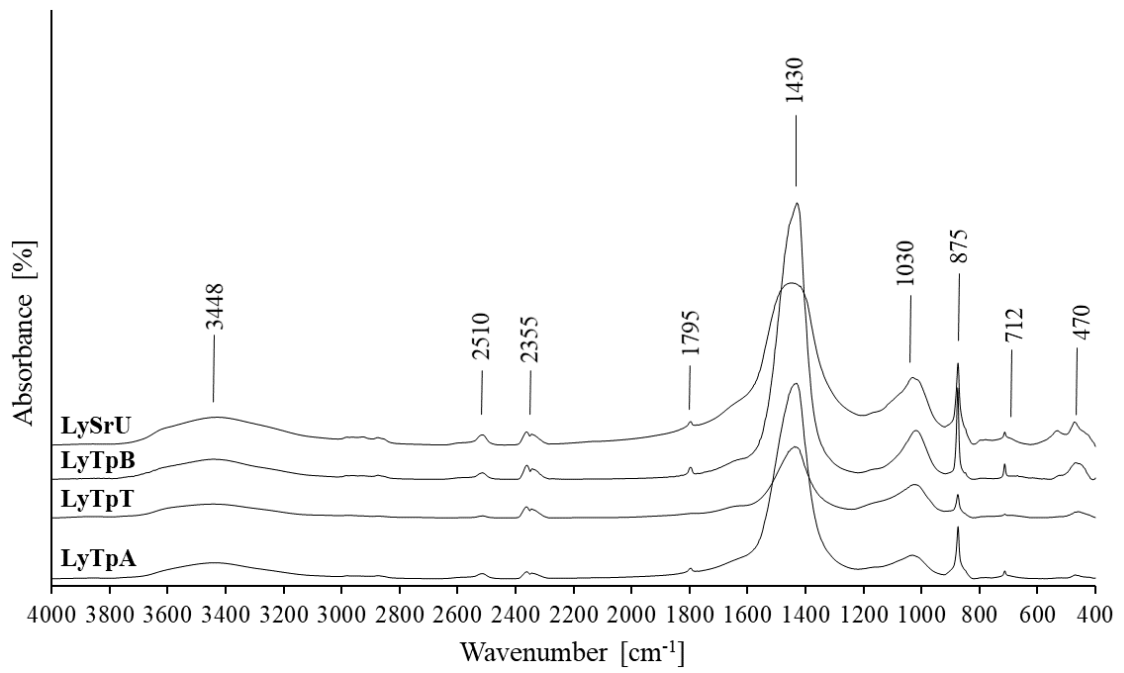
Figure 86. FTIR spectra of binders of Roman lime mortars in Lydia
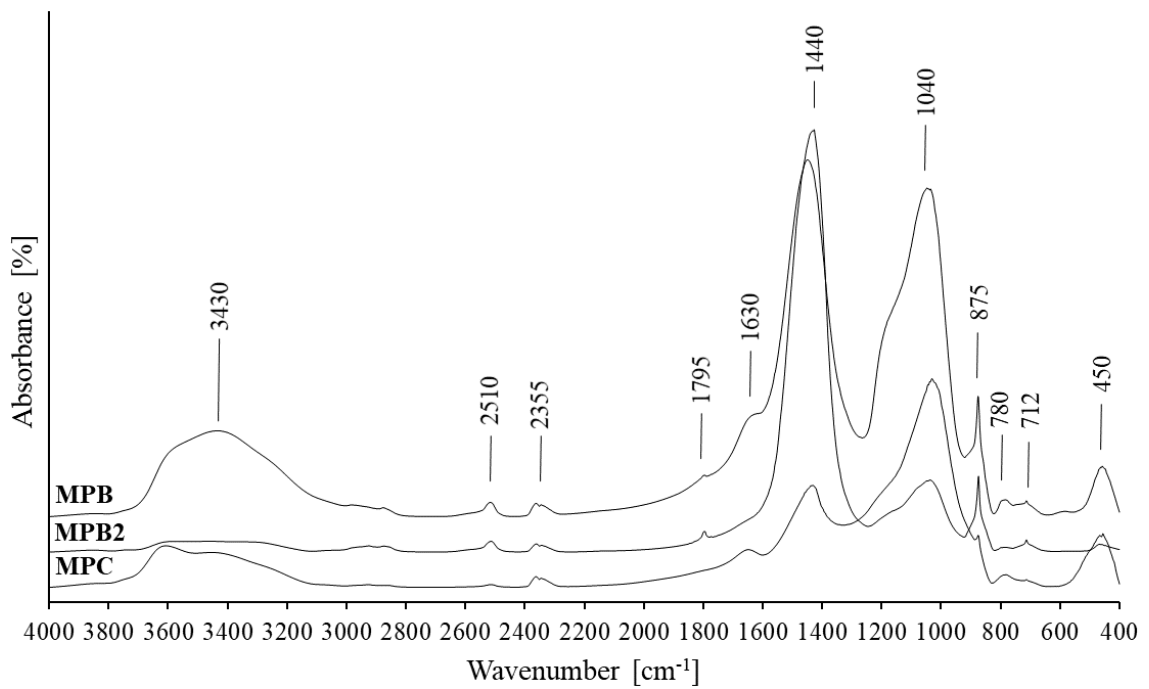
Figure 87. FTIR spectra of binders of Roman lime mortars in Mysia
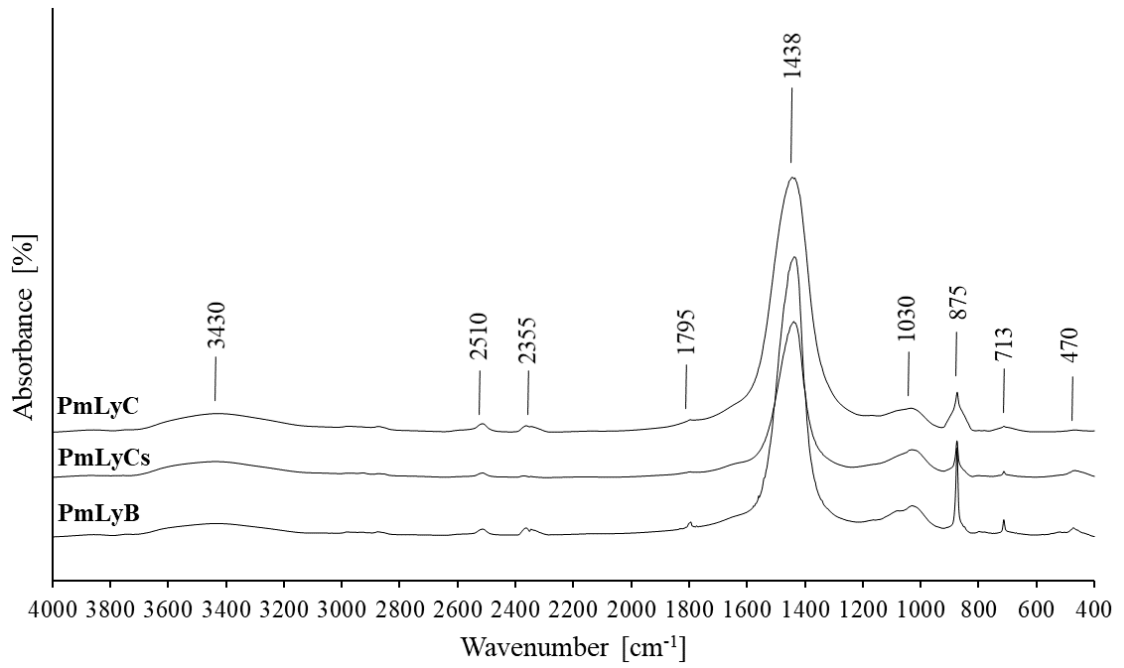
Figure 88. FTIR spectra of binders of Roman lime mortars in Pamphylia.
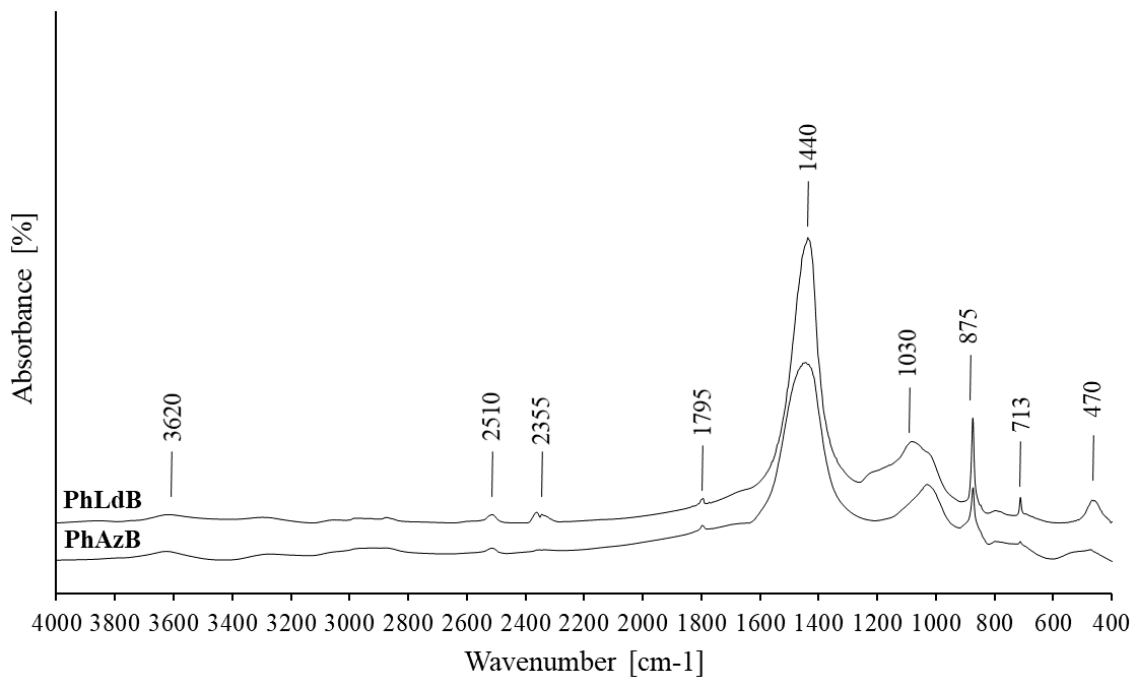
Figure 89. FTIR spectra of binders of Roman lime mortars in Phrygia.

135
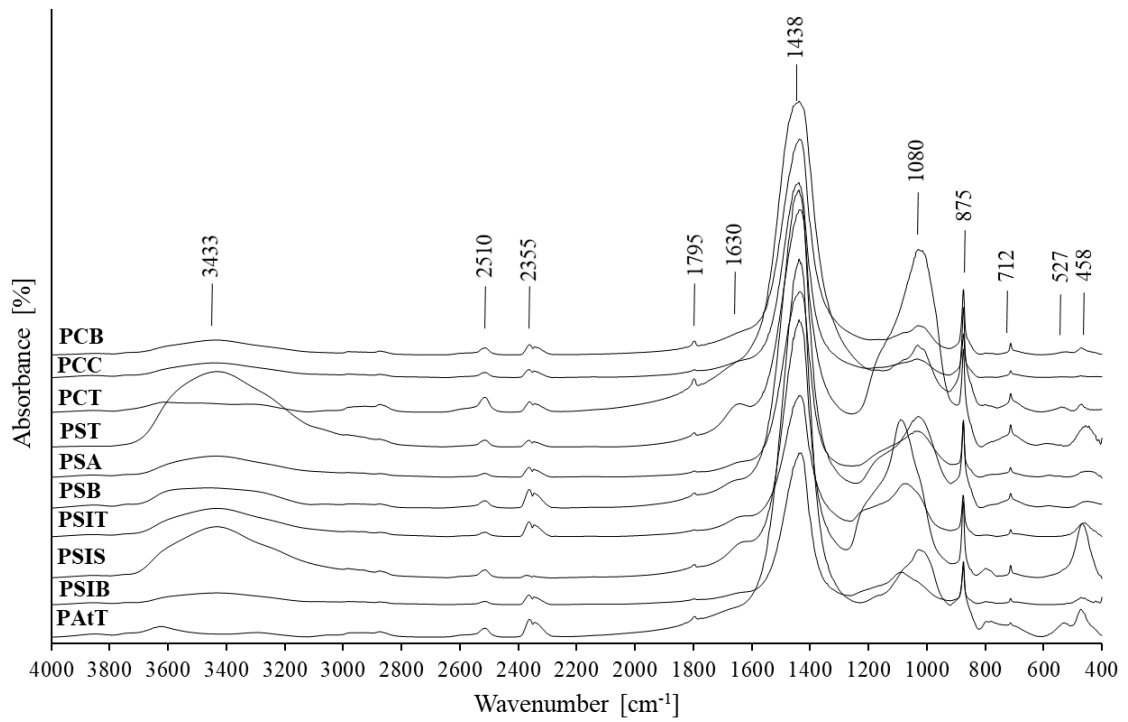
Figure 90. FTIR spectra of binders of Roman lime mortars in Pisidia.
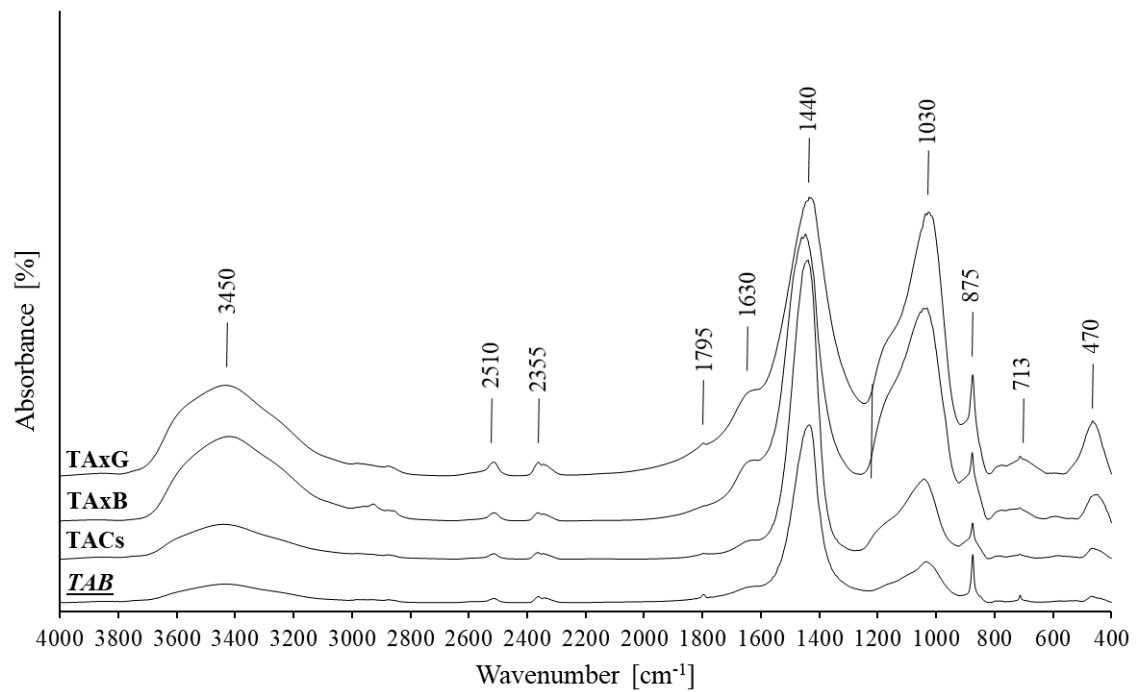
Figure 91. FTIR spectra of binders of Roman lime mortars in Troas

There were no considerable differences between the mineralogical compositions of binders of *opus caementicium* and o*pus signinum* mortars determined by XRD and FTIR analyses.

Mineralogical compositions of binders were determined mainly in previous studies of Turkey, Italy, Spain, and Slovenia (Table 24). References can be found in Table 24. Considering these studies, binders of Roman lime mortars were comprised of mica, diopside, leucite, halite, sanidine, gypsum, kaolinite, analcime, tobermorite, strätlingite, ettringite, plagioclase, chlorite, magnesite, anorthoclase, feldspar, and illite in addition to calcite, quartz, dolomite, muscovite, anorthite, albite, phillipsite and hematite that were defined in binders of lime mortars studied (Table 24).

Table 24. Mineralogical compositions of binders of Roman lime mortars as a result of previous studies.

Country	Case area (Reference)	Method	Cal	Qtz	Dol	Ms	Mi	Di	An	Lct	Hl	Sa	Gp	Anl	Tbr	St	Etr	Al	Pl	Chl	Mgs	Ano	Fsp	Ill	Kln	Ph	Hem	Oth
	Samples of this study	XRD	+	+	+	+			+									+								+	+	
TURKEY	Sagalassos (*Degryse et al. 2002*)	XRD							+	+		+																+
TURKEY	Pergamon (*Özkaya 2005*)	XRD	+	+																								
TURKEY	Soli-Pompeiopolis (*Stanislao et al. 2011*)	XRD, SEM-EDS	+												+		+											
TURKEY	Aigai and Nysa (*Uğurlu Sağın 2012*)	XRD	+	+		+			+									+										
TURKEY	Tarsos and Anavarza (*Polat Pekmezci 2012*)	XRD	+	+	+	+	+						+															
TURKEY	Kyme (*Miriello et al. 2015*)	XRD	+	+			+				+								+	+								+
TURKEY	Myra (*Oğuz et al. 2015*)	XRD	+	+	+																							
TURKEY	Smyrna (*Felekoğlu et al. 2016*)	XRD	+	+																								
ITALY	Sicily (*Rizzo et al. 2008*)	XRD	+	+	+			+	+		+										+	+	+					
ITALY	Rome (*Jackson et al. 2009*)	XRD	+					+		+	+	+		+		+						+						+
ITALY	Rome (*Jackson et al. 2011*)	XRD	+					+		+				+		+												+
ITALY	Narni (*Cantisani et al. 2002; Drdácký et al. 2013*)	XRD	+												+													
ITALY	Lecce (*Gulotta et al. 2016*)	FTIR	+																									
ITALY	Tivoli (*Columbu et al. 2017*)	XRD	+	+		+				+			+				+											+
OTHER COUNTRIES	Pollentia, Spain (*Genestar et al. 2006*)	XRD	+	+																								
OTHER COUNTRIES	Augusta Emerita, Spain (*Robador et al. 2010*)	XRD	+	+			+		+																			
OTHER COUNTRIES	Mošnje, Slovenia (*Kramar et al. 2011*)	XRD	+	+	+	+																						
OTHER COUNTRIES	Uxama Argela, Spain (*Alonso-Olazabal et al. 2019*)	XRD	+	+																				+	+			+

3.12. Chemical Compositions of Binders

The oxide compositions of fine matrices (binder) of mortars were determined by SEM-EDS analysis. Results indicated that binders were composed of high amount of CaO (32-88%) and SiO_2 (7-60%), and moderate amount of Al_2O_3 (2-16%) and MgO (0-14%) and lower amounts of Fe_2O_3 (0-6%), K_2O (0-3%), SO_3 (0-3%) and Na_2O_3 (0-3%) (Table 25 and Table 26). There was no significant difference between the results of chemical analyses of *opus caementicium* and *opus signinum* mortars.

EDS analysis presented magnesium content of more than 5% with lower siliceous content between 8-11% in some cases (IPrB, IPrT, LTIT, LTIS, LyTpB, LyTpT). These mortars, except LyTpB, were composed of dolomitic aggregates confirmed by XRD analysis showing the presence of dolomite. The presence of magnesium may also indicate a dolomitic binder as LyTpB which was classified as DL80 previously. *Opus signinum* mortar (*IPrB*) had the highest ratio of MgO which can be attributed that the magnesium was from the ceramics and not the lime binder.

The differences in Fe_2O_3 and Al_2O_3 content may be derived from the pozzolanic aggregates, and the difference in MgO content may be due to the type of lime used. This information can be also regarded as the use of dolomitic aggregates in the Ionia, Lycia, and Lydia regions.

When compared to results with previous studies, binders were found to be almost similar chemical compositions with binders used in Roman lime mortars from Kyme, Aigai, Nysa, Tarsos, Anavarza in Turkey, Rome, Pompeii and Narni in Italy, and Mošnje in Slovenia (Table 5). References were given in Table 5. These results showed that binders of Roman lime mortars were composed of a high amount of carbonated lime and a minor amount of magnesium, silica, alumina, and iron.

Table 25. Chemical compositions of binders of *opus caementicium* mortars determined by SEM-EDS (%).

Region Name	CaO	MgO	SiO₂	Al₂O₃	FeO	K₂O	SO₃	Na₂O₃
Aiolis (1 Sample)	78	0.7	16	4	1	0.4	–	–
Caria (5 Samples)	48-82 63±14.4 (ave.)	1-7 3±2.8 (ave.)	12-32 24±8.1 (ave.)	4-15 7±4.8 (ave.)	1-4 2±1.3 (ave.)	0-2 1±0.8 (ave.)	–	–
Ionia (11 Samples)	35-81 63±15.1 (ave.)	1-14 5±4.3 (ave.)	11-51 21±12.7 (ave.)	4-10 7±2.1 (ave.)	1-4 3±0.9 (ave.)	0-1 0.3±0.5 (ave.)	–	0-3 1±0.9 (ave.)
Lycia (5 Samples)	61-77 71±7.8 (ave.)	3-9 5±2.5 (ave.)	9-23 17±6.5 (ave.)	2-6 4±2.0 (ave.)	0-4 2±1.6 (ave.)	0-1 0.2±0.5 (ave.)	0-1 0.2±0.4 (ave.)	–
Lydia (4 Samples)	47-79 64±13.2 (ave.)	1-7 4±2.6 (ave.)	14-36 22±9.7 (ave.)	4-9 7±2.2 (ave.)	2-3 2±0.5 (ave.)	0-2 1±0.8 (ave.)	–	–
Mysia (3 Samples)	16-75 43±29.9 (ave.)	1-3 2±0.8 (ave.)	18-60 42±21.7 (ave.)	4-12 9±4.1 (ave.)	1-6 3±2.7 (ave.)	0-3 1±1.6 (ave.)	–	–
Pamphylia (3 Samples)	68-88 78±10.3 (ave.)	1-3 2±0.9 (ave.)	7-19 13±5.7 (ave.)	2-5 4±1.9 (ave.)	1-5 3±1.7 (ave.)	0-1 0.2±0.4 (ave.)	–	–
Phrygia (2 Samples)	59-64 61±3.9 (ave.)	1-4 3±1.9 (ave.)	25-31 28±4.8 (ave.)	4-6 5±2.0 (ave.)	2-3 2±0.5 (ave.)	0-0.5 0.2±0.3 (ave.)	–	–
Pisidia (10 Samples)	35-80 59±15.7 (ave.)	1-3 2±0.7 (ave.)	11-50 28±13.9 (ave.)	3-14 7±3.4 (ave.)	1-4 2±0.9 (ave.)	0-3 1±1.1 (ave.)	–	–
Troas (3 Samples)	32-58 41±15.1 (ave.)	1-7 3±3.1 (ave.)	30-51 42±11.3 (ave.)	7-12 10±2.4 (ave.)	1-2 1±0.2 (ave.)	1-2 2±0.4 (ave.)	–	–

Table 26. Chemical compositions of binders of *opus signinum* mortars determined by SEM-EDS (%).

Region Name	CaO	MgO	SiO$_2$	Al$_2$O$_3$	FeO	K$_2$O	Na$_2$O$_3$
Aiolis (*1 Sample*)	71	1	21	5	1	–	–
Caria (*4 Samples*)	37-52 44±6.3 (ave.)	2-9 4±3.3 (ave.)	31-39 35±4.1 (ave.)	8-16 12±3.4 (ave.)	1-3 2±1.0 (ave.)	0-2 1±1.0 (ave.)	0-1 0.2±0.3 (ave.)
Lycia (*4 Samples*)	68-85 75±9.6 (ave.)	2-10 4±0.7 (ave.)	7-22 15±6.1 (ave.)	2-6 4±1.8 (ave.)	0-2 1±1.2 (ave.)	–	–
Troas (*1 Sample*)	60	2	26	8	2	2	–

The chemical composition of binders was also characterized in terms of three different concentrations by using triangular diagrams (Figure 92-95). EDS analyses showed that some samples were relatively close to pure carbonate phases and the rest of the samples presented a variable composition enriched in silicon, aluminum, and iron (Figure 92). The majority of mortars presented a magnesium content of less than 5% (Figure 93). Most of binders presented SiO_2 content of less than 40% and Al_2O_3 content of less than 15%. (Figure 94). All samples had less than 5% of Fe_2O_3 and they showed presented a variable composition enriched in silicon and aluminum (Figure 95).
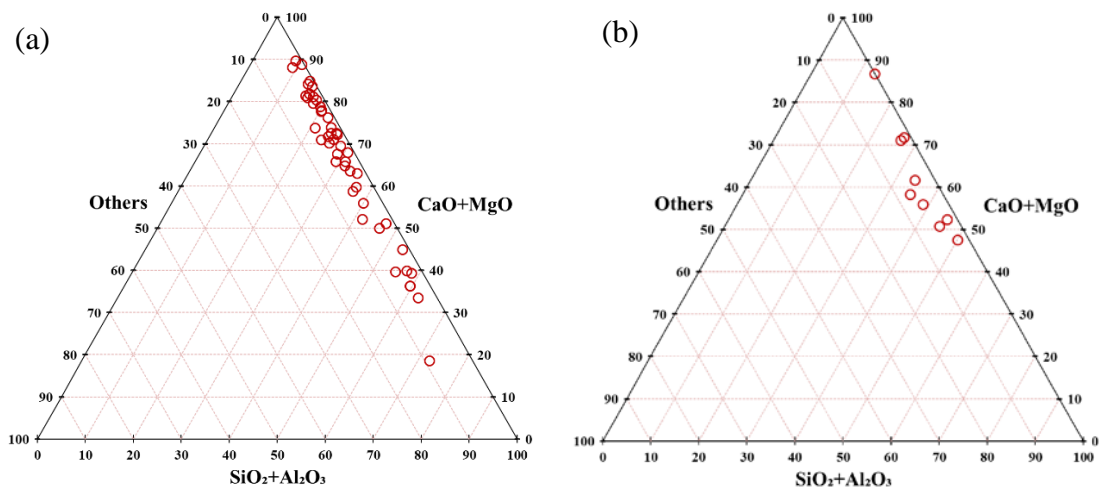
Figure 92. Triangular diagram (CaO+MgO-SiO$_2$+Al$_2$O$_3$-Others) of chemical compositions of binder of *opus caementicium* (a) and *opus signinum* (b).
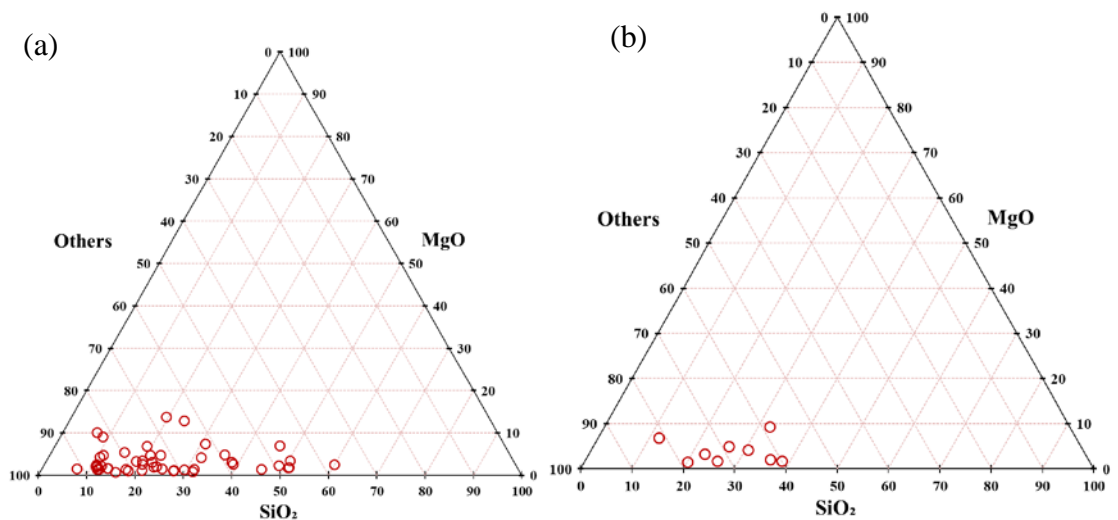
Figure 93. Triangular diagram (MgO-SiO$_2$-Others) of chemical compositions of binder of *opus caementicium* (a) and *opus signinum* (b)
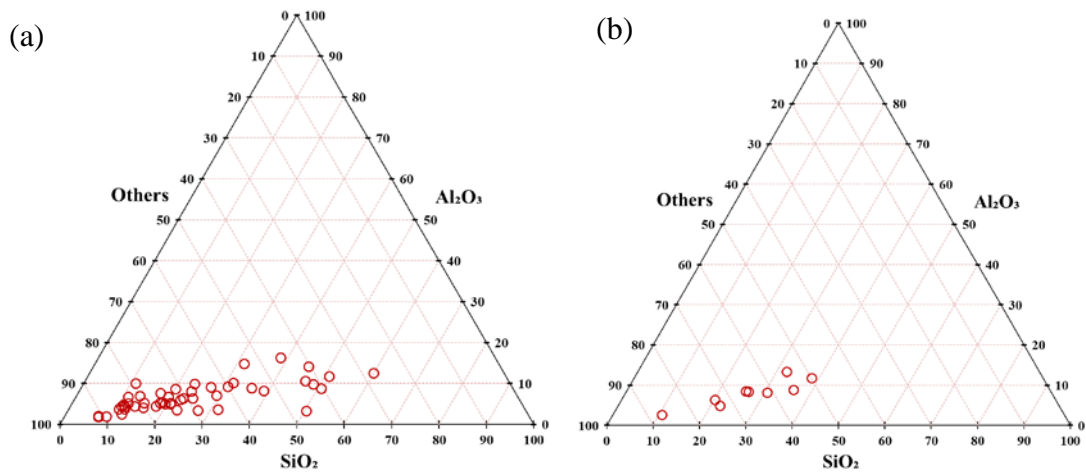
Figure 94.   Triangular diagram (Al₂O₃-SiO₂-Others) of chemical compositions of binder
of *opus caementicium* (a) and *opus signinum* (b).
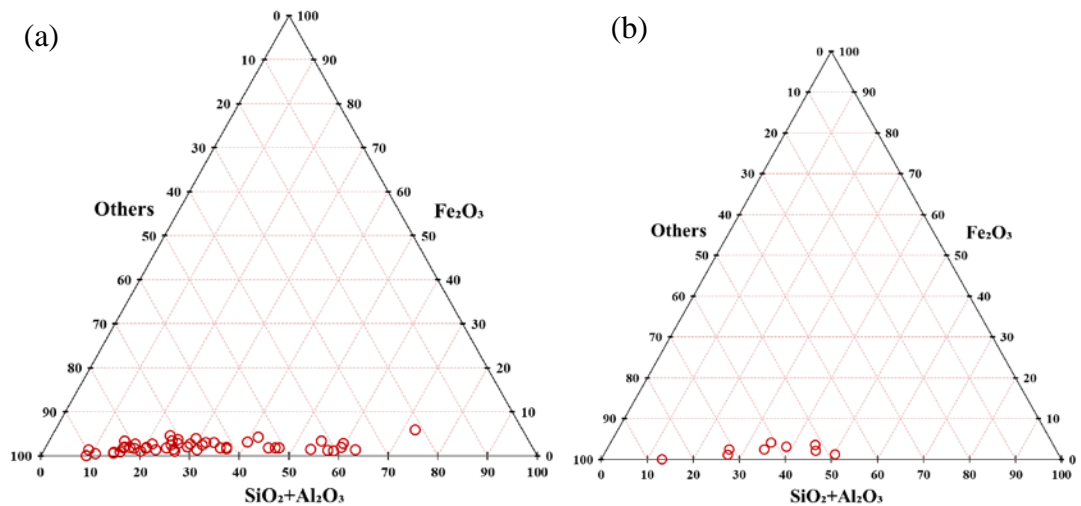
Figure 95.   Triangular diagram (Fe₂O₃-SiO₂+ Al₂O₃-Others) of chemical compositions of
binder of *opus caementicium* (a) and *opus signinum* (b).

3.13. Microstructural Properties of Binders

Microstructural properties of binders in Roman lime mortars were detected by
SEM-EDS analyses to understand the reaction between pozzolanic aggregates and lime.
The SEM microphotograph of studied samples indicated the composition of binder and
different interactions between binder and aggregate in the pores. Images showed that the
lime penetrated inside the pores of the aggregates forming carbonates and reacting with
the silicates were observed with different magnifications (Figure 96 and Figure 97).

Strong adhesion between pozzolanic aggregates and lime, which make mortars stiff, hard, and compact, were also identified in the SEM images (Figure 96 and Figure 97).

Fine mortar matrices comprised of small sized pozzolans and lime, showed a compact structure due to aggregates well-embedded in the matrices (Figure 96 and Figure 97). This compact structure may be thanks to the well mixing carried out during the production of Roman mortars.
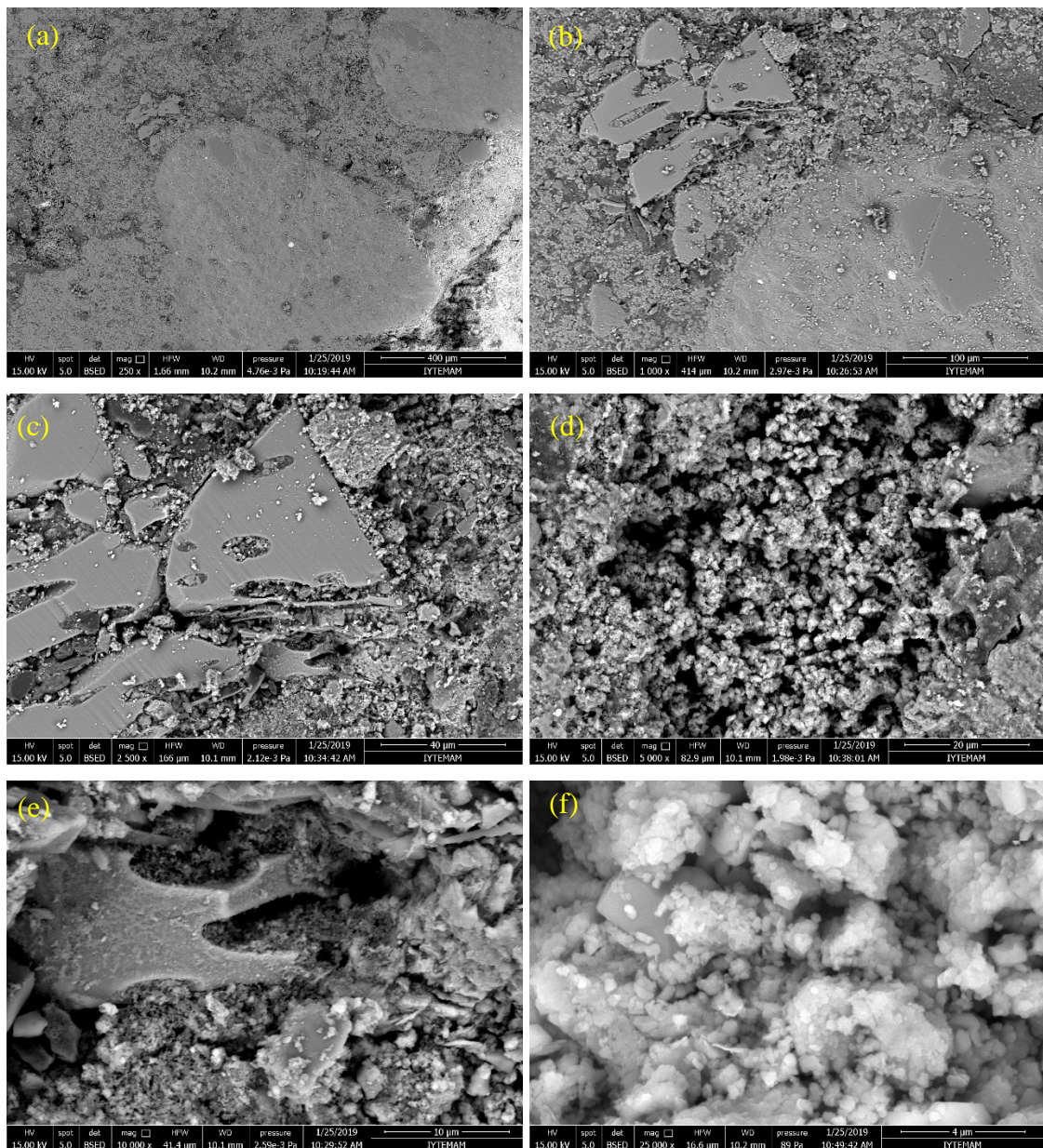
Figure 96.SEM images of mortar of ITCs from Ionia at magnifications of 250 (a), 1000 (b), 2500 (c), 5000 (d), 10000 (e) and 25000 (f).
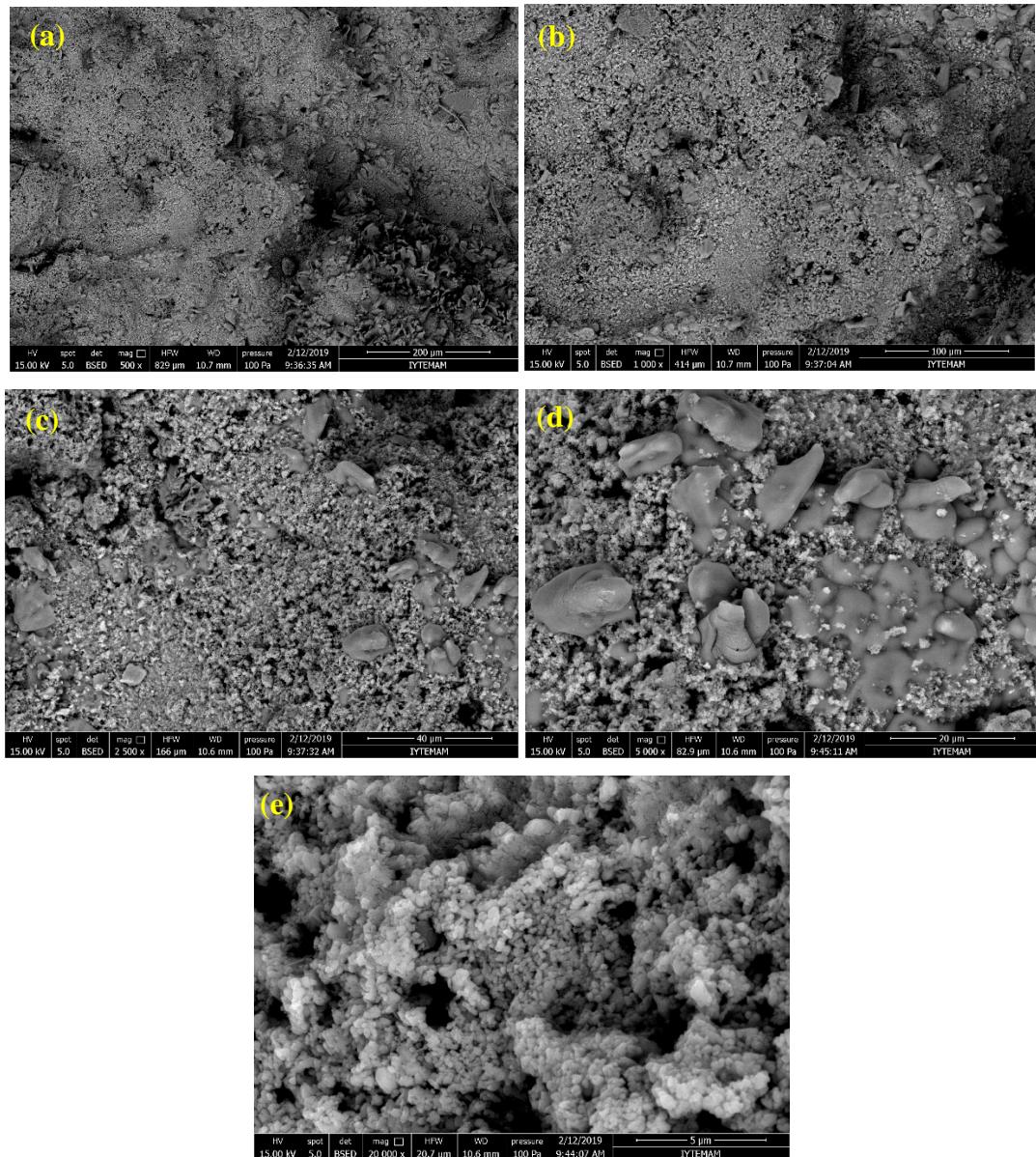
Figure 97. SEM images of mortar of LTIS from Lycia at magnifications of 500 (a), 1000
(b), 2500 (c), 5000 (d) and 20000 (e).

3.14. Hydraulic Properties of Binders

The hydraulic properties of fine mortar matrices (binders) were determined by
thermogravimetric analysis (TGA) and hydraulic index (H.I.).

3.14.1. Thermogravimetric Analysis

In order to examine the hydraulic properties of Roman lime binders, the weight losses at temperatures between 200–600 °C and 600–900 °C were determined by thermogravimetric analyses (TGA). Weight losses of binder parts of mortars at between 200–600 °C were due to the loss of structurally bound water (H_2O) of clay minerals (e.g., kaolinite, sepiolite, and chlorite) and hydraulic products. These hydraulic compounds, such as calcium silicate or aluminate hydrates, originated from the reaction of lime with pozzolanic or volcanic materials. Weight loss at temperatures between 600–900 °C was due to the release of carbon dioxide gas (CO_2) during the decomposition of carbonate phases (Bakolas et al. 1998; Moropoulou, Bakolas, and Bisbikou 2000). According to these explanations, the ratio of the percentage of weight losses due to CO_2/H_2O between 1 and 10 indicated the hydraulic character of Roman lime mortars (Figure 103-107).

Studies revealed that non-hydraulic lime mortars commonly contain CO_2 over 30% and structurally bound water (H_2O) lower than 3%. However, in hydraulic lime mortars, CO_2 content was less than 30% and H_2O content more than 3% (Moropoulou, Bakolas, and Bisbikou 2000).

Table 27. Structural H_2O and CO_2 amounts and CO_2/H_2O values of Roman lime mortars.

Region Name	Weight Loses [%]		CO_2/H_2O
	200-600 °C [Struc. H_2O]	600-900 °C [CO_2]	
Aiolis *(2 Samples)*	3.90-4.23	33.70-35.77	7.97-9.18
Caria *(9 Samples)*	3.25-6.52	28.34-5.07	4.50-10.79
Ionia *(11 Samples)*	4.33-9.55	25.65-38.49	2.69-8.88
Lycia *(9 Samples)*	2.89-9.45	27.77-43.17	4.52-14.15
Lydia *(4 Samples)*	3.78-3.97	22.11-33.11	5.14-8.76
Mysia *(3 Samples)*	4.18-8.19	7.55-23.31	1.81-5.87
Pamphylia *(3 Samples)*	2.82-3.85	30.97-38.90	8.05-13.81
Phrygia *(2 Samples)*	3.66-4.95	31.19-32.64	6.59-8.52
Pisidia *(10 Samples)*	3.30-7.48	20.20-39.50	2.70-9.47
Troas *(4 Samples)*	4.58-5.97	21.24-28.03	3.60-5.83

In this study, CO_2/H_2O ratios of lime mortars were found in the range of 1.81-14.15 (Table 27, Appendix F). CO_2/H_2O ratios were between 1.81-12.94 and 2.77-14.15

for o*pus ceamentium* and *opus signinum* mortars, respectively. These results revealed that all the Roman lime mortars with a few exceptions could be regarded as hydraulic (Figure 98).

The hydraulicity of the mortars can be originated due to the use of pozzolanic aggregates in the production of mortars. However, exceptions CEB, CKC, IMA, IMG, IMS, *LPtB*, PmLyB, and PmLyC may be due to the mistakes in an experiment process.

CO_2/H_2O ratios of Roman lime mortars were investigated in many studies from Turkey (1.1-6.4), Italy (0.3-7.5), Portugal (2.4-8.0) and Spain (1.7-11.1). References were given in Table 2-4. Results indicated that mortars were hydraulic showing CO_2/H_2O ratios less than 10 parallel to the results of this study.
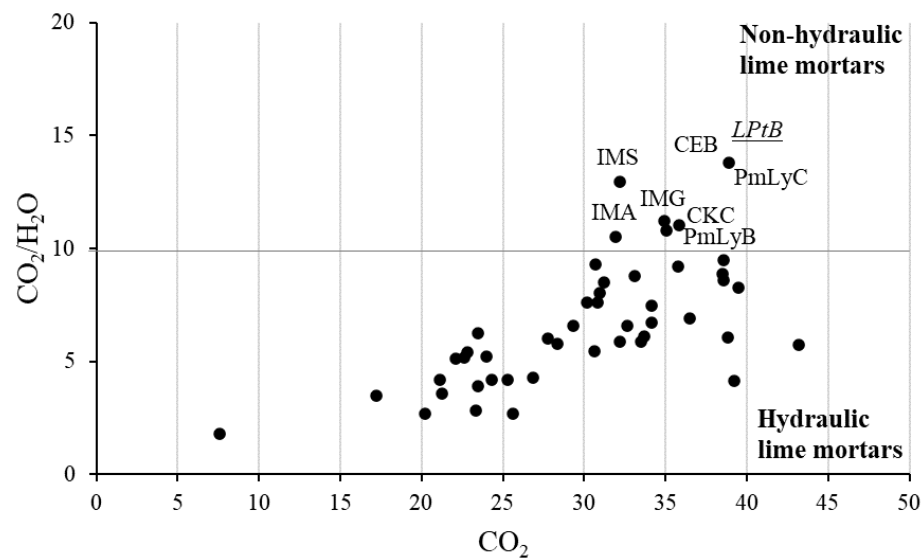
Figure 98. Hydraulic classification of Roman lime mortars by CO_2/H_2O.

3.14.2. Hydraulic Index

The hydraulic index calculated by SEM-EDS analysis of the binder was used to determine the hydraulic properties of mortars. The hydraulic index was defined according to the Boynton formula mentioned previous chapter (Boynton 1980).

Hydraulic indexes of binders from all regions were in the range of 0.1-4.2 (Figure 99). Binders of o*pus ceamentium and opus signinum* mortars showed hydraulic indexes between 0.1-4.2 and 0.1-1.5, respectively. Hydraulic indexes of 12% of binders were

between 0.1-0.2 and can be regarded as weakly hydraulic. Hydraulic indexes of 32% of binders between 0.2-0.4 and can be regarded as moderately hydraulic. Hydraulic indexes of the 56% of binders were more than 0.4 and can be regarded as highly hydraulic.

In addition, 22% of lime lumps showed silicate content more than 5%. These samples can be as highly and moderately hydraulic due to the presence of a high quantity of silicates.

Figure 99. Hydraulic indexes of binders of Roman lime mortars.

Determination of hydraulic indexes of binders also mentioned in a few previous studies such as Ephesus, Kyme, Tarsos, Anavarza, and Amastris (Kuleli 2005; Miriello et al. 2011; Polat Pekmezci 2012; Kurugöl and Güleç 2015). Hydraulic indexes of binders were between 0.1-1.3 for Ephesus mortars, 0.05-0.26 for Kyme mortars, 0.01-0.36 for Tarsos and Anavarza mortars, and 0.6-1.6 for Amastris mortars (Kuleli 2005; Miriello et al. 2011; Polat Pekmezci 2012; Kurugöl and Güleç 2015). Considering these results, binders of these mortars had non-hydraulic property in addition to weakly hydraulic, moderately hydraulic, and highly hydraulic behaviors of mortars which studied before. However, the majority of mortars from previous studies indicated the same hydraulic properties with analyzed mortars in this study showing hydraulic index greater than 0.1 (Kuleli 2005; Miriello et al. 2011; Polat Pekmezci 2012; Kurugöl and Güleç 2015).

CHAPTER 4

CONCLUSION

The properties of Roman lime mortars -*opus caementicium* and *opus signinum*-collected from twenty-six archaeological sites in Western Anatolia were determined to understand whether there was a common production technology of lime mortar in the Roman Empire by making a comparison between Europe and Western Anatolia.

All mortars from the archaeological sites in Western Anatolia were relatively compact due to the well adhering of aggregates to the lime.

Opus caementicium mortars were used in various types of structures, while *opus signinum* mortars were generally used in water-related structures such as bath and cistern. *Opus caementicium* mortars had whitish and grayish color, while *opus signinum* mortars were light brownish with crushed brick/tile/ceramic additions. The color of fine aggregates of o*pus caementicium* and *opus signinum* mortars were "white, gray, brown", and "white, pink, reddish brown", respectively. Regarding the shapes of aggregates, the angular shape was predominant in both type of mortars.

The mortars were low dense and high porous. *Opus signinum* samples were relatively less dense and more porous than o*pus caementicium* ones due to the use of crushed brick aggregates. The various distribution of pore sizes could be attributed to the nonhomogeneous characteristics of mortars.

Lime/aggregate ratios of mortars varied between 1:4-3:2 parallel to ideal lime/aggregate ratios given in historic Roman sources. The average lime/aggregate ratio was found 1:1. Aggregates coarser than 1 mm formed the major fraction of total aggregates. Small differences in raw material compositions could be regarded as the use of local raw material sources.

The compressive strength values of the mortars were found in the range of 2-12 MPa and this range corresponded to NHL3.5 type of lime based on the compressive strength of laboratory mortars after 28 days.

Lime used in the production of mortars was high calcium lime (fat lime) which carbonated to the small-sized micritic calcite crystals. Lime showed non-hydraulic behavior and can be classified as CL 90 hydrated lime. Lime lumps presented spongy texture of calcite crystals which can be the indicators of the hot lime mix method.

Fine aggregates (pozzolans) of *opus caementicium* mortars were rhyolite and dacite (silicic rocks) composed of quartz, feldspar (albite, anorthite), and mica (biotite, muscovite) minerals. All the grayish fine aggregates matched with rhyolite fragments. The fine aggregates of *opus signinum* mortars could not be examined in terms of geochemical characteristics.

Fine mortar matrices (binders) of Roman lime mortars comprised of calcite, quartz, feldspar, and mica minerals. Calcite was originated from carbonated lime, while quartz and other minerals were from fine aggregates. Feldspars and biotite can be originated from volcanic aggregates. No significant differences were observed between properties *opus caementicium* and *opus signinum* mortars by means of lime/aggregate ratio, particle size distribution, type of lime, the mineralogical and chemical compositions, hydraulicity and pozzolanicity.

Fine mortar matrices (binders) were composed of a high amount of carbonated lime and a minor amount of magnesium, silica, alumina, and iron. Fine mortar matrices comprised of small sized pozzolans and lime, showed a compact structure due to aggregates well-embedded in the matrices.

Fine aggregates were composed of mainly silica, alumina, and iron. They presented irregular morphology and consisted of small-sized amorphous particles with small crystal structures.

The mortars were hydraulic due to the use of pozzolanic rhyolite and dacite aggregates. They reacted with lime to produce calcium silicate hydrate and/or calcium aluminate hydrate that provide high mechanical strength and durability to the mortars. Majority of samples had parallel results regarding compressive strength, pozzolanicity and the hydraulicity.

This study indicated that properties of Roman lime mortars were similar in different geographical regions of Western Anatolia, and there was also a common mortar technology produced using local raw material sources throughout the Roman Empire. Results were found consistent with the evaluation of literature review. Overall results may be attributed to the production of a standard quality mortar with local materials in different geographical regions of the Roman Empire.

REFERENCES

Adam, Jean-Pierre. 2005. *Roman Building: Materials and Techniques*. London and New York: Routledge.

Akdeniz, Engin. 2007. "Kadıkalesi Kazısı Miken Buluntuları (Mycenaean Findings from the Excavations of Kadıkalesi)." *Arkeoloji Dergisi* 9: 35–70.

Arandigoyen, M., B. Bicer-Simsir, J. I. Alvarez, and D. A. Lange. 2006. "Variation of Microstructure with Carbonation in Lime and Blended Pastes." *Applied Surface Science* 252 (20): 7562–71.

Artioli, Gilberto, Michele Secco, and Anna Addis. 2019. "The Vitruvian Legacy: Mortars and Binders before and after the Roman World." *European Mineralogical Union Notes in Mineralogy* 20: 151–202.

Ashurts, John, and Francis G. Dimes. 1990. *Mortars of Stone Buildings in Conservation of Building and Decorative Stone*. Oxford: Butterworth-Heinemann.

Aslan Özkaya, Özlem. 2005. "Properties of Roman Bricks and Mortars Used in Serapis Temple in Bergama." Master's Thesis, IYTE.

Aslan Özkaya, Özlem, and Hasan Böke. 2009. "Properties of Roman Bricks and Mortars Used in Serapis Temple in the City of Pergamon." *Materials Characterization* 60 (9): 995–1000.

ASTM. 1985. "Standard Test Method for Determination of the Point Load Strength Index of Rock 1." *Rock Mechanics* 22 (2): 1–9.

Baki, Vahiddin Alperen, Safa Nayır, Şakir Erdoğdu, and İlker Ustabaş. 2020. "Determination of the Pozzolanic Activities of Trachyte and Rhyolite and Comparison of the Test Methods Implemented." *International Journal of Civil Engineering* 18 (9): 1053–66.

Bakolas, A., G. Biscontin, A. Moropoulou, and E. Zendri. 1995. "Characterization of the Lumps in the Mortars of Historic Masonry." *Thermochimica Acta* 269/270: 809–16.

Bakolas, A., G. Biscontin, A. Moropoulou, and E. Zendri. 1998. "Characterization of Structural Byzantine Mortars by Thermogravimetric Analysis." *Thermochimica Acta* 321 (1–2): 151–60.

Belfiore, C. M., G. V. Fichera, M. F. La Russa, A. Pezzino, S. A. Ruffolo, G. Galli, and D. Barca. 2015. "A Multidisciplinary Approach for the Archaeometric Study of Pozzolanic Aggregate in Roman Mortars: The Case of Villa Dei Quintili (Rome, Italy)." *Archaeometry* 57 (2): 269–96.

Benedetti, D., S. Valetti, E. Bontempi, C. Piccioli, and L. E. Depero. 2004. "Study of Ancient Mortars from the Roman Villa of Pollio Felice in Sorrento (Naples)." *Applied Physics A: Materials Science and Processing* 79 (2): 341–45.

Benedetto, Claudia Di, Sossio Fabio Graziano, Vincenza Guarino, Concetta Rispoli, Priscilla Munzi, Vincenzo Morra, and Piergiulio Cappelletti. 2018. "Romans' Established Skills: Mortars from D46b Mausoleum, Porta Mediana Necropolis, Cuma (Naples)." *Mediterranean Archaeology and Archaeometry* 18 (5): 131–46.

Bieniawski, Zdzisław Tadeusz. 1975. "The Point-Load Test in Geotechnical Practice." *Engineering Geology* 9 (1): 1–11.

Borsoi, G., A. Santos Silva, P. Menezes, A. Candeias, and J. Mirão. 2019. "Analytical Characterization of Ancient Mortars from the Archaeological Roman Site of Pisões (Beja, Portugal)." *Construction and Building Materials* 204: 597–608.

Boynton, Robert. S. 1980. *Chemistry and Technology of Lime and Limestone*. 2nd Edition. New York: John Wiley & Sons.

Cantisani, E., A. Cecchi, I. Chiaverini, F. Fratini, C. M. Del Fa, E. Pecchioni, and S. Rescici. 2002. "The Binder of the Romen Concrete of the Ponte Di Augusto at Narni (Italy)." *Periodico Di Mineralogia* 71: 113–23.

Cardoso, I., M. F. Macedo, F. Vermeulen, C. Corsi, A. Santos Silva, L. Rosado, A. Candeias, and J. Mirao. 2014. "A Multidisciplinary Approach to the Study of Archaeological Mortars from the Town of Ammaia in the Roman Province of Lusitania (Portugal)." *Archaeometry* 56 (1): 1–24.

Cazalla, O., C. Rodriguez-Navarro, E. Sebastian, G. Cultrone, and M. J. De la Torre. 2000. "Aging of Lime Putty: Effects on Traditional Lime Mortar Carbonation." *Journal of the American Ceramic Society* 83 (5): 1070–76.

Chen, Xudong, Shengxing Wu, and Jikai Zhou. 2013. "Influence of Porosity on Compressive and Tensile Strength of Cement Mortar." *Construction and Building Materials* 40: 869–74.

Columbu, S., C. Lisci, F. Sitzia, G. Lorenzetti, M. Lezzerini, S. Pagnotta, S. Raneri, et al. 2018. "Mineralogical, Petrographic and Physical-Mechanical Study of Roman Construction Materials from the Maritime Theatre of Hadrian's Villa (Rome, Italy)." *Measurement* 127: 264–76.

Columbu, Stefano, Fabia Sitzia, and Guido Ennas. 2017. "The Ancient Pozzolanic Mortars and Concretes of Heliocaminus Baths in Hadrian's Villa (Tivoli, Italy)." *Archaeological and Anthropological Sciences* 9 (4): 523–53.

Cowan, Henry J. 1977. *The Master Builders: A History of Structural and Environmental Design from Ancient Egypt to the Nineteenth Century*. New York: John Willey & Sons.

Cowper, A D. 1998. *Lime and Lime Mortars*. (First published in 1927 for the Building Research Station by HM Stationery Office, London), Dorset: Donhead Publishing Ltd.

Davey, Norman. 1961. *A History of Building Materials*. London: Phoenix House.

Degryse, Patrick, Jan Elsen, and Marc Waelkens. 2002. "Study of Ancient Mortars from Sagalassos (Turkey) in View of Their Conservation." *Cement and Concrete Research* 32 (9): 1457–63.

De Luca, Raffaella. 2014. "Methodological Approach to the Study of Archaeological Mortars and Plasters from Mediterranean Sites." *Plinius* 40: 68–75.

Diamond, Sidney. 1976. "A Review of Alkali-Silica Reaction and Expansion Mechanisms 2. Reactive Aggregates." *Cement and Concrete Research* 6 (4): 549–60.

Diler, Adnan. 2008. "Bodrum Yarımadası Leleg Yerleşimleri, Pedasa, Mylasa, Damlıboğaz (Hydai), Kedrai (Sedir Adası), Kissebükü (Anastasiapolis) ve Mobolla Kalesi Yüzey Araştırmaları 2004-2005." *Araştırma Sonuçları Toplantısı XXIV. II*, 479–500.

Drdácký, M., F. Fratini, D. Frankeová, and Z. Slížková. 2013. "The Roman Mortars Used in the Construction of the Ponte Di Augusto (Narni, Italy) - A Comprehensive Assessment." *Construction and Building Materials* 38: 1117–28.

Duman, Bahadır. 2013. "Son Arkeolojik Araştırmalar ve Yeni Bulgular Işığında Tripolis Ad Maeandrum." *Cedrus I*.

Eckel, Edwin Clarence. 1905. *Cements, Limes, and Plasters; Their Materials, Manufacture, and Properties.* 1st ed. New York,: Wiley,.

Ergenç, D., F. Rafael, N. Aly, O. Henry, and S. Hemeda. 2019. "Interpretation of Scientific Data Derived from Analytical Techniques Used in the Characterisation of Roman Mortars." In *5th Historic Mortars Conference HMC2019*, edited by José Ignacio Álvarez, José María Fernández, Iñigo Navarro, and Rafael Sirera. Pamplona, Spain, 19-21 June.

Ergenç, Duygu, and Rafael Fort. 2019. "Multi-Technical Characterization of Roman Mortars from Complutum, Spain." *Measurement* 147: 106876.

Ergenç, Duygu, Rafael Fort, and Serdar. H. Öztaner. 2016. "Characterization of Roman Mortars of Nysa in the Ancient Caria, Turkey." In *4th Historic Mortars Conference HMC2016*, edited by Ioanna Papayianni, Maria Stefanidou, and Vasiliki Pachta. Santorini, Greece, 10-12 October.

Erkanol, Demir, and Abdülkerim Aydındağ. 2013. "İller Mermer ve Doğal Taş Potansiyel Alan Belirleme Etüt Raporları." *MTA Doğal Kaynaklar Ve Ekonomi Bülteni* 16: 147–56.

Farci, Alessio, Deborah Floris, and Paola Meloni. 2005. "Water Permeability vs. Porosity in Samples of Roman Mortars." *Journal of Cultural Heritage* 6 (1): 55–69.

Felekoğlu, B., E. Gödek, A. Ersoy, M. Kuşoğlu, and A. Hasözbek. 2016. "Physical, Mechanical and Microstructural Characterization of Basilica Plasters and Bouleuterion Mortars in Smyrna Agora." *Mediterranean Archaeology and Archaeometry* 16 (1): 193–202.

Feuser, Stefan. 2011. "The Roman Harbour of Alexandria Troas, Turkey." *International Journal of Nautical Archaeology* 40 (2): 256–73.

Franquelo, M. L., M. D. Robador, V. Ramírez-Valle, A. Durán, M. C. Jiménez De Haro, and J. L. Pérez-Rodríguez. 2008. "Roman Ceramics of Hydraulic Mortars Used to Build the Mithraeum House of Mérida (Spain)." *Journal of Thermal Analysis and Calorimetry* 92 (1): 331–35.

Genestar, Catalina, Carmen Pons, and Ángeles Más. 2006. "Analytical Characterisation of Ancient Mortars from the Archaeological Roman City of Pollentia (Balearic Islands, Spain)." *Analytica Chimica Acta* 557 (1–2): 373–79.

Gourdin, William H., and W. David Kingery. 2016. "The Beginnings of Pyrotechnology : Neolithic and Egyptian Lime Plaster." *Journal of Field Archaeology* 2 (1): 133–50.

Gulotta, D., L. Toniolo, F. D'Andria, C. Polito, V. Capogrosso, S. Mosca, A. Nevin, and G. Valentini. 2016. "Characterization of Archaeological Mortars from Messapian and Roman Sites in Lecce (Italy)." In *4th Historic Mortars Conference HMC2016*, edited by Ioanna Papayianni, Maria Stefanidou, and Vasiliki Pachta. Santorini, Greece, 10-12 October.

Hamidi, Moussa, Larbi Kacimi, Martin Cyr, and Pierre Clastres. 2013. "Evaluation and Improvement of Pozzolanic Activity of Andesite for Its Use in Eco-Efficient Cement." *Construction and Building Materials* 47: 1268–77.

Holmes, Stafford, and Michael Wingate. 1997. *Building with Lime*. London: Intermediate Technology Publications.

Hughes, John J., and Alick B. Leslie. 2001. "The Petrography of Lime Inclusions in Historic Lime Based Mortars." In *Proc 8th Euroseminar on Microscopy Applied to Building Materials*, 359– 364. September 4–7 Athens.

İnan, Jale. 1998. *Toroslar'da Bir Antik Kent. Lyrbe? – Seleukeia? Arkeoloji ve Sanat Yayınları. Kazı Monografileri Dizisi 5*. İstanbul.

Izaguirre, Ana, Javier Lanas, and José Ignacio Álvarez. 2010. "Ageing of Lime Mortars with Admixtures: Durability and Strength Assessment." *Cement and Concrete Research* 40 (7): 1081–95.

Izzo, F., C. Grifa, C. Germinario, M. Mercurio, A. De Bonis, L. Tomay, and A. Langella. 2018. "Production Technology of Mortar-Based Building Materials from the Arch of Trajan and the Roman Theatre in Benevento, Italy." *European Physical Journal Plus* 133 (9): 1–12.

Jackson, M. D., P. Ciancio Rossetto, C. K. Kosso, M. Buonfiglio, and F. Marra. 2011. "Building Materials of the Theatre of Marcellus, Rome." *Archaeometry* 53 (4): 728–42.

Jackson, M. D., J. M. Logan, B. E. Scheetz, D. M. Deocampo, C. G. Cawood, F. Marra, M. Vitti, and L. Ungaro. 2009. "Assessment of Material Characteristics of Ancient Concretes, Grande Aula, Markets of Trajan, Rome." *Journal of Archaeological Science* 36 (11): 2481–92.

Jedrzejevska, Hanna. 1981. "Ancient Mortars as Criterion in Analysis of Old Architecture." In *Proceedings of Symposium on Mortars, Cements and Grouts Used in the Conservation of Historic Buildings*, 311–29. Rome, Italy, 3-6 November.

Karlsson, Lars, Jesper Blid, Olivier Henry, and Ragnar Hedlund. 2012. "Labraunda 2011 : A Preliminary Report on the Swedish Excavations with an Appendix by R. Hedlund." *Opuscula: Annual of the Swedish Institutes at Athens and Rome* 5: 49–87.

Kaya, Mehmet Ali. 2005. "Anadolu'da Roma Eyaletleri; Sınırlar ve Roma Yönetimi." *Tarih Araştırmaları Dergisi*. Ankara Üniversitesi.

Kingery, W. David, Pamela B. Vandiver, and Martha Prickett. 1988. "The Beginnings of Pyrotechnology, Part II: Production and Use of Lime and Gypsum Plaster in the Pre-Pottery Neolithic Near East." *Journal of Field Archaeology* 15 (2): 219–44.

Kızıl, Abuzer, and Taylan Doğan. 2018. "Euromos Güney Nekropolis'te Ortaya Çıkarılan Geometrik ve Arkaik Dönem Mezarları." *TÜBA-AR* 23: 137–55.

Kozlu, Hale. 2010. "Kayseri Yöresindeki Tarihi Harçların Karakterizasyonu ve Onarım Harçlarının Özellikleri." PhD. Thesis, ITÜ.

Kramar, S., V. Zalar, M. Urosevic, W. Körner, A. Mauko, B. Mirtič, J. Lux, and A. Mladenović. 2011. "Mineralogical and Microstructural Studies of Mortars from the Bath Complex of the Roman Villa Rustica Near Mošnje (Slovenia)." *Materials Characterization* 62 (11): 1042–57.

Kretzchmer, Fritz. 2010. *Antik Roma'da Mimarlık ve Mühendislik*. Arkeoloji ve Sanat Yayınları.

Krumnacher, Paul J. 2001. "Lime and Cement Technology : Transition from Traditional to Standardized Treatment." Msc. Thesis, Virginia Polytechnic Institute and State University.

Kuleli, Esin. 2005. "Efes Yamaç Evler 2'de, 1, 2 ve 4 Nolu Evler Örneğinde Roma Dönemi Harçları Araştırılması." PhD. Thesis, DEU.

Kumar, Rakesh, and Bishwajit Bhattacharjee. 2003. "Porosity, Pore Size Distribution and in Situ Strength of Concrete." *Cement and Concrete Research* 33 (1): 155–64.

Kurugöl, Sedat, and Ahmet Güleç. 2012. "Physico-Chemical, Petrographic, and Mechanical Characteristics of Lime Mortars in Historic Yoros Castle (Turkey)." *International Journal of Architectural Heritage* 6 (3): 322–41.

Kurugöl, Sedat, and Ahmet Güleç. 2015. "Physico-Chemical , Petrographical and Mechanical Properties of Mortars Used in an Ancient Roman Basilica in Amasra / Turkey." *Gazi University Journal of Science* 28 (4): 609–21.

Lanas, Javier, and José Ignacio Alvarez. 2003. "Masonry Repair Lime-Based Mortars: Factors Affecting the Mechanical Behavior." *Cement and Concrete Research* 33 (11): 1867–76.

Lancaster, Lynne. 2019. "Pozzolans in Mortar in the Roman Empire: An Overview and Thoughts on Future Work." In *Mortiers et Hydraulique En Méditerranée Antique*, edited by Iván Fumadó Ortega and Sophie Bouffier, 31–39.

Laycock, E. A., D. Pirrie, F. Clegg, A. M. T. Bell, and P. Bidwell. 2019. "An Investigation to Establish the Source of the Roman Lime Mortars Used in Wallsend, UK." *Construction and Building Materials* 196: 611–25.

Lea, Frederick Measham. 1940. "Investigations on Pozzolanas." *Building Research*, Technical paper, 1 (27): 1–63.

Leone, G., A. De Vita, A. Magnani, and C. Rossi. 2016. "Characterization of Archaeological Mortars from Herculaneum." *Thermochimica Acta* 624: 86–94.

Lugli, Giuseppe. 1957. *La Tecnica Edilizia Romana: Con Particolare Riguardo a Roma e Lazio*. Edited by Scienze e Lettere. Rome: Giovanni Bardi.

Luxán, Maria Pilar, Francisco J. Madruga, and Julio Saavedra. 1989. "Rapid Evaluation of Pozzolanic Activity of Natural Products by Conductivity Measurement." *Cement and Concrete Research* 19 (1): 63–68.

MacDonald, William L. 1982. *The Architecture of the Roman Empire*. New Haven and London: Yale University Press.

Maitre, R.W. Le, A. Streckeisen, B. Zanettin, M. J. Le Bas, B. Bonin, and P. Bateman. 2002. *Igneous Rocks: A Classification and Glossary of Terms: Recommendations of the International Union of Geological Sciences Subcommission on the Systematics of Igneous Rocks*. 2nd ed. Cambridge: Cambridge University Press.

Margalha, M. G., A. S. Silva, M. do Rosário Veiga, J. de Brito, R. J. Ball, and G. C. Allen. 2013. "Microstructural Changes of Lime Putty during Aging." *Journal of Materials in Civil Engineering* 25 (10): 1524–32.

Mascolo, G., M. C. Mascolo, A. Vitale, and O. Marino. 2010. "Microstructure Evolution of Lime Putty upon Aging." *Journal of Crystal Growth* 312 (16–17): 2363–68.

Massazza, Franco. 1998. "10 - Pozzolana and Pozzolanic Cements." In *Lea's Chemistry of Cement and Concrete (Fourth Edition)*, edited by Peter C Hewlett, Fourth Edi, 471–635. Oxford: Butterworth-Heinemann.

Midtgaard, Mette, Isabelle Brajer, and Michelle Taube. 2020. "Hot-Mixed Lime Mortar: Historical and Analytical Evidence of Its Use in Medieval Wall Painting Plaster." *Journal of Architectural Conservation* 26 (3): 235–46.

Miriello, D., F. Antonelli, C. Apollaro, A. Bloise, N. Bruno, M. Catalano, S. Columbu, et al. 2015. "A Petro-Chemical Study of Ancient Mortars from the Archaeological Site of Kyme (Turkey)." *Periodico Di Mineralogia* 84 (3A): 497–517.

Miriello, D., D. Barca, A. Bloise, A. Ciarallo, G. M. Crisci, T. De Rose, C. Gattuso, F. Gazineo, and M. F. La Russa. 2010. "Characterisation of Archaeological Mortars from Pompeii (Campania, Italy) and Identification of Construction Phases by Compositional Data Analysis." *Journal of Archaeological Science* 37 (9): 2207–23.

Miriello, D., A. Bloise, G. M. Crisci, C. Apollaro, and A. La Marca. 2011. "Characterisation of Archaeological Mortars and Plasters from Kyme (Turkey)." *Journal of Archaeological Science* 38 (4): 794–804.

Mitchell, Stephen, and Marc Waelkens. 1987. "Sagalassus and Cremna 1986." *Anatolian Studies* 37: 37–47.

Moreno-Alcaide, Manuel, and José Manuel Compaña-Prieto. 2018. "Roman Plasters and Mortars from Ancient Cosa (Tuscany-Italy). Mineralogical Characterisation and Construction from Domus 10.1 (House with Cryptoporticus)." *Journal of Archaeological Science: Reports* 19 (February): 127–37.

Moropoulou, Antonia, Asterios Bakolas, and Sophia Anagnostopoulou. 2005. "Composite Materials in Ancient Structures." *Cement and Concrete Composites* 27 (2): 295–300.

Moropoulou, Antonia, Asterios Bakolas, and Katerina Bisbikou. 2000. "Investigation of the Technology of Historic Mortars." *Journal of Cultural Heritage* 1 (1): 45–58.

Munsell Color. 2013. *Munsell Soil Color Charts : With Genuine Munsell Color Chips*. 2009 year revised. Grand Rapids, MI : Munsell Color.

Nikolić, E., A. Radivojević, I. Delić-Nikolić, and D. Rogić. 2016. "Roman Mortars from the Amphitheatre of Viminacium." In *4th Historic Mortars Conference HMC2016*, edited by Ioanna Papayianni, Maria Stefanidou, and Vasiliki Pachta. Santorini, Greece, 10-12 October.

Nolle, Johannes. 2015. *Sikkeler, Agaclar ve Alimler: Selge*. AKMED.

Odler, Ivan, and Maxie Rößler. 1985. "Investigations on the Relationship between Porosity, Structure and Strength of Hydrated Portland Cement Pastes. II. Effect of Pore Structure and of Degree of Hydration." *Cement and Concrete Research* 15 (3): 401–10.

Oğuz, Cem, Fikret Türker, and Niyazi Uğur Koçkal. 2015. "Andriake Limani'nda Roma, Bizans ve Selçuklu Dönemi Harçlarin Özellikleri." *Teknik Dergi/Technical Journal of Turkish Chamber of Civil Engineers* 26 (1): 6993–7013.

Olazabal, A. A., C. A. Fernández, J. J. Echevarría, L. Ortega, and G. P. Antón. 2019. "Roman Mortars of Floor Substrates and Walls from Arroyo de La Dehesa de Velasco Site Petrographic and Mineralogical Characterization." In *5th Historic Mortars HMC2019*, edited by José Ignacio Álvarez, José María Fernández, Iñigo Navarro, and Rafael Sirera. Pamplona, Spain, 19-21 June.

Ontiveros-Ortega, Esther, Oliva Rodríguez-Gutiérrez, and Antonio D. Navarro. 2016. "Mineralogical and Physical-Chemical Characterisation of Roman Mortars Used for Monumental Substructures on the Hill of San Antonio, in the Roman City of Italica (Prov. Baetica, Santiponce, Seville, Spain)." *Journal of Archaeological Science: Reports* 7: 205–23.

Özhanlı, Mehmet. 2013. "Pisidia Antiokheiası Kazısı 2012." *ANMED (Anadolu Akdenizi Arkeoloji Haberleri* 11: 14–21.

Papayianni, Ioanna, Vasiliki Pachta, and Maria Stefanidou. 2013. "Analysis of Aancient Mortars and Design of Compatible Repair Mortars: The Case Study of Odeion of the Archaeological Site of Dion." *Construction and Building Materials* 40: 84–92.

Pavía, Sara, and Susana Caro. 2008. "An Investigation of Roman Mortar Technology through the Petrographic Analysis of Archaeological Material." *Construction and Building Materials* 22 (8): 1807–11.

Peter, Nicholson. 1850. *Encyclopedia of Architecture*. 2 volumes. New York: Fry & Co.

Polat Pekmezci, Işıl. 2012. "Çukurova Bölgesindeki (Kilikya) Bazı Tarihi Yapılarda Kullanılan Harçların Karakterizasyonu ve Onarım Harçları Için Öneriler." PhD. Thesis, ITÜ.

Rasch, Jürgen. 1985. "Die Kuppel in Der Römischen Architektur: Entwicklung, Formgebung, Konstruktion." *Architectura* 15: 117–139.

Richard, C., C. Mielenz, P. Leslie, P. Witte, and J. Glantz Omar. 1950. *Effect of Calcinatoin on Natural Pozzolans*. Edited by T E Stanton and R F Blanks. *Symposium on Use of Pozzolanic Materials in Mortars and Concretes*. West Conshohocken, PA: ASTM International.

RILEM. 1980. "Tests Defining the Structure." *Materials and Construction* 13 (73).

Rizzo, G., L. Ercoli, B. Megna, and M. Parlapiano. 2008. "Characterization of Mortars from Ancient and Traditional Water Supply Systems in Sicily." *Journal of Thermal Analysis and Calorimetry* 92 (1): 323–30.

Robador, María Dolores, José Luís Perez-Rodriguez, and Adrian Duran. 2010. "Hydraulic Structures of the Roman Mithraeum House in Augusta Emerita, Spain." *Journal of Archaeological Science* 37 (10): 2426–32.

Robertson, Alastair H. F., Osman Parlak, and Ülvi Can Ünlügenç. 2013. *Geological Development of Anatolia and the Easternmost Mediterranean Region. Geological Society of London*. 2013/12/18. Vol. 372. Geological Society of London.

Rodriguez-Navarro, Carlos, Eric Hansen, and William S. Ginell. 1998. "Calcium Hydroxide Crystal Evolution upon Aging of Lime Putty." *Journal of American Ceramic Society* 81 (11): 3032–34.

Sánchez-Moral, S., L. Luque, J. C. Cañaveras, V. Soler, J. Garcia-Guinea, and A. Aparicio. 2005. "Lime-Pozzolana Mortars in Roman Catacombs: Composition, Structures and Restoration." *Cement and Concrete Research* 35 (8): 1555–65.

Santos, Ana Rita, Maria do Rosário Veiga, António Santos Silva, Jorge de Brito, and José Ignacio Álvarez. 2018. "Evolution of the Microstructure of Lime Based Mortars and Influence on the Mechanical Behaviour: The Role of the Aggregates." *Construction and Building Materials* 187: 907–22.

Saraçoğlu, Aslı. 2011. "Hellenistic and Roman Unguentaria from the Necropolis of Tralleis." *Anadolu*. Ankara Üniversitesi, DTCF, Arkeoloji Bölümü, Ana Bina, 06100 Sıhhiye-Ankara: Ankara University.

Schiller, K. K. 1971. "Strength of Porous Materials." *Cement and Concrete Research* 1 (4): 419–22.

Şerifaki, Kerem, Elif Uğurlu Sağın, and Hasan Böke. 2020. "Microstructural Characteristics of Mortars Prepared by Hot Lime Mix." *Gradjevinar* 72 (11): 991–1000.

Silva, Denise A., Hans Rudolf Wenk, and Paulo J. M. Monteiro. 2005. "Comparative Investigation of Mortars from Roman Colosseum and Cistern." *Thermochimica Acta* 438 (1–2): 35–40.

Stanislao, Corrado, C. Rispoli, G. Vola, P. Cappelletti, V. Morra, and M. De Gennaro. 2011. "Contribution to the Knowledge of Ancient Roman Seawater Concretes: Phlegrean Pozzolan Adopted in the Construction of the Harbour at Soli-Pompeiopolis (Mersin, Turkey)." *Periodico Di Mineralogia* 80 (3): 471–88.

Stock, Friederike, Anna Pint, Barbara Horejs, Sabine Ladstätter, and Helmut Brückner. 2013. "In Search of the Harbours: New Evidence of Late Roman and Byzantine Harbours of Ephesus." *Quaternary International* 312: 57–69.

Topličić-Ćurčić, Gordana A., Zoran J. Grdić, Nenad S. Ristić, Dušan Z. Grdić, Petar B. Mitković, Igor S. Bjelić, and Ana J. Momčilović-Petronijević. 2014. "Characterization of Roman Mortar From the Mediana Archeological Site." *Tehnički Vjesnik* 21 (1): 191–97.

Tuna, Numan. 1995. "Araştırma Sonuçları Toplantısı." Vol. 12: 167.

Uğurlu Sağın, Elif. 2012. "Characteristics of Roman Mortars Produced from Natural and Artificial Pozzolans in Aigai and Nysa." PhD. Thesis, IYTE.

Uğurlu Sağın, Elif, Hasan Böke, Nadir Aras, and Şerife Yalçın. 2012. "Determination of $CaCO_3$ and SiO_2 Content in the Binders of Historic Lime Mortars." *Materials and Structures* 45 (6): 841–49.

UNI EN 16085. 2012. "Conservation of Cultural Property - Methodology for Sampling from Materials of Cultural Property - General Rules."

UNI EN 16572. 2015. "Conservation of Cultural Heritage - Glossary of Technical Terms Concerning Mortars for Masonry, Renders and Plasters Used in Cultural Heritage," no. 112.

UNI EN 17187. 2020. "Conservation of Cultural Heritage - Characterization of Mortars Used in Cultural Heritage."

UNI EN 459-1. 2001. "Building Lime - Part 1: Definitions, Specifications and Conformity Criteria."

Velosa, A. L., J. Coroado, M. R. Veiga, and F. Rocha. 2007. "Characterisation of Roman Mortars from Conímbriga with Respect to Their Repair." *Materials Characterization* 58 (11-12 SPEC. ISS.): 1208–16.

Velosa, A. L., R. Veiga, J. Coroado, and V. M. Ferreira. 2010. "Materials, Technologies and Practice in Historic Heritage Structures," 235–57.

Vicat, L. J. 2003. *Mortars and Cements*. (First published in 1837 by John Weale, High Holborn, London), Dorset: Donhead Publishing Ltd.

Vitruvius, P. 1960. *Vitruvius : The Ten Books on Architecture*. Edited by M.H. Morgan. (First published in 1914. Edited by M.H. Morgan), New York: Dover Publications.

Waelkens, Marc. 1989. "Hellenistic and Roman Influence in the Imperial Architecture of Asia Minor." *Bulletin Supplement (University of London. Institute of Classical Studies)*, no. 55: 77–88.

Ward-Perkins, John Bryan. 1994. *Roman Imperial Architecture*. New Haven and London: Yale University Press.

Ward-Perkins, John Bryan. 2003. *History of World Architecture: Roman Architecture*. New York: Phaidon Press.

Willet, Rinse. 2020. *The Geography of Urbanism in Roman Asia Minor*. Equinox publishing; Sheffield and Bristol.

Wingate, Michael. 1985. *Small-Scale Lime-Burning: A Practical Introduction*. London: Intermediate Technology Publications.

Yaseen, I. A. B., H. Al-Amoush, M. Al-Farajat, and A. Mayyas. 2013. "Petrography and Mineralogy of Roman Mortars from Buildings of the Ancient City of Jerash, Jordan." *Construction and Building Materials* 38: 465–71.

Yegül, Fikret. 2007. "When a Theatron Is Not a Theater: 'a Place for Viewing' in Magnesia on the Meander." *Journal of Roman Archaeology* 20: 578–582.

Yegül, Fikret, and Diane Favro. 2019. *Roman Architecture and Urbanism: From the Origins to Late Antiquity*. Cambridge University Press.

Yu, Lehua, Shuangxi Zhou, and Wenwu Deng. 2015. "Pozzolanic Activity of Volcanic Rocks from Southern Jiangxi Province, China." *Journal of Sustainable Cement-Based Materials* 5 (3): 176–98.

Zamba, I. C., M. G. Stamatakis, F. A. Cooper, P. G. Themelis, and C. G. Zambas. 2007. "Characterization of Mortars Used for the Construction of Saithidai Heroon Podium (1st Century AD) in Ancient Messene, Peloponnesus, Greece." *Materials Characterization* 58 (11-12 SPEC. ISS.): 1229–39.

APPENDIX A

BASIC PHYSICAL PROPERTIES OF MORTARS

Sample Name	Apparent Density (g/cm^3)	Porosity (by volume - %)
ACyH	1.35±0.29	48.21±13.76
ACyT	1.68±0.03	35.41±0.81
CEB	1.69±0.06	36.49±1.04
CKC	1.79±0.02	30.99±0.44
CKCs	1.69±0.05	33.1±1.42
CLB1	1.58±0.02	37.39±1.98
CLB2	1.66±0.00	36.26±0.04
CStB	1.43±0.13	42.21±4.07
CStT	1.45±0.03	42.03±1.02
CTrG	1.77±0.05	33.03±2.41
CTrB	1.70±0.02	33.85±1.59
IAnAq	1.76±0.12	33.34±2.62
IAnB	1.52±0.11	44.27±3.86
IMA	1.69±0.03	37.38±0.91
IMG	1.71±0.29	29.02±1.07
IMS	1.86±0.02	30.99±0.14
IPyH	1.79±0.13	31.29±3.37
IPrB	1.56±0.20	38.30±7.12
IPrH	1.74±0.04	35.08±1.57
IPrT	1.74±0.02	34.94±0.62
ITCs	1.82±0.14	30.97±5.96
ITT	1.58±0.08	37.62±3.08
LPtB	1.20±0.13	53.21±4.77
LPtC	1.51±0.37	42.38±13.10
LPtT	1.60±0.20	39.34±7.12
LTlB	1.89±0.02	25.99±2.37
LTlS	1.80±0.01	33.62±3.93
LTlT	1.81±0.12	32.24±5.84

Sample Name	Apparent Density (g/cm^3)	Porosity (by volume - %)
LXA	1.50±0.00	42.50±0.49
LXB	1.69±0.42	34.95±14.35
LXT	1.93±0.56	27.20±19.43
LySrU	1.73±0.12	34.43±3.73
LyTpA	1.78±0.02	33.07±1.85
LyTpB	1.77±0.08	32.72±3.36
LyTpT	1.82±0.01	30.52±0.79
MPB	1.63±0.00	36.77±0.41
MPB2	1.72±0.08	34.00±7.45
MPC	1.57±0.12	38.74±4.82
PhAzB	1.72±0.03	34.77±0.09
PhLdB	1.81±0.04	31.65±3.91
PCT	1.86±0.08	28.50±3.25
PCB	1.78±0.01	32.04±2.07
PCC	1.75±0.31	32.33±11.92
PmLyB	1.65±0.04	38.03±1.23
PmLyCs	1.63±0.06	37.73±2.62
PmLyC	1.40±0.04	45.67±1.84
PAtT	1.84±0.15	34.36±6.23
PSlB	1.55±0.03	39.76±0.46
PSlS	1.65±0.13	36.52±5.30
PSlT	1.33±0.02	48.03±0.59
PSB	1.46±0.14	41.42±1.76
PSA	1.40±0.07	44.80±2.51
PST	1.35±0.26	44.96±12.15
TAB	1.52±0.09	43.94±1.48
TACs	1.64±0.02	36.44±0.64
TAxB	1.53±0.04	39.45±1.72
TAxG	1.62±0.02	35.75±0.19

APPENDIX B

MECHANICAL PROPERTIES OF MORTARS

Sample Name	Width (w) (mm)	Diameter (D) (mm)	Load (P) (kN)	A (mm^2)	De^2 (mm^2)	De (mm)	I_s (MPa)	F	Is$_{(50)}$ (MPa)	S_c (MPa)	$S_{c(ave)}$ (MPa)
ACyH	30	25	0.15	750	954.93	30.90	0.16	0.81	0.13	2.40	2.63±0.33
	30	20	0.15	600	763.94	27.64	0.20	0.77	0.15	2.86	
ACyT	32.5	25	0.4	812.5	1034.51	32.16	0.39	0.82	0.32	6.02	4.89±1.61
	50	30	0.4	1500	1909.86	43.70	0.21	0.94	0.20	3.75	
CEB	30	20	0.3	600	763.94	27.64	0.39	0.77	0.30	5.71	5.79±0.10
	52.5	30	0.65	1575	2005.35	44.78	0.32	0.95	0.31	5.86	
CKC	32.5	30	1.3	975	1241.41	35.23	1.05	0.85	0.89	17.00	17.15±0.21
	47.5	35	2	1663	2116.76	46.01	0.94	0.96	0.91	17.29	
CKCs	25	25	0.4	625	795.77	28.21	0.50	0.77	0.39	7.38	12.22±6.84
	35	25	1.2	875	1114.08	33.38	1.08	0.83	0.90	17.06	
CLB1	35	25	0.3	875	1114.08	33.38	0.27	0.83	0.22	4.27	3.21±1.49
	50	25	0.2	1250	1591.55	39.89	0.13	0.90	0.11	2.16	
CLB2	37.5	25	0.3	937.5	1193.66	34.55	0.25	0.85	0.21	4.04	4.49±0.63
	35	30	0.4	1050	1336.90	36.56	0.30	0.87	0.26	4.94	
CStB	35	20	0.5	700	891.27	29.85	0.56	0.79	0.44	8.45	10.49±2.89
	32.5	20	0.7	650	827.61	28.77	0.85	0.78	0.66	12.53	
CStT	37.5	30	0.35	1125	1432.39	37.85	0.24	0.88	0.22	4.10	3.50±0.84
	50	35	0.35	1750	2228.17	47.20	0.16	0.97	0.15	2.91	
CTrG	30	20	0.35	600	763.94	27.64	0.46	0.77	0.35	6.67	5.21±2.06
	50	30	0.4	1500	1909.86	43.70	0.21	0.94	0.20	3.75	
CTrB	40	25	0.5	1000	1273.24	35.68	0.39	0.86	0.34	6.41	7.89±2.09
	50	30	1	1500	1909.86	43.70	0.52	0.94	0.49	9.36	
IAnAq	32.5	20	0.2	650	827.61	28.77	0.24	0.78	0.19	3.58	6.27±3.80
	32.5	20	0.5	650	827.61	28.77	0.60	0.78	0.47	8.95	
IAnB	42.5	25	0.2	1063	1352.82	36.78	0.15	0.87	0.13	2.45	2.01±0.63
	52.5	25	0.15	1313	1671.13	40.88	0.09	0.91	0.08	1.56	
IMA	37.5	20	0.4	750	954.93	30.90	0.42	0.81	0.34	6.41	4.96±2.05
	45	25	0.3	1125	1432.39	37.85	0.21	0.88	0.18	3.51	
IMG	35	30	0.3	1050	1336.90	36.56	0.22	0.87	0.19	3.70	4.63±1.32
	40	30	0.5	1200	1527.89	39.09	0.33	0.90	0.29	5.57	
IMS	25	25	0.2	625	795.77	28.21	0.25	0.77	0.19	3.69	2.74±1.34
	32.5	20	0.1	650	827.61	28.77	0.12	0.78	0.09	1.79	
IPyH	45	25	0.3	1125	1432.39	37.85	0.21	0.88	0.18	3.51	6.56±4.32
	30	25	0.6	750	954.93	30.90	0.63	0.81	0.51	9.61	
IPrB	41	25	0.3	1025	1305.07	36.13	0.23	0.86	0.20	3.77	4.54±1.09
	42.5	30	0.5	1275	1623.38	40.29	0.31	0.91	0.28	5.31	

Sample Name	Width (w) (mm)	Diameter (D) (mm)	Load (P) (kN)	A (mm²)	De² (mm²)	De (mm)	I_s (MPa)	F	$Is_{(50)}$ (MPa)	S_c (MPa)	$S_{c(ave)}$ (MPa)
IPrH	45	20	0.3	900	1145.92	33.85	0.26	0.84	0.22	4.17	5.25±1.53
	47.5	30	0.65	1425	1814.37	42.60	0.36	0.93	0.33	6.33	
IPrT	35	25	0.3	875	1114.08	33.38	0.27	0.83	0.22	4.27	7.03±3.90
	42.5	25	0.8	1063	1352.82	36.78	0.59	0.87	0.52	9.79	
ITCs	45	25	0.45	1125	1432.39	37.85	0.31	0.88	0.28	5.27	5.24±0.03
	55	30	0.6	1650	2100.85	45.83	0.29	0.96	0.27	5.22	
ITT	27.5	25	0.55	687.5	875.35	29.59	0.63	0.79	0.50	9.43	11.48±2.89
	52.5	30	1.5	1575	2005.35	44.78	0.75	0.95	0.71	13.52	
**LPtB**	32.5	25	0.2	812.5	1034.51	32.16	0.19	0.82	0.16	3.01	2.93±0.11
	30	20	0.15	600	763.94	27.64	0.20	0.77	0.15	2.86	
LPtC	35	20	0.15	700	891.27	29.85	0.17	0.79	0.13	2.54	2.12±0.60
	35	20	0.1	700	891.27	29.85	0.11	0.79	0.09	1.69	
**LPtT**	30	20	0.35	600	763.94	27.64	0.46	0.77	0.35	6.67	5.37±1.83
	27.5	20	0.2	550	700.28	26.46	0.29	0.75	0.21	4.08	
**LTlB**	–	–	–	–	–	–	–	–	–	–	_n.d._
LTlS	–	–	–	–	–	–	–	–	–	–	_n.d._
LTlT	32.5	25	0.3	812.5	1034.51	32.16	0.29	0.82	0.24	4.52	7.02±3.54
	30	20	0.5	600	763.94	27.64	0.65	0.77	0.50	9.52	
LXA	42.5	20	0.2	850	1082.25	32.90	0.18	0.83	0.15	2.91	2.65±0.37
	22.5	20	0.1	450	572.96	23.94	0.17	0.72	0.13	2.38	
**LXB**	30	25	0.3	750	954.93	30.90	0.31	0.81	0.25	4.81	4.53±0.40
	42.5	30	0.4	1275	1623.38	40.29	0.25	0.91	0.22	4.25	
LXT	30	25	0.7	750	954.93	30.90	0.73	0.81	0.59	11.22	10.29±1.32
	37.5	30	0.8	1125	1432.39	37.85	0.56	0.88	0.49	9.36	
LySrU	40	22	0.6	880	1120.45	33.47	0.54	0.83	0.45	8.49	11.45±4.18
	52.5	35	1.8	1838	2339.58	48.37	0.77	0.99	0.76	14.40	
LyTpA	25	20	0.25	500	636.62	25.23	0.39	0.74	0.29	5.48	4.43±1.49
	35	20	0.2	700	891.27	29.85	0.22	0.79	0.18	3.38	
LyTpB	25	20	0.2	500	636.62	25.23	0.31	0.74	0.23	4.39	5.76±1.94
	27.5	20	0.35	550	700.28	26.46	0.50	0.75	0.38	7.13	
LyTpT	25	20	0.4	500	636.62	25.23	0.63	0.74	0.46	8.78	17.15±3.33
	45	30	0.4	1350	1718.87	41.46	0.23	0.92	0.21	4.06	
MPB	27.5	20	0.2	550	700.28	26.46	0.29	0.75	0.21	4.08	4.98±1.28
	57.5	30	0.7	1725	2196.34	46.87	0.32	0.97	0.31	5.88	
MPB2	25	20	0.2	500	636.62	25.23	0.31	0.74	0.23	4.39	5.00±0.87
	50	30	0.6	1500	1909.86	43.70	0.31	0.94	0.30	5.62	
MPC	25	20	0.2	500	636.62	25.23	0.31	0.74	0.23	4.39	4.96±0.81
	25	25	0.3	625	795.77	28.21	0.38	0.77	0.29	5.54	
PhAzB	–	–	–	–	–	–	–	–	–	–	_n.d._
PhLdB	37.5	30	0.9	1125	1432.39	37.85	0.63	0.88	0.55	10.53	11.46±1.31
	30	20	0.65	600	763.94	27.64	0.85	0.77	0.65	12.38	
PCT	35	30	0.7	1050	1336.90	36.56	0.52	0.87	0.45	8.64	11.70±4.33
	25	25	0.8	625	795.77	28.21	1.01	0.77	0.78	14.76	
PCB	25	25	0.4	625	795.77	28.21	0.50	0.77	0.39	7.38	6.67±1.01
	22.5	20	0.25	450	572.96	23.94	0.44	0.72	0.31	5.95	
PCC	30	25	0.7	750	954.93	30.90	0.73	0.81	0.59	11.22	10.41±1.14
	30	25	0.6	750	954.93	30.90	0.63	0.81	0.51	9.61	

Sample Name	Width (w) (mm)	Diameter (D) (mm)	Load (P) (kN)	A (mm^2)	De^2 (mm^2)	De (mm)	I$_s$ (MPa)	F	Is$_{(50)}$ (MPa)	S$_c$ (MPa)	S$_{c(ave)}$ (MPa)
PmLyB	37.5	30	0.2	1125	1432.39	37.85	0.14	0.88	0.12	2.34	2.82±0.67
	25	20	0.15	500	636.62	25.23	0.24	0.74	0.17	3.29	
PmLyCs	35	25	0.5	875	1114.08	33.38	0.45	0.83	0.37	7.11	5.59±2.15
	27.5	20	0.2	550	700.28	26.46	0.29	0.75	0.21	4.08	
PmLyC	60	30	0.35	1800	2291.83	47.87	0.15	0.98	0.15	2.85	3.68±1.18
	32.5	25	0.3	812.5	1034.51	32.16	0.29	0.82	0.24	4.52	
PAtT	55	25	0.5	1375	1750.70	41.84	0.29	0.92	0.26	5.01	4.38±0.89
	50	30	0.4	1500	1909.86	43.70	0.21	0.94	0.20	3.75	
PSlB	45	25	0.7	1125	1432.39	37.85	0.49	0.88	0.43	8.19	7.90±0.41
	35	20	0.45	700	891.27	29.85	0.50	0.79	0.40	7.61	
PSlS	40	20	0.5	800	1018.59	31.92	0.49	0.82	0.40	7.62	8.57±1.34
	22.5	20	0.4	450	572.96	23.94	0.70	0.72	0.50	9.52	
PSlT	25	25	0.35	625	795.77	28.21	0.44	0.77	0.34	6.46	6.71±0.35
	30	30	0.5	900	1145.92	33.85	0.44	0.84	0.37	6.96	
PSB	25	20	0.1	500	636.62	25.23	0.16	0.74	0.12	2.19	2.48±0.41
	25	25	0.15	625	795.77	28.21	0.19	0.77	0.15	2.77	
PSA	35	30	0.1	1050	1336.90	36.56	0.07	0.87	0.06	1.23	2.70±2.08
	30	30	0.3	900	1145.92	33.85	0.26	0.84	0.22	4.17	
PST	37.5	25	0.3	937.5	1193.66	34.55	0.25	0.85	0.21	4.04	5.23±1.68
	30	25	0.4	750	954.93	30.90	0.42	0.81	0.34	6.41	
**TAB**	52.5	25	0.7	1313	1671.13	40.88	0.42	0.91	0.38	7.27	6.17±1.55
	45	30	0.5	1350	1718.87	41.46	0.29	0.92	0.27	5.08	
TACs	27.5	20	0.25	550	700.28	26.46	0.36	0.75	0.27	5.09	6.70±2.27
	37.5	35	0.8	1313	1671.13	40.88	0.48	0.91	0.44	8.31	
TAxB	50	30	0.9	1500	1909.86	43.70	0.47	0.94	0.44	8.43	8.97±0.77
	47.5	35	1.1	1663	2116.76	46.01	0.52	0.96	0.50	9.51	
TAxG	45	25	0.4	1125	1432.39	37.85	0.28	0.88	0.25	4.68	4.63±0.08
	50	35	0.55	1750	2228.17	47.20	0.25	0.97	0.24	4.57	

APPENDIX C

LIME/AGGREGATE RATIOS OF MORTARS

Sample Name	Lime [%]	Aggregate [%]	Lime/Aggregate
ACyH	60.7	39.3	3/2
ACyT	42.1	57.9	3/4
CEB	27.6	72.4	1/3
CKC	57.6	42.4	3/2
CKCs	31.1	68.9	1/2
CLB1	39.5	60.5	2/3
CLB2	24.7	75.3	1/3
CStB	29.4	70.6	1/2
CStT	42.7	57.3	3/4
CTrG	20.8	79.2	1/4
CTrB	37.6	62.4	2/3
IAnAq	29.9	70.1	1/2
IAnB	51.9	48.1	1/1
IMA	37.2	62.8	2/3
IMG	30.7	69.3	1/2
IMS	35.6	64.4	1/2
IPyH	32.4	67.6	1/2
IPrB	65.5	34.5	2/1
IPrH	46.5	53.5	1/1
IPrT	52.5	47.5	1/1
ITCs	35.1	64.9	1/2
ITT	34.1	65.9	1/2
LPtB	64.9	35.1	2/1
LPtC	71.3	28.7	5/2
LPtT	61.9	38.1	3/2
LTlB	86.3	13.7	6/1
LTlS	91.5	8.5	11/1
LTlT	78.0	22.0	7/2
LXA	40.6	59.4	2/3
LXB	45.8	54.2	1/1

Sample Name	Lime [%]	Aggregate [%]	Lime/Aggregate
LXT	54.2	45.8	1/1
LySrU	21.5	78.5	1/4
LyTpA	34.8	65.2	1/2
LyTpB	22.5	77.5	1/4
LyTpT	13.7	86.3	1/6
MPB	23.6	76.4	1/3
MPB2	22.8	77.2	1/4
MPC	21.7	78.3	1/4
PhAzB	31.4	68.6	1/2
PhLdB	59.8	40.2	3/2
PCT	93.3	6.7	14/1
PCB	88.6	11.4	8/1
PCC	96.5	3.5	28/1
PmLyB	54.7	45.3	1/1
PmLyCs	61.4	38.6	3/2
PmLyC	70.7	29.3	5/2
PAtT	18.7	81.3	1/4
PSlB	61.8	38.2	3/2
PSlS	61.2	38.8	3/2
PSlT	80.2	19.8	4/1
PSB	43.7	56.3	3/4
PSA	28.7	71.3	1/3
PST	69.5	30.5	2/1
TAB	32.9	67.1	1/2
TACs	27.7	72.3	1/3
TAxB	20.0	80.0	1/4
TAxG	24.5	75.5	1/3

APPENDIX D

PARTICLE SIZE DISTRIBUTION OF AGGREGATES

Sample Name	Particle Size Distributions of Aggregates			
	1180µm [%]	500µm [%]	53µm [%]	<53µm [%]
ACyH	40.39	25.86	29.24	3.00
ACyT	20.49	52.47	25.16	1.22
CEB	58.94	21.48	18.68	0.63
CKC	59.84	12.80	22.55	2.64
CKCs	37.03	48.46	11.18	1.47
CLB1	43.33	15.12	36.90	3.18
CLB2	54.51	11.41	30.57	3.11
CStB	47.66	22.51	26.66	2.30
CStT	44.76	16.65	34.67	3.14
CTrG	48.62	24.16	25.86	1.36
CTrB	51.16	24.84	22.37	1.43
IAnAq	55.72	20.35	21.19	2.48
IAnB	43.79	19.48	34.54	1.09
IMA	18.64	26.35	51.95	2.67
IMG	24.00	26.97	47.00	1.20
IMS	43.69	18.06	30.42	4.09
IPyH	32.06	31.77	33.95	2.95
IPrB	67.73	11.93	15.87	1.37
IPrH	45.50	19.11	31.71	1.56
IPrT	74.74	8.27	12.23	1.66
ITCs	68.44	15.67	13.84	1.63
ITT	43.44	29.30	26.10	0.92
LPtB	43.76	26.63	27.58	2.68
LPtC	5.98	36.52	57.17	2.67
LPtT	65.62	18.88	13.51	1.04
LTlB	26.90	36.58	28.02	2.31
LTlS	39.15	19.78	10.29	1.22
LTlT	71.57	12.20	7.22	0.71

Sample Name	Particle Size Distributions of Aggregates			
	1000µm [%]	500µm [%]	53µm [%]	<53µm [%]
LXA	38.63	9.68	45.35	4.43
LXB	80.11	6.60	9.63	1.14
LXT	3.01	7.53	82.02	4.91
LySrU	53.43	24.08	21.46	0.97
LyTpA	47.02	20.85	29.67	1.23
LyTpB	53.69	23.22	21.68	1.08
LyTpT	60.84	22.67	15.54	0.86
MPB	33.47	36.30	29.59	0.32
MPB2	33.85	35.15	29.94	0.58
MPC	59.43	22.63	16.52	1.21
PhAzB	44.95	37.96	15.71	0.81
PhLdB	31.84	26.90	36.57	2.26
PCT	0.91	37.64	49.74	8.86
PCB	10.24	28.58	48.81	5.42
PCC	3.44	45.63	40.53	5.01
PmLyB	34.74	25.35	36.16	2.77
PmLyCs	31.56	19.59	43.58	3.88
PmLyC	8.97	16.79	68.31	3.97
PAtT	59.52	20.96	18.18	1.07
PSlB	51.13	24.25	22.44	1.40
PSlS	34.94	29.23	32.40	2.18
PSlT	10.44	33.61	49.46	2.32
PSB	25.82	24.78	43.69	4.93
PSA	21.55	20.25	51.68	4.94
PST	16.43	26.69	50.99	4.70
TAB	45.17	43.94	9.84	0.21
TACs	38.03	36.16	23.88	1.08
TAxB	30.80	53.72	14.39	0.59
TAxG	48.41	37.30	12.92	0.91

APPENDIX E

IMAGES OF AGGREGATES USED IN MORTARS AFTER SIEVE ANALYSES

Sample Name	1180 μm	500 μm	53 μm	53 μm<
ACyH				
ACyT				
CEB				
CKC				
CKCs				

0   2 cm

Sample Name	1180 μm	500 μm	53 μm	53 μm<
CLB1				
CLB2				
CStB				
CStT				
CTrG				
CTrB				

0   2 cm

Sample Name	1180 μm	500 μm	53 μm	53 μm<
IAnAq				
IAnB				
IMA				
IMG				
IMS				
IPyH				

0   2 cm

Sample Name	1180 μm	500 μm	53 μm	53 μm<
IPrB				
IPrH				
IPrT				
ITCs				
ITT				
LPtB			not available	

0 _____ 2 cm

Sample Name	1180 μm	500 μm	53 μm	53 μm<
LPtC	not available	not available		
LPtT				not available
LTIB				not available
LTIS		not available		not available
LTIT				
LXA				

0   2 cm

175

Sample Name	1180 μm	500 μm	53 μm	53 μm<
LXB				
LXT				
LySrU				
LyTpA				
LyTpB				
LtTpT				

0 _____ 2 cm

Sample Name	1180 μm	500 μm	53 μm	53 μm<
MPB				
MPB2				
MPC				
PhAzB				
PhLdB				
PCT	not available			

0   2 cm

Sample Name	1180 μm	500 μm	53 μm	53 μm<
PCB				
PCC	not available	not available		not available
PmLyB				
PmLyCs				
PmLyC				not available
PAtT				

0 ⬛⬛⬛⬜⬜ 2 cm

178

Sample Name	1180 μm	500 μm	53 μm	53 μm<
PSIB				
PSIS				
PSIT				
PSB				
PSA				
PST				

0   2 cm

Sample Name	1180 μm	500 μm	53 μm	53 μm<
TAB				
TACs				
TAxB				
TAxG				
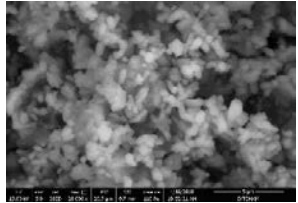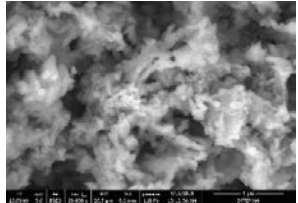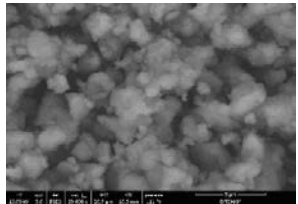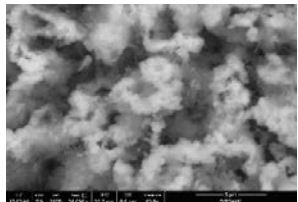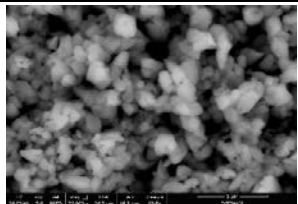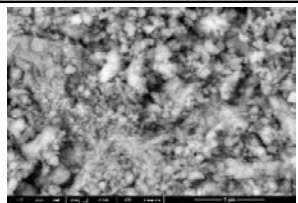
0   2 cm
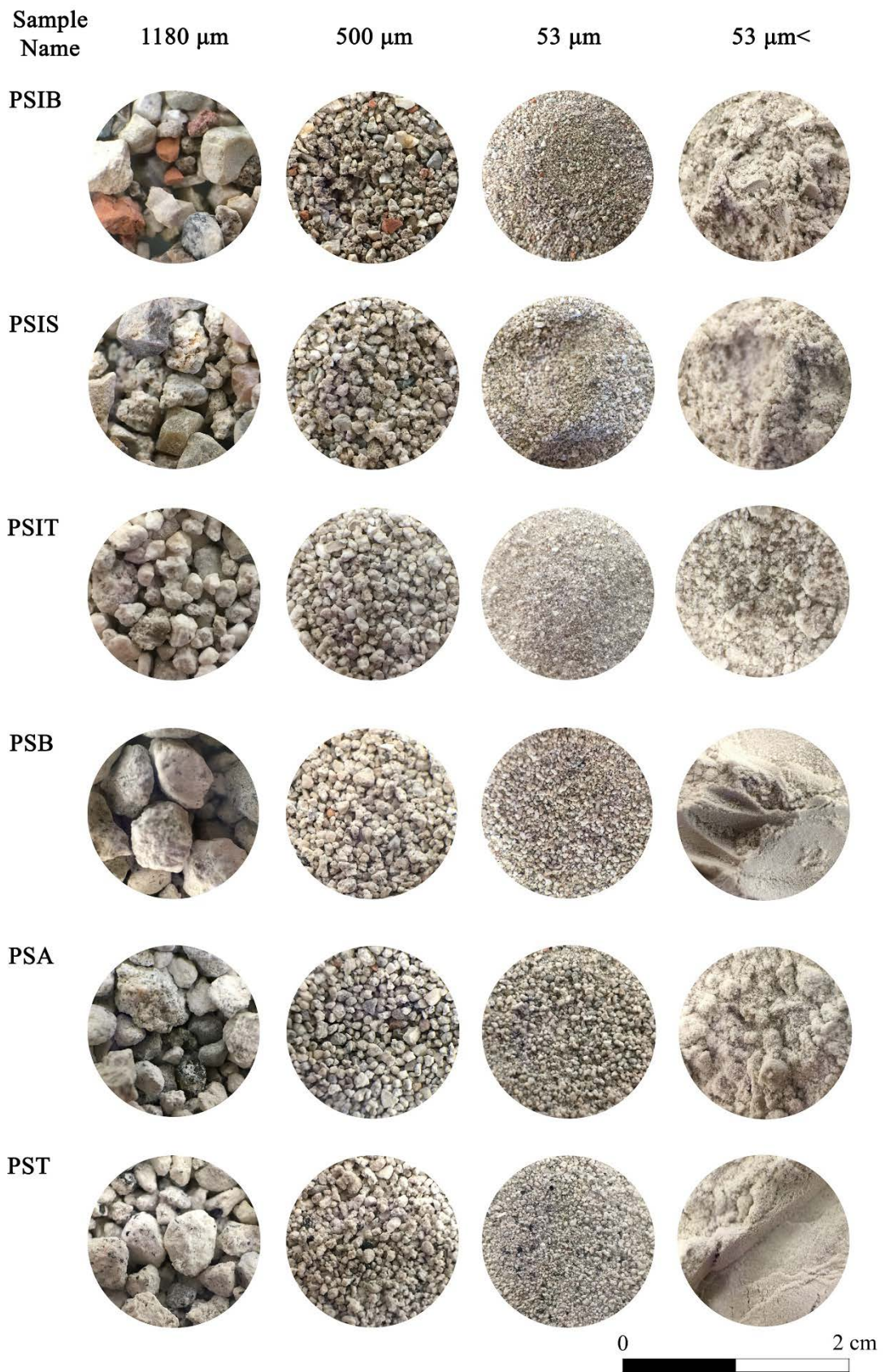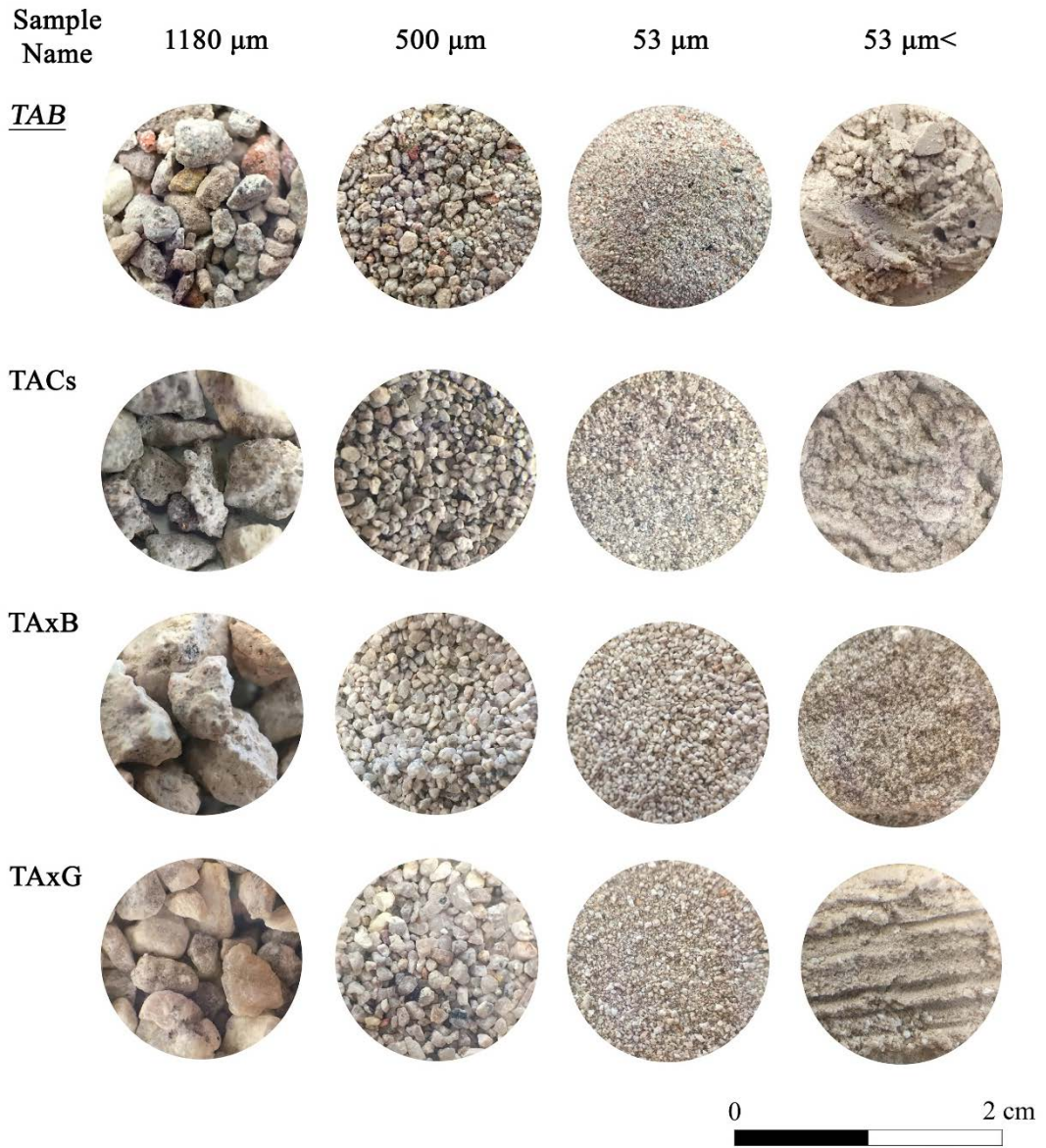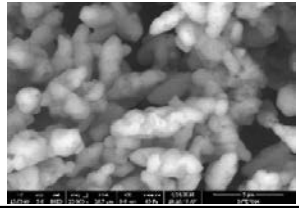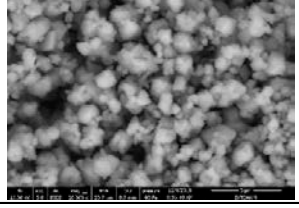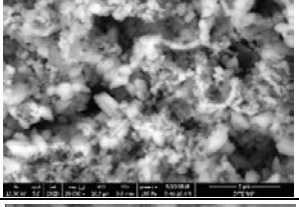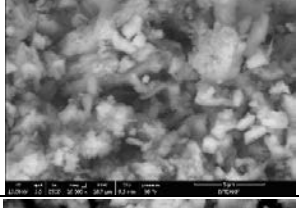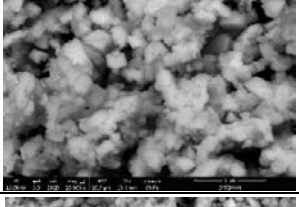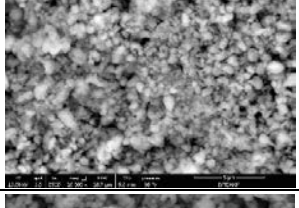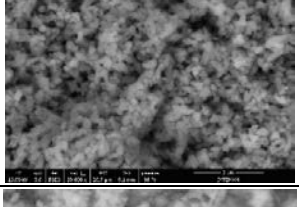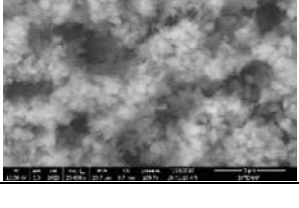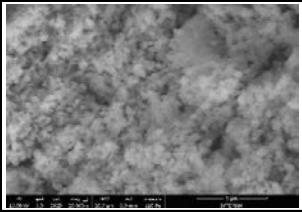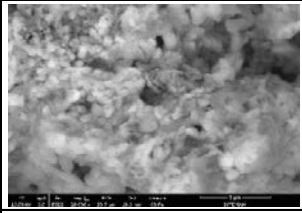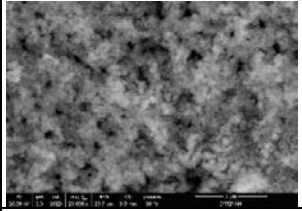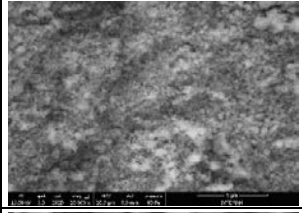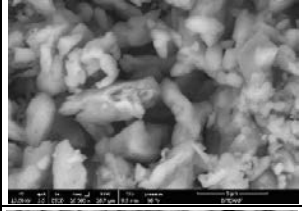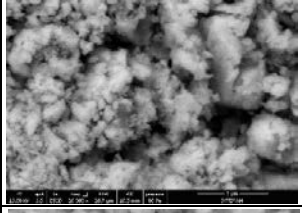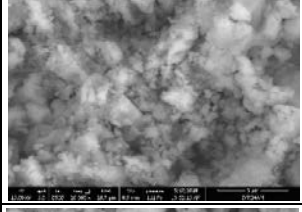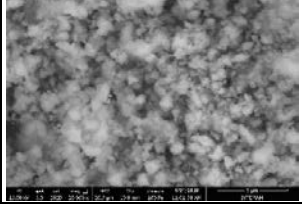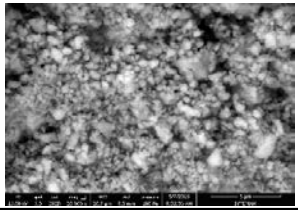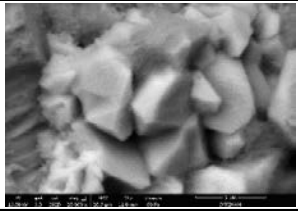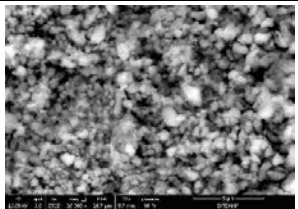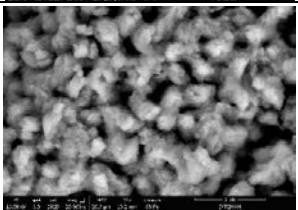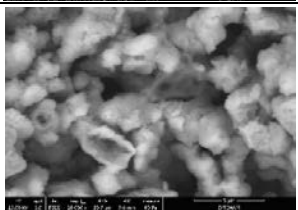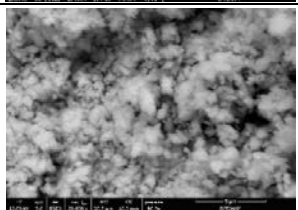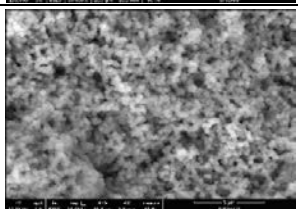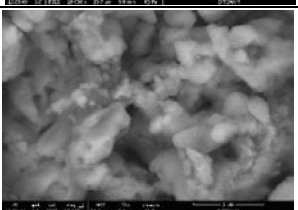
APPENDIX F
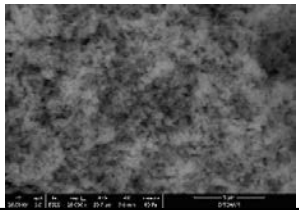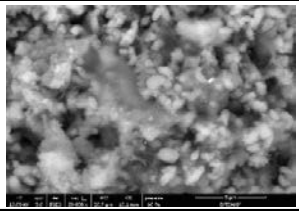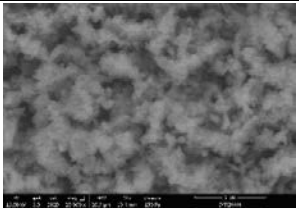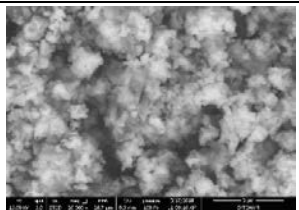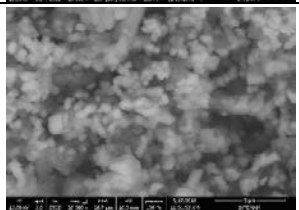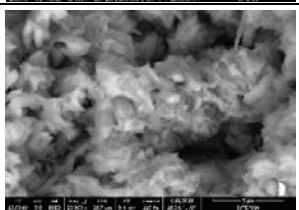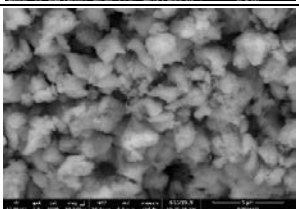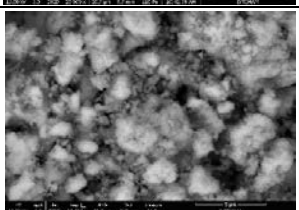
CHEMICAL COMPOSITION OF LIME LUMPS
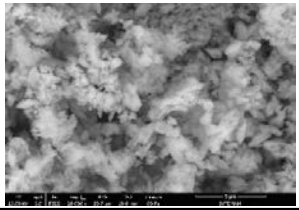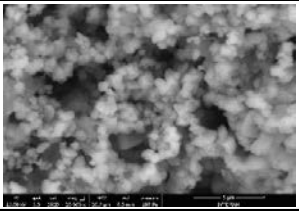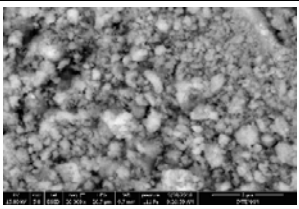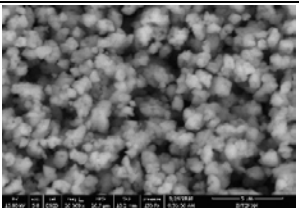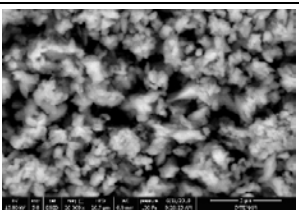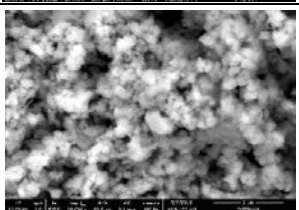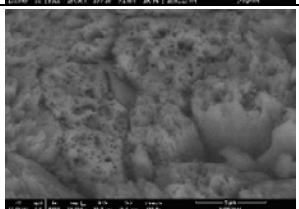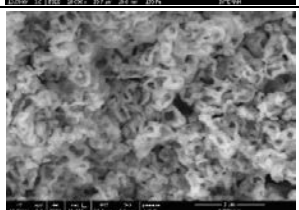
Sample Code	CaO [%]	MgO [%]	SiO$_2$ [%]	Al$_2$O$_3$ [%]	FeO [%]	P$_2$O$_5$ [%]	Image [mag 20.000x]
ACyH	90.79	-	6.80	2.40	-	-	
ACyT	96.01	-	1.80	2.18	-	-	
CEB	93.86	-	3.19	2.96	-	-	
CKC	91.06	0.84	6.14	1.96	-	-	
CKCs	97.13	-	2.03	0.84	-	-	
CLB1	95.75	1.16	1.40	1.69	-	-	
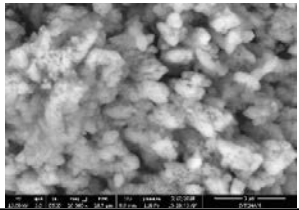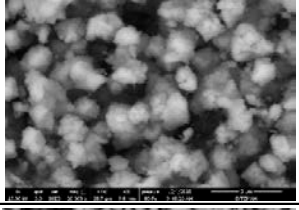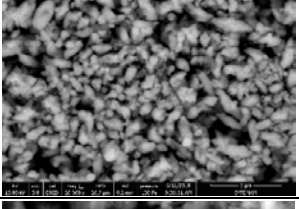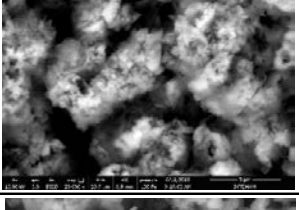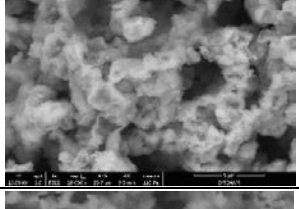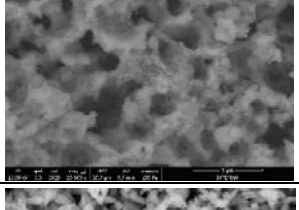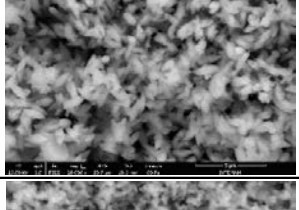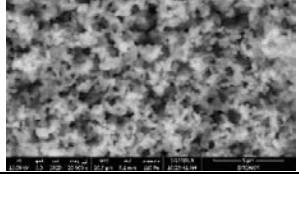
Sample Code	CaO [%]	MgO [%]	SiO₂ [%]	Al₂O₃ [%]	FeO [%]	P₂O₅ [%]	Image [mag 20.000x]
CLB2	92.14	0.64	2.96	4.26	-	-	
CStB	92.82	1.06	3.90	2.23	-	-	
CStT	88.07	1.02	5.49	5.42	-	-	
CTrG	90.93	3.74	4.24	1.09	-	-	
CTrB	93.37	1.78	4.17	0.67	-	-	
IAnAq	92.12	3.32	3.00	1.03	0.81	-	
IAnB	95.43	1.18	1.32	2.06	-	-	
IMA	88.31	3.26	3.54	4.89	-	-	
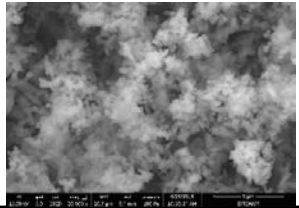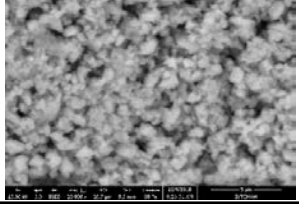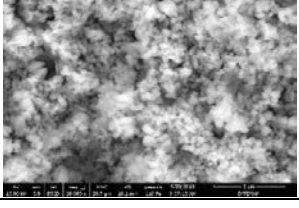
Sample Code	CaO [%]	MgO [%]	SiO$_2$ [%]	Al$_2$O$_3$ [%]	FeO [%]	P$_2$O$_5$ [%]	Image [mag 20.000x]
IMG	96.34	0.84	2.41	0.41	-	-	
IMS	87.91	-	5.99	6.10	-	-	
IPyH	98.34	0.89	-	0.76	-	-	
IPrB	94.51	0.94	1.87	2.07	-	0.63	
IPrH	98.20	0.81	0.23	0.76	-	-	
IPrT	94.89	1.52	2.34	1.26	-	-	
ITCs	96.60	-	2.65	0.75	-	-	
ITT	89.11	0.24	5.22	5.43	-	-	

Sample Code	CaO [%]	MgO [%]	SiO$_2$ [%]	Al$_2$O$_3$ [%]	FeO [%]	P$_2$O$_5$ [%]	Image [mag 20.000x]
__LPtB__	86.93	0.75	8.75	3.57	-	-	
LPtC	92.45	1.06	3.79	2.19	0.51	-	
__LPtT__	99.57	-	0.43	-	-	-	
LTlB	90.63	4.12	1.98	3.27	-	-	
LTlS	92.10	4.50	2.15	1.25	-	-	
LTlT	91.31	4.10	3.15	0.85	-	0.59	
LXA	98.50	-	0.91	0.60	-	-	
__LXB__	97.74	0.63	1.25	0.38	-	-	

Sample Code	CaO [%]	MgO [%]	SiO$_2$ [%]	Al$_2$O$_3$ [%]	FeO [%]	P$_2$O$_5$ [%]	Image [mag 20.000x]
LXT	97.74	-	0.74	1.52	-	-	
LySrU	85.93	2.98	6.50	4.59	-	-	
LyTpA	96.15	-	2.73	1.12	-	-	
LyTpB	78.68	6.66	11.60	3.06	-	-	
LyTpT	85.67	1.16	10.14	3.03	-	-	
MPB	90.74	0.49	4.14	4.63	-	-	
MPB2	92.46	-	1.30	6.25	-	-	
MPC	88.51	0.90	7.20	3.39	-	-	

Sample Code	CaO [%]	MgO [%]	SiO$_2$ [%]	Al$_2$O$_3$ [%]	FeO [%]	P$_2$O$_5$ [%]	Image [mag 20.000x]
PAB	97.13	-	0.75	2.13	-	-	
PhLdB	94.56	0.69	3.95	1.26	-	-	
PmLyB	92.75	0.23	3.30	2.60	0.39	-	
PmLyCs	90.18	3.18	4.33	2.31	-	-	
PmLyC	96.34	0.69	2.17	0.80	-	-	
PCT	93.49	1.69	2.39	2.14	-	0.30	
PCB	92.09	-	4.37	3.54	-	-	
PCC	97.30	0.70	-	2.01	-	-	

Sample Code	CaO [%]	MgO [%]	SiO$_2$ [%]	Al$_2$O$_3$ [%]	FeO [%]	P$_2$O$_5$ [%]	Image [mag 20.000x]
PAtT	84.63	4.82	7.04	3.51	-	-	
PSlB	91.01	0.53	5.25	3.21	-	-	
PSlS	92.39	1.86	4.66	1.08	-	-	
PSlT	89.15	1.80	9.05	-	-	-	
PSB	97.95	-	0.81	1.24	-	-	
PSA	97.37	-	0.50	2.13	-	-	
PST	85.60	-	2.24	12.16	-	-	
TAB	96.96	-	1.00	2.04	-	-	

Sample Code	CaO [%]	MgO [%]	SiO$_2$ [%]	Al$_2$O$_3$ [%]	FeO [%]	P$_2$O$_5$ [%]	Image [mag 20.000x]
TACs	92.67	0.97	2.81	3.54	-	-	
TAxB	87.77	0.22	6.40	5.60	-	-	
TAxG	91.86	1.57	3.75	2.82	-	-	

APPENDIX G

POZZOLANIC ACTIVITIES OF AGGREGATES

Sample Name	Electrical Conductivity [mS/cm]		Difference in Electrical Conductivity [mS/cm]
	Before	**After**	
ACyH	7.72	1.04	6.68
ACyT	7.78	4.26	3.52
CEB	7.87	2.09	5.78
CKC	7.67	2.21	5.46
CKCs	7.74	3.34	4.40
CLB1	7.89	1.50	6.39
CLB2	7.77	3.46	4.31
CStB	7.86	0.46	7.40
CStT	7.85	0.87	6.98
CTrG	7.64	2.47	5.17
CTrB	7.86	1.05	6.82
IAnAq	7.71	1.89	5.82
IAnB	7.69	4.20	3.49
IMA	7.67	1.58	6.10
IMG	7.81	4.39	3.42
IMS	7.66	5.50	2.16
IPyH	7.65	2.51	5.14
IPrB	7.67	3.97	3.70
IPrH	7.78	4.20	3.58
IPrT	7.58	4.06	3.52
ITCs	7.78	1.30	6.48
ITT	7.76	0.94	6.82
LPtB	7.69	0.87	6.83
LPtC	7.77	3.75	4.02
LPtT	7.70	1.23	6.47
LTlB	7.78	1.34	6.44
LTlS	7.77	2.79	4.98

Sample Name	Electrical Conductivity [mS/cm]		Difference in Electrical Conductivity [mS/cm]
	Before	After	
LTlT	7.75	1.09	6.66
LXA	8.20	5.66	2.54
LXB	7.82	3.67	4.15
LXT	8.03	4.60	3.43
LySrU	7.71	2.14	5.57
LyTpA	7.80	4.00	3.80
LyTpB	7.79	0.50	7.29
LyTpT	7.72	0.51	7.21
MPB	7.72	1.99	5.74
MPB2	7.85	2.05	5.80
MPC	7.73	6.54	1.19
PhAzB	7.67	3.36	4.31
PhLdB	7.75	2.37	5.38
PCT	7.75	1.14	6.61
PCB	7.78	2.51	5.27
PCC	7.77	0.75	7.02
PmLyB	7.96	3.27	4.69
PmLyCs	7.64	3.81	3.83
PmLyC	7.76	2.32	5.44
PAtT	7.69	4.76	2.93
PSlB	7.75	0.64	7.11
PSlS	7.72	1.09	6.63
PSlT	7.65	0.61	7.04
PSB	7.89	3.15	4.74
PSA	7.76	3.43	4.33
PST	7.79	0.63	7.17
TAB	7.86	0.33	7.53
TACs	7.70	0.96	6.74
TAxB	7.73	0.36	7.38
TAxG	7.80	0.32	7.48

APPENDIX H

STRUCTURAL H_2O AND CO_2 RATIOS OF MORTARS

Sample Name	Weight Loses [%]		CO_2/H_2O
	200-600 °C [Structural H_2O]	600-900 °C [CO_2]	
ACyH	4.23	33.70	7.97
ACyT	3.90	35.77	9.18
CEB	2.73	37.18	13.63
CKC	3.25	35.07	10.79
CKCs	5.46	32.18	5.89
CLB1	3.77	23.48	6.23
CLB2	4.38	22.63	5.17
CStB	8.14	22.56	2.77
CStT	4.36	21.17	4.86
CTrG	4.90	28.34	5.78
CTrB	6.52	29.31	4.50
IAnAq	9.55	25.65	2.69
IAnB	4.33	38.49	8.88
IMA	3.04	31.95	10.52
IMG	3.12	34.95	11.21
IMS	2.49	32.20	12.94
IPyH	6.30	26.85	4.26
IPrB	5.09	34.16	6.71
IPrH	5.30	36.50	6.89
IPrT	4.58	34.14	7.45

Sample Name	Weight Loses [%]		CO$_2$/H$_2$0
	200-600 °C [Structural H$_2$O]	600-900 °C [CO$_2$]	
ITCs	4.22	22.83	5.40
ITT	4.90	17.19	3.51
LPtB	2.89	40.84	14.15
LPtC	7.53	43.17	5.73
LPtT	7.34	33.17	4.52
LTlB	7.17	38.05	5.31
LTlS	9.45	39.20	4.15
LTlT	6.42	38.82	6.05
LXA	4.60	27.77	6.03
LXB	6.85	36.03	5.26
LXT	5.51	33.70	6.12
LySrU	3.97	30.17	7.60
LyTpA	3.78	33.11	8.76
LyTpB	4.07	30.85	7.59
LyTpT	4.30	22.11	5.14
MPB	8.19	23.31	2.85
MPB2	5.71	33.48	5.87
MPC	4.18	7.55	1.81
PhAzB	3.66	31.19	8.52
PhLdB	4.95	32.64	6.59
PCT	4.49	38.60	8.60
PCB	4.07	38.54	9.47
PCC	4.77	39.50	8.27
PmLyB	3.24	35.83	11.04
PmLyCs	3.85	30.97	8.05
PmLyC	2.82	38.90	13.81

Sample Name	Weight Loses [%]		CO_2/H_2O
	200-600 °C [Structural H_2O]	600-900 °C [CO_2]	
PAtT	4.46	29.33	6.58
PSlB	5.62	30.61	5.44
PSlS	5.79	24.34	4.20
PSlT	3.30	30.70	9.29
PSB	6.00	25.26	4.21
PSA	5.02	21.12	4.21
PST	7.48	20.20	2.70
TAB	4.80	28.03	5.83
TACs	5.97	23.44	3.93
TAxB	5.91	21.24	3.60
TAxG	4.58	24.00	5.24

APPENDIX I

TGA CURVES OF BINDERS BY REGIONS

AIOLIS

CARIA

IONIA

LYCIA

LXA
LXT
LTIB
LTIS
LTIT
LXB
LPtB
LXT
LPtT

LYDIA

LyTpA
LySrU
LyTpT
LyTpB

MYSIA

MPC
MPB:
MPB

PAMPHYLIA

PmLyC
PmLyCs
PmLyB

PHRYGIA

PISIDIA

TROAS
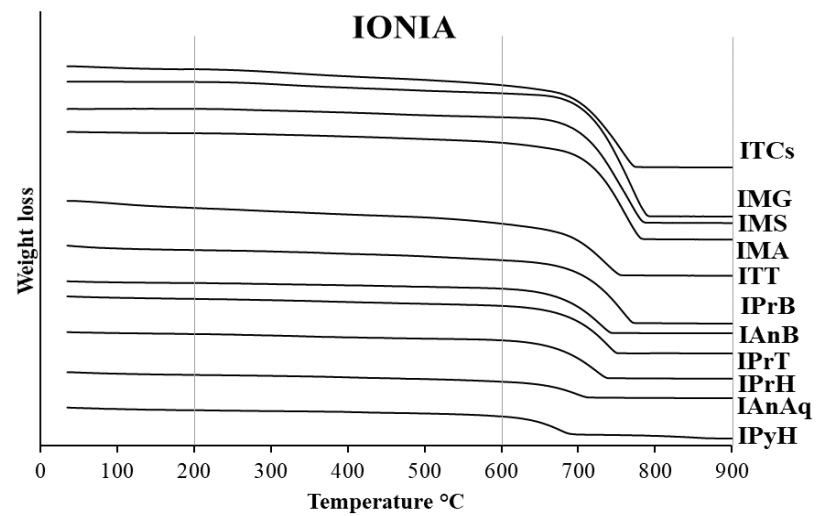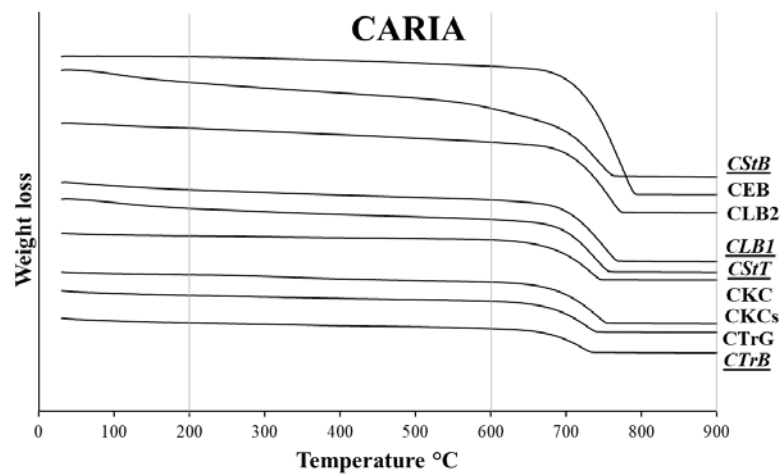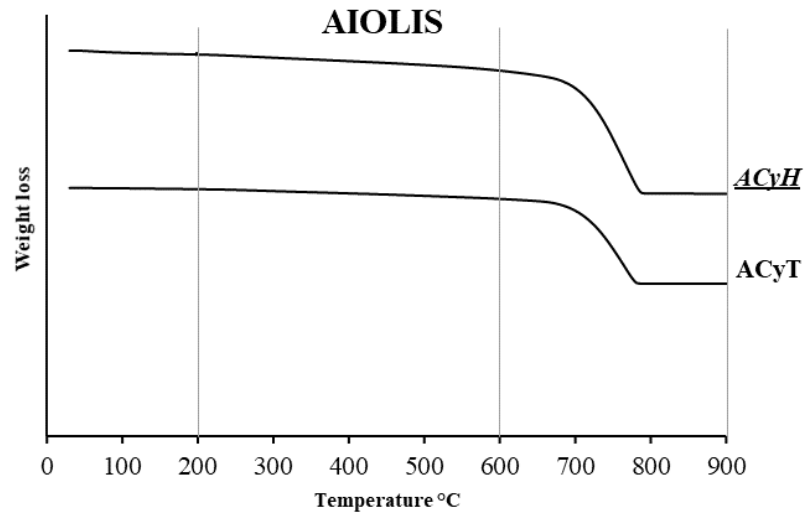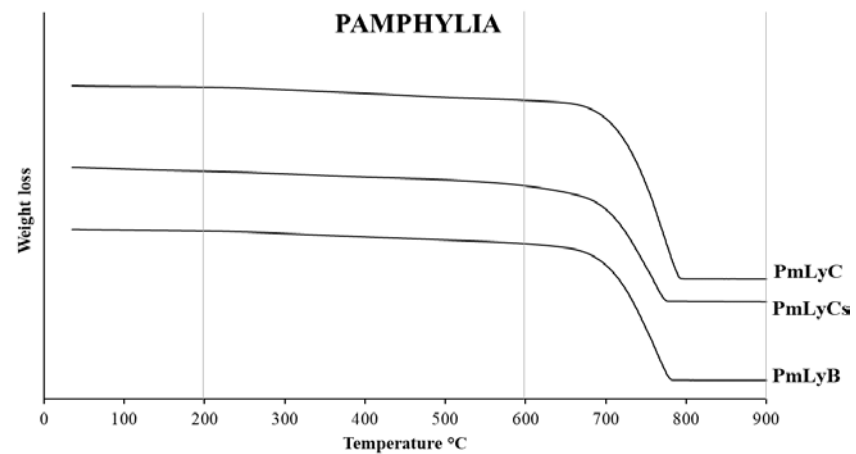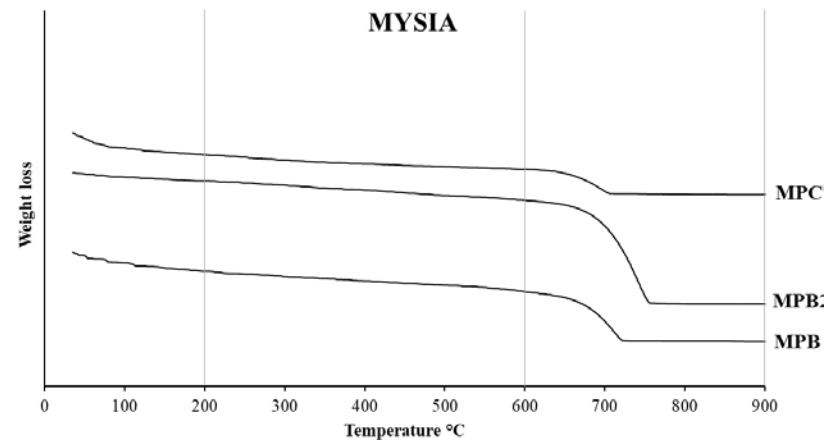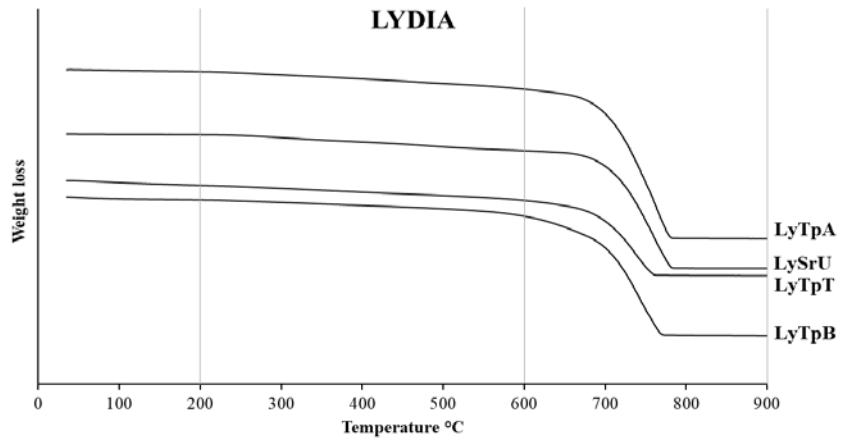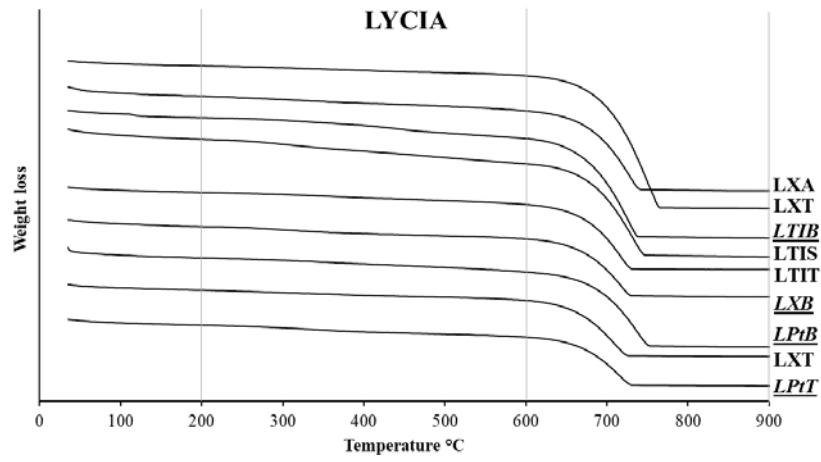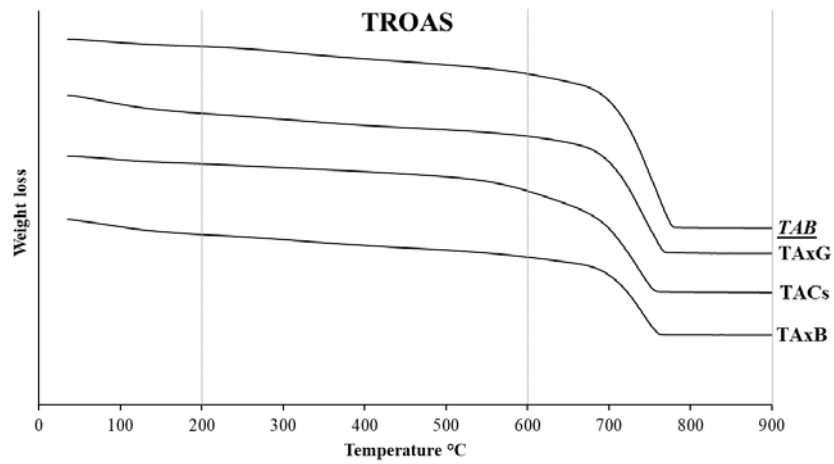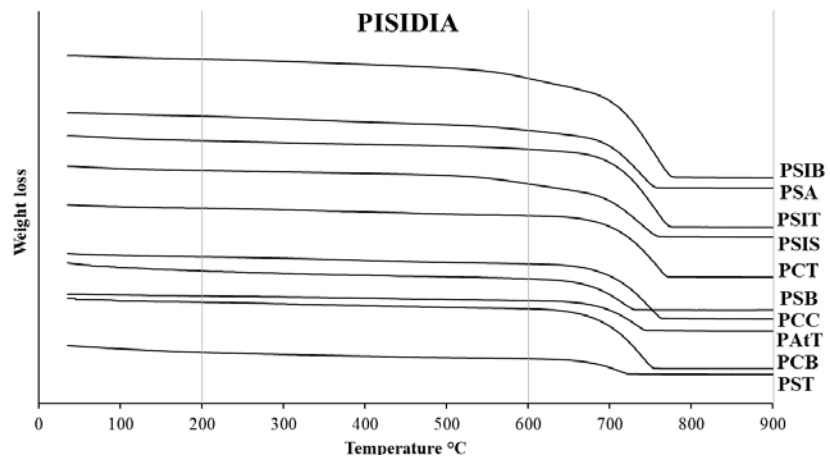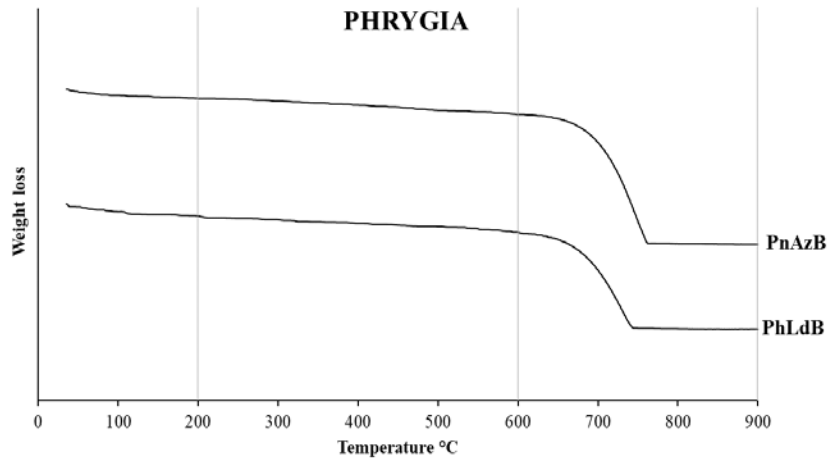
APPENDIX J

RELATIONSHIP BETWEEN MECHANICAL STRENGTH
AND OTHER PARAMETERS

Sample Name	Compressive Strength [MPa]	Difference in Electrical Conductivity [mS/cm]	Hydraulicity [CO_2/H_2O]	Porosity [%]	SiO_2 content of aggregates [%]	CaO content of aggregates [%]	Binder content [%]
ACyH	2.63	6.68	7.97	48.21	83.86	0.93	60.7
ACyT	4.89	3.52	9.18	35.41	90.55	0.16	42.1
CEB	5.79	5.78	13.63	36.49	71.30	0.55	27.6
CKC	17.15	5.46	10.79	30.99	57.69	1.40	57.6
CKCs	12.22	4.40	5.89	33.1	86.40	1.25	31.1
CLB1	3.21	6.39	6.23	37.39	83.10	1.89	39.5
CLB2	4.49	4.31	5.17	36.26	75.78	0.00	24.7
CStB	10.49	7.40	2.77	42.21	91.32	0.00	29.4
CStT	3.50	6.98	4.86	42.03	91.02	0.16	42.7
CTrG	5.21	5.17	5.78	33.03	79.60	0.00	20.8
CTrB	7.89	6.82	4.50	33.85	89.25	0.00	37.6
IAnAq	6.27	5.82	2.69	33.34	77.08	0.00	29.9
IAnB	2.01	3.49	8.88	44.27	72.42	0.00	51.9
IMA	4.96	6.10	10.52	37.38	76.16	0.48	37.2
IMG	4.64	3.42	11.21	29.02	61.47	0.88	30.7
IMS	2.74	2.16	12.94	30.99	62.18	0.00	35.6
IPyH	6.57	3.70	4.26	38.30	72.27	1.32	32.4
IPrB	4.54	5.14	6.71	31.29	69.77	0.69	65.5
IPrH	5.25	3.58	6.89	35.08	53.00	2.73	46.5
IPrT	7.03	3.52	7.45	34.94	52.11	5.71	52.5
ITCs	5.24	6.48	5.40	30.97	78.48	0.00	35.1
ITT	11.47	6.82	3.51	37.62	89.08	0.38	34.1
LPtB	2.94	6.83	14.15	53.21	79.10	4.64	64.9
LPtC	2.12	4.02	5.73	42.38	89.61	1.86	71.3
LPtT	5.37	6.47	4.52	39.34	87.80	1.02	61.9
LTlB	*n.d.*	6.44	7.60	25.99	83.42	1.03	86.3

Sample Name	Compressive Strength [MPa]	Difference in Electrical Conductivity [mS/cm]	Hydraulicity [CO_2/H_2O]	Porosity [%]	SiO_2 content of aggregates [%]	CaO content of aggregates [%]	Binder content [%]
LTlS	*n.d.*	4.98	5.31	33.62	69.41	3.42	91.5
LTlT	7.02	6.66	8.76	32.24	66.03	7.05	78.0
LXA	2.65	2.54	7.59	42.50	56.05	10.43	40.6
LXB	4.53	4.15	5.14	34.95	66.35	5.01	45.8
LXT	10.29	3.43	4.15	27.20	67.25	1.59	54.2
LySrU	11.45	5.57	6.05	34.43	82.81	0.00	21.5
LyTpA	4.43	3.80	6.03	33.07	76.69	1.65	34.8
LyTpB	5.76	7.29	5.26	32.72	89.94	0.17	22.5
LyTpT	6.42	7.21	6.12	30.52	89.37	0.00	13.7
MPB	4.98	5.74	2.85	36.77	87.16	0.79	23.6
MPB2	5.00	5.80	5.87	34.00	87.94	2.68	22.8
MPC	4.96	1.19	1.81	38.74	89.46	0.38	21.7
PhAzB	*n.d.*	4.31	8.52	34.77	78.09	0.00	31.4
PhLdB	11.46	5.38	8.60	31.65	86.32	2.64	59.8
PCT	11.70	6.61	9.47	38.03	75.76	0.00	93.3
PCB	6.67	5.27	8.27	37.73	73.71	4.07	88.6
PCC	10.42	7.02	6.59	45.67	88.64	0.49	96.5
PmLyB	2.82	3.83	8.05	28.50	78.87	1.52	54.7
PmLyCs	5.59	5.44	13.81	32.04	77.98	1.07	61.4
PmLyC	3.68	4.69	11.04	32.33	82.05	0.64	70.7
PAtT	4.38	2.93	6.58	34.36	73.52	0.00	18.7
PSlB	7.90	4.74	4.21	39.76	90.09	0.72	61.8
PSlS	8.57	7.11	5.44	36.52	89.33	1.73	61.2
PSlT	6.71	6.63	4.20	48.03	92.96	1.11	80.2
PSB	2.48	7.04	9.29	41.42	80.91	1.35	43.7
PSA	2.70	4.33	4.21	44.80	82.21	5.12	28.7
PST	5.22	7.17	2.70	44.96	91.76	0.00	69.5
TAB	6.17	7.53	5.83	43.94	91.24	0.00	32.9
TACs	6.70	6.74	3.93	36.44	92.61	0.00	27.7
TAxB	8.97	7.38	3.60	39.45	93.05	0.96	20.0
TAxG	4.63	7.48	5.24	35.75	90.52	0.80	24.5

VITA

PERSONEL INFORMATION

Surname, Name: Taşcı, Burcu
Date and place of birth:
E-mail addresses: burcutasci@iyte.edu.tr, burcutasci89@gmail.com

EDUCATION

Ph.D., İzmir Institute of Technology, Graduate School of Engineering and Sciences, Department of Architectural Restoration, Turkey **(2015-2021)**

Thesis: "Properties of Lime Binders and Aggregates of Roman Mortars in Western Anatolia"

Ph.D. Scholarship (YÖK / YUDAB), The University of Navarra, Department of Chemistry, MATCH Research Group, Spain **(2019-2020)**

Project: "Optimization of New Lime Restoration Mortars by the Combined Action of Admixtures and Pozzolanic Materials"

Erasmus Exchange Student, Uppsala University, Department of Art History, Cultural Heritage and Sustainability, Sweden **(2017-2018)**

Project: "Changes in Cultural Heritage Activities: New Goals and Benefits for Economy and Society"

M.Sc., Dokuz Eylül University, The Graduate School of Natural and Applied Sciences, Department of Architecture, Restoration, Turkey **(2012-2015)**

Thesis: "Evaluation of the Conservation Issues of the Multi-layered Settlements: The Case Study of Foça (Phokaia), Turkey"

B.Arch., Dokuz Eylül University, Department of Architecture, Turkey (Graduate ranking first in the faculty) **(2007-2012)**

ACADEMIC EXPERIENCES

Research Assistant, İzmir Kâtip Çelebi University, Department of Architecture (2014-2016)

Research Assistant, İzmir Institute of Technology, Department of Architectural Restoration (2016-2018)

Research Assistant, İzmir Kâtip Çelebi University, Department of Architecture (since 2018)